# DEVELOPMENT OF INTELLIGENT MONITORING SYSTEM (IMS) MODULES FOR THE AQUISTORE $CO_2$ STORAGE PROJECT

Final Technical Report – Deliverable D5

*Prepared for:*

AAD Document Control

National Energy Technology Laboratory
U.S. Department of Energy
626 Cochrans Mill Road
PO Box 10940, MS 921-107
Pittsburgh, PA 15236-0940

Cooperative Agreement No. DE-FE0026516
Project Period: October 1, 2015 – September 30, 2018
Cooperative Agreement No. DE-FE0026516
DUNS No. 102280781

*Prepared by:*

Nicholas A. Azzolina
José A. Torres
Saurabh Chimote
Lawrence J. Pekot
Matthew E. Burton-Kelly
Neil W. Dotzenrod
Nicholas W. Bosshart
Chantsalmaa Dalkhaa
Scott C. Ayash
Chunxiao Li
David V. Nakles
Charles D. Gorecki
Heidi M. Vettleson

Energy & Environmental Research Center
University of North Dakota
15 North 23rd Street, Stop 9018
Grand Forks, ND 58202-9018
Phone (701) 777-5120; Fax (701) 777-5181
nazzolina@undeerc.org

2018-EERC-11-19

November 14, 2018

## EERC DISCLAIMER

LEGAL NOTICE This research report was prepared by the Energy & Environmental Research Center (EERC), an agency of the University of North Dakota, as an account of work sponsored by the U.S. Department of Energy (DOE) National Energy Technology Laboratory. Because of the research nature of the work performed, neither the EERC nor any of its employees makes any warranty, express or implied, or assumes any legal liability or responsibility for the accuracy, completeness, or usefulness of any information, apparatus, product, or process disclosed or represents that its use would not infringe privately owned rights. Reference herein to any specific commercial product, process, or service by trade name, trademark, manufacturer, or otherwise does not necessarily constitute or imply its endorsement or recommendation by the EERC.

## ACKNOWLEDGMENT

This material is based upon work supported by the U.S. Department of Energy, National Energy Technology Laboratory under Award No. DE-FE0026516.

## DOE DISCLAIMER

This report was prepared as an account of work sponsored by an agency of the United States Government. Neither the United States Government, nor any agency thereof, nor any of their employees, makes any warranty, express or implied, or assumes any legal liability or responsibility for the accuracy, completeness, or usefulness of any information, apparatus, product, or process disclosed, or represents that its use would not infringe privately owned rights. Reference herein to any specific commercial product, process, or service by trade name, trademark, manufacturer, or otherwise does not necessarily constitute or imply its endorsement, recommendation, or favoring by the United States Government or any agency thereof. The views and opinions of authors expressed herein do not necessarily state or reflect those of the United States Government or any agency thereof.

## TABLE OF CONTENTS



Continued . . .

**TABLE OF CONTENTS (continued)**

## LIST OF FIGURES



Continued . . .

## LIST OF FIGURES (continued)



Continued . . .

## LIST OF FIGURES (continued)



## LIST OF TABLES

# DEVELOPMENT OF INTELLIGENT MONITORING SYSTEM (IMS) MODULES FOR THE AQUISTORE $CO_2$ STORAGE PROJECT

## EXECUTIVE SUMMARY


The monitoring data generated at a $CO_2$ storage site can quickly result in large amounts of data, often requiring significant labor- and time-intensive efforts to process and analyze before being able to make operational decisions. Implementing an intelligent monitoring system (IMS) can reduce the associated data-processing and analysis costs, which can thereby improve the efficiency of the monitoring process and enable real-time operational decision-making.

The Energy & Environmental Research Center (EERC) has completed a 3-year project focused on developing an IMS comprising new workflows, algorithms, and a user interface for the automation and integration of geologic carbon dioxide ($CO_2$) storage site-monitoring and simulation data. The design for the IMS was based on using injection and monitoring data acquired from Aquistore, an operating $CO_2$ storage project. Managed by the Petroleum Technology Research Centre, the Aquistore Project is injecting $CO_2$ captured from SaskPower's coal-fired Boundary Dam Power Station into a deep saline formation for geologic storage. Using data from the Aquistore Project provided a real-world basis to develop an IMS.

The IMS consists of a database that stores the monitoring measurements (IMS Database) and a graphical user interface (IMS GUI) used to retrieve data from that database. Lastly, the IMS Workflow defines the linkage between the IMS GUI and the IMS Database.

The IMS GUI is divided into seven modules that address specific aspects of the monitoring system:

**Module 1 (Well Monitoring Measurements):** This module allows the user to plot time-series results of injection well measurements. These time-series plots provide information to the user about changes in these measurements over time and relationships between measurements. Module 1 includes six measurements: $CO_2$ mass injection rate (Qg) measured at an injection meter building prior to the $CO_2$ being injected into the subsurface and five measurements collected at the injection well: wellhead temperature (WHT), wellhead pressure (WHP), bottomhole temperature (BHT), bottomhole pressure (BHP), and annulus pressure (ANP).

**Module 2 (Distributed Temperature System [DTS] Measurements):** The DTS acquires temperature measurements from 33 discrete temperature sensors located along the length of the 4.5-inch tubing within the injection wellbore, providing a time-series temperature profile of the injection well (two-dimensional data with time). Module 2 provides the user with two different options for displaying these DTS temperature measurements: DTS temperature profiles (Module 2A – Temperature versus depth at a given time) and DTS time-series temperature or temperature gradient heat maps (Module 2B – Temperature versus time and depth).

**Module 3 (BHT and BHP Analysis):** This module provides a decision framework for evaluating new BHT or BHP measurements given a set of operating conditions. Module 3 uses a set of "action levels," or threshold values, to identify exceedances of normal operating limits.

**Module 4 (DTS Analysis):** Module 4 provides a decision framework for evaluating new DTS temperature measurements given the combined effects of 1) the $CO_2$ injection rate and 2) the $CO_2$ injection duration on the measured DTS wellbore temperature profile.

**Module 5 (Continuous Modeling Refinement [CMR] Analysis):** The CMR component of the IMS integrates continuous and periodic monitoring data with reservoir performance simulations. The primary purpose of the CMR process is to evaluate whether the reservoir simulation can reproduce the observed behavior of the $CO_2$ plume within a reasonable error tolerance. As part of the IMS, the CMR process compares the predicted $CO_2$ plume behavior with observed $CO_2$ plume behavior given a set of injection and monitoring measurements, the geologic model, and reservoir simulations. The CMR module automatically adjusts the simulation model until the predicted $CO_2$ plume matches the observed $CO_2$ as closely as possible. Failure of the reservoir simulations to adequately predict the observed $CO_2$ plume informs the operator that there may be a deficiency in the simulation or a subsurface condition that is outside of normal operating limits. Conversely, if the CMR process rapidly and accurately predicts the observed $CO_2$ plume, it provides the operator with greater confidence that the subsurface conditions are consistent with normal operating limits.

**Module 6 ($CO_2$ Plume Boundary):** This module provides the user with a visual output for exploring the quality of the results obtained from Module 5 against the observed $CO_2$ plume contour, which was previously defined from time-lapse seismic analysis of pre- and post-$CO_2$ injection 3-D seismic measurements (4-D seismic).

**Module 7 (System Evaluation):** Module 7, the last module in the IMS, integrates the action levels for DTS, BHT, and BHP and the outcome from the CMR analysis of Module 5, into a graphical assessment of whether the system is operating within normal limits. Module 7 produces a set of color-coded outputs that flag for the operator the need to evaluate other modules within the IMS or to implement further actions to control the storage site.

Compared with the traditional manual processing, interpretation, and integration workflows, this IMS allows a carbon capture and storage (CCS) site operator to more efficiently monitor and manage $CO_2$ injection and subsurface conditions. This technology advanced the state-of-the-science for IMSs and contributes to the U.S. Department of Energy Carbon Storage Program goals of developing and validating technologies to ensure $CO_2$ storage permanence and to improve reservoir storage efficiency while ensuring containment effectiveness. This report discusses the injection and monitoring data used to develop the IMS; describes the database, data workflow, IMS programming and system requirements, and modules included in the IMS; and provides examples from the IMS interface and its outputs.

# DEVELOPMENT OF INTELLIGENT MONITORING SYSTEM (IMS) MODULES FOR THE AQUISTORE $CO_2$ STORAGE PROJECT

## INTRODUCTION

The Energy & Environmental Research Center (EERC) has completed a 3-year project focused on developing new workflows, algorithms, and a user interface to automate the integration of carbon dioxide ($CO_2$) storage site-monitoring and simulation data as part of an intelligent monitoring system (IMS). Compared with traditional manual processing, interpretation, and integration workflows, this IMS allows a carbon capture and storage (CCS) site operator to more efficiently monitor and manage $CO_2$ injection and subsurface conditions.

The concept of implementing an IMS to monitor and manage subsurface injection is widespread in the oil and gas exploration and production (E&P) industry for production control and optimization, surrogate modeling as an alternative to computationally intensive full numerical simulation, and virtual sensing (Khan and others, 2015; Chai and others, 2014; Bravo and others, 2013). When oil fields deploy an IMS, these fields, or sometimes individual wells within fields, are often referred to as intelligent fields, e-fields, i-completions, smart wells, and/or digital fields. A key aspect of these intelligent fields is that they integrate real-time data from wells and reservoirs to obtain critical information about the overall performance and state of the operation (Khan and others, 2015; Silva and others, 2012).

While the application of an IMS in oil and gas E&P activities is relatively common, applications as part of $CO_2$ storage projects are much less common. However, $CO_2$ storage projects stand to gain substantial benefit from implementing such a system. Federal requirements under the Underground Injection Control (UIC) Program for $CO_2$ Geologic Sequestration require testing and monitoring as part of the Class VI permit application implemented throughout the project to demonstrate the safe operation of the injection well and track the position of the $CO_2$ plume and pressure front (U.S. Environmental Protection Agency [EPA], 2018a). In addition, the reporting requirements under Subpart RR of the 45Q tax credit for $CO_2$ sequestration require facilities that conduct geologic sequestration by injecting $CO_2$ for long-term containment in subsurface geologic formations, including UIC Class VI wells, to develop and implement an EPA-approved site-specific monitoring, reporting and verification (MRV) plan (U.S. Environmental Protection Agency, 2018b). Therefore, monitoring is an integral component of $CO_2$ storage projects.

Monitoring plans for $CO_2$ storage projects often contain several technologies, each with their own collection frequency (e.g., continuous, periodic). In addition, the variety of monitoring technologies used often results in multiple different and disparate data types. As such, monitoring data generated at a $CO_2$ storage site can quickly result in large amounts of data, which then require a significant labor- and time-intensive effort to process and analyze the data before using this information to make decisions about the state of the operation. Implementing an IMS can reduce the associated data-processing and analysis time and costs, thereby improving monitoring efficiency and enabling real-time operational decision-making.

The IMS discussed in this report integrates continuous monitoring data (pressure, temperature, and $CO_2$ injection rate measurements), periodic monitoring data (seismic data and

well logs), and reservoir performance simulations (which have been tuned and improved with monitoring data) with software algorithms linked to a user interface for visualization and real-time decision-making support. This body of work advances the state of the science for intelligent monitoring at geologic $CO_2$ storage sites.

The remainder of this report discusses the injection and monitoring data used to develop the IMS; summarizes the database, data workflow, IMS programming and system requirements, and modules included in the IMS; and provides examples from the IMS interface and its outputs.

## IMS INJECTION AND MONITORING DATA

The design for the IMS was based on using injection and monitoring data acquired by SaskPower and the Petroleum Technology Research Centre (PTRC) at the Aquistore $CO_2$ Storage Site of the Boundary Dam Power Station located near Estevan, Saskatchewan, Canada (hereafter the "Storage Site") (Figure 1). SaskPower's Boundary Dam Power Station is a coal-fired electric generating facility. In October 2014, the Boundary Dam Power Station completed a refurbishment program that included retrofitting $CO_2$ capture facilities onto the power plant. The majority of the captured $CO_2$ from the power plant is transported via pipeline and used for enhanced oil recovery (EOR) at the Weyburn Oil Unit, which is also located in Saskatchewan. However, the portion of the captured $CO_2$ that is not used for EOR is transported via pipeline to the nearby Storage Site for dedicated geologic storage and isolation from the atmosphere (Global CCS Institute, 2018) (Figure 2). The target geologic reservoirs for dedicated geologic storage of the $CO_2$ are the Deadwood and Black Island Formations, approximately 10,500 feet beneath the surface.

Since the Storage Site serves as overflow storage for $CO_2$ not being sold for EOR, the $CO_2$ injection has been intermittent, with periods of varying injection rate and duration. However, the Storage Site provides an ideal case study for development an IMS because 1) the project is an active $CO_2$ storage demonstration project injecting into saline formations that are representative of potential target reservoirs of future commercial deep saline $CO_2$ storage projects and 2) the Storage Site is deploying multiple monitoring technologies, which collectively offer a variety of data types applicable for deep saline $CO_2$ storage.

### Continuous Monitoring Measurements

The specific continuous monitoring measurements used in the IMS include:

- $CO_2$ mass injection rate (Qg), measured at an injection meter building prior to the $CO_2$ being injected into the subsurface.
- Five different measurements collected at the injection well: wellhead temperature (WHT), wellhead pressure (WHP), bottomhole temperature (BHT), bottomhole pressure (BHP), and annulus pressure (ANP).
- Distributed temperature system (DTS) temperature measurements acquired at 33 discrete sensors located along the length of a 4.5-inch tubing within the injection wellbore.

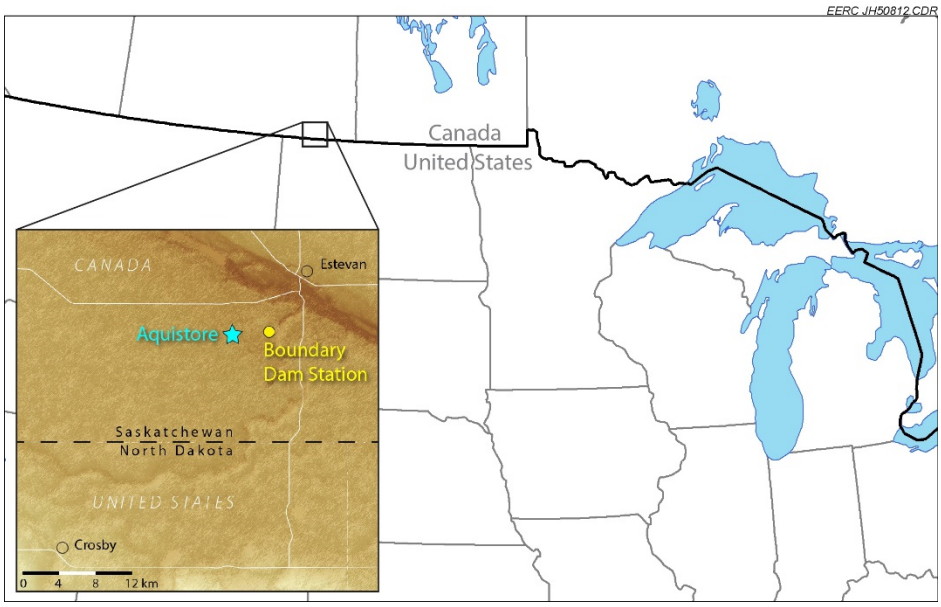


Figure 1. Location of the Aquistore $CO_2$ storage project and Boundary Dam Power Station, the source of the $CO_2$, in southeastern Saskatchewan, Canada (modified from Peck and others, 2014).

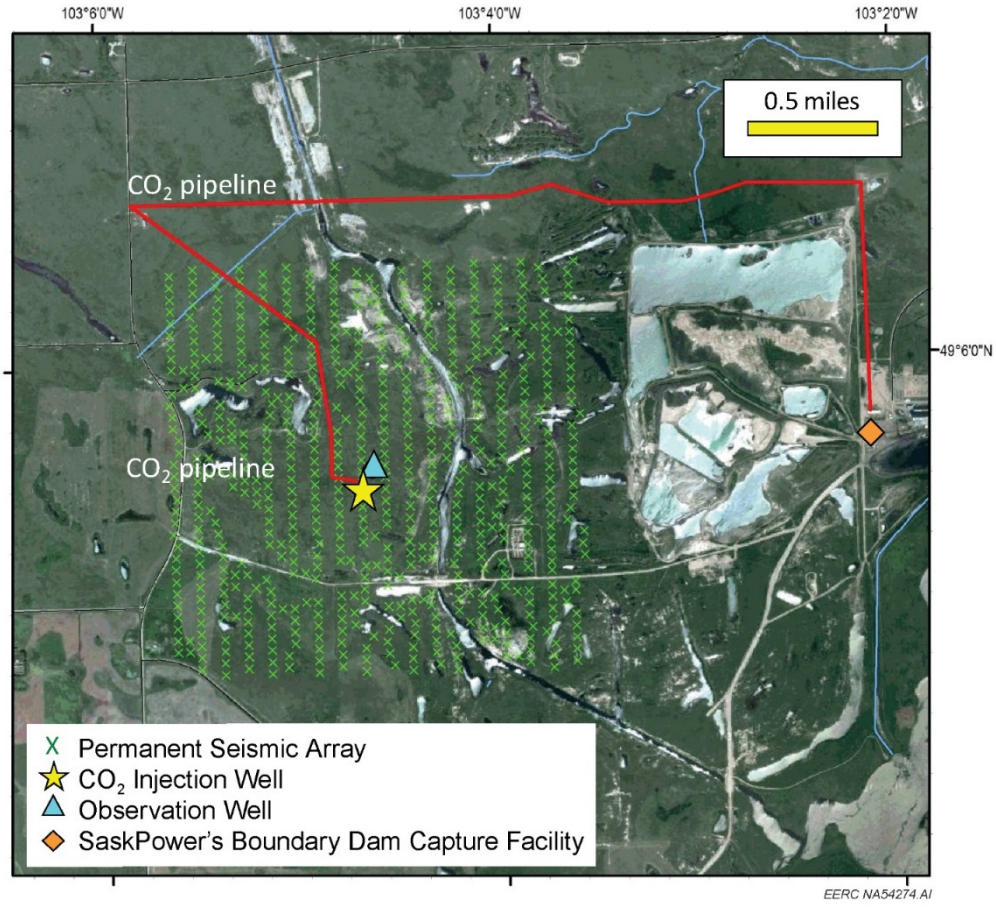


Figure 2. Map of the Storage Site showing the locations of the Boundary Dam $CO_2$ capture facility, $CO_2$ pipeline to the $CO_2$ injection well, observation well, and permanent surface seismic array (source: courtesy of Petroleum Technology Research Centre).

The default unit of measurement for Qg is pounds per hour (lb/hr). Figure 3 provides a schematic of the injection well. The WHT and WHP gauges are located in the wellhead of the injection well and provide information about the temperature and pressure of the injected $CO_2$ at the surface. The default units of measurement for temperature and pressure are degrees Fahrenheit (°F) and pounds per square inch (psi), respectively. The IMS uses the casing-conveyed BHT and BHP gauges located at 10,374 ft, which provide information about the BHT and BHP conditions. Figure 3 also shows the DTS line along the injection well tubing (DTS line). The DTS temperature measurements acquired at the injection well include 33 discrete temperature measurements at increments of approximately 328 ft from the surface to 10,203 ft. Lastly, the ANP is a measurement of the pressure in the space between the tubing and the production casing. This space is filled with water plus a small quantity of nitrogen at the top and sealed with the wellhead annulus valve at the surface and at the bottom by the production packer. The ANP is monitored at the surface in the wellhead where the annulus connects to the pressure management system (not shown in Figure 3). The measurements of Qg, WHT, WHP, BHT, BHP, and ANP constitute continuous or high-acquisition frequency measurements collected at 1-minute intervals.

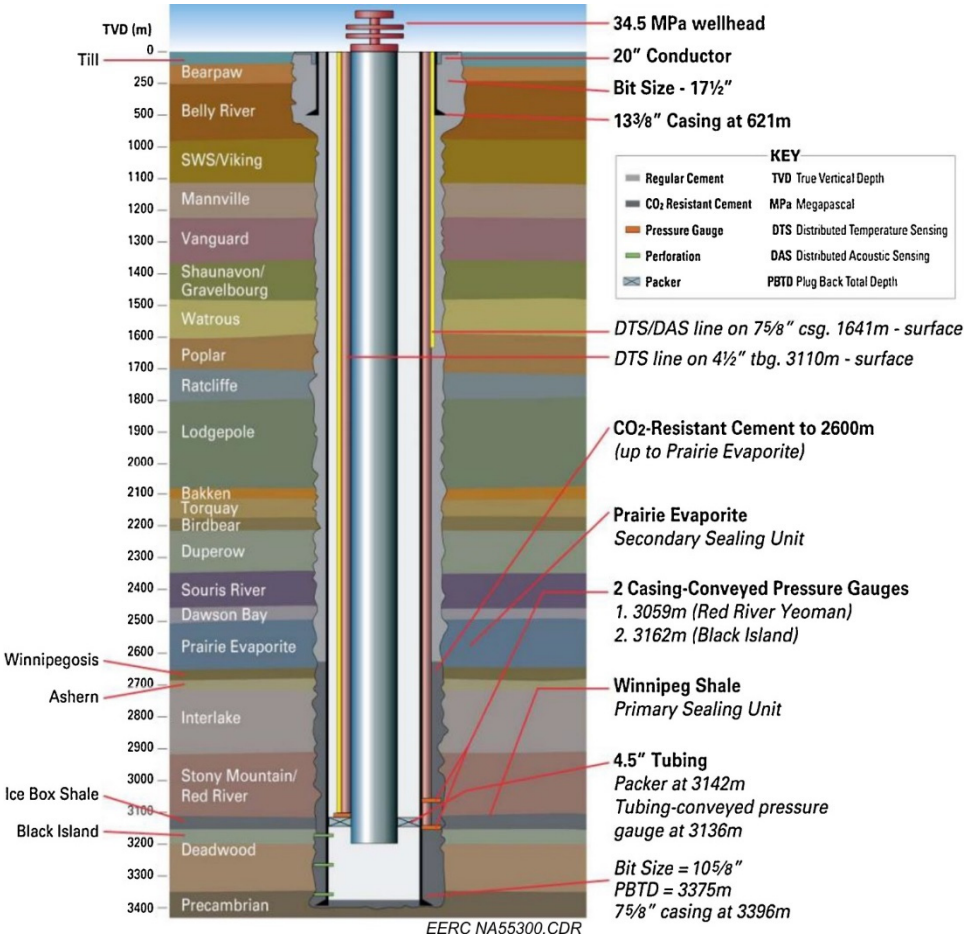


Figure 3. Well schematic for the $CO_2$ injection well (source: Lee and others, 2018).

While the observation well also includes casing- and tubing-conveyed BHT and BHP gauges, these data are not included in the IMS as these devices no longer function properly.

**Definition of Normal Operating Limits and Action Levels**

As part of its effort at the Storage Site, PTRC conducted an extensive review of the monitoring data that have been collected, including additional measurements beyond those incorporated into the IMS, and concluded that there have been no failures of the storage unit, e.g., $CO_2$ migration outside of the target injection horizon or leakage along the $CO_2$ injection wellbore. Thus the data set used to develop the IMS is referred to in this document as representative of "normal operating limits" under a range of $CO_2$ injection conditions and contains the observed data which provide the basis for quantifying decision thresholds. Specifically, the IMS uses monitoring data acquired from the injection well from April 15, 2015, through July 31, 2017, to establish a set of "action levels" or threshold values that could be used to identify exceedances of normal operating limits. These action levels represent a retrospective analysis applied to the historical data set rather than an autonomous system that begins at the start of $CO_2$ injection, learns from the data, and derives action levels in real time. Nevertheless, these action levels provide a basis for decision-making about future monitoring measurements (i.e., acquired after July 31, 2017).

The action levels were incorporated into the IMS, focusing on three continuous monitoring measurements: DTS temperature, BHT, and BHP. The treatment of periodic monitoring measurements is handled through the coupling of seismic interpretation, geologic modeling, and numerical reservoir simulations, as described in the next section.

**Periodic Monitoring Measurements**

Three-dimensional (3-D) surface seismic measurements were acquired periodically at the Storage Site using the permanent geophone array shown in Figure 2. In addition, well log measurements (spinner surveys and pulsed-neutron logs [PNLs]) were acquired periodically from the injection well and the observation well. These seismic and well log measurements represent lower acquisition frequency data because, unlike the continuous measurements that were acquired at 1-minute intervals, these measurements were acquired periodically with relatively long time spans between measurements (e.g., 1 year or more). These periodic measurements were incorporated into the IMS through a process called "Continuous Modeling Refinement" (CMR), which integrates continuous and periodic monitoring data with reservoir performance simulations.

The primary purpose of the CMR process is to evaluate whether the reservoir simulation can reproduce the observed behavior of the $CO_2$ plume within a reasonable error tolerance. As a monitoring tool for managing $CO_2$ injection and subsurface conditions, the CMR process informs the operator about whether the predicted $CO_2$ plume behavior is consistent with observed $CO_2$ plume behavior given a set of injection and monitoring data, the geologic model, and reservoir simulations. The CMR module automatically adjusts the simulation model until the predicted $CO_2$ plume matches the observed $CO_2$ as closely as possible. Failure of the reservoir simulations to adequately predict the observed $CO_2$ plume may reflect a deficiency in the simulation or a subsurface condition that is outside of normal operating limits. Conversely, if the CMR process

rapidly and accurately predicts the observed $CO_2$ plume, then this outcome provides the operator with greater confidence that subsurface conditions are sufficiently represented within the geologic model and the $CO_2$ plume behavior can be reasonably predicted by simulations using that model.

The CMR process is the most complex component within the IMS because of the integration of multiple data types, linkage of several subcomponents, and interface with commercial reservoir simulation software. As a result, a general overview and results of the CMR are presented in the main body of this text. A detailed description of the CMR process is provided in Appendix A.

## IMS DESCRIPTION

The IMS comprises a database that stores the monitoring measurements and CMR outputs (IMS Database) and a graphical user interface (IMS GUI) with which the user interacts to retrieve data from the IMS Database. Lastly, the IMS Workflow defines the linkage between the IMS GUI and the IMS Database. This section provides an overview of the IMS Database and IMS Workflow, in addition to a brief description of the IMS programming. The IMS Modules section provides a detailed description of the IMS GUI and the individual modules that make up the IMS.

### IMS Database

#### *SaskPower Database*

Site injection and monitoring data acquired by SaskPower and PTRC are stored in a secure database at the EERC (IMS Database). Over the course of the project, SaskPower shared daily data from the Storage Site for over 100 sensors formatted to report one sensor reading per minute (60 measurements per hour or 1440 measurements per day per sensor). These sensor data are recorded in SaskPower's plant data collection system, which is an automated system provided by ABB Ltd. These measurements are then permanently stored on a separate server system, which is a PI Historian System.

#### *Data Importation and Extraction*

The IMS was developed to run from the IMS Database stored on EERC servers. The IMS Database interfaced with the PI Historian System to retrieve injection and monitoring data. The PI Historian System has a Microsoft Excel® (Excel) add-in that allows users to retrieve the data by a specified frequency, from every 0.5 seconds to every 24 hours. Throughout the course of the project, the IMS Database acquired updates from the PI Historian System at either daily frequency or, in some cases, in batches of longer periods of time, e.g., 1 month of data.

The Excel data from the PI Historian System were manually imported into the IMS Database and processed through a Microsoft Structured Query Language Stored Procedure (T-SQL). Each column of sensor data was processed independently, and a series of quality assurance checks were performed prior to importing the Storage Site data into the IMS Database. The first check was to determine if the sensor exists in the raw data master source table (MST) for the raw data. Next, the data were inserted into the MST, where the time stamp column was the identifier for the row (year,

month, day, hour, and minute). This process was completed after all columns (sensors) were checked and uploaded. Error checking for valid data occurred at the time the data were imported. For example, if the sensor data reported for a specific time stamp contained nonnumeric values, then an update statement was executed to insert a NULL value at the current time stamp and sensor column. Any invalid data types were treated as null data (missing data) in the IMS Database.

The IMS Database is a relational database, which offers the advantages of structured data, security/privileges, speed, and ease of access. Data management through SQL allows for querying, adding, and changing the data. The IMS Database resides on a Windows 2012 Server operating system and 2012 SQL Server R2, which provides the required processing speed and data protection. Interface between the IMS Database and other data analysis tasks is handled through SQL queries. These queries provide outputs formatted for use in the data-processing tasks and for reports that are displayed in the graphical user interface (IMS GUI).

The IMS Database includes data from April 15, 2015 (the start of $CO_2$ injection) through July 31, 2017 (the last valid day in the IMS Database). This represents over 2 years of injection and monitoring data and more than 1 million rows of data.

### *Security Features*

The IMS Database includes multiple features to prevent data loss and to ensure that the data are secure from unauthorized access (e.g., "hacking"). For example, the IMS is hosted on a server disk rack array configured as RAID 6, a redundant array of independent disks, which protects the data from hardware failures. A full backup of the IMS Database is performed daily, and a shadow backup is performed twice daily. A continuous log file of the IMS Database transactions is maintained so that the data can be recovered exactly up to a precise point in time. In addition to these measures, an off-site backup copy of the IMS Database is maintained on an encrypted drive in case of an on-site system failure. Several security features are implemented on the server to prevent unauthorized access, such as limiting user access and making the IMS Database only accessible through the domain within the EERC; hence physical files are protected. All of the connections to the IMS Database are encrypted. Finally, the EERC Server Administrator tracks the security, and when "brute force" attacks are detected, the Internet protocol address of the attack machine is blocked for 10 minutes. If the attack continues, then the attack machine is blocked for up to 2 years. The EERC Server Administrator receives e-mail or text notification as soon as a potential threat to the database is detected.

## IMS Data Workflow

The IMS Data Workflow maps the flow of data from the Storage Site to the IMS Database and then through one of six paths, which reflect the different types of measurements and the degree of processing between the IMS Database and the IMS GUI (Figure 4):

- **Path 1** is raw continuous data (as reported from SaskPower to the EERC) from the IMS Database to the IMS GUI and provides the user with real-time monitoring information from seven different measurements, i.e., Qg, WHT, WHP, BHT, BHP, ANP, and DTS measurements from 33 sensors along the injection well.

- **Path 2** processes the DTS temperature sensor measurements or BHT and BHP measurements from the raw data through a set of algorithms. These algorithms compare new measurements against a set of action levels to assess whether the site is or is not operating within normal limits.

- **Path 3** processes a subset of the measurements of the raw data through preprocessing routines and then feeds these processed data into a CMR Module, which uses the monitoring data to generate an automated history match between the simulated $CO_2$ plume and the 3-D seismic-interpreted $CO_2$ plume obtained from the periodic data.

- **Path 4** takes outputs from the CMR Module and sends these to the IMS Database for storage.

- **Path 5** retrieves outputs from the CMR Module that are saved in the IMS Database and sends these to the IMS GUI.

- **Path 6** retrieves a static image of the most current 3-D seismic-interpreted $CO_2$ plume from the IMS database.

The IMS Modules section provides additional details about how the paths illustrated in the IMS Data Workflow are performed within the IMS.

### IMS Programming

After various programming languages were considered, Python was selected as the programming language for the IMS (Python Core Team, 2018). Python is a high-level, general-purpose programming language that can be applied to many different classes of problems (Python Software Foundation, 2018). The IMS was developed using Python Version 2.7. Additional details about the programming and system requirements of the IMS are summarized in Appendix B.

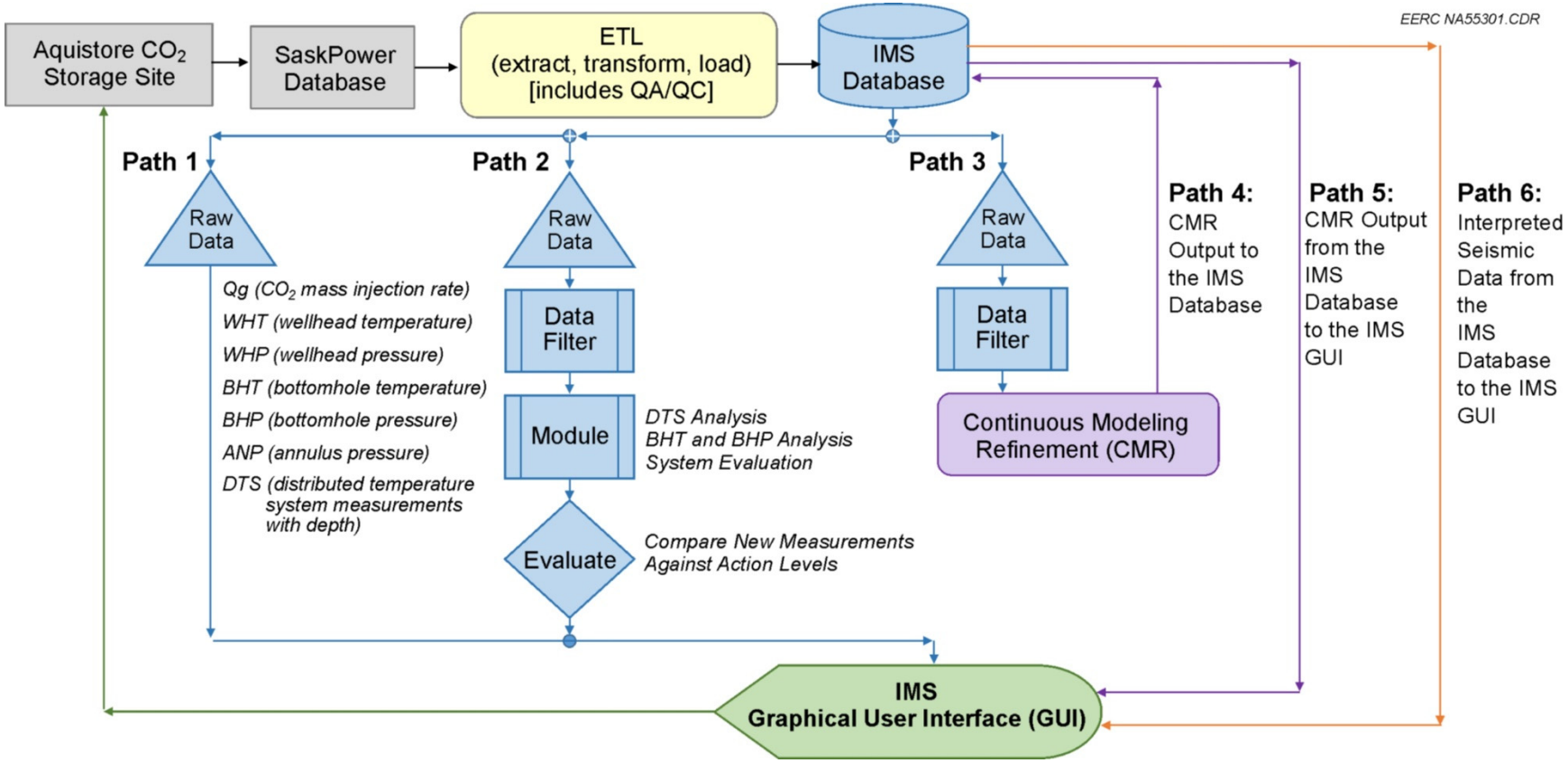


Figure 4. IMS Data Workflow showing the flow of data from the Storage Site to the IMS Database and then to one of six paths for handling the analyses of the sensor measurements, the continuous refinement of reservoir models (history-matching automation and seismic data integration), and the graphical display of data.

## IMS MODULES

### Launching the IMS

The user launches the IMS by clicking on the IMS shortcut (Windows Batch File) in the directory within which the IMS has been installed on the user's computer (Figure 5). The IMS shortcut will launch the main window of the IMS.

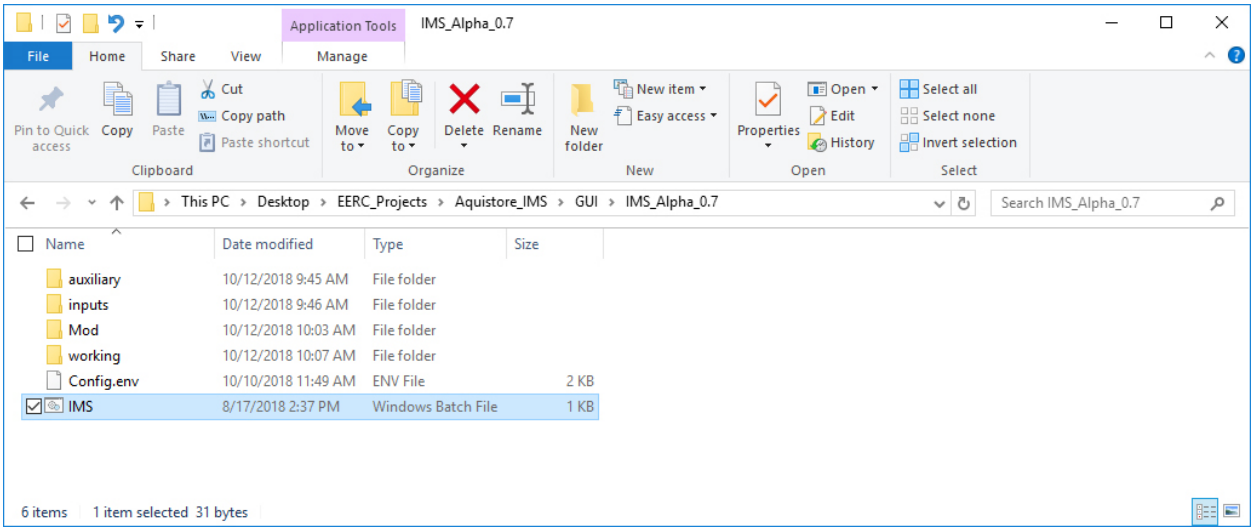


Figure 5. Windows Explorer screen showing the IMS installation files and the Windows Batch File that is used to launch the IMS.

The IMS GUI is divided into seven modules, which are separate pages within the user interface that address specific aspects of the monitoring system (Figure 6):

Module 1) Well Monitoring Measurements
Module 2) DTS Measurements (DTS Profiles [2A] and DTS Time-Series [2B])
Module 3) BHT and BHP Analysis
Module 4) DTS Analysis
Module 5) CMR Analysis
Module 6) $CO_2$ Plume Boundary
Module 7) System Evaluation

Each module serves a specific function that provides information to the CCS site operator. Module 7, System Evaluation, integrates multiple modules together into a single page. The remainder of this section provides the details for launching and executing each module.

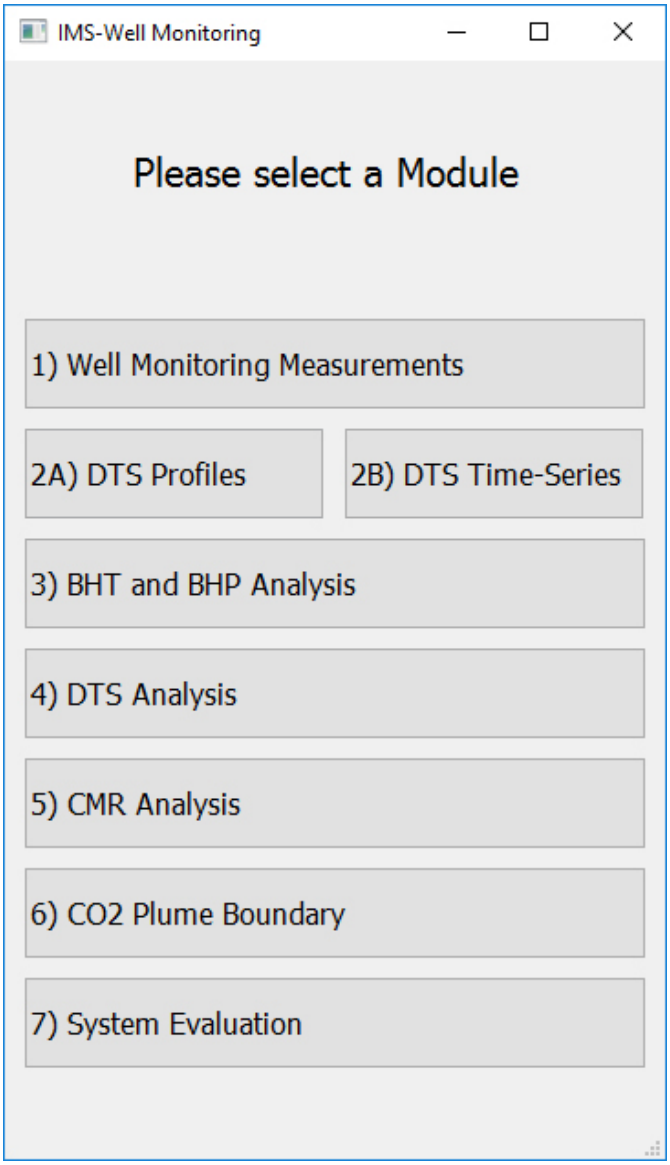


Figure 6. Module Selection Window for the IMS GUI.

**Module 1 – Well Monitoring Measurements**

The purpose of Module 1 is to allow the user to plot time-series results of injection well measurements. These time-series plots provide information to the user about changes in these measurements over time and relationships between measurements. Module 1 includes six measurements: Qg, WHT, WHP, BHT, BHP, and ANP. Module 1 does not include the DTS measurements as these are handled in Module 2.

To launch Module 1, the user clicks on the "1) Well Monitoring Measurements" button from the Module Selection Window (Figure 6). This will launch Module 1 and open the default page (Figure 7).

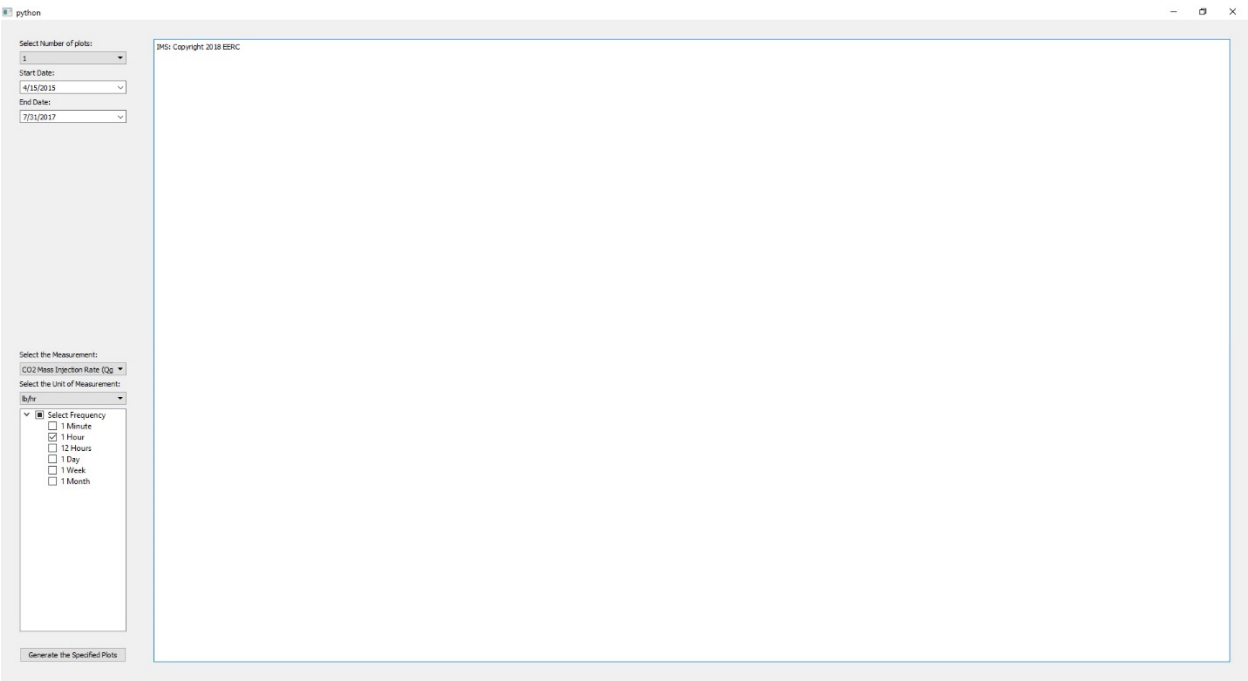


Figure 7. Default page for Module 1 – Well Monitoring Measurements.

Module 1 allows the user to choose from one of three different plotting options from the "Select Number of plots" dropdown menu in the upper left-hand corner of the page: single plot, double plot, or multiple axis plot.

### *Single-Plot Option*

Selecting the single-plot option (Select Number of plots = 1) allows the user to plot one measurement versus time. The default date range is currently set to a Start Date of April 15, 2015 (the beginning of $CO_2$ injection) and an End Date of July 31, 2017 (the last valid date in the IMS Database). However, the user may select any date range within this period by modifying the Start Date and End Date. A calendar feature has been incorporated into Module 1, which allows the user to select a Start Date or End Date using a monthly calendar (Figure 8).

After selecting a Start Date and End Date, the user must select one of the six measurements from the "Select the Measurement" dropdown list: $CO_2$ mass injection rate (Qg), WHP, WHT, BHP, BHT, or AN) (Figure 9).

The default units of measurement for the IMS are Imperial units, as these are the units of measurement reported by the Storage Site and stored in the IMS Database. However, the IMS GUI provides an option for converting to metric units under the "Select the Unit of Measurement" dropdown menu (Figure 10). The default and (metric) units for each measurement are listed as follows:

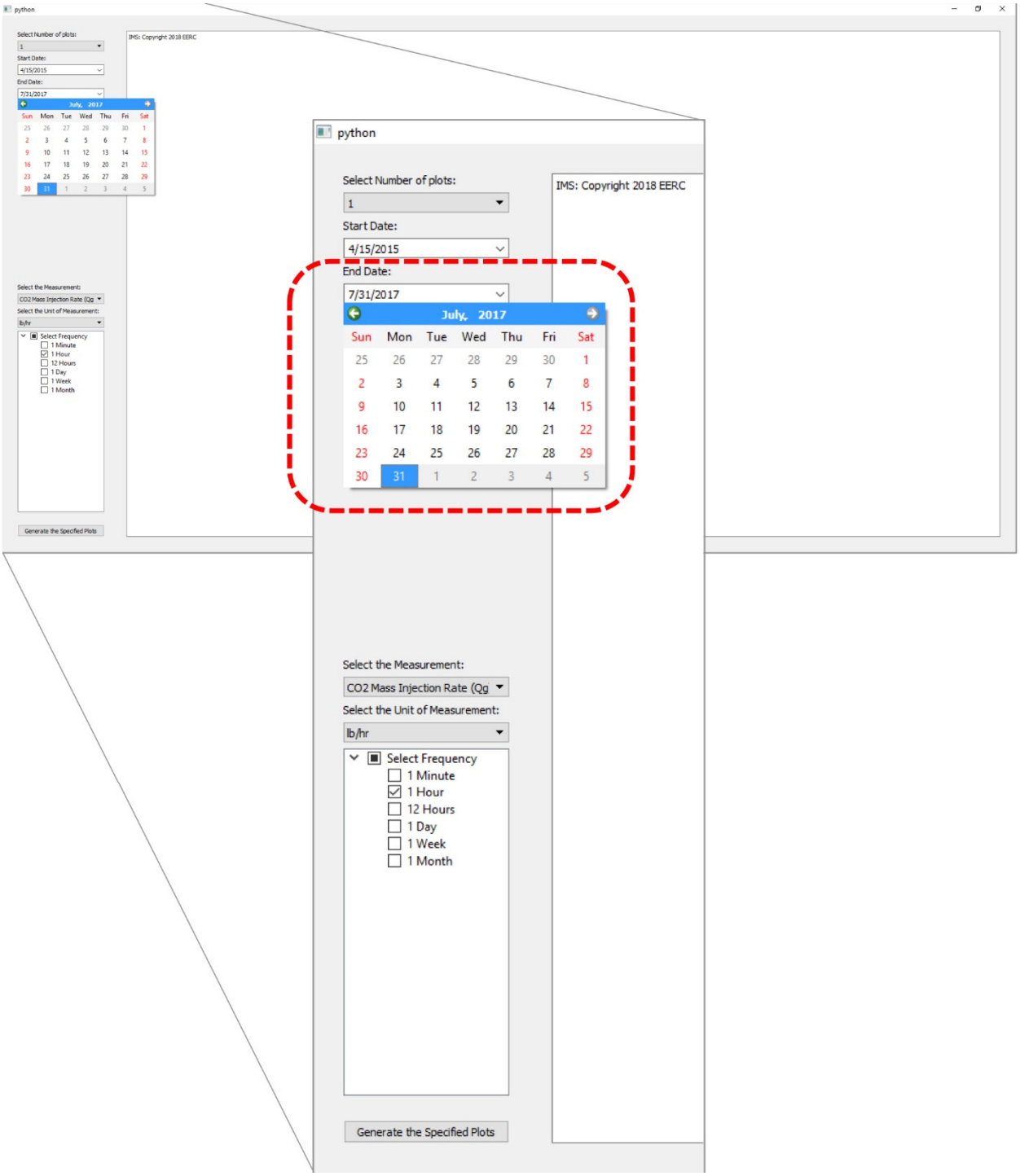


Figure 8. Illustration of the calendar feature for selecting an End Date in Module 1.

- $CO_2$ mass injection rate (Qg): pounds per hour (lb/hr) or metric tons per day (metric tons/day)
- WHP, BHP, and ANP: pounds per square inch (psi) or kilopascals (kPa)
- WHT and BHT: degrees Fahrenheit (°F) or degrees Celsius (°C)

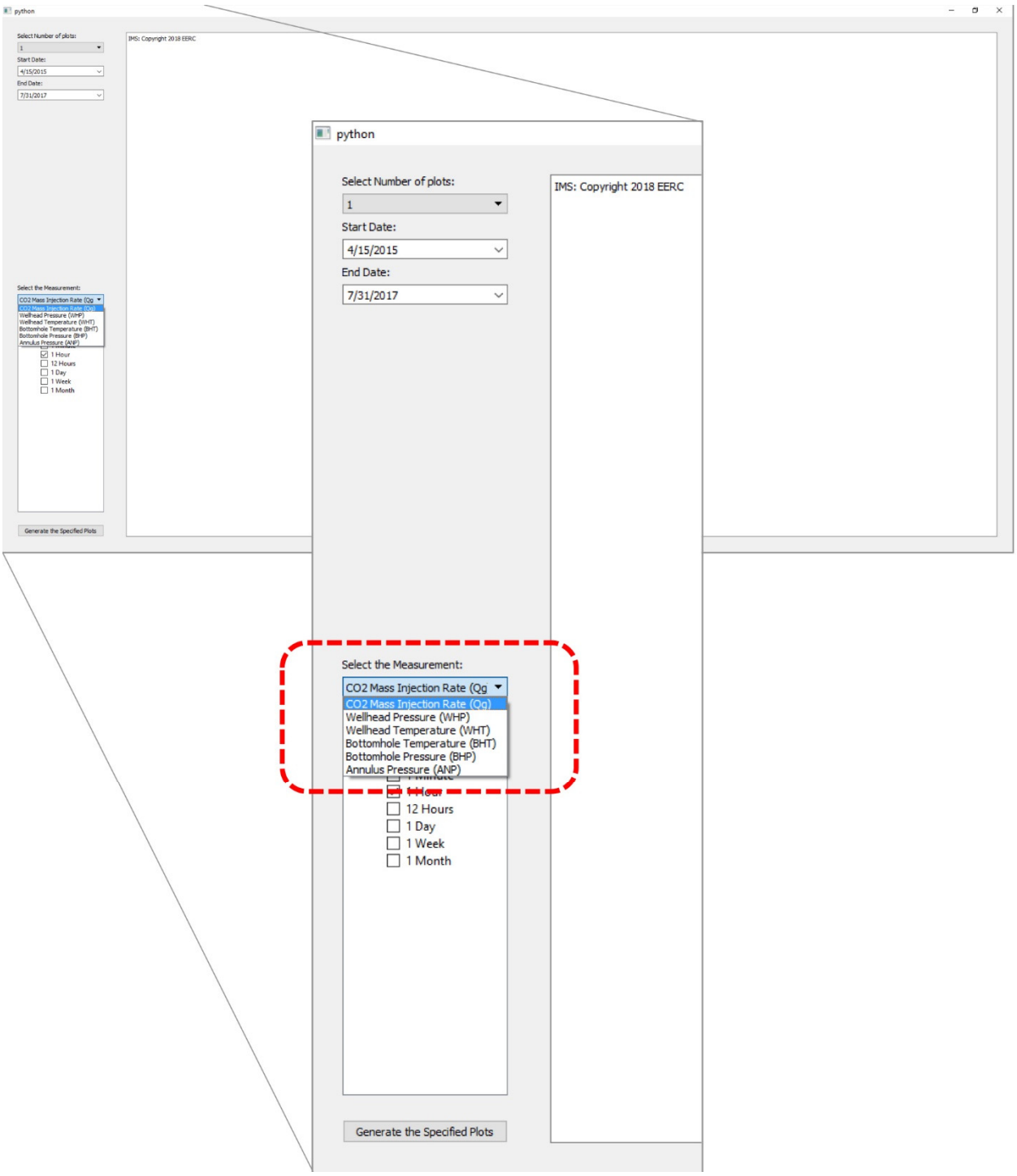


Figure 9. Illustration of the dropdown menu for selecting one of six measurements in Module 1.

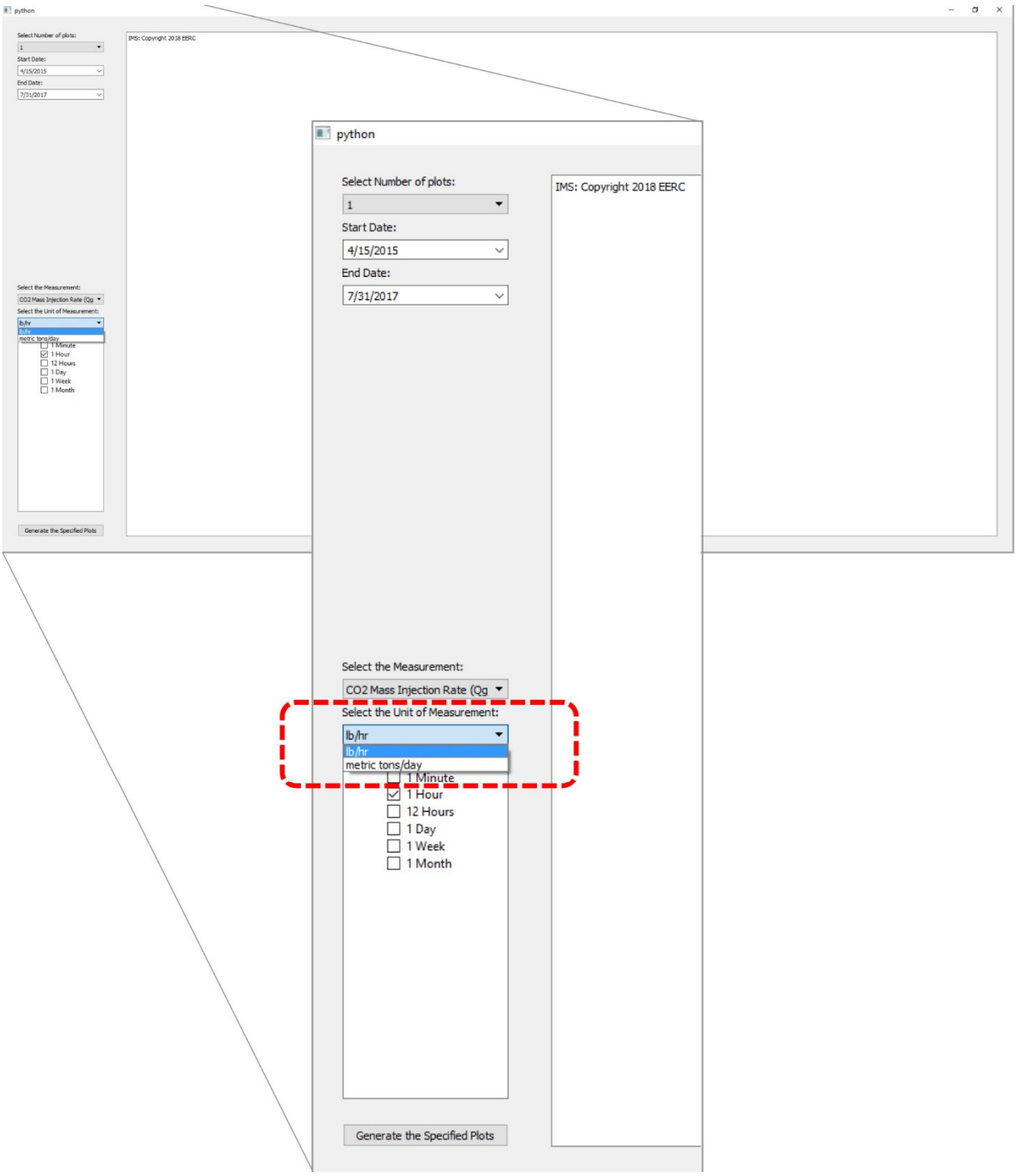


Figure 10. Illustration of the dropdown menu for selecting the unit of measurement in Module 1.

Lastly, the user must select the frequency of the measurement to plot from six options (Figure 11):

- 1 minute
- 1 hour
- 12 hours
- 1 day
- 1 week
- 1 month

The 1-minute frequency option reports the data in their native (as-acquired) frequency. The other frequencies use the 1-minute data in the IMS Database to compute averages for the reduced-frequency options. For example, the 1-hour frequency returns the average of sixty measurements for each hour, while the 1-day frequency returns the average of $24 \times 60 = 1440$ measurements for each day. There are multiple reasons why the user may want to select a frequency of greater than 1 minute. First, the 1-minute frequency option is data-intensive, which results in slower plotting. For example, plotting 1-minute data across the entire data range is approximately 1.2 million data points, whereas plotting 1-day data across that same date range results in only 840 data points. Second, measurements acquired every 1 minute capture a significant amount of variability attributable to differences between the measurement acquisition rate and the rates at which physical processes occur (e.g., pressure dissipation from the wellbore into the formation or heat transfer between the wellbore and the formation). This variability can make the plot look noisy, which detracts from an image that could inform the user about trends in measurement values over time. Therefore, averaging the 1-minute data into longer periods like 1 hour or 1 day helps to smooth the data and provides a clearer picture of the measurement value trends over time. While it might be argued that a CCS operator using the IMS should work with 1-minute data since 1-hour or 1-day averages will increase the time-to-detection, waiting for an hour or a day will help reduce false alarms (false positives) every few minutes resulting from the above-discussed variability in measurements. That said, the user has the option to select the desired data frequency and has the option to select multiple frequencies (e.g., 1 hour and 1 day), which will overlay both results on the same plot.

Once the user has selected a date range, measurement, unit of measurement, and frequency, the final step is to click the "Generate the Specified Plots" button in the lower left-hand corner of Module 1, which will retrieve the data from the IMS Database and generate the specified plot. Figure 12 shows an example of plotting Qg versus time for the date range from April 15, 2015, to July 31, 2017, and a frequency of 12 hours. This plot shows the start of $CO_2$ injection at the beginning of the date record, cessation of $CO_2$ injection from approximately June through December 2015, and an extended period of $CO_2$ injection with variable injection rates from approximately December 2015 through March 2017.

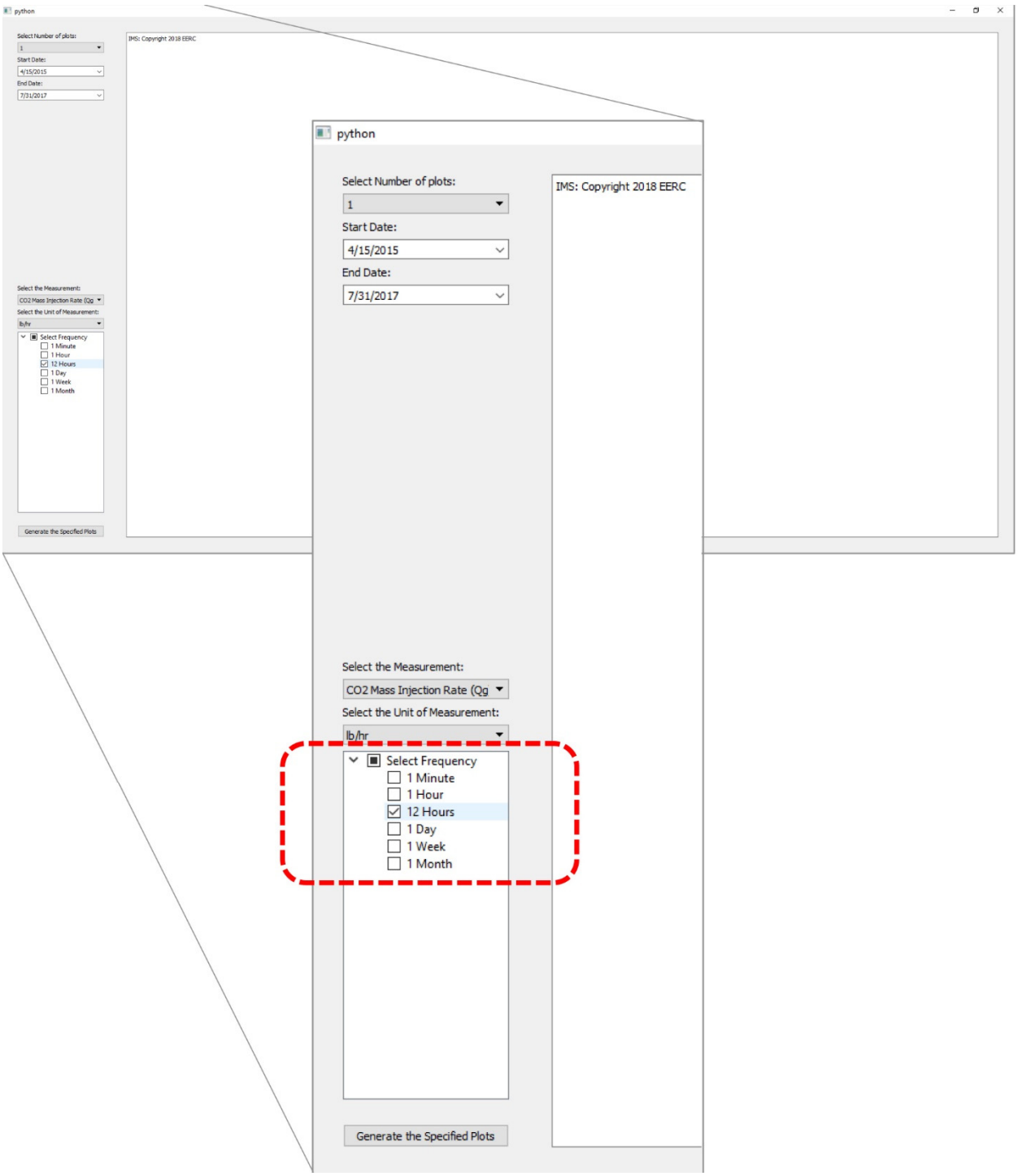


Figure 11. Illustration of the "Select Frequency" option in Module 1 showing the selection of "12 Hours."

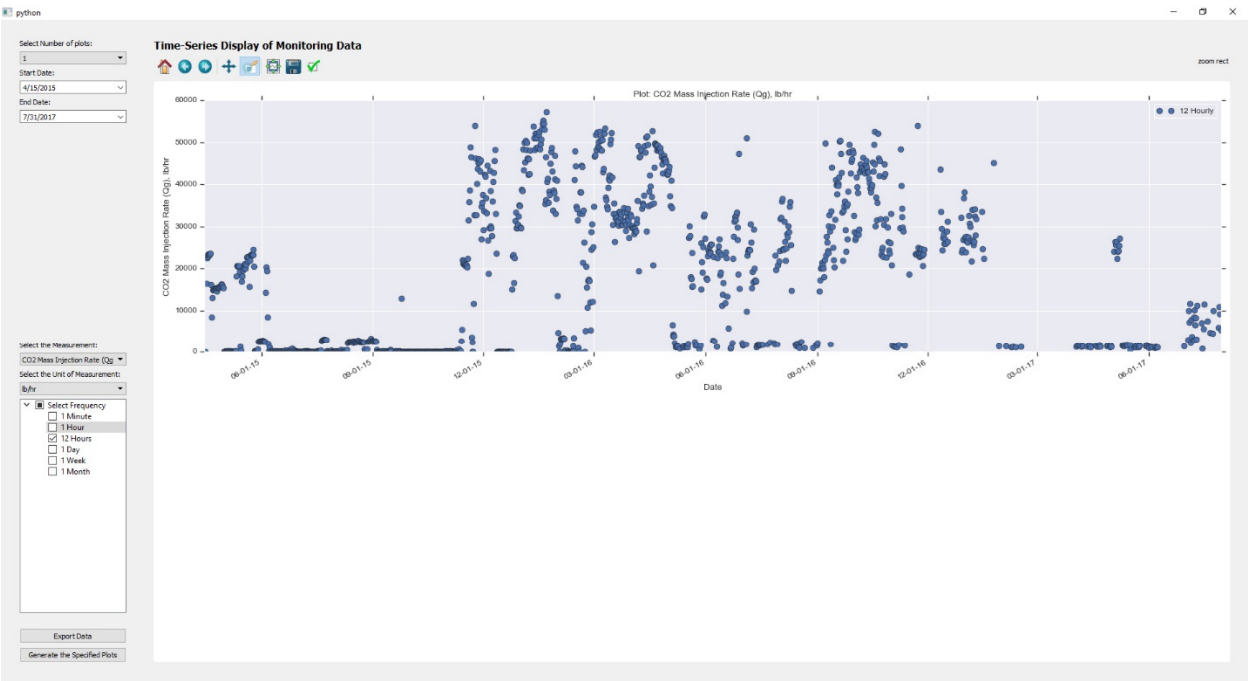


Figure 12. Module 1 single-plot option showing Qg versus time from April 15, 2015, to July 31, 2017, for a frequency period of 12 hours.

The initial plot will display default x- and y-axis labels, symbols, and scales. The user may modify these features by using the formatting tools at the top of the module page. These tools include the following features and are consistent across all IMS modules (Figure 13):

- ***Home*** – resets the plot to the original (default) view
- ***Left arrow*** – goes back to the previous view
- ***Right arrow*** – scrolls forward to the next view
- ***Pan/Zoom*** – allows the user to either pan (move up/down or left/right) within the plot or zoom to a specific portion of the plot using the mouse
- ***Zoom to rectangle*** – allows the user to draw a rectangle over the plot and zoom the image within that rectangle
- ***Configure subplots*** – allows the user to modify the spacing of the plot layout, for example, the width of the top, bottom, left, and right borders
- ***Save*** – allows the user to save the plot as one of several image file types
- ***Edit*** – allows the user to edit symbols, lines, and axes to tailor the plot to specific needs

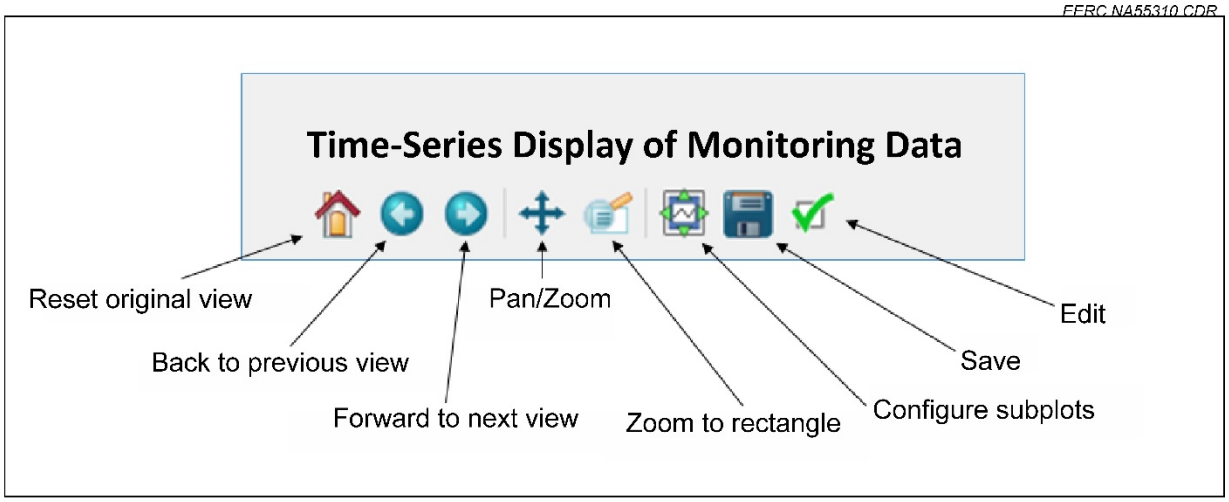


Figure 13. Description of the formatting tools available in Module 1 and all subsequent modules.

***Double-Plot Option***

Selecting the double-plot option (Select Number of plots = 2) allows the user to plot two measurements versus time in two separate panels. The process is essentially the same as the one described above for the single-plot option – the user must select a date range, measurement, unit of measurement, and frequency. However, the user must make these selections for both measurements, completing them in sequence for one measurement and then again for the second measurement. The final step is to click the "Generate the Specified Plots" button in the lower left-hand corner of Module 1, which will retrieve the data from the IMS Database and generate the two specified plots. The user may also select multiple frequencies (e.g., 1 hour and 1 day), which will overlay both frequencies on the same plot for a given measurement. In addition, the user may plot one frequency for the top plot and a different frequency for the bottom plot.

Figure 14 shows an example of the double-plot option with Qg in the top panel and BHT in the bottom panel for the date range from April 15, 2015, to July 31, 2017, and a frequency of 12 hours. This double-plot option provides information to the user about the relationship between these two variables. For example, periods with increasing Qg are associated with decreasing BHT. Conversely, periods of no significant $CO_2$ injection correspond with either flat (horizontal) or increasing BHT as the wellbore returns toward the geothermal baseline of approximately 234°F.

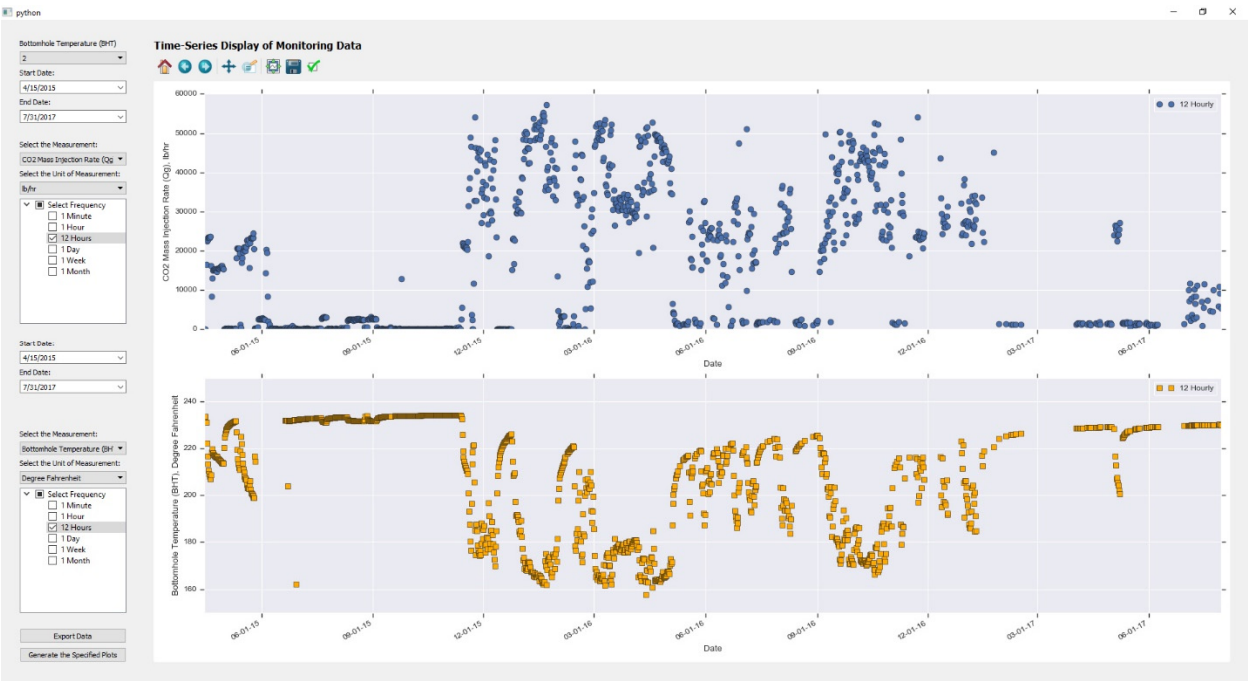


Figure 14. Module 1 double-plot option showing Qg (top panel) and BHT (bottom panel) versus time.

### *Multiple-Axis Plot Option*

While the double-plot option allows the user to compare relationships between two measurements, plotting these measurements in two separate panels can make directly comparing these measurements challenging. In addition, the user may want to compare more than two measurements along the same time-series. The multiple-axis plot option (select number of plots = multiple axes) allows the user to plot up to three different measurements onto a single graph, with one measurement plotted on the primary (left-hand) y-axis and up to two measurements plotted on the secondary (right-hand) y-axis. The multiple-axis option, therefore, allows the user to more effectively examine relationships among three different measurements over the same time-series.

Figure 15 shows an example of the multiple-axis plot option with Qg plotted on the primary y-axis and BHT and BHP plotted on the secondary y-axes for the date range from April 15, 2015, to July 31, 2017. This multiple-axis display shows the decreasing BHT with increasing Qg (similar to the double-plot option example) and also the increasing BHP with increasing Qg. For example, beginning around December 24, 2015, the black dotted line (Qg) increases from zero to over 50,000 lb/hr, while the blue dashed line (BHT) decreases from a baseline of 234° to nearly 160°F. Conversely, the gold dashed line (BHP) increases from a baseline value of approximately 4940 psi to a maximum value of nearly 6000 psi during this period. Plots like these can help the user to explore different combinations of measurements and assess whether the changes in measurement values in response to $CO_2$ injection are consistent with past and/or expected performance trends.


Figure 15. Module 1 multiple-axis plot option showing Qg, BHT, and BHP versus time.

### Module 2 – DTS Measurements

Unlike WHT, WHP, BHT, BHP, and ANP, which provide time-series measurements at one discrete location in the injection well (one-dimensional data with time), the DTS acquires temperature measurements from 33 discrete temperature sensors located along the length of the 4.5-inch tubing within the injection wellbore, which provides a time-series temperature profile of the injection well (two-dimensional data with time). Module 2 provides the user with two different options for displaying these DTS temperature measurements: DTS temperature profiles (Module 2A – temperature versus depth at a given time) and DTS time-series temperature or temperature gradient heat maps (temperature versus time and depth, Module 2B).

#### *Module 2A – DTS Profiles*

The DTS temperature profile is a plot of temperature on the x-axis and sensor depth on the y-axis. As described in Azzolina and others (2018), when there is no $CO_2$ injection occurring at the Storage Site, the DTS temperature profile at the injection well slowly returns to the local geothermal gradient, which was determined to follow a quadratic (second-order polynomial) of the form:

$$T_{\mathrm{DTS}} = 48.1 - 0.02699Z - 0.00000087Z^2 \qquad \text{[Eq. 1]}$$

Where:

$T_{\mathrm{DTS}}$ = temperature measurement within the DTS temperature profile (°F)

$Z$ = depth below ground surface (feet), where 0 is surface and −10,203 feet is the depth of the base of the injection well

In response to $CO_2$ injection, the DTS temperature profile changes, as several factors will influence the temperature along the wellbore. These factors primarily include 1) the temperature of the $CO_2$ at the time of injection; 2) the thermal properties of the wellbore casing, cement, and surrounding rock and formation fluids; 3) the thermal properties of the injected $CO_2$; 4) the Qg; and 5) the number of consecutive days of $CO_2$ injection (Ramey, 1962).

Module 2A allows the user to evaluate the daily average DTS temperature profile over a date range to assess the change in this profile from baseline conditions (i.e., no $CO_2$ injection). To launch Module 2A, the user clicks on the "2A) DTS Profiles" button from the Module Selection Window (Figure 6). This will launch Module 2A and open the default page (Figure 16).

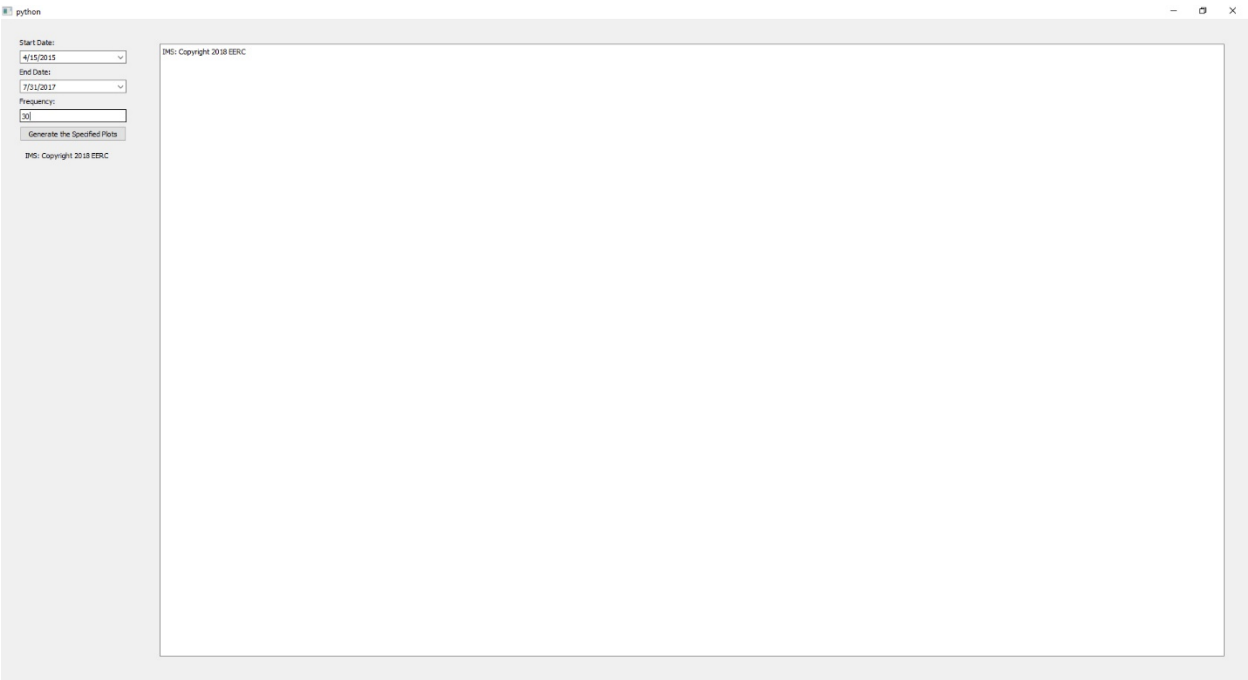


Figure 16. Default page for Module 2A – DTS Profiles.

Similar to Module 1, the user must select a Start Date and End Date to define the date range for the plot. A calendar feature, identical to that in Module 1 (see Figure 8), has been incorporated into Module 2A, which allows the user to select a Start Date or End Date using a monthly calendar.

The third input required from the user is "Frequency." Since the DTS is collecting 33 measurements along the length of the injection well, plotting the DTS temperature profile over a date range quickly results in a crowded plot that is difficult to interpret. Therefore, Module 2A allows the user to select a frequency, which is the number of days between measurements. For example, if the user selects the entire available date range (Start Date = April 15, 2015, and End

Date = July 31, 2017) and a frequency of "30," then Module 2A will return the daily average value for every 30th record from the IMS Database (every 30th calendar day) from the Start Date to the End Date, as illustrated in Figure 17. For example, if the user selects a Start Date of December 1, 2015, and an End Date of March 1, 2016, and a frequency of "30," then Module 2 will return the daily average temperature profile for December 1, 2015, December 30, 2015, January 29, 2016, and February 28, 2016. Selecting a longer date range and larger Frequency allows the user to assess the long-term, average conditions of the DTS temperature profile.

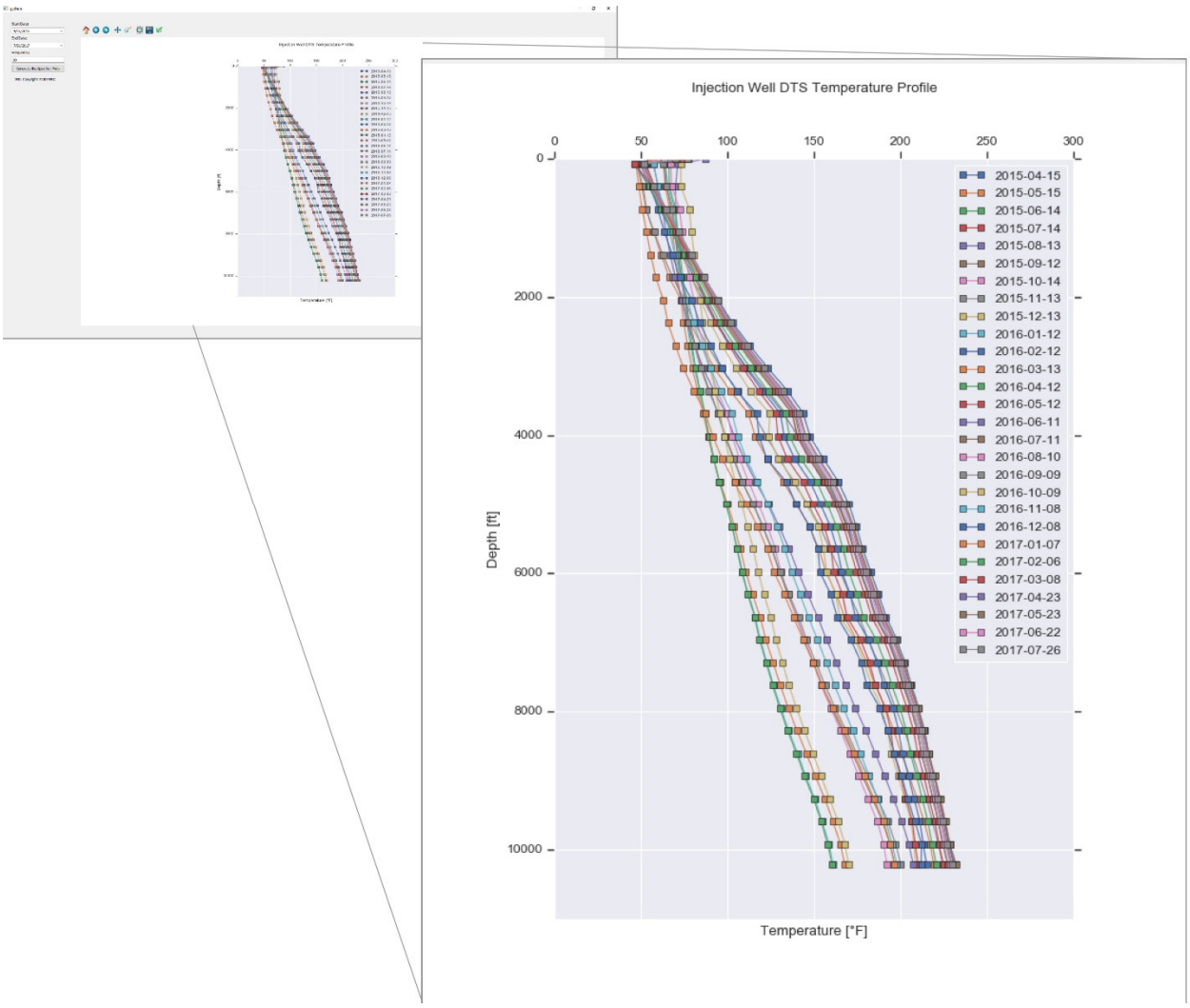


Figure 17. Module 2A plot showing the full date range (April 15, 2015, to July 31, 2017) and frequency = 30.

Alternatively, the user may want to investigate a narrower date range and select a smaller frequency, which provides information about the DTS temperature profile within a specific period of operation. For example, Figure 18 illustrates a scenario where the user has selected a period just prior to $CO_2$ injection (Start Date = December 24, 2015) up to a period where $CO_2$ injection

temporarily ceases (End Date = January 10, 2016) and a frequency of "1," which returns the daily average DTS temperature profile (i.e., the average of 1440 measurements for each DTS sensor) for each day within the selected date range. The dark blue colored line in Figure 18 is the DTS temperature profile for December 24, 2015, which shows the baseline condition (no $CO_2$ injection); subsequent days show the decrease in the DTS temperature profile in response to $CO_2$ injection and recovery towards baseline after $CO_2$ injection ceased.

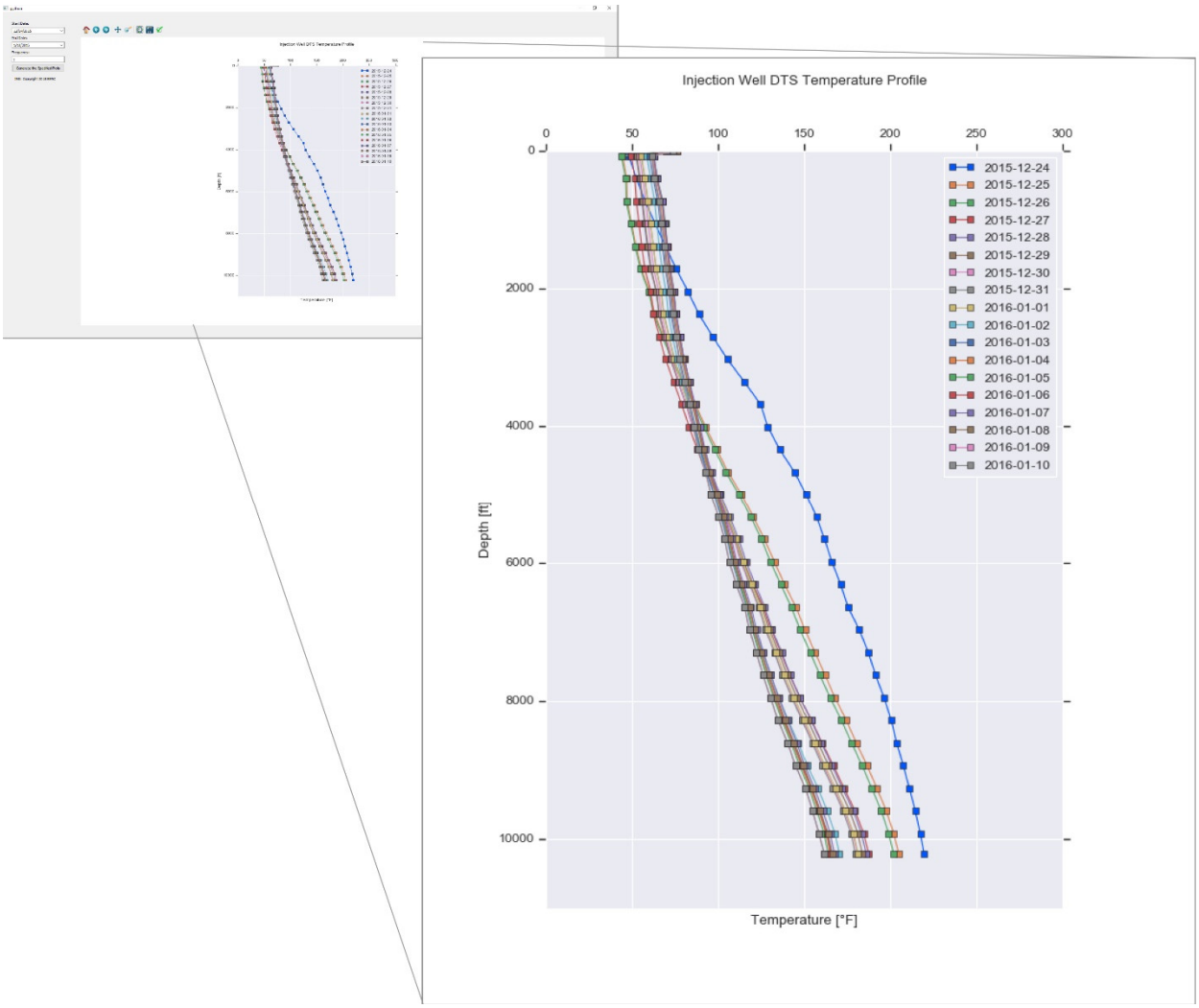


Figure 18. Module 2A plot showing data from December 24, 2015, to January 10, 2016, and frequency = 1; i.e., an average DTS temperature profile for each sensor located along the length of the injection well is determined for each day within the selected date range.

### *Module 2B – DTS Time-Series*

Module 2B allows the user to evaluate the daily average DTS temperature or temperature gradient as a function of both depth and time. To launch Module 2B, the user clicks on the "2B) DTS Time-Series" button from the Module Selection Window (Figure 6). This will launch Module 2B and open the default page (Figure 19).

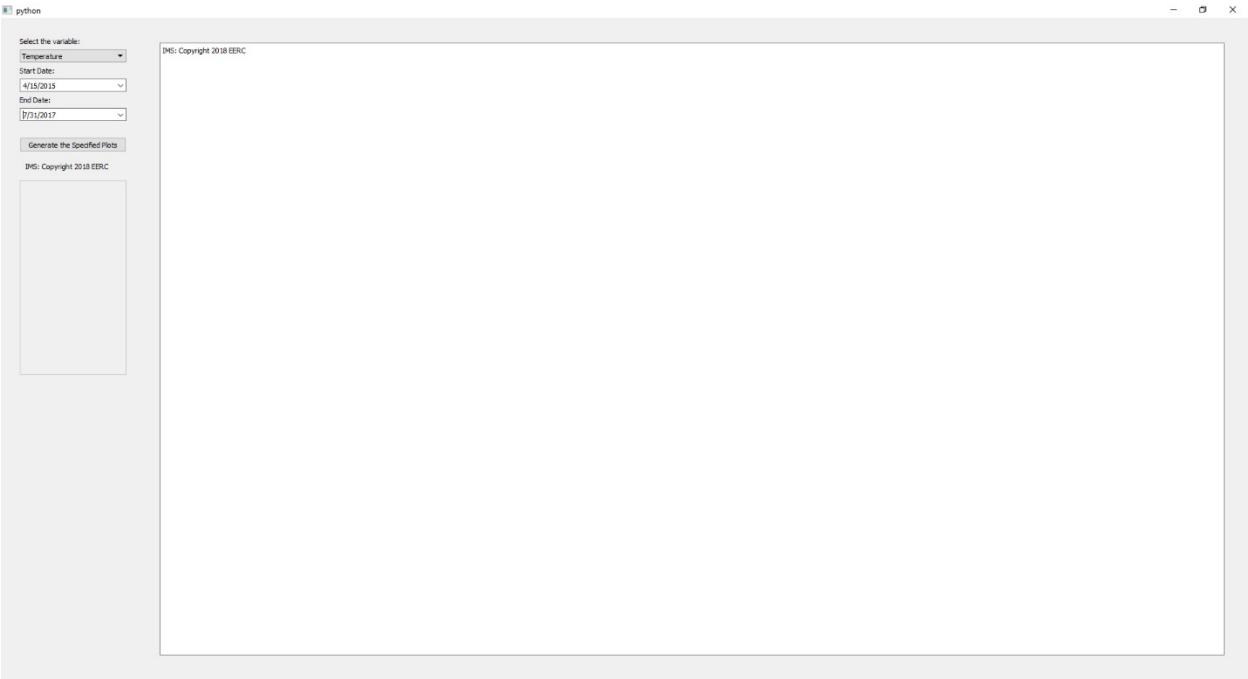


Figure 19. Default page for Module 2B – DTS Time-Series.

Similar to Module 2A, the user must select a Start Date and End Date to define the date range for the plot. As such, a calendar feature has been incorporated into Module 2B identical to that which was incorporated into Module 1 (see Figure 8), which allows the user to select a Start Date or End Date using a monthly calendar.

Next, the user must select either "Temperature" or "Temperature Gradient" from the dropdown menu, "Select the Variable," in the upper left-hand corner of Module 2B. The final step is to click the "Generate the Specified Plots" button, which will retrieve the data from the IMS Database and generate the plot.

Plotting temperature versus time in Module 2B shows the changing temperature profile of the injection well in response to the injection of $CO_2$ or, conversely, recovery of the injection well temperature profile following the cessation of $CO_2$ injection. For example, Figure 20 shows the DTS temperature from December 10, 2015, through February 6, 2016. Module 2B uses a heat map (color ramp), with blue shading for cooler temperature and red shading for warmer temperature. As shown in the figure, when there is no or little $CO_2$ injection (the period from December 12 to

December 24, 2015), the DTS temperature profile reflects the baseline temperature profile, with increasing temperatures below approximately 3000 feet attributable to the geothermal gradient at the Storage Site. However, in response to $CO_2$ injection (the period from December 24, 2015, through January 31, 2016), the DTS temperature profile decreases, with cooler temperatures measured along the length of the injection well throughout that period (a greater proportion of blue shading). Variability in the color shading over the period of $CO_2$ injection is caused by variability in the $CO_2$ mass injection rate. Also shown in Figure 20, the DTS temperature profile returns to the baseline temperature profile following the cessation of $CO_2$ injection at the end of January 2016.

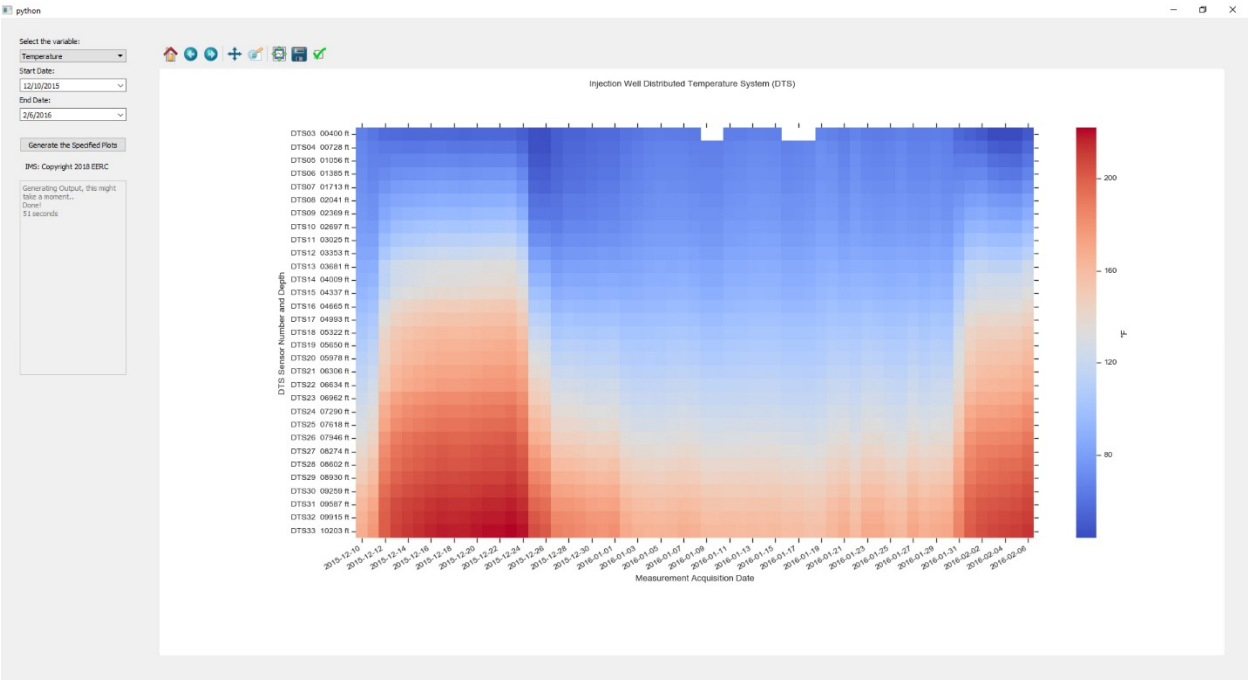


Figure 20. Module 2B plot showing DTS temperature data from December 10, 2015, to February 6, 2016.

The DTS temperature gradient refers to the difference in temperature between sensors divided by the distance between sensors. For example, if the temperatures measured at sensors 02 and 03 were 53° and 57°F, respectively, and these sensors were separated by a distance of 328 feet, then the temperature gradient between these two sensors was 0.012°F/ft ([57° – 53°F]/ 328 ft). Plotting temperature gradient versus time in Module 2B shows the changing temperature gradient of the injection well in response to the injection of $CO_2$ or, conversely, return of the injection well temperature gradient when $CO_2$ injection ceases. Figure 21 shows the same date range as the previous figure but now displays the temperature gradient. Module 2B again uses a heat map, shading smaller temperature gradients in blue and larger temperature gradients in red. As shown in the figure, when there is no or little $CO_2$ injection (the period from December 12 to December 24, 2015), the DTS temperature gradient reflects the baseline temperature gradient, with

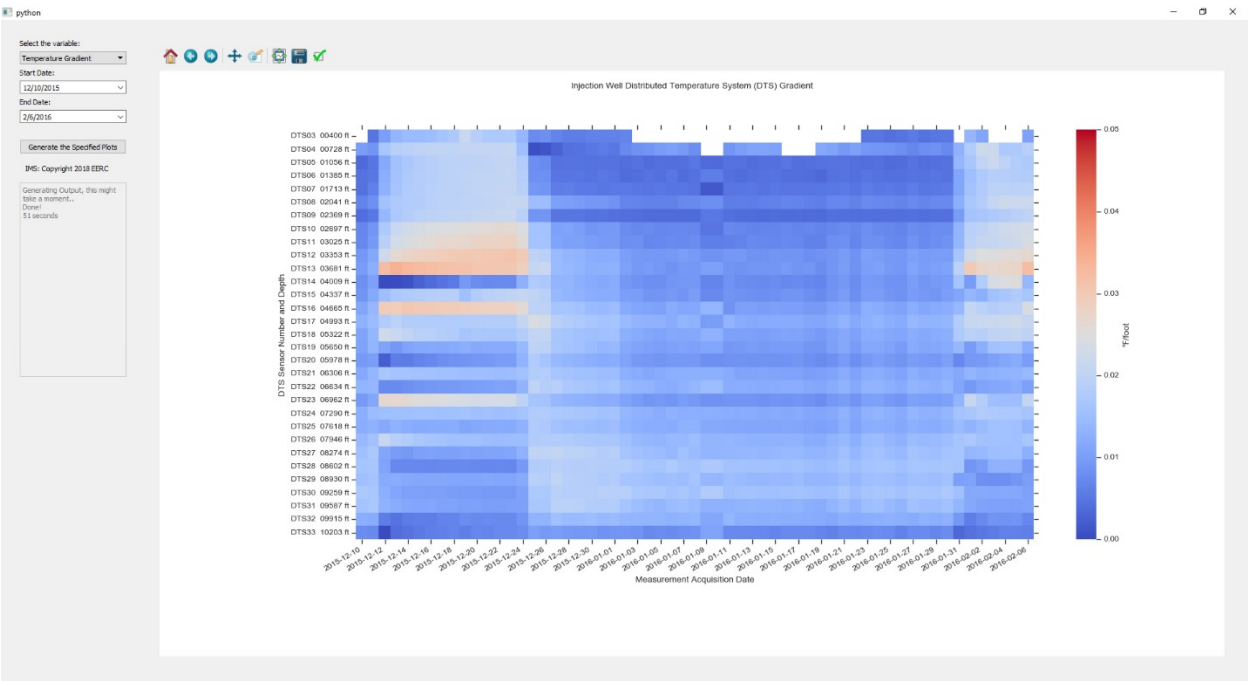


Figure 21. Module 2B plot showing DTS temperature gradient data from December 10, 2015, to February 6, 2016.

a zone of higher gradient from approximately 2697 to 3681 ft. However, in response to $CO_2$ injection (the period from December 24, 2015, through January 31, 2016), the DTS temperature gradient becomes more uniform, as the wellbore is shaded almost entirely blue (i.e., a temperature gradient generally less than 0.02°F/ft). Plotting temperature gradient, as opposed to temperature, may offer a more localized indication of unusual temperature changes suggestive of a loss in wellbore integrity at that depth.

### Module 3 – BHT and BHP Analysis

As previously described, Modules 1 and 2 provide the user with real-time measurement results for wellhead/bottomhole pressure and temperature or DTS measurements, respectively. These modules correspond to Path 1 in the IMS Data Workflow – raw data reported from the Storage Site to the EERC and subsequently retrieved from the IMS Database to the IMS GUI. However, Modules 1 and 2 minimally process the measurements, and the responsibility is on the IMS user to interpret the information and make decisions about whether the measurement values and trends are consistent with normal operating limits. Modules 3 and 4, which represent Path 2 in the IMS Data Workflow, are different in that the measurements are processed through a set of algorithms to compare new measurements against a set of action levels for the purpose of assessing whether the Storage Site is or is not operating within normal limits. Module 3 provides action levels for BHT and BHP measurements and is discussed in the remainder of this section; Module 4 provides a basis for decision-making about the DTS temperature profile measurements and is discussed in the next section.

The goal of Module 3 is to evaluate whether the measured BHT and/or BHP are within normal operating limits using action levels that were developed given a set of operating conditions. New measurements of either BHT or BHP that are beyond these action levels may indicate subsurface conditions that are outside of normal operating limits. The remainder of this section describes the individual components of Module 3. Appendix C provides a more detailed discussion of the statistical methods used to derive the action levels for these continuous measurements.

### *BHT Analysis*

#### *BHT Response to $CO_2$ Injection*

The IMS uses data from the casing-conveyed BHT gauge located at 10,374 ft. When there is no $CO_2$ injection occurring at the Storage Site, the measured BHT in the injection well is approximately 234°F, consistent with the formation-specific geothermal gradient. For example, Figure 22 shows time-series plots of BHP, BHT, and Qg for the period from April 15, 2015, through July 31, 2017. The period from approximately June 21, 2015, through November 12, 2015, represents a period with little to no $CO_2$ injection, as Qg was at or near zero over this time. Consequently, the measured BHT during this period shows a horizontal line of nearly constant BHT of 234°F (Period A, middle panel of Figure 22). However, in response to $CO_2$ injection, BHT decreases from this baseline value. The intermittent $CO_2$ injection, in which both Qg and the number of days of $CO_2$ injection vary, results in a sawtooth pattern in BHT corresponding to oscillating periods of $CO_2$ injection and shut-in (Period B, middle panel of Figure 22). Finally, after $CO_2$ injection ceases on January 24, 2017, BHT increases toward the preinjection temperature of 234°F (Period C, middle panel of Figure 22).

#### *Action Levels for BHT*

The BHT algorithms in Module 3 provide a prediction of BHT given a set of operating conditions using injection and monitoring data acquired from the injection well during the period from April 15, 2015, through July 31, 2017. Lower-than-expected BHT measurements could indicate that the $CO_2$ mass injection rate, as measured at an injection meter building prior to the $CO_2$ being injected into the subsurface, is not reaching the bottom of the wellbore and, therefore, not lowering BHT as predicted. This result could indicate a loss of $CO_2$ from the injection well. Therefore, the goal of the BHT algorithms was to derive threshold BHT values that define an expected range for normal operating limits such that new BHT measurements outside of this expected range would indicate to the IMS user that they should either investigate further or implement an operational response. These threshold values are referred to as “action levels” because they provide a decision framework to the IMS user about whether or not additional actions are needed given the monitoring result.

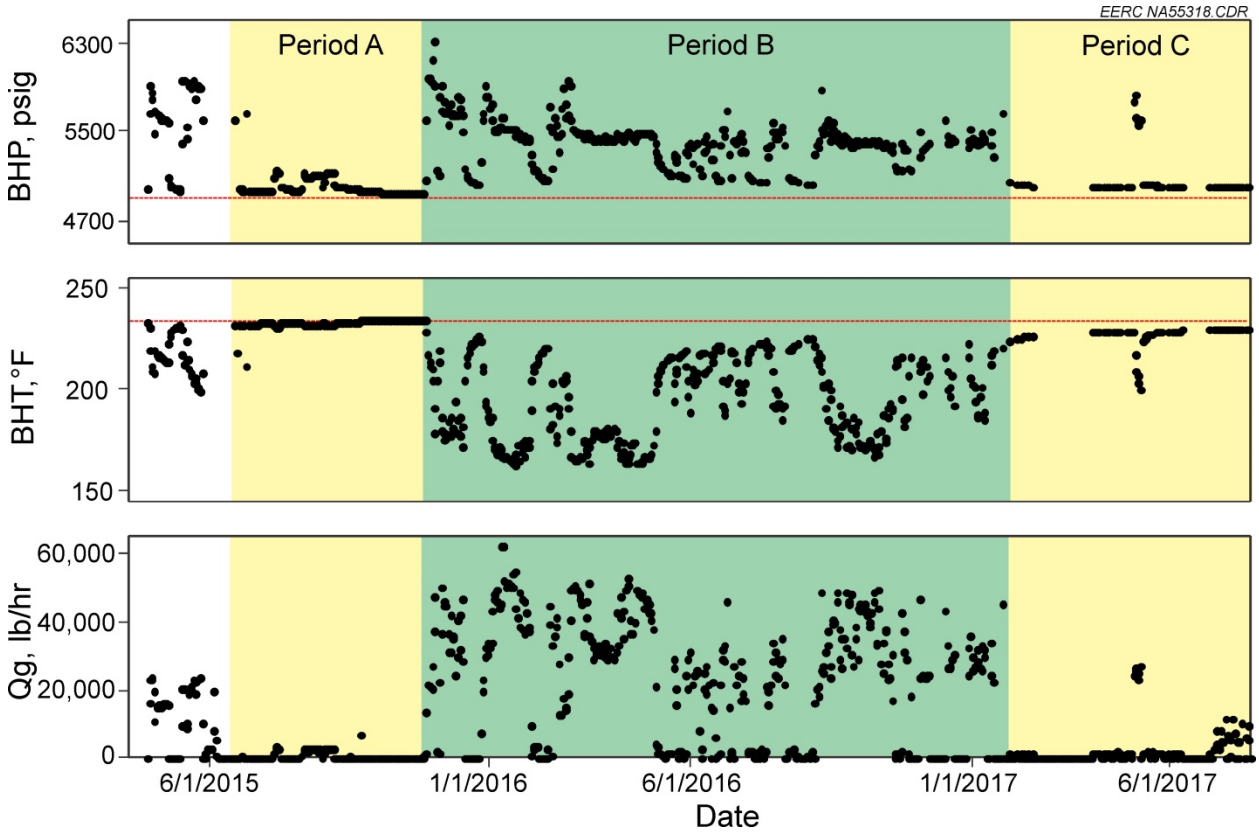


Figure 22. Time-series plots of BHP (top), BHT (middle), and Qg (bottom) from the period beginning April 15, 2015, and ending July 31, 2017. Periods A and C (yellow highlights) show periods of no significant $CO_2$ injection, while Period B (green highlight) corresponds to oscillating periods of $CO_2$ injection and shut-in. The horizontal lines in the top and middle panels reflect the hydrostatic pressure gradient of 4940 psi and static geothermal gradient of 234°F, respectively.

As described in Azzolina and others (2018), the development of BHT action levels explored two different BHT prediction models: one based on heat transfer between the wellbore and surrounding rock and formation fluids (physical model) and one based on empirical correlations between Qg and BHT (empirical model). While the empirical model ignores time dependency and heat transfer, comparison of the two approaches showed that the empirical model was simpler to implement and more robust (i.e., less dependent upon input assumptions) and provided comparable or better sensitivity to detecting change from normal operating conditions than the physical model. Thus the empirical model was selected for calculating action levels for BHT in Module 3.

The empirically derived action levels for BHT were generated using linear regression to estimate an expected value and prediction intervals as a function of Qg (Appendix C). This technique was used to define two action levels: Action Level 1 and Action Level 2. Action Level 1 represents a 2% false-positive rate, and Action Level 2 represents a 1% false-positive rate. Stated differently, fewer than 2% of the BHT measurements acquired from April 15, 2015, through July 31, 2017, plot outside Action Level 1, and fewer than 1% of the BHT measurements acquired

over the same time span plot outside Action Level 2. Thus new BHT measurements (acquired after July 31, 2017) that plot outside of these action levels indicate BHT conditions that do not frequently occur, which may indicate BHT conditions that exceed the normal operating limits observed during the first 2 years of operation at the Storage Site. The fact that one or more BHT measurements occurs outside the action levels does not necessarily mean that there is an operational problem; however, this result does alert the IMS user to the fact that the system is responding differently than the operations up to that point, and further investigation may be warranted.

*BHT Component of Module 3*

To launch Module 3, the user clicks on the "3) BHT and BHP Analysis" button from the Module Selection Window (Figure 6). This will launch Module 3 and open the default page (Figure 23).

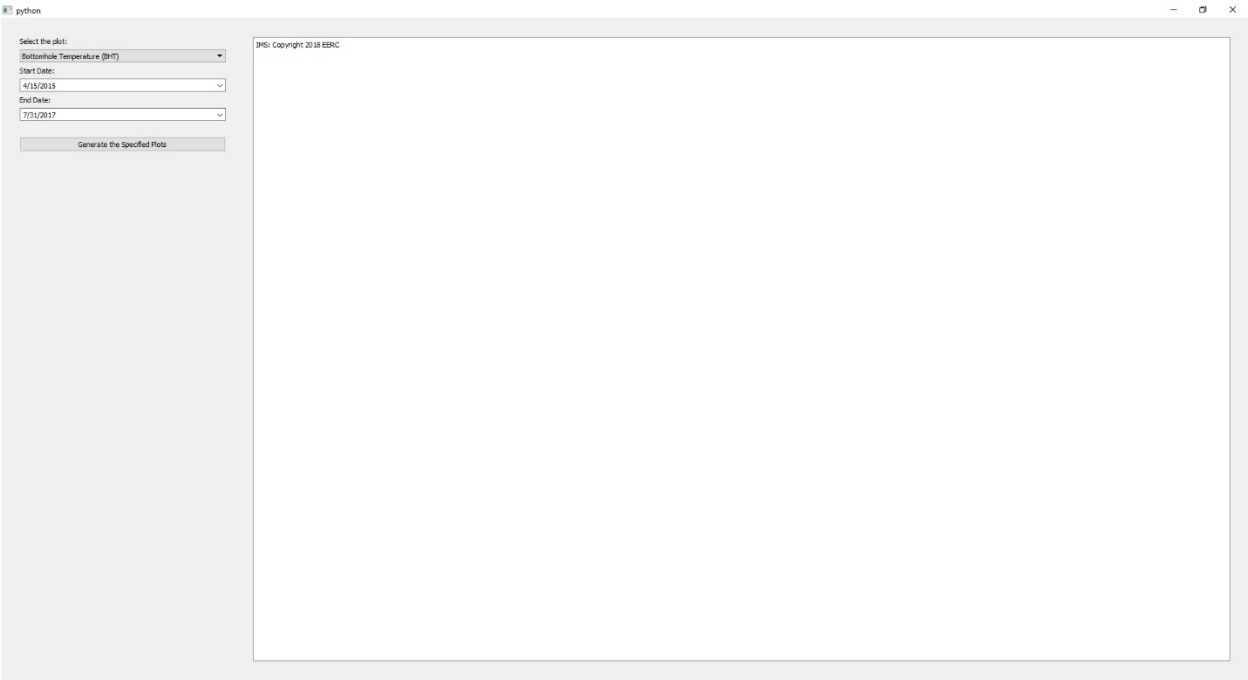


Figure 23. Default page for Module 3 – BHT and BHP Analysis.

The user can then select "Bottomhole Temperature (BHT)" from the dropdown menu in the upper left-hand corner of Module 3. Similar to Module 1, the default date range is currently set to a Start Date of April 15, 2015 (the beginning of $CO_2$ injection) and an End Date of July 31, 2017 (the last valid date in the IMS Database). However, the user may select any date range within this period by modifying the Start Date and End Date. As with the other modules, a calendar feature has been incorporated into Module 3, which allows the user to select a Start Date or End Date using a monthly calendar. Lastly, the user must select "Generate the Specified Plots," which will retrieve the BHT measurements from the IMS Database, calculate the daily average BHT values,

and plot them onto the template of Qg versus BHT action levels. Figure 24 shows the output from Module 3 for the "Bottomhole Temperature (BHT)" and the date range from April 15, 2015, through July 31, 2017. The default template will plot the BHT measurements (black circles), expected value from the regression (green line), Action Level 1 (blue dashed lines), and Action Level 2 (red dotted lines). As shown in the figure and noted above, few measurements plot beyond the action levels. As $CO_2$ injection continues at the Storage Site, additional BHT measurements should plot within these action levels. New BHT measurements that plot outside of these action levels indicate BHT conditions that do not frequently occur, which may indicate BHT conditions that exceed normal operating limits and could trigger an operational response from the IMS user.

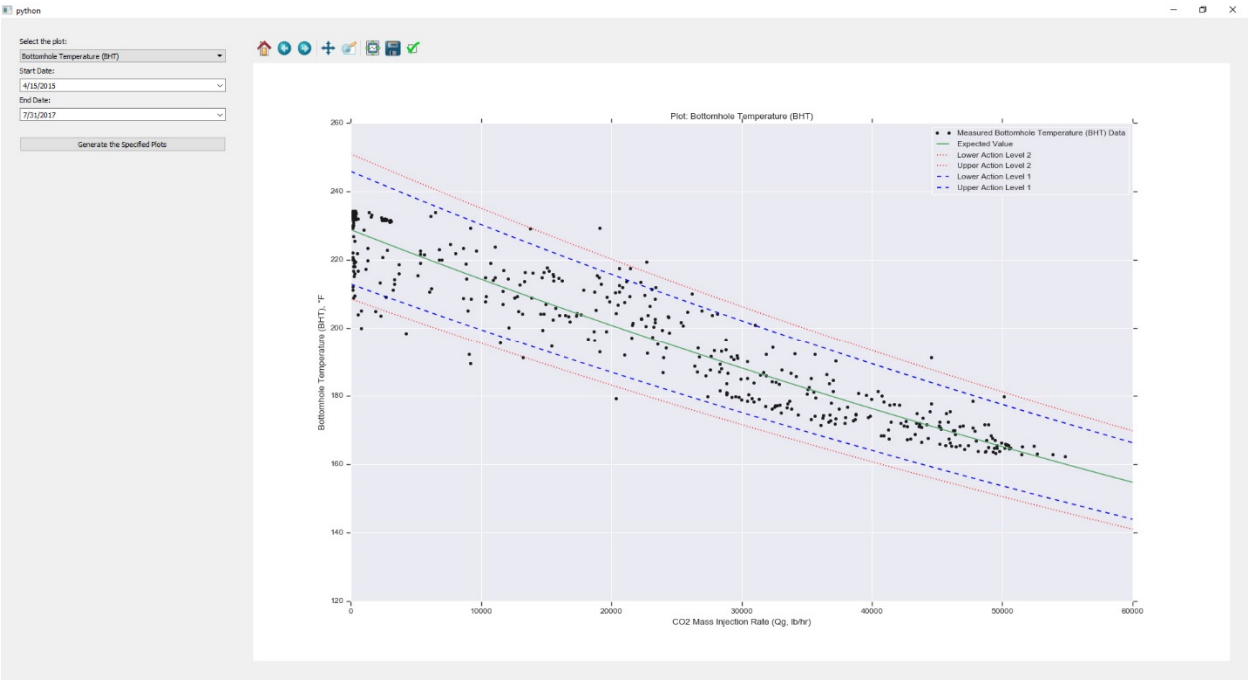


Figure 24. Module 3 crossplot of Qg (x-axis, lb/hr) versus BHT (y-axis, °F) for the date range from April 15, 2015, through July 31, 2017, showing the BHT measurements (black circles), expected value (green line), Action Level 1 (blue dashed lines), and Action Level 2 (red dotted lines).

### *BHP Analysis*

#### *BHP Response to $CO_2$ Injection*

The IMS utilizes BHP measurements acquired at the casing-conveyed pressure gauge located at 10,374 feet in the injection well. Similar to the measurements of BHT, when there is no $CO_2$ injection occurring at the Storage Site, the measured BHP in the $CO_2$ injection well has returned to a value near the initial pore pressure, which is approximately 4940 psig. For example, as previously shown in Figure 22, during the period from June 21, 2015, through November 12, 2015, which represents a period with little-to-no $CO_2$ injection, the measured BHP during this

period shows a horizontal line at 4940 psig (Period A, top panel of Figure 22). However, in response to $CO_2$ injection, BHP increases from this baseline value, resulting in a sawtooth pattern in BHP that corresponds to oscillating periods of $CO_2$ injection of varying magnitude and duration, including shut-in (Period B, top panel of Figure 22). These sawtooth patterns in BHP in response to $CO_2$ injection are roughly the inverse of the patterns observed for BHT, which decreases in response to $CO_2$ injection. Finally, after $CO_2$ injection ceases on January 24, 2017, BHP begins to decrease and return to the preinjection baseline of 4940 psig (Period C, top panel of Figure 22).

*Action Levels for BHP*

Numerical modeling of $CO_2$ injection into a deep saline formation is well established in the literature, and commercial software packages such as Computer Modelling Group Ltd.'s (CMG's) GEM (Nghiem, 2002) are capable of modeling multiphase fluid flow like the $CO_2$-brine system at the Aquistore Storage Site (e.g., Gorecki and others, 2009; Pruess and others, 2003; Jiang and others, 2017). However, the IMS modules for BHP are designed for rapid calculations that do not rely on interfaces between the IMS Database and third-party software packages. Consequently, the IMS modules require analytical or semianalytical solutions for modeling BHP in response to $CO_2$ injection. While analytical solutions exist (e.g., Noh and others, 2007; Azizi and Cinar, 2013), the $CO_2$ injection characteristics of the Storage Site complicate using analytical models to estimate BHP. As previously described, the intermittent $CO_2$ injection causes nonconstant flow rates, temperature variations in the wellbore and near-wellbore formation, and history-dependent performance effects surrounding the wellbore. Existing analytical solutions cannot account for these types of characteristics and are, therefore, not appropriate for estimating BHP at this Storage Site.

However, in terms of providing information to the Storage Site operator to more efficiently monitor and manage $CO_2$ injection and subsurface conditions, predicting BHP is perhaps less important than knowing how the measured BHP relates to the normally expected injectivity regime of the target injection horizon at a given $CO_2$ injection rate. On this basis, the approach used to derive BHP action levels for the IMS integrates the relationships among Qg, BHT, and rock geomechanics to estimate the Qg that corresponds to the matrix- and/or fracture-flow regimes that may exist in the reservoir. The expected BHP response during $CO_2$ injection determined for the matrix- and fracture-flow regimes represent the BHP action levels of the IMS. Measured BHPs outside of the expected BHP response range at a given Qg inform the operator of a potential change in subsurface conditions resulting in a reservoir response outside normal operating limits. Appendix C provides a detailed discussion of the derivation of these matrix- and fracture-flow regimes and action levels for BHP.

The BHP component of Module 3 includes three regions for BHP: Zone I, Zone II, and Zone III (Figure 25). Zone 1 (blue region) represents the lower boundary of normal operating conditions for matrix or fracture flow. New BHP measurements plotting within Zone I could indicate either failure of the casing-conveyed pressure gauge or that the $CO_2$ injection has fractured the formation, resulting in no commensurate increase in BHP with increasing Qg. Zone II (green region) represents the normal operating conditions. New BHP measurements falling within this region are within the expected injectivity regime of either matrix or fracture flow. Lastly, Zone III (red

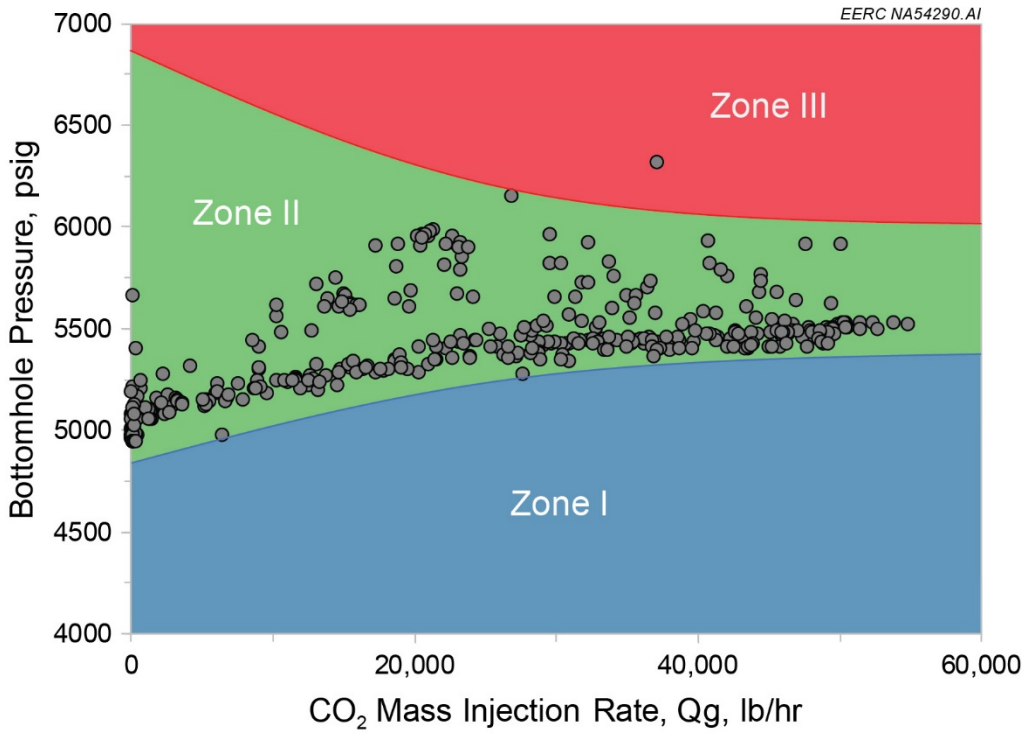


Figure 25. Crossplot of Qg vs. BHP illustrating the injection-dependent action levels for BHP.

region) represents a region of above-normal BHP. For example, new BHP measurements plotting in Zone III when Qg exceeds 40,000 lb/hr indicate that the injectivity is less than predicted, which could indicate potential problems with one or more of the four injection intervals. This decision-making framework forms the basis of the BHP component of Module 3.

*BHP Component of Module 3*

The user can launch the BHP component of Module 3 by selecting "Bottomhole Pressure (BHP)" from the dropdown menu in the upper left-hand corner of Module 3. Again, the user must provide a Start Date, End Date, and select "Generate the Specified Plots," which will retrieve the BHP measurements from the IMS Database, calculate the daily average BHP values, and plot them onto the template of Qg versus BHP action levels. Figure 26 shows the output from Module 3 for the "Bottomhole Pressure (BHP)" and the date range from April 15, 2015, through July 31, 2017. The default template will plot the BHP measurements (black circles), Zone I/II action level (blue dashed line), and Zone II/III action level (red dotted line). As shown in the figure, few measurements plot beyond the action levels. As $CO_2$ injection continues at the Storage Site, additional BHP measurements should plot within these action levels. New BHP measurements that plot outside of these action levels indicate BHP conditions that do not frequently occur, which may indicate BHT conditions that exceed normal operating limits and could trigger further investigation and/or an operational response from the IMS user. The fact that one or more BHP measurements occur in either Zone I or Zone III does not necessarily mean that there is an operational problem; however, this result does alert the IMS user to the fact that the system is responding differently than the operations up to that point and further investigation may be warranted.

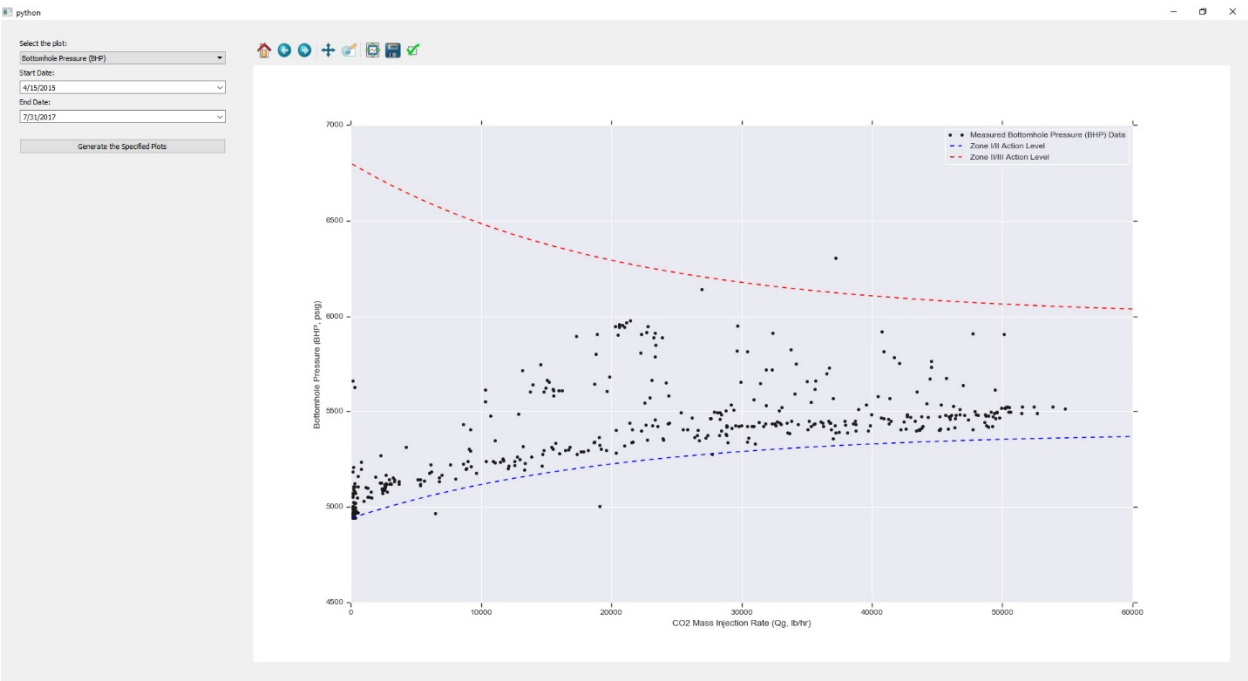


Figure 26. Module 3 crossplot of Qg (x-axis, lb/hr) versus BHP (y-axis, psig) for the date range from April 15, 2015, through July 31, 2017, showing the BHP measurements (black circles), Zone I/II action level (blue dashed line), and Zone II/III action level (red dotted line).

### *Combined BHT and BHP Option*

The last option within Module 3 is to generate a combined BHT and BHP plot, which generates two panels with BHT plotted in the top panel and BHP plotted in the bottom panel. The user can launch this option from Module 3 by selecting "Bottomhole Temperature (BHT) and Bottomhole Pressure (BHP)" from the dropdown menu in the upper left-hand corner of Module 3. Again, the user must provide a Start Date, End Date, and select "Generate the Specified Plots," which will retrieve the BHT and BHP measurements from the IMS Database, calculate the daily average BHT and BHP values, and plot these onto the templates of Qg versus BHT or BHP action levels. Figure 27 shows the output from Module 3 for the "Bottomhole Temperature (BHT) and Bottomhole Pressure (BHP)" and the date range from April 15, 2015, through July 31, 2017. The default formatting for the combined plot is the same as the default formatting previously described for each individual plot of BHT and BHP.

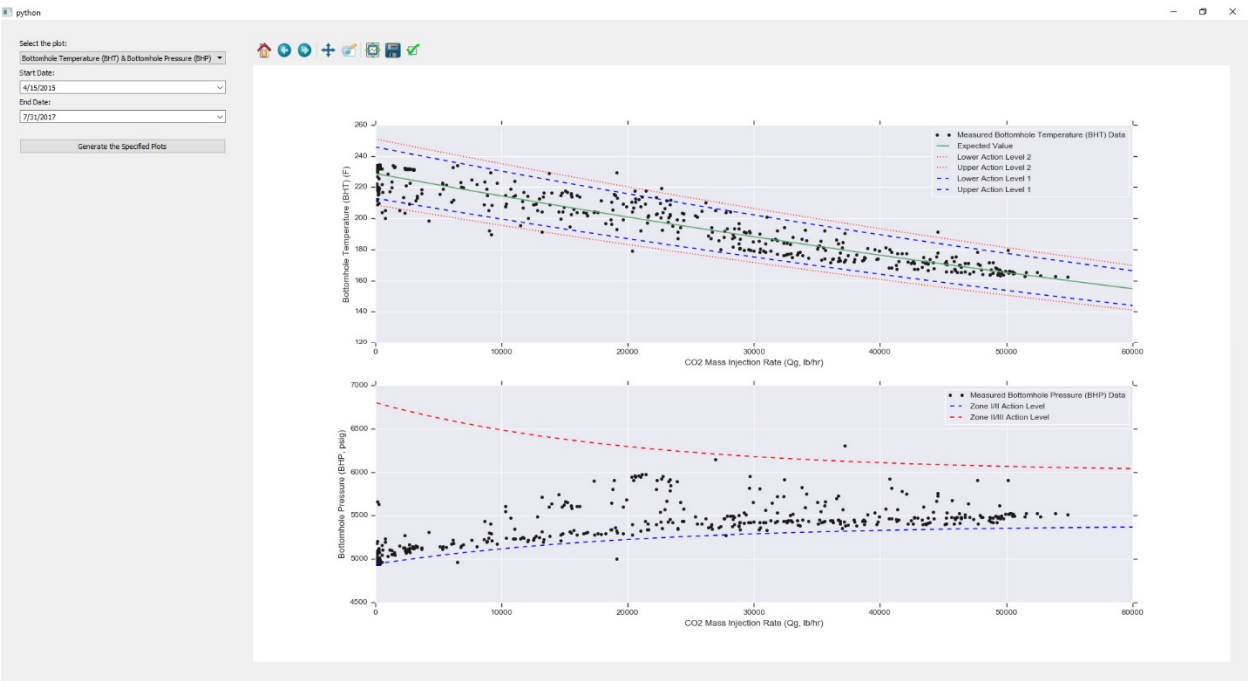


Figure 27. Module 3 crossplot of the combined BHT and BHP plot option showing Qg (x-axis, lb/hr) versus (top) BHT (y-axis, °F) or (bottom) BHP (y-axis, psig) for the date range from April 15, 2015, through July 31, 2017.

### Module 4 – DTS Analysis

A detailed comparison of DTS temperature profiles versus DTS temperature gradients showed that the profiles were less variable than the gradients and, therefore, provided better overall sensitivity for detecting change from normal operating conditions. As a result, Module 4 was developed to provide a basis for decision-making based only on the DTS temperature profile measurements and not temperature gradients. Whereas Module 2 allows the user to plot the DTS measurements as either profiles or time-series graphs, Module 4 incorporates action levels for the DTS temperature profile measurements, providing a decision-making framework for identifying new DTS measurements that are outside of normal operating limits.

#### *Effects of $CO_2$ Injection Rate and Duration on Wellbore Temperature Profiles*

As described in Azzolina and others (2018), the Storage Site receives intermittent $CO_2$ from SaskPower's Boundary Dam $CO_2$ capture facility, which results in periods with and without $CO_2$ injection. In addition, Qg varies as a function of the mass of $CO_2$ sent from the capture facility to the Storage Site. For example, for the period from April 15, 2015, through July 31, 2017, 33% of the days had no $CO_2$ injection. When $CO_2$ was injected, Qg was most frequently between 1000 and 50,000 lb/hr; however, there were days where Qg was less than or greater than this range (Figure 28). This variability in Qg affects the wellbore temperature profile response to $CO_2$ injection, as the heat transfer between the wellbore and the surrounding formation is affected by

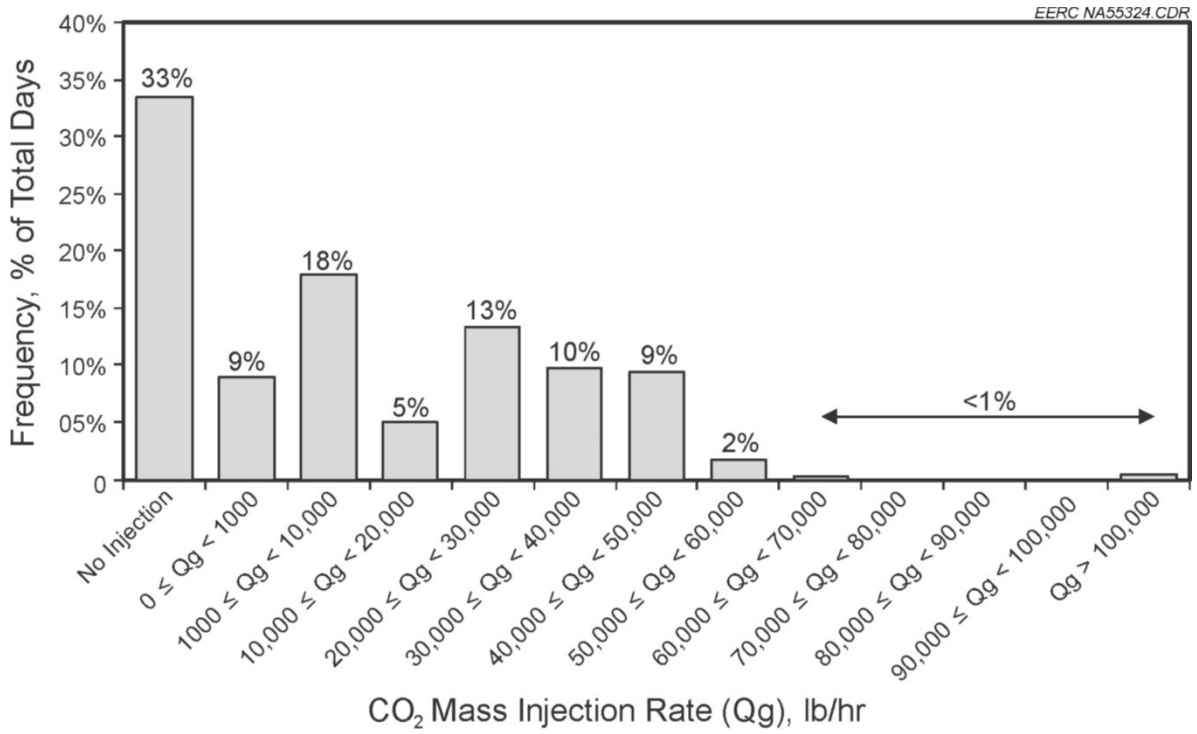


Figure 28. Histogram showing the frequency percentage (percent of the total number of days) of the Qg for the period from April 15, 2015, through July 31, 2017.

the average wellbore temperature and the enthalpy and specific heat of the wellbore fluids (McAdams, 1942; Ramey, 1962; Willhite, 1967; Wu and Pruess, 1990). Thus decision-making based upon whether the DTS temperature profile response is or is not within normal operating limits must account for the variability in Qg.

In addition to the variability in Qg, the intermittent injection of $CO_2$ results in different periods of injection duration (i.e., different lengths of consecutive days of injection), including periods with no $CO_2$ injection where the wellbore temperature profile rebounds toward the baseline geothermal gradient. For example, again for the period from April 15, 2015, through July 31, 2017: 1) there were only five periods with an injection duration of more than 20 consecutive days, with the longest period of continuous $CO_2$ injection consisting of 89 consecutive days and 2) there were five periods with more than ten consecutive days with no $CO_2$ injection, with the longest period of no $CO_2$ injection of 44 consecutive days.

These changes in the injection duration also affect the wellbore temperature profile response to $CO_2$ injection. Heat losses between the wellbore and the formations are large initially but decrease with time as thermal resistance to the flow of heat builds up in the formation (Ramey, 1962; Willhite, 1967). Consequently, decision-making based on whether the DTS temperature profile response is or is not within normal operating limits must also account for the variability in injection duration.

Module 4 addresses the combination of the effects of variability in Qg and injection duration on the DTS temperature profile by defining three groups of conditions and then providing action levels that are group-specific. Investigation into the sensitivity of the DTS temperature profile to the injection duration showed that the wellbore reached its minimum temperature profile relatively rapidly (in less than 5 days) and that Qg played a more significant role in determining the DTS temperature profile than the injection duration. An assessment of the combined effects of Qg and the injection duration resulted in the use of the following three combinations for the derivation of action levels for the DTS temperature profile measurements in the injection well:

- **Group A:** Qg < 10,000 lb/hr and consecutive days < 5
- **Group B:** Qg < 10,000 lb/hr and consecutive days ≥ 5
- **Group C:** Qg ≥ 10,000 lb/hr

These three combinations of Qg and/or injection duration provided optimum sensitivity for detecting changes from normal operating conditions. Further parsing of the DTS measurement record into more groups resulted in fewer measurements in each group and commensurately wider action intervals (i.e., more uncertainty and, therefore, less sensitivity for detecting change).

Figure 29 shows the DTS temperature profiles for the injection well grouped according to the three combinations of Qg and consecutive days of $CO_2$ injection. Module 4 uses percentiles for each of the 33 DTS sensors to define action levels for the three groups. The DTS temperature profile of the injection well in response to $CO_2$ injection does not result in a linear function with depth, nor a quadratic or simple nonlinear function. Consequently, regression techniques were not used to derive action levels as a function of depth. Instead, pointwise intervals were derived for each DTS sensor depth. These percentiles were set to provide a 2% action level (Action Level 1) and a 1% action level (Action Level 2). There is less than 2% or 1% probability that a new DTS measurement would fall below Action Levels 1 or 2, respectively, under normal operating conditions. These action levels were incorporated into Module 4 to provide the user with a visual assessment tool for the DTS temperature profile measurements.

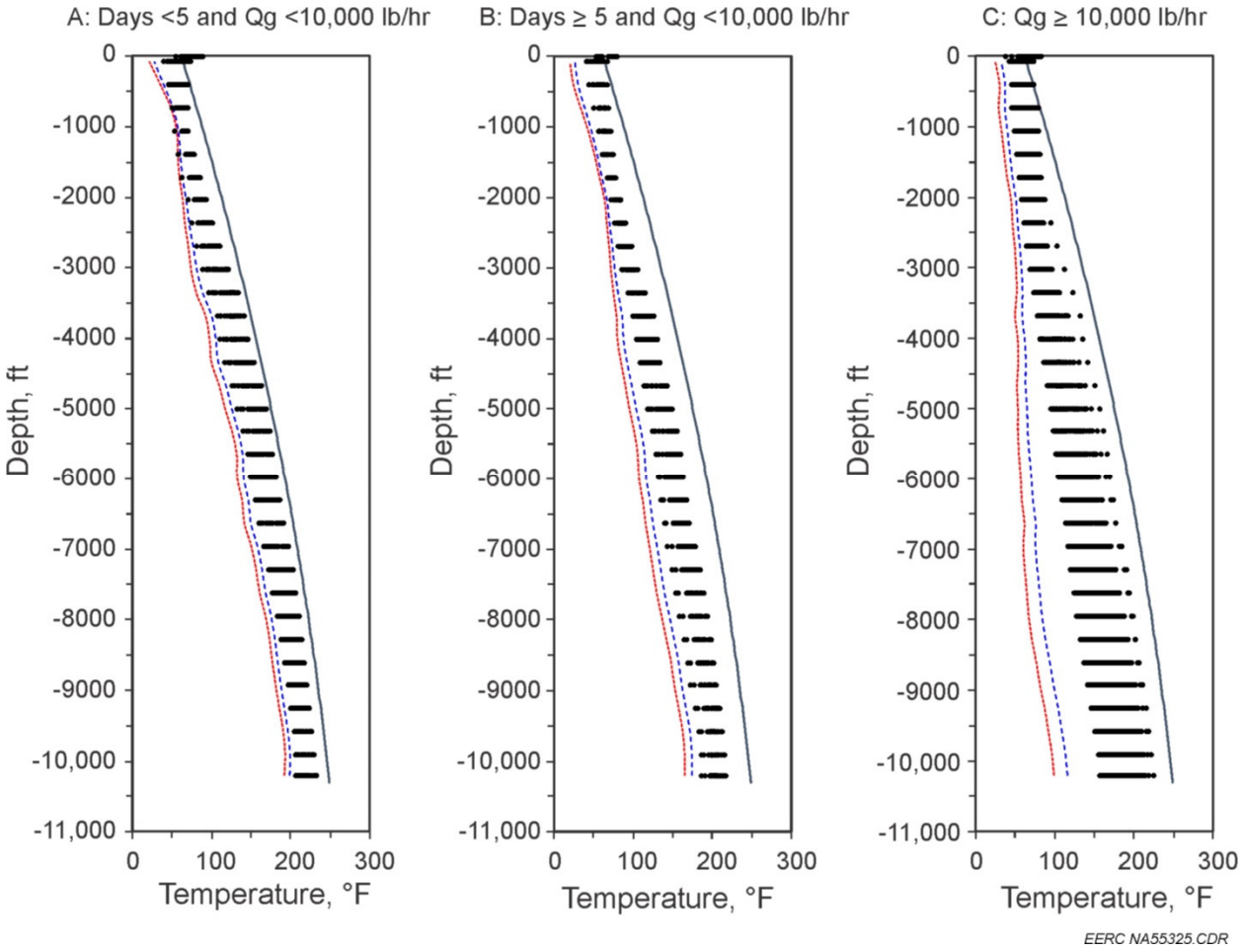


Figure 29. Average daily DTS temperature profiles acquired at the injection well during the period from April 15, 2015, through July 31, 2017, grouped by three combinations: A) $CO_2$ Qg < 10,000 lb/hr and number of cumulative days of $CO_2$ injection < 5 days, B) Qg < 10,000 lb/hr and ≥ 5 days, and C) Qg ≥ 10,000 lb/hr. The black lines to the right show a fit of the upper 95% prediction limit of the Equation 1 fit to the baseline (no $CO_2$ injection) DTS measurements. The blue and red dashed lines to the left represent the group-specific 2% (Action Level 1) and 1% (Action Level 2) action levels, respectively.

### *Using Module 4*

To launch Module 4, the user clicks on the "4) DTS Analysis" button from the Module Selection Window (Figure 6). This will launch Module 4 and open the default page (Figure 30).

From the default page, the user can select which group of measurements to plot from the dropdown menu in the upper left-hand corner of the page:

A. Days < 5 and Qg < 10,000 lb/hr
B. Days ≥ 5 and Qg < 10,000 lb/hr
C. Qg ≥ 10,000 lb/hr

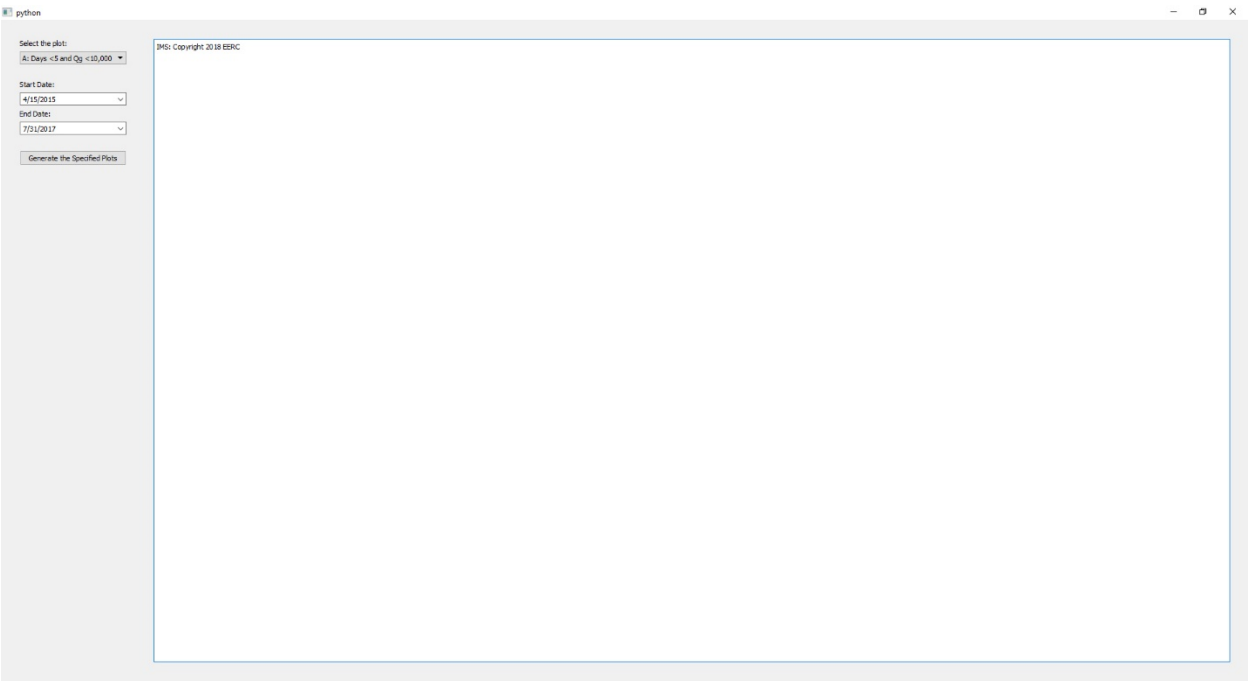


Figure 30. Default page for Module 4 – DTS Analysis.

Similar to other modules, the default date range is currently set to a Start Date of April 15, 2015 (the beginning of $CO_2$ injection) and an End Date of July 31, 2017 (the last valid date in the IMS Database). However, the user may select any date range within this period by modifying the Start Date and End Date. As with the other modules, a calendar feature has been incorporated into Module 4, which allows the user to select a Start Date or End Date using a monthly calendar. Lastly, the user must select "Generate the Specified Plots," which will retrieve the DTS temperature measurements from the IMS Database, calculate the daily average DTS temperature values, and plot them onto the group-specific template with their respective action levels.

Figures 31, 32, and 33 shows the output from Module 4 for Groups A, B, and C, respectively, for the date range from April 15, 2015, through July 31, 2017. The default template will plot the DTS temperature measurements (black circles), baseline geothermal gradient (solid black line), Action Level 1 (blue dashed line), and Action Level 2 (red dotted line). As shown in the figure, few existing measurements plot beyond the action levels. As $CO_2$ injection continues at the Storage Site, additional BHT measurements should plot within these action levels. New BHT measurements that plot outside of these action levels indicate DTS temperature conditions that do not frequently occur, which may indicate wellbore temperature conditions that exceed normal operating limits and could trigger an operational response from the IMS user. The significantly wider action levels for Group C ($Qg \geq 10{,}000$ lb/hr) reflects the greater variability in the wellbore temperature profile when $CO_2$ injection rates exceeded this value. In addition, this group of measurements had greater variability in the injection duration.

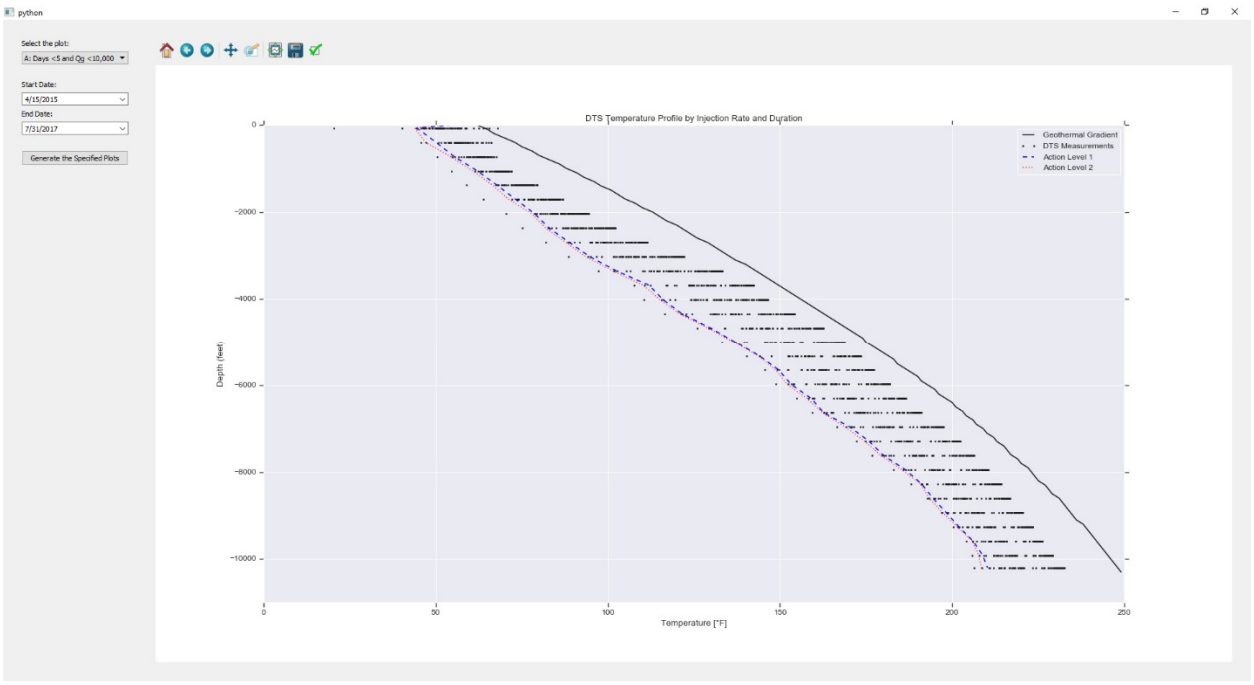


Figure 31. Module 4 plot for Group A (days < 5 and Qg < 10,000 lb/hr).

EERC NA55328.CDR

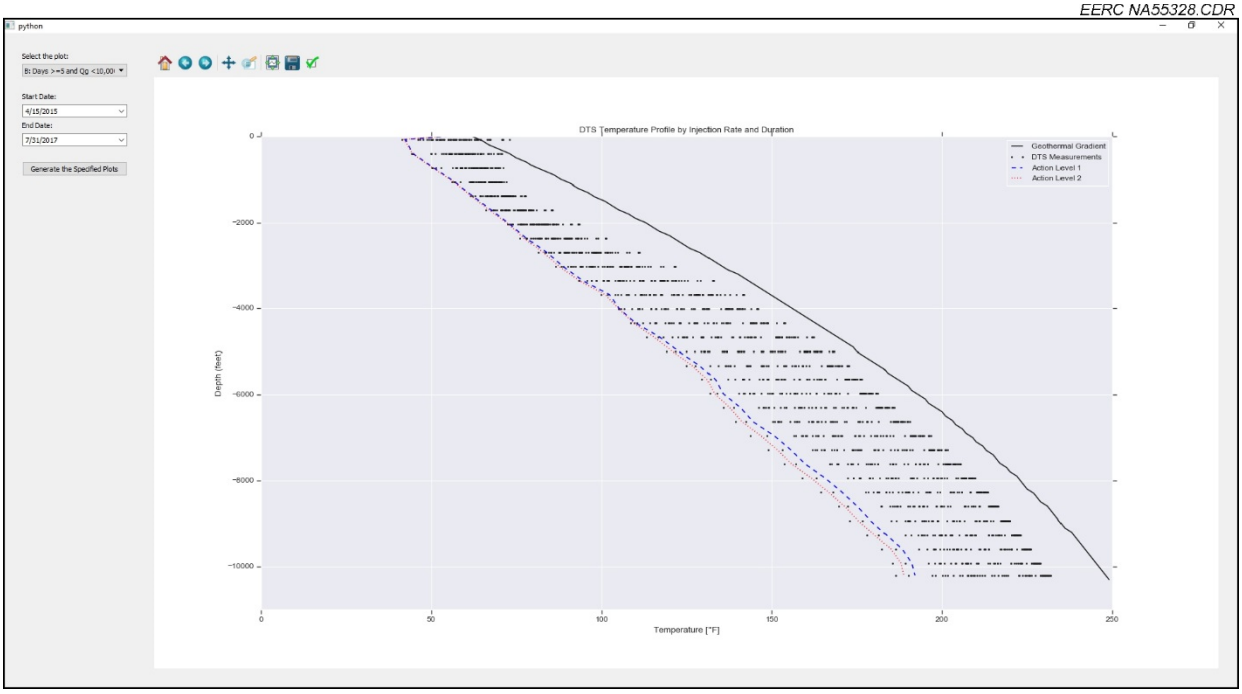


Figure 32. Module 4 plot for Group B (days ≥ 5 and Qg < 10,000 lb/hr).

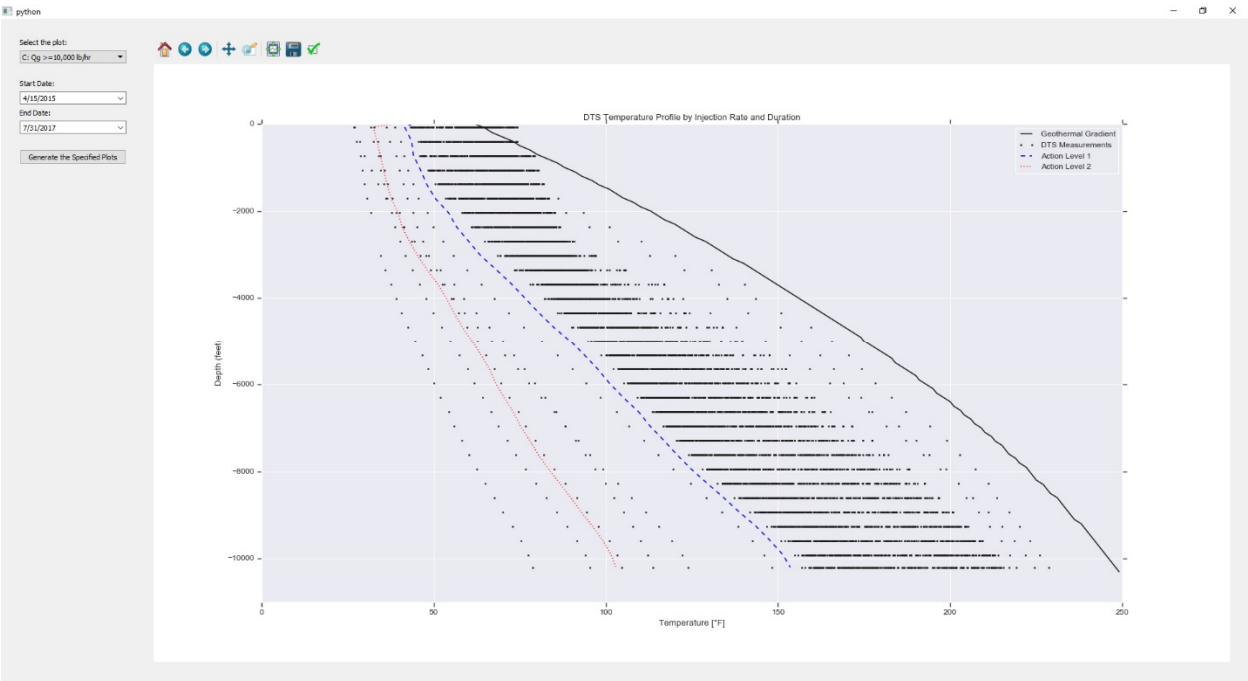


Figure 33. Module 4 plot for Group C (Qg ≥ 10,000 lb/hr).

## Module 5 – CMR Analysis

### *CMR Overview*

Module 5, CMR Analysis, is the IMS GUI entry point for executing the automated history-match (AHM) workflow. The CMR component of the IMS integrates continuous and periodic monitoring data with reservoir performance simulations. The primary purpose of the CMR process is to evaluate whether the reservoir simulation can reproduce the observed behavior of the $CO_2$ plume within a reasonable error tolerance. In this context, the observed $CO_2$ plume is an interpreted $CO_2$ plume image that was generated through seismic time-lapse analysis from pre- and post-$CO_2$ injection 3-D seismic measurements (4-D seismic).

As a monitoring tool for managing $CO_2$ injection and subsurface conditions, the CMR process informs the operator about whether the predicted $CO_2$ plume behavior is consistent with the observed $CO_2$ plume behavior given a set of injection and monitoring measurements, the geologic model, and reservoir simulations. Failure of the reservoir simulations to adequately predict the observed $CO_2$ plume may reflect a subsurface condition that is outside of normal operating limits or an inaccuracy within the simulation. Conversely, if the CMR process rapidly and accurately predicts the observed $CO_2$ plume, then this outcome provides the operator with greater confidence that the subsurface conditions are consistent with normal operating limits.

The CMR process consists of two complementary methods, a forward-modeling workflow and an inverse-modeling workflow, that are used in combination to best match simulation results with seismic monitoring data (Figure 34). The forward-modeling workflow uses pre-$CO_2$ injection

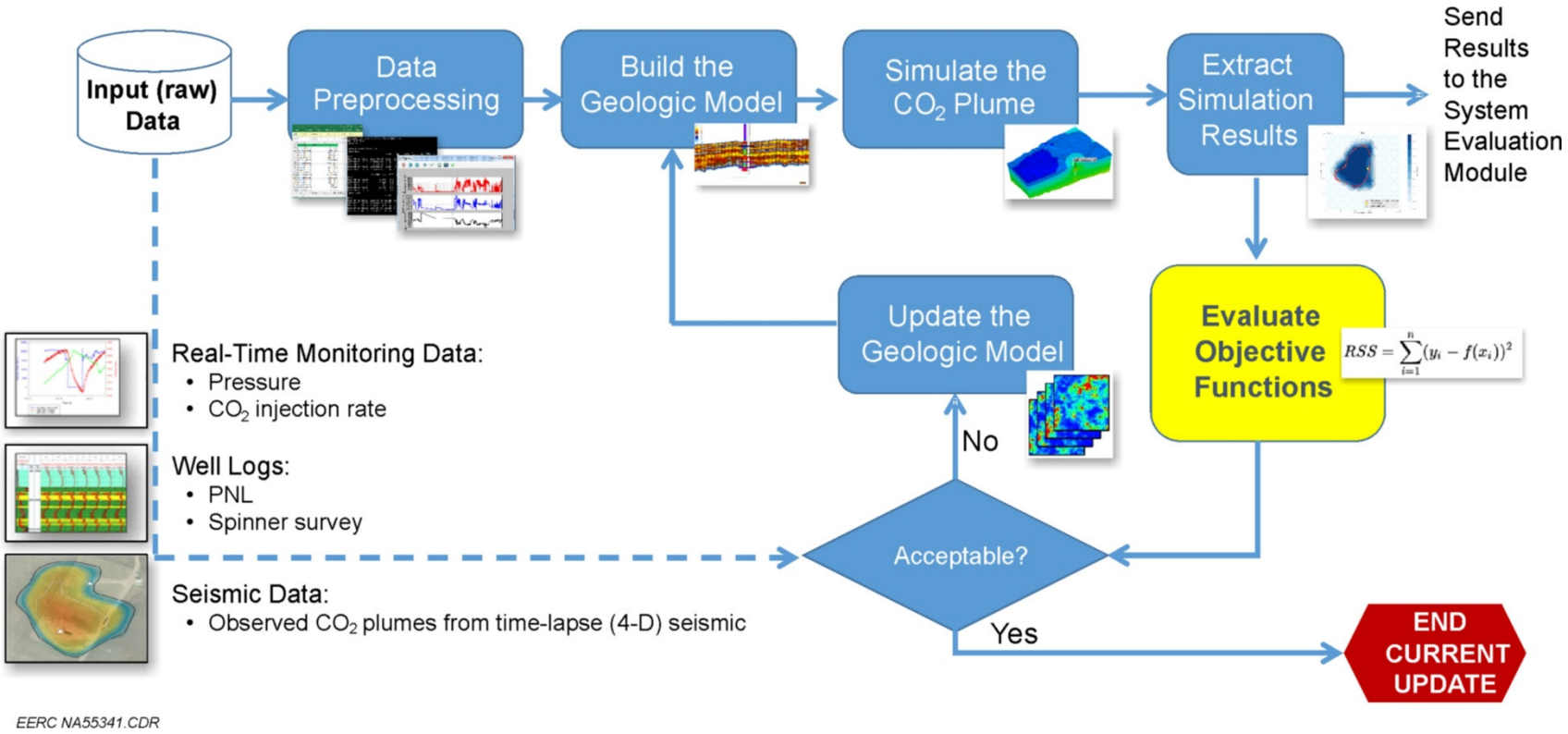


Figure 34. Diagram showing the different steps in the CMR process.

3-D seismic and well log measurements to characterize and create a geologic model of the subsurface that includes structure, facies, and petrophysical properties. This static geologic model is then used for dynamic reservoir simulations of the $CO_2$ behavior in the subsurface in response to $CO_2$ injection. The output from this forward-modeling workflow is the simulated $CO_2$ plume dimensions (lateral extent and depth of the $CO_2$ plume within the reservoir). The initial forward-modeling process is a manual (assisted) set of tasks supervised by specially trained staff in the reservoir simulation software. The quality of this initial forward-modeling process is evaluated by comparing the simulation results against a set of objective functions, such as how closely the predicted BHP matches the measured BHP from the monitoring well and how accurately the simulated $CO_2$ behavior in the reservoir matches the timing and extent captured by the spinner and PNL logs. This initial forward-modeling outcome is then fed into the inverse-modeling workflow.

The inverse-modeling workflow uses the dimensions of an interpreted (observed) $CO_2$ plume that was generated through seismic time-lapse analysis from pre- and post-$CO_2$ injection 3-D seismic measurements (4-D seismic). If the dimensions of the simulated $CO_2$ plume from the forward-modeling workflow match the observed $CO_2$ plume within a defined error criterion referred to as the "local objective function" (LOF), then the workflow is complete. However, if the LOF is not met, then additional adjustments are made to update the porosity and/or permeability of the initial geologic model, and this updated geologic model is fed back into the forward-modeling workflow. This updated geologic model is then used to simulate a new $CO_2$ plume for comparison against the observed $CO_2$ plume. This iterative process continues until the LOF is either achieved (i.e., LOF $\leq$ 10%) or until the process reaches the maximum number of iterations (e.g., ten iterations).

The CMR process is the most complex module within the IMS because of the integration of multiple data types, linkage of several component submodules, and interface with commercial reservoir simulation software. Appendix A provides a detailed explanation about the CMR assumptions and workflows, the AHM algorithms, and the Python coding used to implement the AHM processes. While the CMR process is complex, Module 5 requires minimal intervention from the operator. The algorithms that integrate data and execute the AHM operations run "behind the scenes," with the operator simply needing to start the AHM calculation by pressing the "LAUNCH" button. However, CMR requires a specific local configuration, which is explained below.

### *Using Module 5*

To run Module 5, the user clicks on the "5) CMR Analysis" button from the Module Selection Window (Figure 6). This will launch Module 5 and open the default page (Figure 35).

From the default page, the user can select to run either the full numerical simulation model, which is computationally intensive and takes several hours to run, or the sector model, which is a reduced form of the full model and has a simulation time that is between 10- to 60-fold less than the full numerical simulation model. Appendix A discusses the full simulation model and the sector model in greater detail. The user makes the model selection from the "Select the model type" dropdown menu in the upper left-hand corner of the page. Next, the user can make a selection from

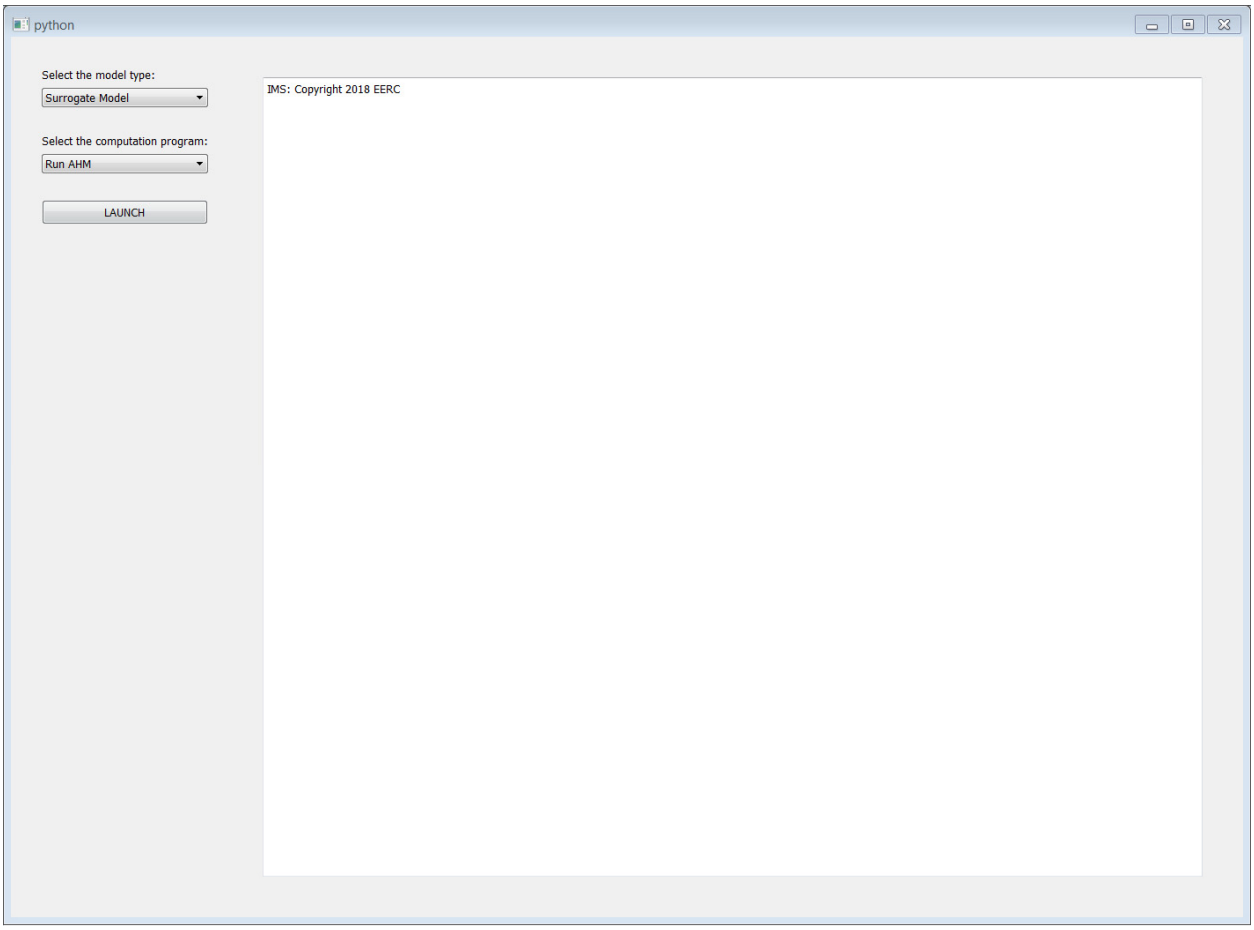


Figure 35. Default page for Module 5 – CMR Analysis.

the "Select the computation program" dropdown menu in the upper left-hand corner of the page. In the current version of the IMS, the only option for this menu is "Run AHM," which will execute the automated history-match routine. The reason for having this input field in the IMS is to allow flexibility for potential future edits to the IMS that may wish to display other computational program outputs. Lastly, to run the AHM, the user selects the "LAUNCH" button.

The AHM workflow links CMG tools with Python scripts to compare the observed $CO_2$ plume from the 4-D seismic time-lapse analysis and the simulated $CO_2$ plume from dynamic simulations using an LOF. Figure 36 shows an example of the Module 5 results from one application using three iterations of the AHM workflow. The output is a series of text statements for each iteration showing the results for the three components of the LOF (Appendix A):

- **Agree:** This is a term in the numerator of the LOF, which measures the agreement between observed and simulated $CO_2$ plumes.

- **Disagree:** This is a term in the numerator of the LOF, which measures the disagreement between observed and simulated $CO_2$ plumes.

- **LOF:** This is the result of the LOF for comparing observed and simulated $CO_2$ plumes.

As shown in the example, the Agree/Disagree/LOF outputs change with each iteration of the AHM workflow. Module 5 tracks these values for each iteration, and the results should converge toward a minimum LOF value with additional iterations. In this example, the first iteration results in Agree/Disagree/LOF outputs of 4.3898, 26.9822, and 6.1466, respectively (Figure 36, top red box). Then, in the second iteration, the Agree term increases to 5.1894, the Disagree term decreases to 25.8354, and the LOF decreases to 4.9785 (Figure 36, middle red box). Lastly, in the third iteration, the Agree term decreases from the second iteration down to 5.0914, the Disagree term increases from the second iteration up to 26.0587, and the LOF increases from the second iteration up to 5.1182 (Figure 36, bottom red box). Therefore, in this example, the second iteration represents the minimum LOF and the final stopping point of the AHM workflow.

This example shows a case where the AHM stopped by reaching a maximum number of iterations, which was set to three iterations for the purposes of illustration. The maximum number of iterations criterion avoids spending simulation time on unnecessary iterations when the results are changing significantly from the baseline condition, or when the AHM algorithm might need an excessive period of time to find a better solution. If the AHM fails to converge using a reduced number of iterations, then this could indicate that something changed in the system or that some significant structural feature is missing in the geologic model, and because of these factors, warning flags should be raised in the AHM workflow. Rapid convergence (few iterations) suggests that the $CO_2$ plume is behaving within predicted limits. Conversely, greater disagreement means that the $CO_2$ plume is NOT behaving within predicted limits; therefore, the model is taking longer to converge or is not converging.

The AHM workflow contains three stopping criteria:

1. LOF is smaller than a predefined tolerance (e.g., 10%)

2. LOF is higher than the predefined tolerance (e.g., 10%), but there is an inflection point when changes are considered in the LOF over successive iterations

3. The maximum number of iterations is reached, which indicates a higher degree of uncertainty between observed and simulated $CO_2$ plumes and failure of the AHM workflow to achieve the LOF. Case 3 does not necessarily mean that there is an unacceptable level of risk for the Storage Site; however, this outcome indicates to the operator that the observed subsurface behavior of the $CO_2$ plume is outside of the expected range, which is an indication that the geologic model may need to be reexamined or other inputs must be reevaluated; i.e., human intervention is required

The default tolerance for the LOF is currently set to 10%, and the maximum number of iterations is currently set to 10. These default values can be tailored to the specific monitoring requirements of the storage site.

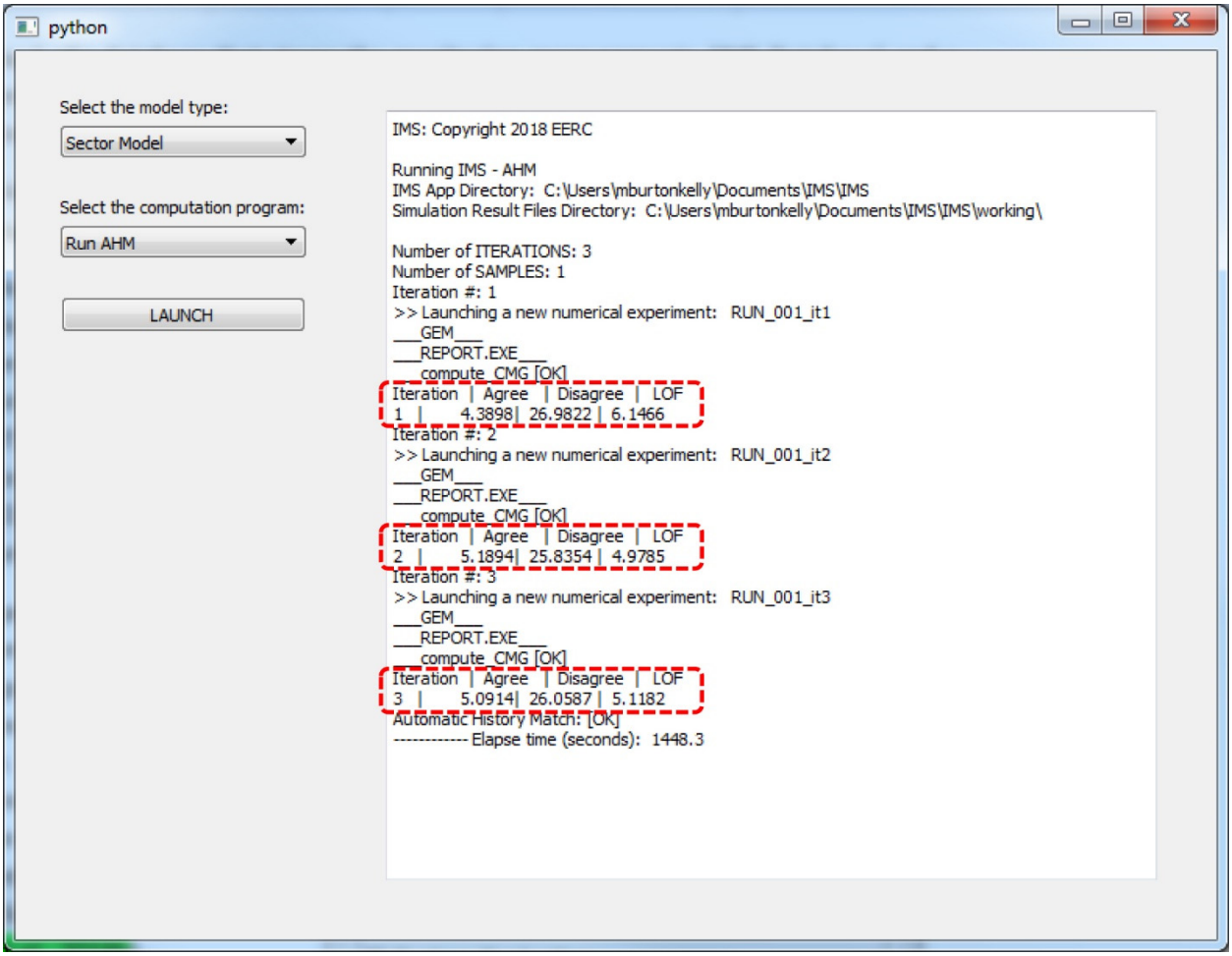


Figure 36. Results displayed in the Module 5 – CMR Analysis panel after the AHM simulation is finished.

### *CMR Configuration*

The CMR module requires a number of input files to successfully execute the AHM algorithm. The core of the IMS AHM calculations are done by CMG's reservoir simulator, GEM; therefore, the input files need to follow some predefined formats explained in the GEM's user manual (Computer Modelling Group Ltd., 2016). Key information is transmitted with the help of template files (report.tmpl and SM.tmpl) that provide a link to the CMG's keyword data system, allowing the IMS to gain access to the reservoir simulation model parameters. Table 1 shows a list containing the main environment and input parameters required by the CMR module.

One of the main outcomes of the AHM is a map comparing the simulated and observed $CO_2$ saturation plume, which can be visualized within Module 6: $CO_2$ Plume Boundary (see next section).

**Table 1. IMS Variables.** The modules that process CMG information to generate maps (Module 5: CMR Analysis and Module 6: $CO_2$ Plume Boundary) require the definition of environment setting variables to execute programs external to IMS. These variables can be defined in a configuration file called "Config.env."

| ITEM/EXAMPLE | COMMENTS |
|---|---|
| [CMG] | Keyword announcing that the following lines will serve to define setting variables regarding CMG applications. |
| GEM=GM201710.EXE | Defines the version of the CMG's Reservoir simulator GEM. |
| GEM-PATH=C:\PROGRAM FILES (X86)\CMG\GEM\2017.10\WIN_X64\EXE\ | Defines the path to the CMG's Reservoir simulator GEM. |
| REPORT-PATH=C:\PROGRAM FILES (X86)\CMG\BR\2017.10\WIN_X64\EXE\ | Defines the path to the CMG's Results Report (Report.exe) postprocessing utility. |
| | |
| [DATA] | Keyword announcing that the following lines will serve to define setting variables regarding AHM inputs. |
| WORKING=C:\IMS\IMS_ALPHA_0.6\WORKING\ | Defines the path that the AHM will use a temporary folder to store files while performing the different numerical experiments. |
| TEMPLATE=C:\IMS\IMS_ALPHA_0.7\INPUTS\SM.TMPL | Defines the filename where the user will place the "GEM" template files containing tokens that identify the AHM parameters. |
| REPORT-TMPL=C:\IMS\IMS_ALPHA_0.6\INPUTS\REPORT.TMPL | Defines the filename where the user will place the "Results Report" template files containing tokens that identify the AHM parameters. |
| INPUTS=C:\IMS\IMS_ALPHA_0.6\INPUTS\ | Defines the path where the user will place the GEM template files containing tokens that identify the model parameters. |
| AUXILIARY=C:\IMS\IMS_ALPHA_0.6\AUXILIARY\ | Defines the path where the user will place supplementary data, required to compute the LOF. |
| | |
| SM-GRID=SM GRID TOP TIME 2015-04-16.TXT | Defines the name of the file that contains information about the Surrogate Model grid (XYZ CMG's format). |
| FM-GRID=REDONESEISMICMOD_00139 GRID TOP_XYZ.TXT | Defines the name of the file that contains information about the Full Model grid (XYZ CMG's format). |
| FM-BIN=CMGBUILDER00 CMGLCUSTOM_2_SRF.TXT | Defines the name of the file that contains information about the 4-D seismic-derived property in the Full Model (SRF CMG's format). |
| SM-BIN=SM_BINARY_SRF.TXT | Defines the name of the file that contains information about the 4-D seismic-derived property in the Sector Model (SRF CMG's format). |
| SM-PERMI=PERMEABILITY_I.INC | Defines the name of the file that contains the permeability 3-D array from the Surrogate Model (SRF CMG's format). |
| SM-PORO=SM_POROSITY.INC | Defines the name of the file that contains the porosity 3-D array from the Surrogate Model (SRF CMG's format). |
| CO2FILE=OUTERPLUME_NAD83_XYS - COPY.TXT | Defines the name of the file that contains the 2-D boundary contour obtained from image processing (X-Y-Z Table). |
| PERF2XYZ=GRID.INC | Defines the name of the file that contains the Perforation 2 layers (XYZ CMG's format). |
| | |
| [PARAMETERS] | Keyword announcing that the following lines will serve to define AHM parameters. |
| NO-OF-SAMPLES=1 | Defines the number of samples, in case multiple realizations are executed. |
| NO-OF-ITERATIONS=3 | Defines the maximum number of iterations. |
| MONITORING-TIME=307 | Defines the date when the monitoring seismic survey was launched. |

### Module 6 – $CO_2$ Plume Boundary

Module 6 ($CO_2$ Plume Boundary) provides the user with a visual output for exploring the quality of the results obtained with the AHM in Module 5 against the observed $CO_2$ plume contour, which was previously defined from time-lapse seismic analysis of pre- and post-$CO_2$ injection 3-D seismic measurements (4-D seismic).

To run Module 6, the user clicks on the "6) $CO_2$ Plume Boundary" button from the Module Selection Window (Figure 6). This will launch Module 6 and open the default page (Figure 37). Next, the user must select the latest AHM output file to display the simulated $CO_2$ plume contour. Figure 38 illustrates the process of navigating the local directory to search for the AHM output of the simulation results file using Windows Explorer. The user launches this search tool by selecting the "Browse" button from the default page. The output file from Module 5 is saved in the working directory where the IMS is installed on the user's computer. The default browse location in Module 6 points the user to this directory.

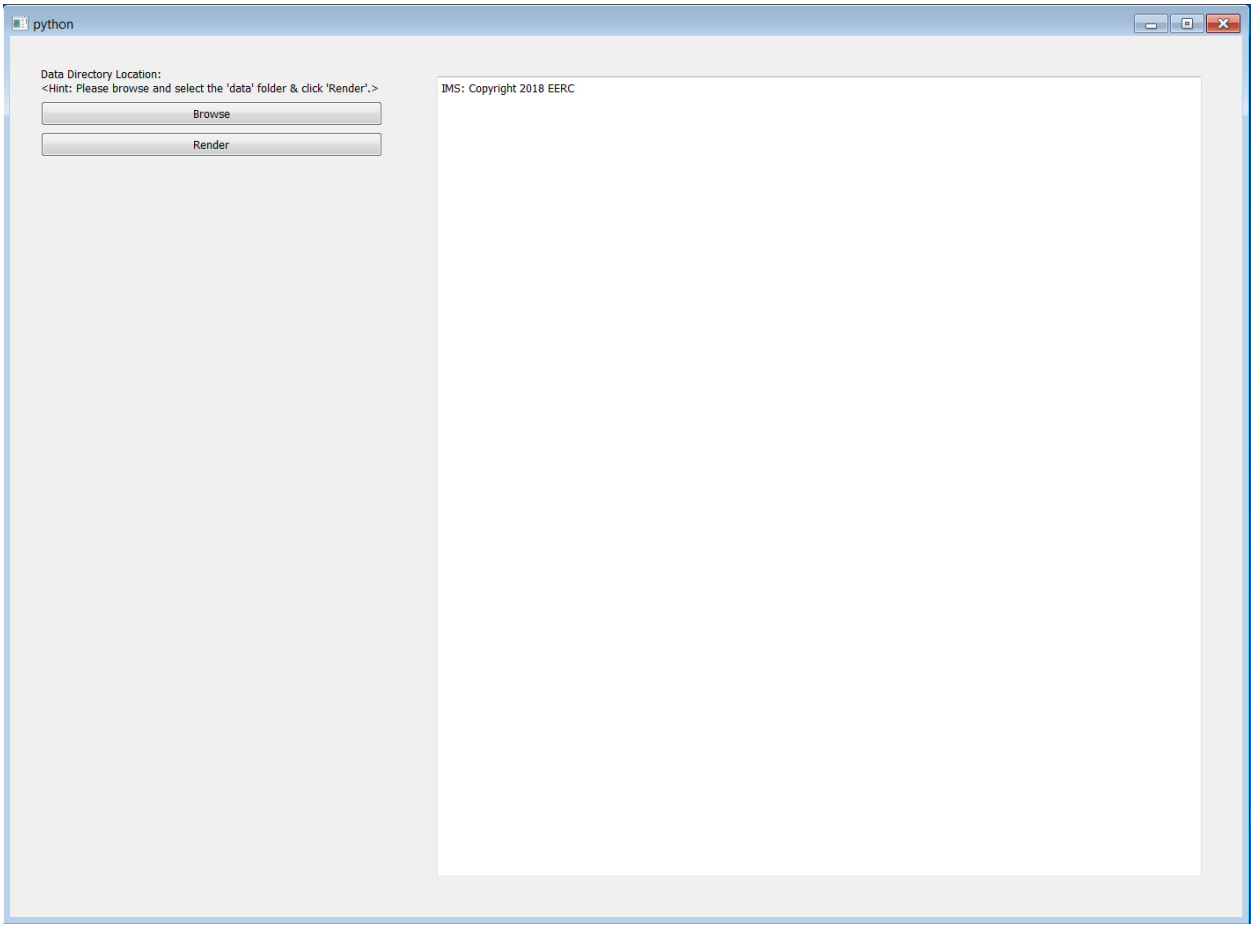


Figure 37. Default page for Module 6 – $CO_2$ Plume Boundary.

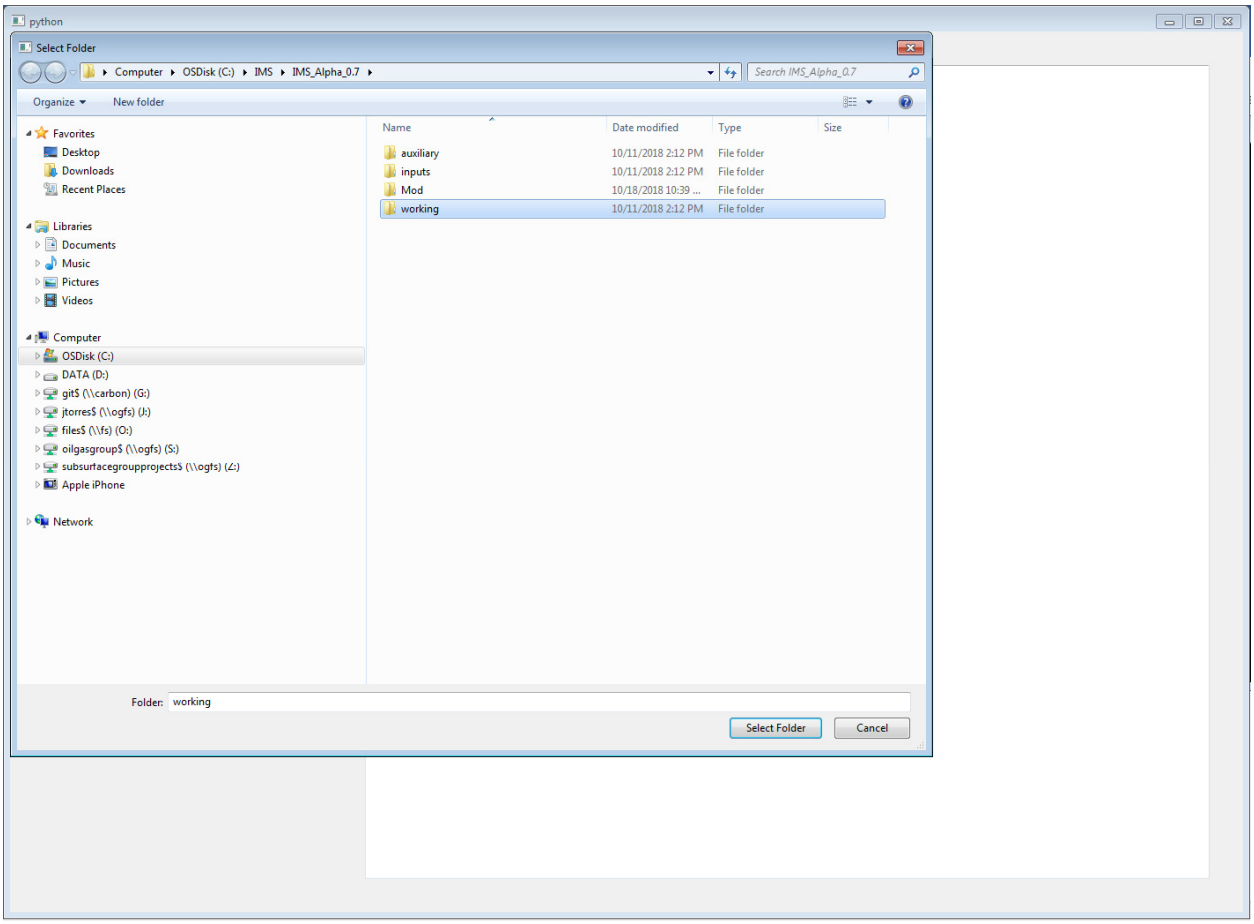


Figure 38. Folder browse navigation window on Module 6 – $CO_2$ Plume Boundary.

Lastly, Figure 39 shows an example output from Module 6 that was developed using AHM simulation and the observed data corresponding to the Aquistore Monitoring Survey 2 (Monitor 2), which was completed on February 2016. Shown in this figure is an outline of the observed $CO_2$ plume boundary (from 4-D seismic data) as compared to the simulated $CO_2$ plume from the AHM executed in Module 5 (red-to-blue contour map). While this example is specific to the Storage Site, the IMS is a general-purpose system that can be extended to handle other operational scenarios and sites.

**Module 7 – System Evaluation**

Module 7 (System Evaluation) is the last module in the IMS and integrates the statistical thresholds for the three continuous measurements from Modules 3 and 4 (DTS, BHT, and BHP) and the outcome from the AHM in Module 5 (stopping criteria) into a graphical assessment of whether the system is or is not operating within normal limits. The purpose of Module 7 is to provide a tool for the operator to quickly assess a set of color-coded outputs and determine whether they need to evaluate other modules within the IMS or implement further actions to control the storage site.

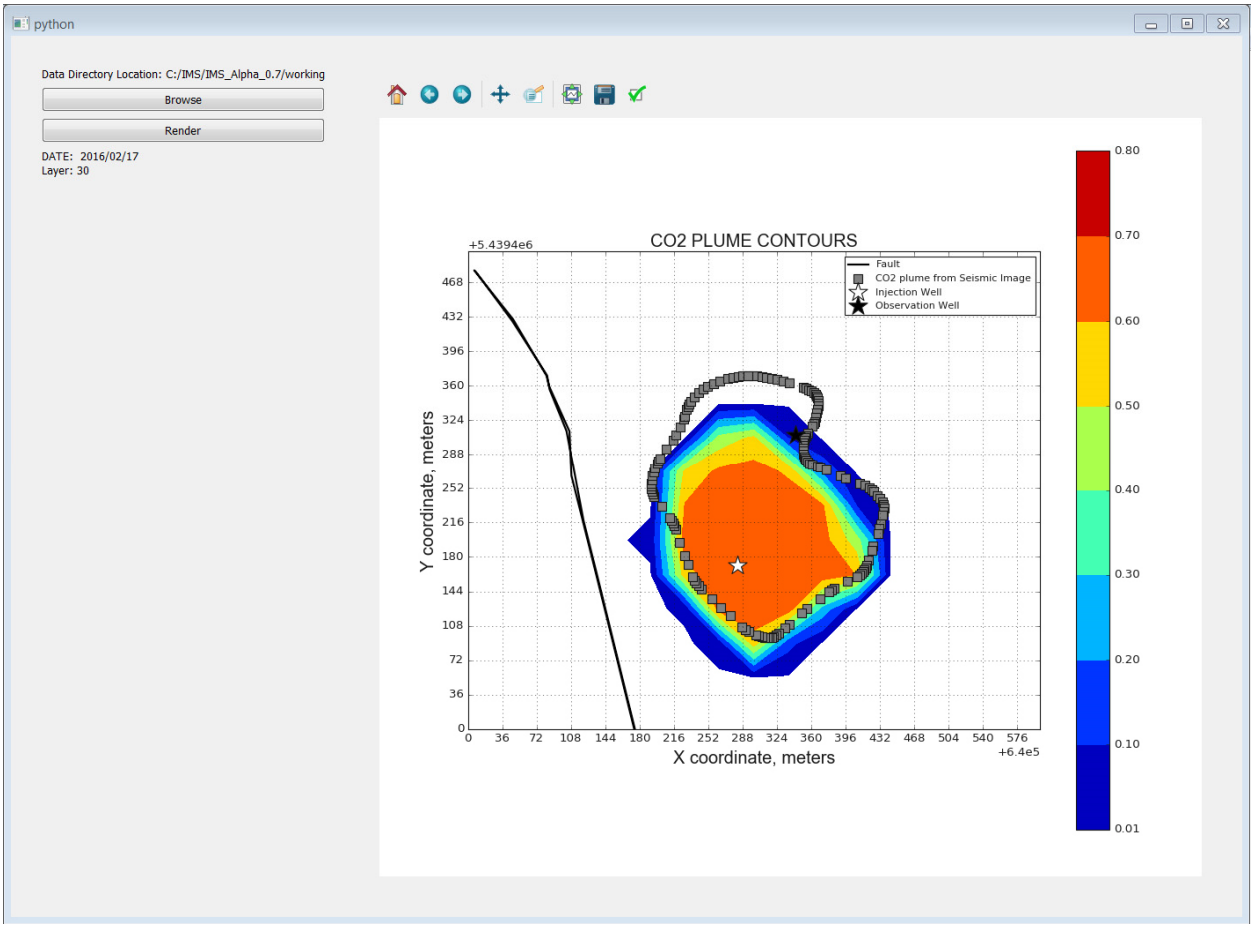


Figure 39. Contour maps shown in Module 6 – $CO_2$ Plume Boundary. The map is a top view of the reservoir, at a depth equivalent to the top layer on Perforation 2. Gray-filled squares represent the seismic-derived $CO_2$ plume contour, while the red to blue contour scale represents the simulation-derived $CO_2$ plume contours. The variable displayed is Gas Saturation. The fault-feature (black line), injection well (white star), and observation well (black star) are shown as references. Results from the simulated $CO_2$ plume were automatically generated by the AHM workflow.

To run Module 7, the user clicks on the "7) System Evaluation" button from the Module Selection Window (Figure 6). This will launch Module 7 and open the default page (Figure 40).

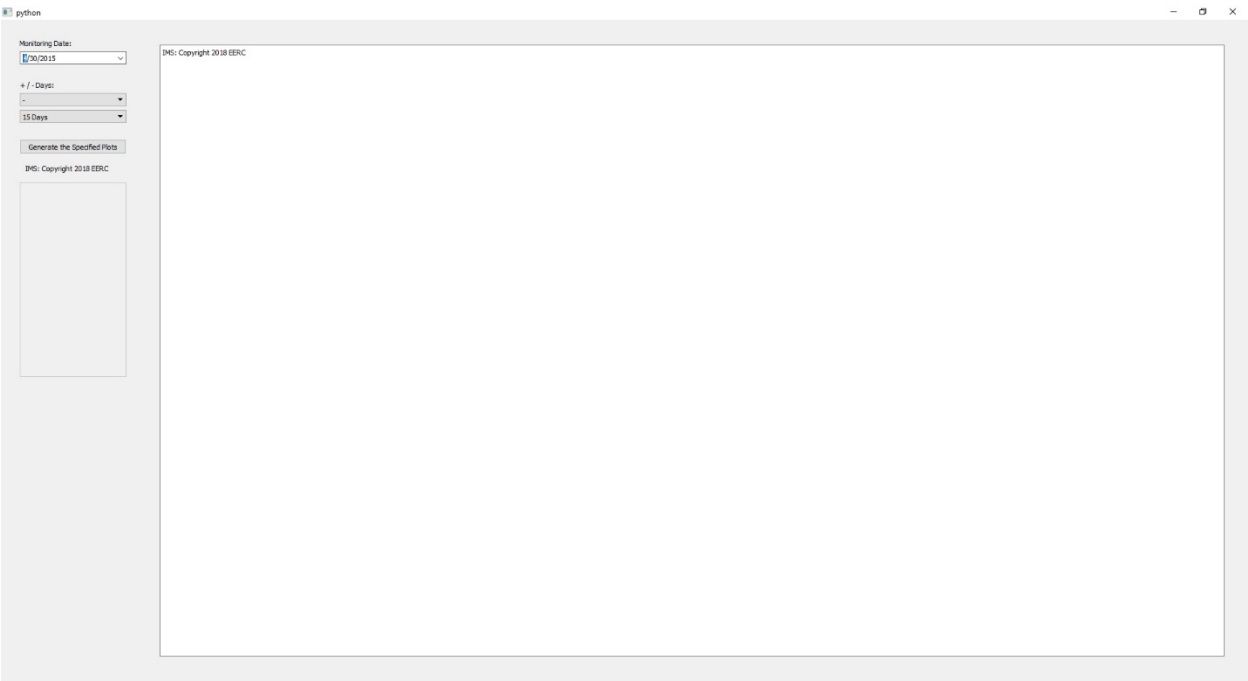


Figure 40. Default page for Module 7 – System Evaluation.

The user must make three selections prior to generating the graphical output: Monitoring Date, +/– Days, and Number of Days. The Monitoring Date is either the Start Date or End Date of the evaluation, depending on which constraint the user wants to provide. A calendar feature has been incorporated into Module 7, which allows the user to select a Monitoring Date using a monthly calendar. Next, the "+/– Days" dropdown menu tells the IMS whether to count forward (+) or backward (–) from the Monitoring Date. The user must then select the length of the evaluation period using the "Number of Days" dropdown menu. The selections include 15, 30, and 45 days from the Monitoring Date (Figure 41). Lastly, the user must select "Generate the Specified Plots."

Module 7 incorporates algorithms to quickly classify new measurements as "Normal" (blue), "Caution" (pink), or "Flag" (red). In addition, NULL (missing) values in the IMS Database or BHP gauge readings less than 4940 psi (initial reservoir pressure) are reported as "possible error" (gray). Module 7 makes several simplifying assumptions to accommodate multiple measurements and action levels. Appendix C describes these algorithms and assumptions in greater detail.

Module 7 is designed with a global false-positive rate of 1% for "Flag" and 2% for "Caution" conditions; therefore, a system evaluation color shading of blue denotes conditions that were observed 98% of the time during the period from April 15, 2015, through July 31, 2017, i.e., conditions established as "normal operating limits." The operator can modify these action levels depending on their specific risk tolerances.

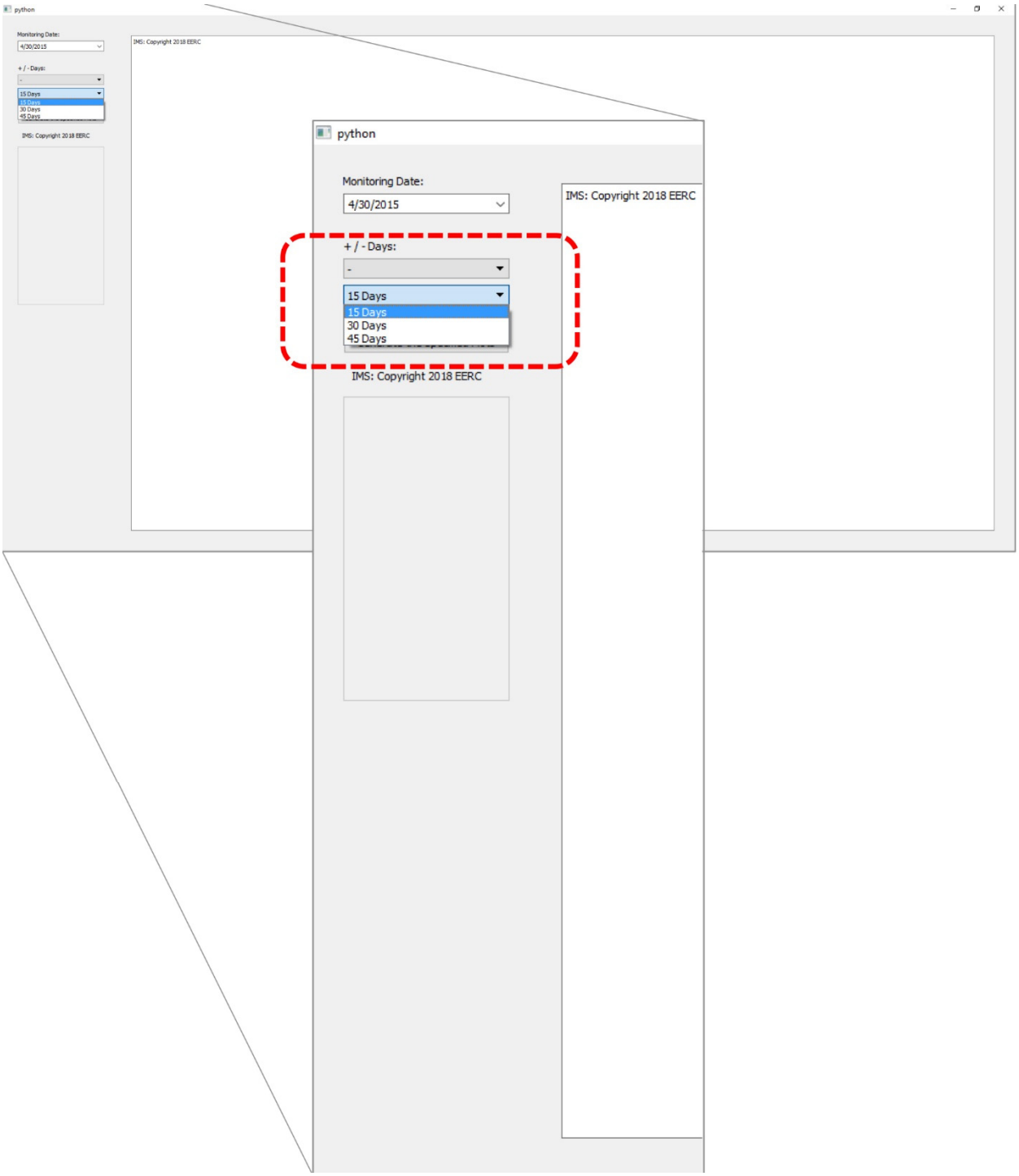


Figure 41. Module 7 example of the dropdown menu for selecting 15, 30, or 45 days.

As shown in the example in Figure 42, the Module 7 output is organized as follows:

- Time (measurement acquisition date) is displayed across the x-axis as columns, with a maximum of 45 columns (+/– 45 days).

- DTS sensor results from DTS02 to DTS33 are displayed from top-to-bottom, which corresponds to the injection well temperature profile, identical to the configuration used in Module 2B (DTS Time-Series – Figure 20). The DTS sensor at the surface, DTS01, is excluded from this analysis, as the temperature measured at this gauge is significantly affected by surface conditions.

- The BHT results are shown at the bottom of the column of DTS sensors, which corresponds with the spatial relationship between the BHT sensor (bottomhole in the injection well) and the bottommost DTS sensor.

- A blank row is inserted between BHT and the last two measurements to distinguish between temperature-related measurements and the other measurements.

- The BHP results are displayed next and use a single row to flag either Zone I (pressure is less than expected) or Zone III outcomes (pressure is greater than expected).

- Lastly, the stopping criteria from the AHM workflow executed in Module 5 are shown in the final row, "CMR." The three stopping criteria for the AHM are the same as those in Module 6, with 1 corresponding to blue (Normal), 2 corresponding to pink (Caution), and 3 corresponding to red (Flag).

The CMR portion of Module 7 requires a processed and interpreted 3-D seismic data set to function. Because of the time required to collect and analyze this type of data, as well as the span of time between repeat seismic surveys (sometimes a year or more), the CMR criterion of the system evaluation has a much longer time to detection than the continuous measurements of DTS, BHT, or BHP.

Figure 42 shows an example where the user has selected a Monitoring Date of December 10, 2015, and +45 days. After "Generate the Specified Plots" is selected, Module 7 will retrieve the DTS, BHT, and BHP measurements from the IMS Database, compare these measurements against respective action levels, and display the results. The CMR component of the module shows normal conditions throughout this period. The example shown in Figure 42 does flag particular days where portions of the DTS temperature profile, BHT, or BHP were outside of their respective 1% (red) or 2% action levels (pink). Even though the action levels were defined using low-probability thresholds, these types of flags are expected to occur during operations because of anomalies that are unrelated to risk events occurring. The user must decide based on the system evaluation results whether to consult other modules within the IMS or whether an operational response is needed.


Figure 42. Module 7 example output showing +45 days from a monitoring date of December 10, 2015.

## SCHLUMBERGER REVIEW OF THE IMS

The IMS development included a technical review by Schlumberger, which was completed during an on-site visit to the EERC on August 21, 2018. Schlumberger was provided with access to a workstation preloaded with a preliminary version of the IMS, including the required software needed to execute the different modules. Appendix D provides the technical memorandum submitted by Schlumberger to the EERC, which presents the findings of its review.

Schlumberger provided valuable feedback with respect to evaluating the IMS interface functionality and capabilities and assessing the utility of integrating the IMS control system architecture with existing commercial systems. The IMS reflects some, but not all, of Schlumberger's comments. For example, the IMS contains the following enhancements that were suggested by Schlumberger:

- **Module Selection Window:** This window now includes module version, copyright, disclaimer, license, and contact information, in addition to a brief description of each module.
- **Module 1 (Well Monitoring Measurements):** This module now includes the ability to plot multiple measurements in a single panel (multiple axes plot option).

- **Module 2 (DTS Measurements):** This module now displays the units of the sampling frequency (days) and allows the user to display either the DTS temperature or temperature gradient as a function of time (Module 2B – DTS Time-Series).

- **Module 5 (CMR Analysis):** This module now includes the simulation time/date in the display screen.

- **Module 6 ($CO_2$ Plume Boundary)[1]:** This module now includes time information for the $CO_2$ plumes and uses more robust color shading for the gas saturation contour map.

Several of Schlumberger's comments could not be addressed in the IMS because of time constraints; however, these additional recommendations are documented in Appendix D and could be integrated into future versions of the IMS.

## FUTURE WORK

The IMS is a first-generation system developed to integrate continuous monitoring data, periodic monitoring data, and reservoir performance simulations with a technical user interface for visualization and for support of real-time decision-making. While the IMS successfully achieves this objective, additional improvements could be made in future versions. For example:

- The action levels for continuous measurements incorporated into the IMS represent a retrospective analysis applied to the historical data set rather than an autonomous system that begins at the start of $CO_2$ injection, learns from the data, and derives action levels in real time. As part of their technical review, Schlumberger noted that future versions should be "real-time capable." Stated differently, a next-generation IMS should "learn from the data" and automatically adjust the action levels as new measurements are acquired, stored in the IMS Database, and processed through a set of algorithms. This type of fully automated system would likely require the coupling of analytical or numerical physics-based models with empirical approaches similar to the ones provided in Appendix C.

- The IMS does not include action levels for the ANP measurement. However, the ANP is potentially a very good diagnostic for assessing well integrity. Additional work to determine ways to incorporate the ANP measurement into a decision framework similar to those used for DTS, BHT, and BHP measurements would improve the ability of the IMS to detect changes from normal operating limits.

- The IMS is built around measurements collected from a single injection well, as the measurement sensors in the observation well no longer function properly. Future systems integrating information from more than one well could provide a more robust decision-making framework for inferring measurements that are outside of normal operating limits.

- The current AHM workflow relies on an observed $CO_2$ plume, which requires the acquisition of new 3-D seismic measurements, processing, and interpretation by a

[1] At the time of Schlumberger's review, Module 6 was referred to as "Module 3 – Area of Review (AOR)." This language was replaced in subsequent IMS versions to more accurately reflect the module output, which includes the $CO_2$ gas saturation and not reservoir pressure.

geophysicist prior to delineating the $CO_2$ plume boundary. This time- and labor-intensive process has a much longer time-to-detection than the continuous measurements. Acknowledging this time- and labor-intensive process was one motivating factor for using continuous measurements like DTS, BHT, and BHP in the IMS. Incorporating automated approaches for integrating seismic measurements, such as the scalable automated semipermanent seismic array (SASSA) (Livers-Douglas and others, 2017), could reduce the time-to-detection and, thereby, more effectively integrate geophysical measurements into the IMS.

## SUMMARY AND CONCLUSIONS

The monitoring data generated at a $CO_2$ storage site can quickly result in large quantities and types of data, often requiring significant labor- and time-intensive efforts to process and analyze before using this information to make decisions about the state of the operation. Implementing an IMS can reduce the associated data-processing and analysis time and costs, thereby improving monitoring efficiency and enabling real-time operational decision-making.

The IMS described in this report successfully implements workflows and algorithms that:

- Handle real-time monitoring data from the Storage Site. This includes continuous and high-frequency period measurements (e.g., BHP and BPT), as well as low-frequency data (i.e., repeat 3-D seismic surveys)

- Store and manage information in a secure database (IMS Database)

- Perform data-preprocessing linked to an automated history-match that includes a forward-modeling workflow and an inverse-modeling workflow, which are used in combination to best match simulation results with seismic monitoring data. This process automatically adjusts the simulation model until the predicted $CO_2$ plume matches the observed $CO_2$ as closely as possible.

- Integrate continuous and periodic data with reservoir simulation.

- Use the continuous monitoring data to model and predict bottomhole conditions in real time.

- Incorporate statistical threshold decision criteria (action levels) for real-time decision support.

Compared with the traditional manual processing, interpretation, and integration workflows, this IMS allows a CCS site operator to more efficiently monitor and manage $CO_2$ injection and subsurface conditions. This technology advanced the state-of-the-science for IMSs and contributes to the U.S. Department of Energy Carbon Storage Program goals of developing and validating technologies to ensure $CO_2$ storage permanence and to improve reservoir storage efficiency while ensuring containment effectiveness.

## REFERENCES


Azizi, E., and Cinar, Y., 2013, Approximate analytical solutions for $CO_2$ injectivity into saline formations: SPE Reservoir Evaluation & Engineering, May 2013, p. 123–133, SPE-165575-PA.

Azzolina, N.A., Torres, J.A., Pekot, L.J., Li, C., and Gorecki, C.D., 2018, Development of intelligent monitoring system (IMS) modules for the aquistore $CO_2$ storage project—data integration algorithms for aiding decision-making about the subsurface risk profile: Revised Topical Report – Deliverable D4 – Data Integration for Risk Profiling, May 22, 2018.

Bravo, C., Saputelli, L., Rivas, F., Perez, A., Nikolaou, M., Zangl, G.; Guzman, N., Mohaghegh, S., and Nunez, G., 2013, State of the art of artificial intelligence and predictive analytics in the E&P Industry – a technology survey: Presented at the SPE Intelligent Energy International, Utrecht, the Netherlands, March 27–29, 2012, SPE 150314.

Chai, C.F., Berg, F., Engbers, P., and Sondak, G., 2014, Smart fields—10 years of experience in intelligent energy and collaboration: Presented at the SPE Intelligent Energy Conference and Exhibition, Utrecht, The Netherlands, April 1–3, 2014, SPE 167872-MS.

Computer Modelling Group Ltd., 2016, GEM user guide: Calgary, Alberta, Canada.

Global Carbon Capture and Storage (CCS) Institute, 2018, Boundary Dam carbon capture and storage: www.globalccsinstitute.com/projects/boundary-dam-carbon-capture-and-storage-project (accessed November 2018).

Gorecki, C.D., Sorensen, J.A., Bremer, J.M., Ayash, S.C., Knudsen, D.J., Holubnyak, Y.I., Smith, S.A., Steadman, E.N., Harju, J.A., 2009, Development of storage coefficients for carbon dioxide storage in deep saline formations: AAD Document Control, U.S. Deparment of Energy, Cooperative Agreement Energy & Environmental Research Center (EERC): University of North Dakota, p. 1–61.

Jiang, T., Pekot, L.J., Jina, L., Peck, W.D., Gorecki, C.D., and Worth, K., 2017, Numerical modeling of the Aquistore $CO_2$ storage project: Energy Procedia, v. 114, p. 4886–4895.

Khan, F., Verbrugge, E., Pars, H., and Okotete, A., 2015, Back to the future—applying lessons learnt to a new generation of digital oil field applications: Presented at the SPE Digital Energy Conference and Exhibition, The Woodlands, TX, USA, March 3–5, 2015, SPE 173443-MS.

Lee, S.Y., Swagera, L., Pekot, L., Piercey, M., Will, R., and Zaluski, W., 2018, Study of operational dynamic data in Aquistore project: International Journal of Greenhouse Gas Control, v. 76, p. 62–77.

Livers-Douglas, A.J., Salako, O., Kovacevich, J.T., Burnison, S.A., Dalkhaa, C., Torres, J.A., Pekot, L.J., and Gorecki, C.D., 2017, Application of seismic trace-based analysis to detect the extent of injected $CO_2$ using modeled seismic data from aquistore: Interim Report – Deliverable D3 – Shot Record Plume Tracking, December 28, 2017.

McAdams, W.H., 1942, Heat transmission, 2d ed.: New York, McGraw-Hill Book Co. Inc.

Nghiem, L., 2002, Compositional simulator for carbon dioxide sequestration: Calgary, Computer Modelling Group.

Noh, M., Lake, W., Bryant, S.L., and Martinez-Araque, A., 2007, Implications of coupling fractional flow and geochemistry for $CO_2$ injection in aquifers: SPE Reservoir Evaluation & Engineering, August, p. 406–414.

Peck, W.D., Klenner, R.C.L., Liu, G., Gorecki, C.D., Ayash, S.C., Steadman, E.N., and Harju, J.A., 2014, Model development of the Aquistore $CO_2$ storage project: Poster presented at the International Conference on Greenhouse Gas Technologies (GHGT-12), Austin, Texas, October 5–9, 2014.

Pruess, K., Xu, T., Apps, J., and Garcia, J., 2003, Numerical modeling of aquifer disposal of $CO_2$: Society of Petroleum Engineers Journal, v. 8 no.1, p. 49–60, SPE-83695-PA, doi: 10.2118/83695-PA.

Python Software Foundation, 2018, General Python FAQ: https://docs.python.org/3/faq/general.html (accessed October 2018).

Python Core Team, 2018, Python—a dynamic, open source programming language: Python Software Foundation, www.python.org/ (accessed 2018).

Ramey, H.J., Jr., 1962, Wellbore heat transmission: Journal of Petroleum Technology, April, p. 427–435.

Silva Jr, M.F., Muradov, K.M., and Davies, D.R., 2012, Review, analysis, and comparison of intelligent well monitoring systems: Presented at the SPE Intelligent Energy International Conference, Utrecht, The Netherlands, March 27–29, 2012, SPE 150195.

U.S. Environmental Protection Agency, 2018a, Underground injection control (UIC)—final Class VI guidance documents: www.epa.gov/uic/final-class-vi-guidance-documents (accessed November 2018).

U.S. Environmental Protection Agency, 2018b, Fact sheet for geologic sequestration and injection of carbon dioxide—Subparts RR and UU: www.epa.gov/sites/production/files/2015-07/documents/subpart-rr-uu-factsheet.pdf (accessed November 2018).

Willhite, G.P., 1967, Over-all heat transfer coefficients in steam and hot water injection wells: Journal of Petroleum Technology, May, p. 607–615.

Wu, Y., and Pruess, K., 1990, An analytical solution for wellbore heat transmission in layered formations: SPE Reservoir Engineering, November, p. 531–538.

# APPENDIX A

# CONTINUOUS MODELING REFINEMENT PROCESS FOR THE INTELLIGENT MONITORING SYSTEM

## TABLE OF CONTENTS

## LIST OF FIGURES



Continued . . .

## LIST OF FIGURES (continued)



## LIST OF TABLES

# CONTINUOUS MODELING REFINEMENT PROCESS FOR THE INTELLIGENT MONITORING SYSTEM

## 1.0 OVERVIEW

### 1.1 IMS Summary

The Energy & Environmental Research Center (EERC) has completed a 3-year project focused on developing new workflows, algorithms, and a user interface for the automation and integration of carbon dioxide ($CO_2$) storage site-monitoring and simulation data as part of an intelligent monitoring system (IMS). The design for the IMS was based on injection and monitoring data acquired by SaskPower and the Petroleum Technology Research Centre (PTRC) at the Aquistore $CO_2$ Storage Site of the Boundary Dam Power Station located near Estevan, Saskatchewan, Canada (hereafter the "Site").

The IMS comprises a database that stores the monitoring measurements (IMS Database) and a graphical user interface (IMS GUI) with which the user interacts to retrieve data from the IMS Database. Lastly, the IMS Workflow defines the linkage between the IMS GUI and the IMS Database.

The IMS GUI is divided into seven modules, which are separate pages within the user interface that address specific aspects of the monitoring system:

Module 1) Well Monitoring Measurements
Module 2) Distributed Temperature System (DTS) Measurements (DTS Profiles and DTS Time-Series)
Module 3) Bottomhole Temperature (BHT) and Bottomhole Pressure (BHP) Analysis
Module 4) DTS Analysis
Module 5) Continuous Modeling Refinement (CMR) Analysis
Module 6) $CO_2$ Plume Boundary
Module 7) System Evaluation

This appendix is specific to the CMR component of the IMS, which affects Modules 5–7 of the IMS. Additional details about the Site, IMS Database, Workflow, GUI, and modules are provided in the final technical report (Azzolina and others, 2018).

### 1.2 Continuous Modeling Refinement

The CMR component of the IMS integrates two types of Site monitoring data: continuous measurements and periodic measurements. These two types of data capture different spatial and temporal scales. For example, the continuous measurements used in the CMR process include the $CO_2$ mass injection rate (Qg) and BHP acquired at the injection well. These Qg and BHP measurements were acquired at 1-minute frequency (1440 measurements per day). There are two types of periodic measurements: well logs and three-dimensional (3-D) seismic. The well log measurements include spinner logs ($CO_2$ flow distribution at the perforated intervals at the

injection well) and pulsed-neutron logs (PNLs) ($CO_2$ arrival and saturation measured at the observation well acquired at the observation well). These well log measurements are two-dimensional (2-D) data, and these measurements were acquired much less frequently (weeks or months between measurements). Lastly, the 3-D seismic data were acquired over the areal extent of the Site and with relatively long periods of time (years) between acquisitions. These continuous and periodic data are integrated through a geologic model of the Site and subsequent dynamic reservoir simulations that predict the $CO_2$ plume behavior in the subsurface in response to $CO_2$ injection. The integration of these measurements into a modeling and simulation workflow encompasses the CMR process.

The primary purpose of the CMR process is to evaluate whether dynamic reservoir simulation can accurately predict the observed dimensions of the $CO_2$ plume observed in the 3-D seismic within a reasonable error tolerance (e.g., 10%). Failure of the reservoir simulation to adequately predict the observed $CO_2$ plume may reflect a subsurface condition that is outside of normal operating limits or a need to characterize and update the geologic model. Conversely, if the CMR process rapidly and accurately predicts the observed $CO_2$ plume, then this outcome provides the operator with greater confidence that the subsurface conditions are consistent with normal operating limits.

The CMR process consists of two complementary methods, a forward-modeling workflow and an inverse-modeling workflow, that are used in combination to best match simulation results with seismic monitoring data (Figure A-1). The forward-modeling workflow uses pre-$CO_2$ injection 3-D seismic and well log measurements to characterize and create a geologic model of the subsurface that includes structure, facies, and petrophysical properties. This static geologic model is then used for dynamic reservoir simulations of the $CO_2$ behavior in the subsurface in response to $CO_2$ injection. The output from this forward-modeling workflow is the simulated $CO_2$ plume dimensions (lateral extent and depth of the $CO_2$ plume within the reservoir). The initial forward-modeling process is a manual (assisted) set of tasks supervised by specially trained staff in the reservoir simulation software. The quality of this initial forward-modeling process is evaluated by comparing the simulation results against a set of objective functions, such as how closely the predicted BHP matches the measured BHP from the monitoring well and how accurately the simulated $CO_2$ behavior in the reservoir matches the timing and extent captured by the spinner and PNL logs. This initial forward-modeling outcome is then fed into the inverse-modeling workflow.

The inverse-modeling workflow uses the dimensions of an interpreted (observed) $CO_2$ plume that was generated through seismic time-lapse analysis from pre- and post-$CO_2$ injection 3-D seismic measurements (4-D seismic). If the dimensions of the simulated $CO_2$ plume from the forward-modeling workflow match the observed $CO_2$ plume within a defined error criterion referred to as the "local objective function" (LOF), then the workflow is complete. However, if the LOF is not met, then additional adjustments are made to update the porosity and/or permeability of the initial geologic model and this updated geologic model is fed back into the forward-modeling workflow. This updated geologic model is then used to simulate a new $CO_2$ plume for comparison against the observed $CO_2$ plume. This iterative process continues until the

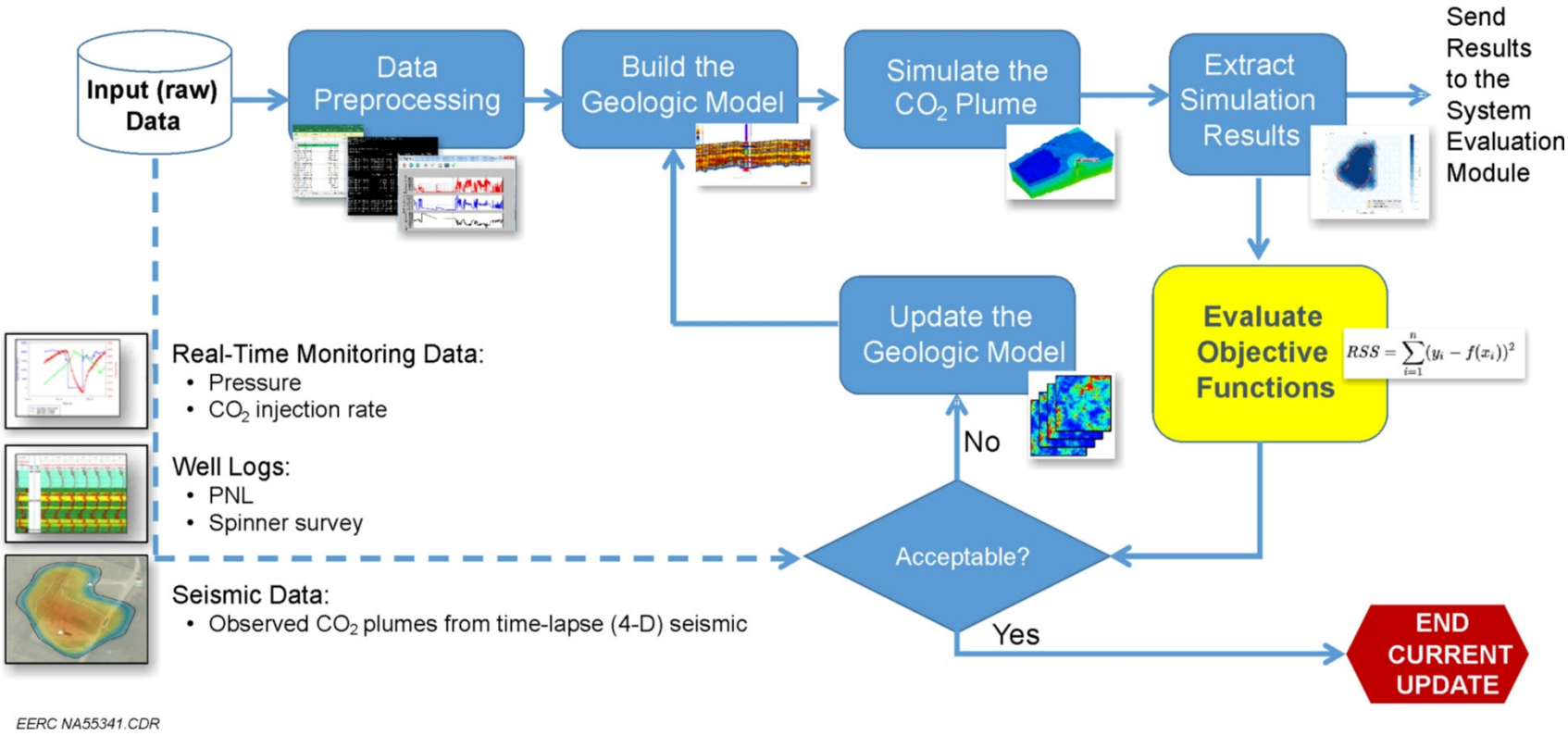


Figure A-1. Diagram showing the different steps in the CMR process.

LOF is either achieved (i.e., LOF ≤10%) or until the process reaches the maximum number of iterations (e.g., ten iterations). Figure A-2 provides an example of this CMR process. The image on the left shows a contour map of the initial simulated $CO_2$ plume as compared to an outline of the observed $CO_2$ plume, and the image on the right shows the results after five iterations of the CMR workflow.

The CMR process is the most complex module within the IMS because of the integration of multiple data types (scale and frequency), linkage of several component submodules, and interface with commercial reservoir simulation software. This appendix provides a detailed overview of the CMR process. There are three main components of this CMR process:

1. Forward-modeling to derive the baseline geologic model and initial simulation output
2. Seismic time-lapse analysis to infer the observed $CO_2$ plume boundary
3. History-matching workflow that links the forward- and inverse-modeling through Module 5 (CMR Analysis) of the IMS

The remainder of this document describes each of these three components in detail.

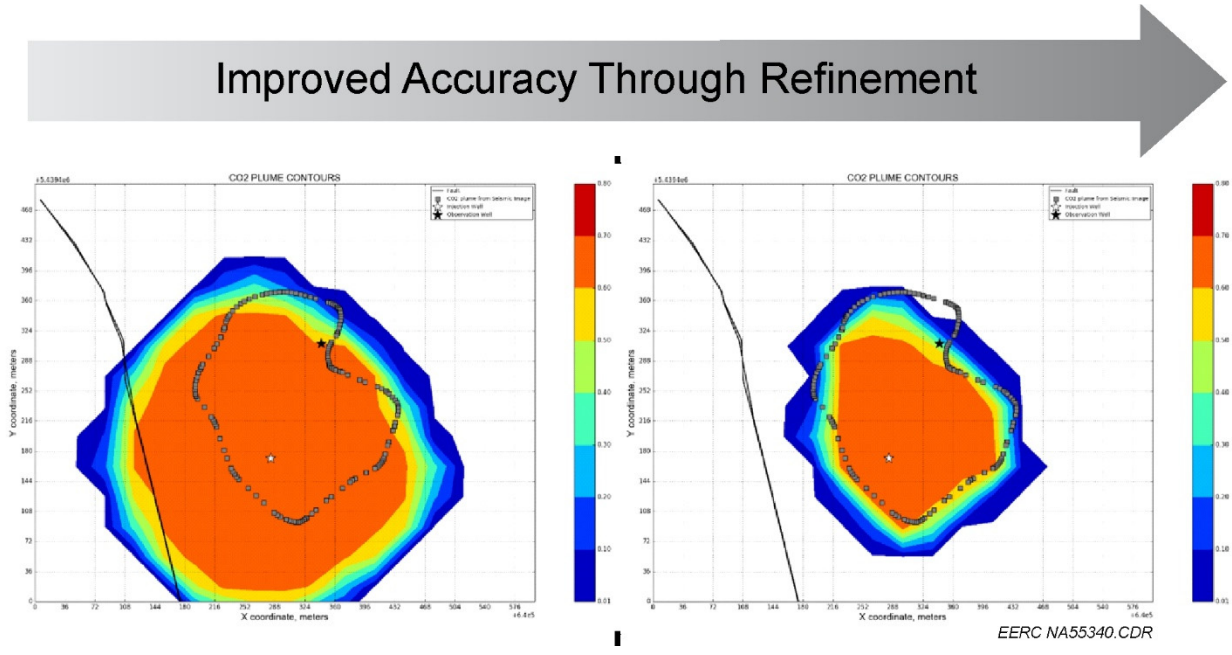


Figure A-2. Illustrative example showing contour maps of the simulated $CO_2$ plume as compared to the observed $CO_2$ plume outline (left) and (right) after five iterations of the CMR workflow. The match of the simulated and observed plume was through the inclusion of a geologic fault and its contribution to block flow.

## 2.0 FORWARD-MODELING TO DERIVE THE BASELINE GEOLOGIC MODEL AND INITIAL RESERVOIR SIMULATION OUTPUT

As part of the Plains $CO_2$ Reduction (PCOR) Partnership, a static geologic model was created in 2014 for the Site using well log data (Peck and others, 2014). The current study improved this 2014 model using a 3-D seismic data set that was acquired at the Site in 2012 prior to the start of $CO_2$ injection (hereafter "Baseline Geologic Model"). Integration of this 3-D seismic data into the Baseline Geologic Model helped improve the accuracy of the model by capturing regional structural features such as a northwestern-southeastern flexural feature that had not previously been evident using only well log data and may be an indication of possible faulting (White and others, 2016). In addition, the seismic data helped inform petrophysical property distributions such as porosity and permeability within the Baseline Geologic Model.

### 2.1 Seismic Time-to-Depth Conversion

White and others (2016) summarize the acquisition and processing parameters for the 2012 3-D seismic data set and provide a discussion about the quality and interpretation of these data. As part of the current study, the EERC expanded this seismic interpretation to pick horizons corresponding to the different perforated intervals in the reservoir in order to more accurately simulate injection into the different intervals. The seismic time data were then converted to depth using a sonic log that was acquired from the injection well. Horizons were picked on both the seismic time data and the depth-converted seismic data. Horizons picked on the 3-D seismic depth data were used to replace the original well-derived layer surfaces and to define the layers in the Baseline Geologic Model (Figure A-3).

### 2.2 Poststack Inversion

Poststack inversion was carried out to derive rock properties from the 3-D seismic data to better inform the porosity and permeability distributions in the Baseline Geologic Model. The interpreted time horizons and the sonic log for the injection well were used to build an initial compressional-wave velocity model (Figure A-4, left panel). Model-based poststack inversion was done using the seismic time data and well log data to produce a compressional-wave volume (Figure A-4, right panel). Inversion parameters were chosen to optimize the match between inversion results and well log data within the different perforated intervals in the reservoir. A statistical wavelet extracted from a single inline intersecting the injection well was used for inversion.

### 2.3 Porosity Volume

The inverted compressional-wave velocity volume was used to calculate a porosity volume. An empirical relationship between compressional-wave velocity and porosity was calculated using Wyllie's time-average equation (Wyllie and others, 1956):

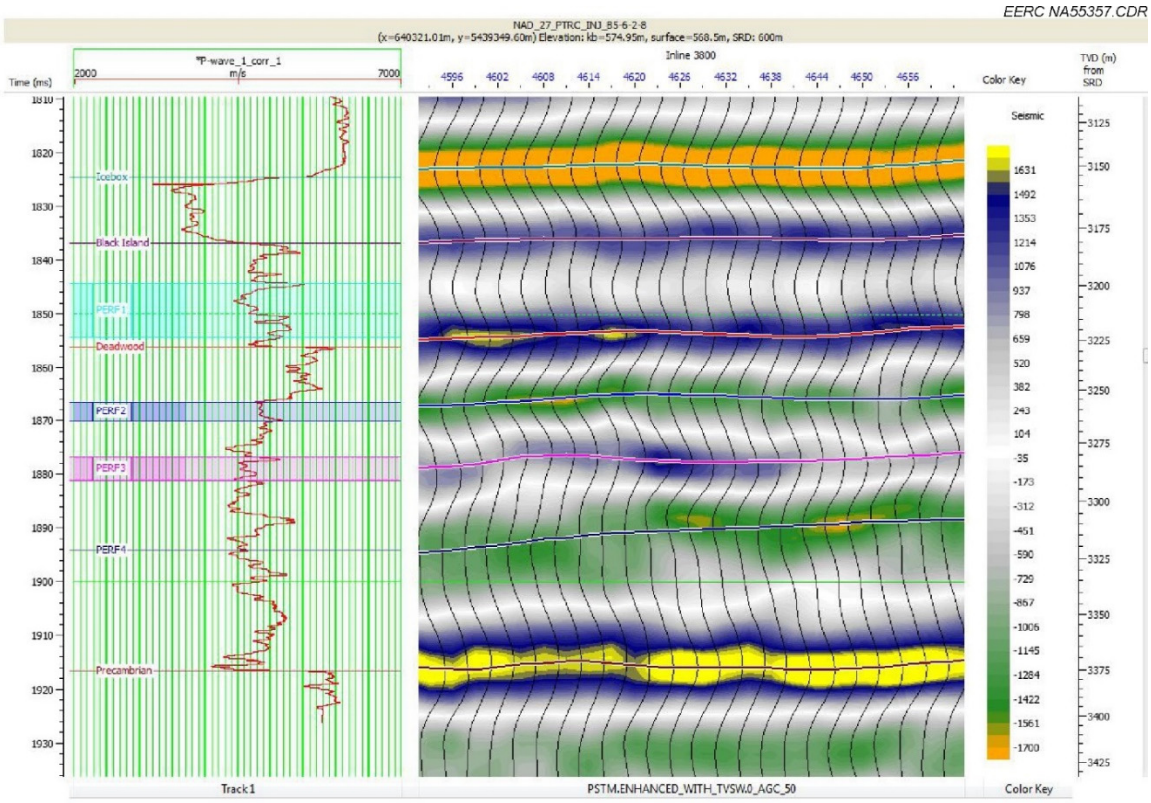


Figure A-3. Left: sonic log for the injection well showing the interpreted formation tops and the four different perforation intervals (PERF 1, 2, 3, and 4). Right: an inline from the 2012 3-D seismic time data set that intersects the injection well. Interpreted horizons are displayed on the seismic cross section with colors corresponding to the specific formation tops. A 50-microsecond window automatic gain control (AGC) was applied to the seismic data to aid horizon interpretation.

$$\frac{1}{v} = \frac{\emptyset}{v_f} + \frac{1-\emptyset}{v_m} \qquad \text{[Eq. 1]}$$

where $\emptyset$ is the total porosity, $v$ is the measured compressional-wave velocity, $v_m$ is the velocity of the rock matrix, and $v_f$ is the velocity of the fluid in the pores. Equation 1 can be rearranged to solve for porosity as shown below:

$$\emptyset = \frac{v_f(v-v_m)}{v(v_f-v_m)} \qquad \text{[Eq. 2]}$$

Constants were assigned for the rock matrix and fluid velocity in Equation 2. The values used were 1623 m/sec for the fluid velocity, assuming a saturated saltwater mud filtrate, and 5500 m/sec for the matrix velocity, assuming a clean sand matrix for the Deadwood Formation. Well log values for the Perforation 2 interval were used to check the accuracy of this empirical relationship. Perforation 2 was selected because additional testing conducted by PTRC has concluded that most of the injected $CO_2$ enters the reservoir through this perforation (PTRC, personal communication). Results indicated that an additional scale factor of 1.2057 was needed, resulting in the following empirical relationship:

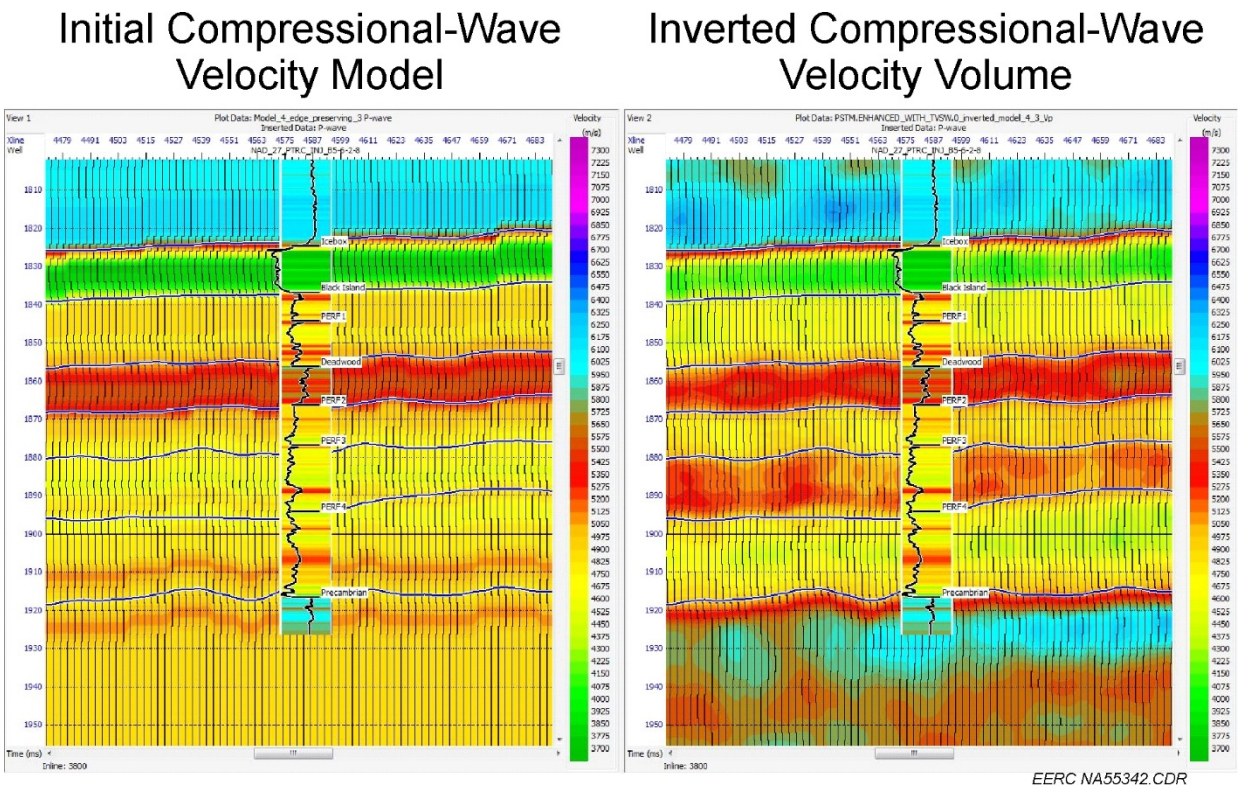


Figure A-4. Color-filled cross sections including the initial compressional-wave velocity model used for poststack inversion (left) and inverted compressional-wave velocity volume generated from poststack inversion (right). Interpreted horizons are shown in blue. The sonic log and formation tops are shown in black overlying the color-filled compressional-wave velocities associated with the sonic logs that are outlined in white.

$$\emptyset = \frac{2776\frac{m}{s}}{v} - 0.5047 \qquad \text{[Eq. 3]}$$

A 3-D porosity volume was calculated using the inverted compressional-wave velocity volume and the empirical relationship in Equation 3 (Figure A-5).

Computed porosities in geologic intervals with clean sand, such as Perforation 2, matched the sonic-porosity values that were measured at the injection well. However, there was an expected mismatch between sonic-porosity values and calculated porosity values for intervals with a higher shale content because the empirical relationship between porosity and compressional-wave velocity was derived for a clean sand matrix. The resulting porosity distributions within each shale interval were normalized to the porosity values measured from core samples that were collected from these shale intervals. This normalization process retained the relative pattern of distribution of porosity values from the seismic data while constraining the range of the distribution according to core sample measurements. Porosities within the sandstone intervals were also normalized to the range of core sample-measured porosities for each zone.

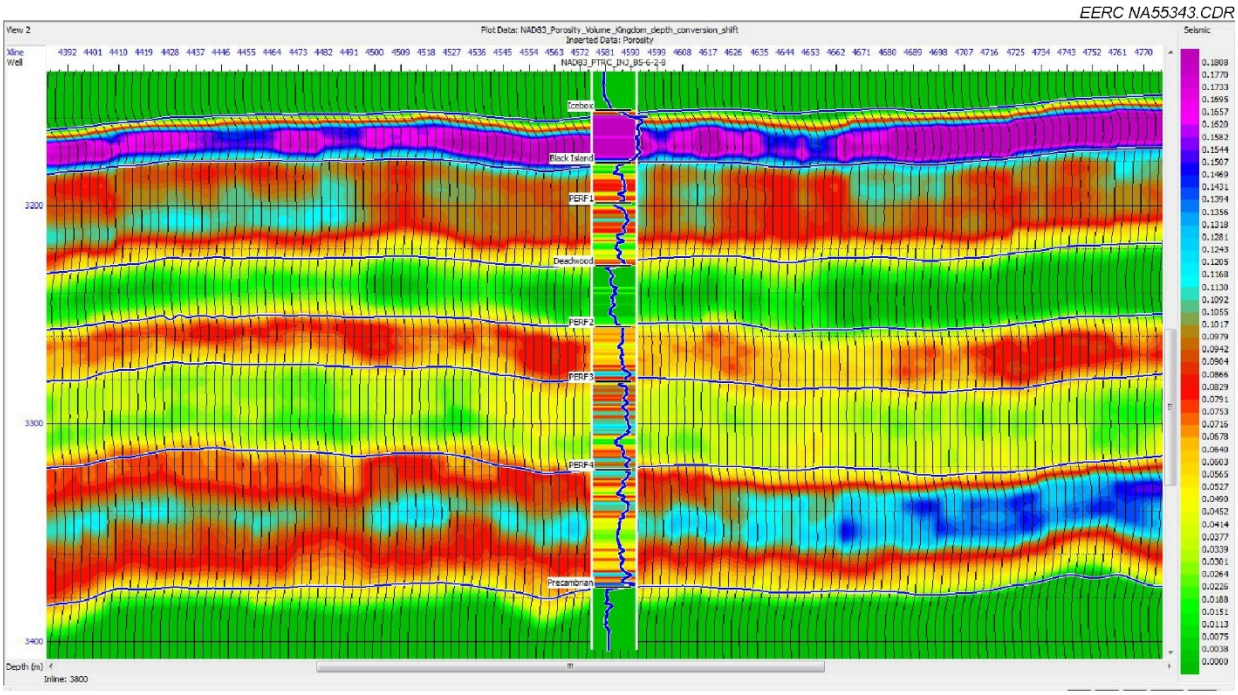


Figure A-5. Color-filled cross section of the calculated porosity. Interpreted horizons are shown in blue. The sonic log and formation tops are shown in black overlying the color-filled porosity values associated with the sonic porosity logs that are outlined in white.

Variogram analysis and per zone porosity/permeability crossplots (generated from core sample measurements) were used to populate the model with permeability values based on the porosity volume. Table A-1 shows the range of porosity and permeability values for each of the intervals within the Baseline Geologic Model.

**Table A-1. Porosity and Permeability Ranges for the Geologic Model Subintervals**

| Zone | Lithology | Porosity, v/v | Permeability, mD |
|---|---|---|---|
| Icebox | Shale | 0.01–0.06 | 0.06–2.10 |
| Black Island | Sandstone | 0.02–0.14 | 0.04–97.00 |
| Black Island Shale | Shale | 0.01–0.06 | 0.06–2.10 |
| Perf 1 Top | Sandstone | 0.02–0.14 | 0.04–97.00 |
| Deadwood | Shale | 0.01–0.06 | 0.06–2.10 |
| Perf 2 Top | Sandstone | 0.03–0.16 | 17.74–271.37 |
| Perf 2 Base | Shale | 0.01–0.06 | 0.06–2.1 |
| Perf 3 Top | Sandstone | 0.03–0.16 | 0.01–312.3 |
| Perf 3 Base | Shale | 0.01–0.06 | 0.06–2.1 |
| Perf 4 Top | Sandstone | 0.03–0.16 | 0.01–312.3 |

The petrophysical properties of the model were then upscaled into a coarser model grid (36-m × 36-m grid cells) that was clipped to the extent of the seismic porosity volume. This upscaling process reduced the model extent and total cell count, enabling numerical simulations to be conducted more efficiently. This Baseline Geologic Model represents the initial (base case) model utilized for generating the initial reservoir simulation output of the $CO_2$ plume distribution.

### 2.4 Initial Simulated $CO_2$ Plume

As described above and illustrated in Figure A-1, the outcome of the forward-modeling process is the simulated $CO_2$ plume dimensions. The initial reservoir simulation output used the Baseline Geologic Model, and the simulation was calibrated with historical injection data using the Computer Modelling Group, Ltd. (CMG) numerical reservoir simulator, GEM, (Computer Modelling Group, Ltd., 2016b) together with the CMG's assisted history-matching tool, CMOST. The best-case reservoir simulation obtained with CMOST (Computer Modelling Group, Ltd., 2016a) (hereafter "Initial Simulated $CO_2$ Plume") provides the initial simulation output used in the first iteration for inverse-modeling using the automated history-matching (AHM) workflow (see Section 4.0). This best-case reservoir simulation represents a human-supervised (assisted) process and incorporates injection and monitoring data from the onset of the injection operation through June 2017. This initial calibration step did not incorporate the observed $CO_2$ plume interpreted from seismic data.

CMOST reservoir simulations were constrained on the historical $CO_2$ injection rate, and the simulation quality was evaluated with three field observations:

- BHP response in the injection well
- Spinner survey data ($CO_2$ flow distribution at the perforated intervals at the injection well)
- PNL data ($CO_2$ arrival and saturation measured at the observation well)

Data preprocessing routines were used prior to converting the $CO_2$ injection rate, and BHP measurements for simulation input (Figure A-1). These data preprocessing steps attempt to minimize the measurement uncertainty prior to converting the observed data into simulation model inputs. The data preprocessing for these inputs included cleaning, filtering, and resampling steps for transforming the raw (unprocessed) data stored in the IMS Database into an input format that is compatible with commercial simulation software. These functionalities used Python scripts and open-source scientific libraries to perform the data query, noise removal, outlier detection, custom-filtering application, and reduction to sizes and rates compatible with simulation models and algorithm performance (Python Core Team, 2018).

Figure A-6 provides an example of the cleaning, filtering, and resampling functionalities used to preprocess continuous monitoring data. Figure A-6a (top panel) shows the $CO_2$ mass injection rate (Qg, tons per day), and Figure A-6b (bottom panel) shows BHP, psi. Three data sets are shown: 1) original raw data set, 1-minute resolution (light blue); 2) cleaned and resampled 1-day resolution (dark blue); and 3) cleaned, resampled, and filtered using a standard deviation factor (stars). The averaging of the measurements from 1-minute to 1-day resolution significantly reduces noise (uncertainty) in the measurements, and the standard deviation factor further eliminates outliers.

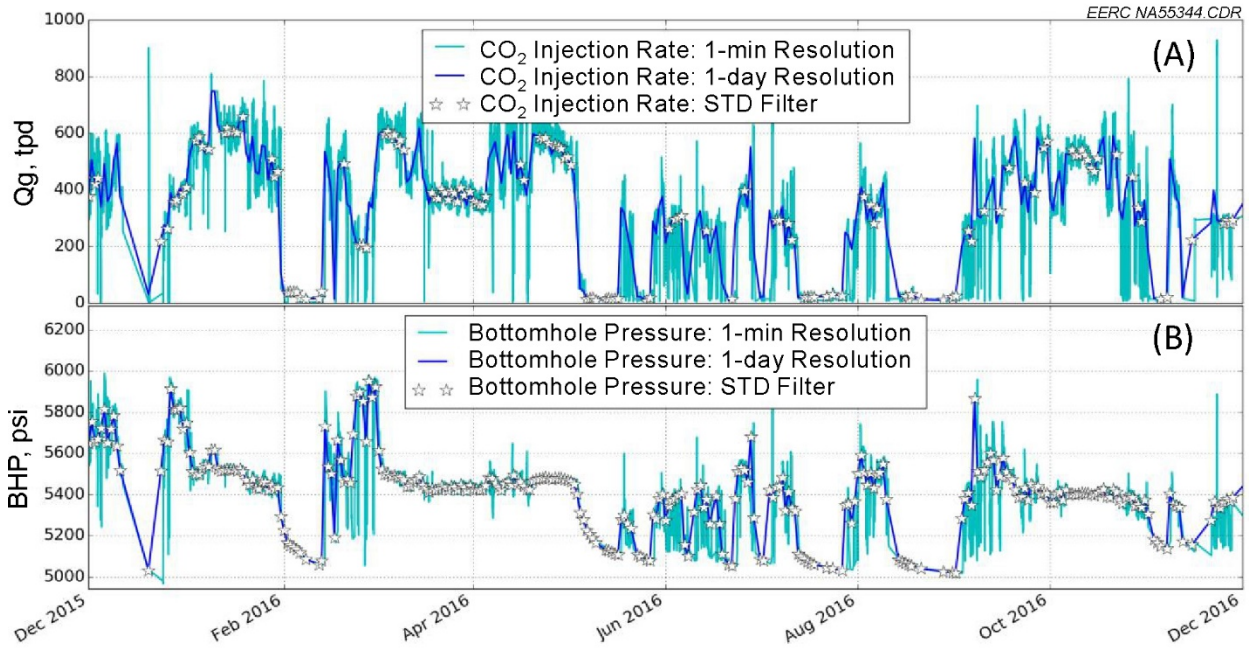


Figure A-6. Example of the data preprocessing steps of cleaning, filtering, and resampling used for continuous monitoring data such as A) $CO_2$ mass injection rate (Qg, tons per day) and B) BHP, psi. Three data sets are shown: 1) original raw data set, 1-minute resolution (light blue); 2) cleaned and resampled 1-day resolution (dark blue); and 3) cleaned, resampled, and filtered using a standard deviation factor (stars).

The integration of the well log data required an external preparation step. Because of the uncertainty associated with well log measurements, human (scientific and engineering) judgment is needed to transform the raw measurements into an interpreted output. These interpretations were done outside of the IMS, and the interpreted well-log measurements were used to evaluate simulation quality.

Well-logging data provide valuable information about the injectivity at each perforation zone (using the gas rate profile obtained from the spinner log) and the interwell heterogeneity between the injection and observation well based on the $CO_2$ breakthrough behavior at the observation well (using the gas saturation profile obtained from the PNL). Figures A-7 and A-8 show examples of the successfully calibrated simulation models using periodic logging data. This step is important to reduce uncertainty in injection performance prediction and provide better simulated $CO_2$ plume prediction accuracy. Figure A-7 shows the simulated and calculated gas rate profiles versus depth from the spinner survey data collected in April 2015. Spinner surveys can provide valuable information about the injectivity of perforation zones, which help with tuning the well index in the simulation model at selected dates for history matching. As a simplifying assumption, the reservoir simulation assumes that the well index does not change, unless there is

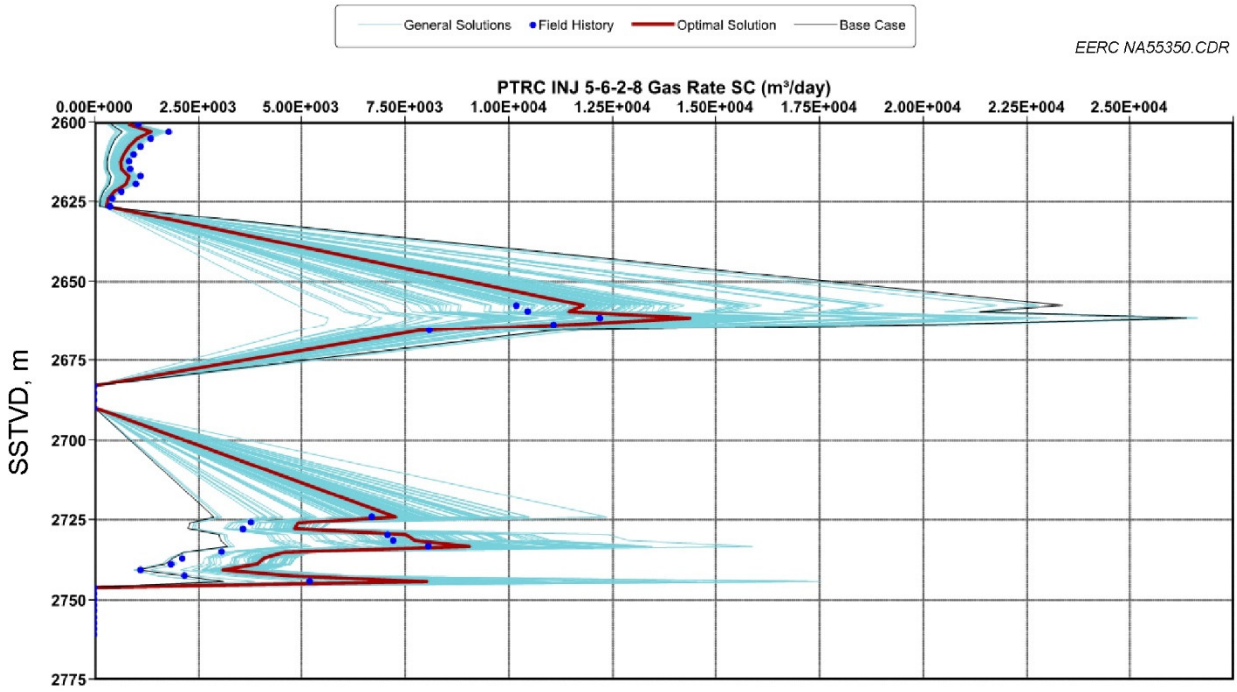


Figure A-7. Vertical gas rate profile ($m^3$/day) at the injection well in April 2015. Blue circles are measured data points from the spinner log injectivity profile. Simulated results were obtained with the CMOST AHM study. The solid black line is the simulation base case, and the solid red line is the optimal simulation case. Other simulation results (multiple realizations) are shown as light blue lines.

a significant effect observed from spinner surveys. Figure A-8 displays the simulated and calculated saturation of the $CO_2$ that arrived at the observation well from the PNL data collected in February 2016. Once breakthrough occurred in the observation well, subsequent PNL logs provided little information about the $CO_2$ plume distribution (unless breakthrough timing varies for each perforation interval).

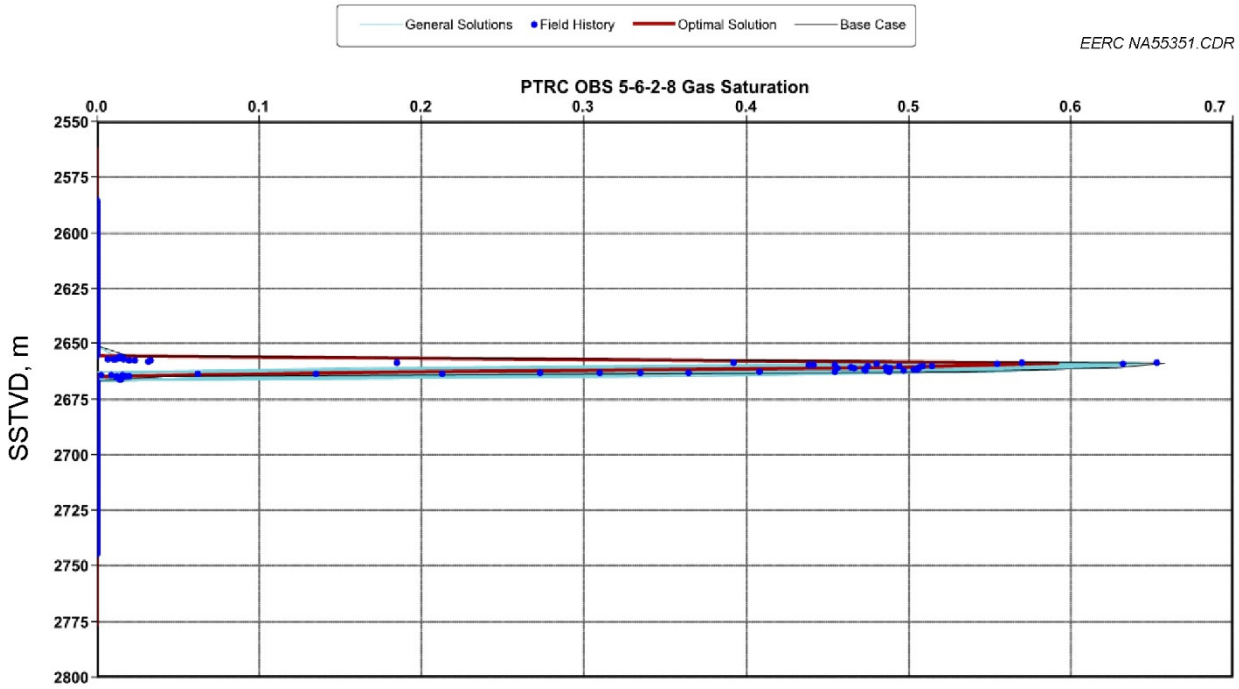


Figure A-8. Vertical gas saturation profile at the observation well on February 2016. Blue circles are measured data points from the PNL profile. Simulated results were obtained with the CMOST AHM study. The solid black line is the simulation base case, and the solid red line is the optimal simulation case. Other simulation results (multiple realizations) are shown as light blue lines.

Approximately 140 numerical simulations were generated during the AHM process. The optimal (best) case had a global history-matching error of 6.5%. Figure A-9 shows a time-series plot of the predicted BHP from the reservoir simulations as compared to the measured BHP for the general solutions (blue lines) and the optimal solution (red line). The results from this optimal numerical simulation were used as the Initial Simulated $CO_2$ Plume into the AHM workflow.

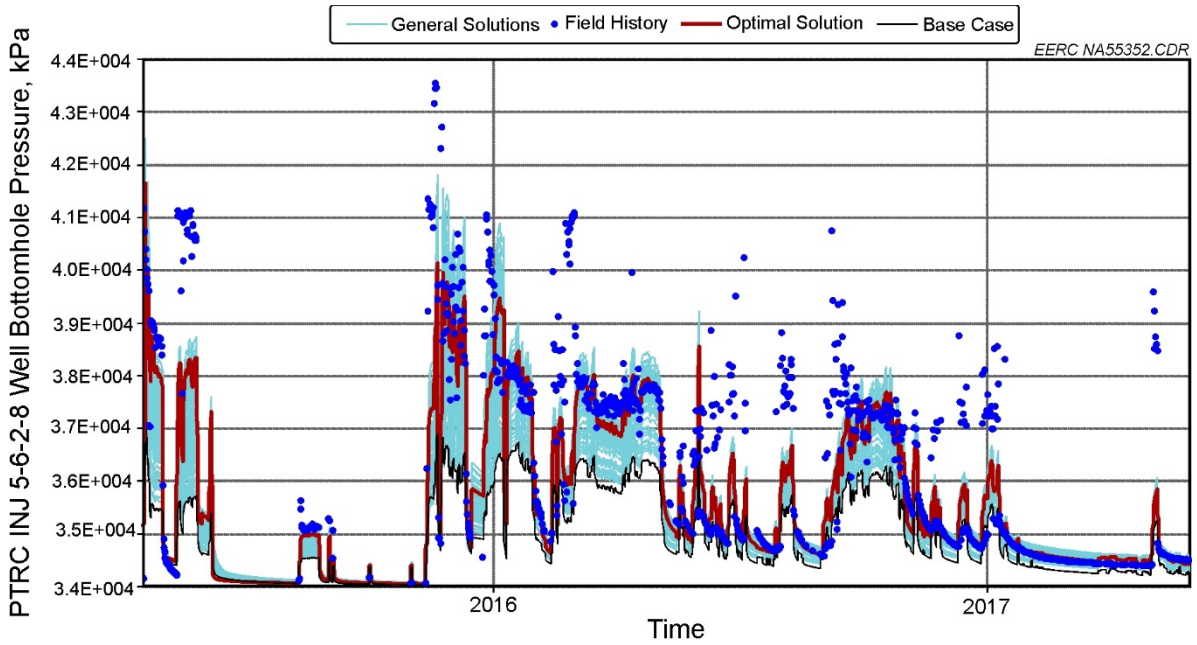


Figure A-9. Time-series showing the BHP at the injection well. Blue circles are measured data points from the BHP gauge. Simulated results were obtained with the CMOST AHM study. The solid black line is the simulation base case, and the solid red line is the optimal simulation case. Other simulation results (multiple realizations) are shown as light blue lines.

## 3.0 DERIVING THE OBSERVED $CO_2$ PLUME BOUNDARY

### 3.1 Seismic Time-Lapse Analysis

Time-lapse 3-D seismic data often referred to as 4-D seismic due to the addition of the time dimension acquired from the Site were used to estimate the $CO_2$ plume boundary. Conventional time-lapse analysis was applied to the data set to generate an interpreted $CO_2$ plume image. This interpreted $CO_2$ plume image is considered the empirical evidence (with uncertainty) of what is occurring in the subsurface and provides the input to the inverse-modeling workflow (Figure A-1).

The 4-D seismic data used to generate an interpreted $CO_2$ plume image included a preinjection baseline and a postinjection seismic survey using a permanent seismic array installed at the Site to collect repeat seismic data as part of the monitoring program on an as needed basis (months to years) (Figure A-10). White and others (2015) describe in detail the parameters of this permanent seismic array. Several sources have been tested and deployed to collect data using the permanent array, including dynamite, vibroseis, and a permanently installed orbital vibrator referred to as the Accurately Controlled, Routinely Operated Signal System (or ACROSS) source (White and others, 2015; Nakatsukasa and others, 2016). The 4-D seismic data input into the history-matching workflow were acquired during a preinjection survey conducted in March 2012 and a postinjection survey conducted in February 2016 (Monitor 2) using the permanent array and dynamite sources. Roach and others (2017) discuss the acquisition and processing parameters for these two data sets.

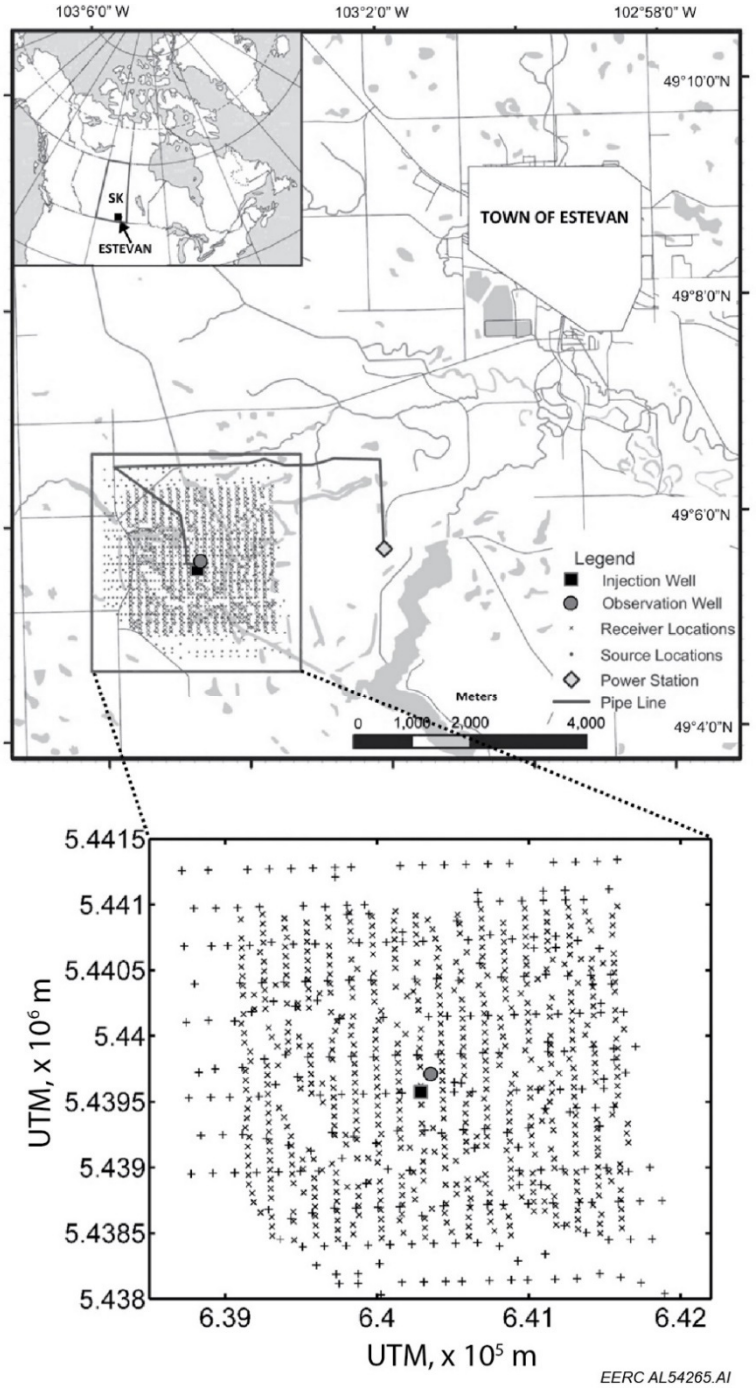


Figure A-10. Map showing the location of the Site including the permanent seismic array and injection and observation wells (Roach and others, 2017) UTM means universal transverse mercator.

### 3.2 4-D Seismic Difference and Normalized Root Mean Squared

Standard 4-D analysis of the pre- and postinjection seismic data sets resulted in the interpretation of change in the reservoir due to injected $CO_2$, which is indicated by differences in the amplitude and/or arrival time of the reservoir reflections. To quantify these differences, normalized root mean squared (nRMS) values were calculated over the different perforated intervals in the reservoir. Differences in the reservoir are evident in the Perforation 2 interval. The nRMS values computed over the Perforation 2 interval indicate the extent of change in the reservoir between the pre- and postinjection seismic data sets (Figure A-11).

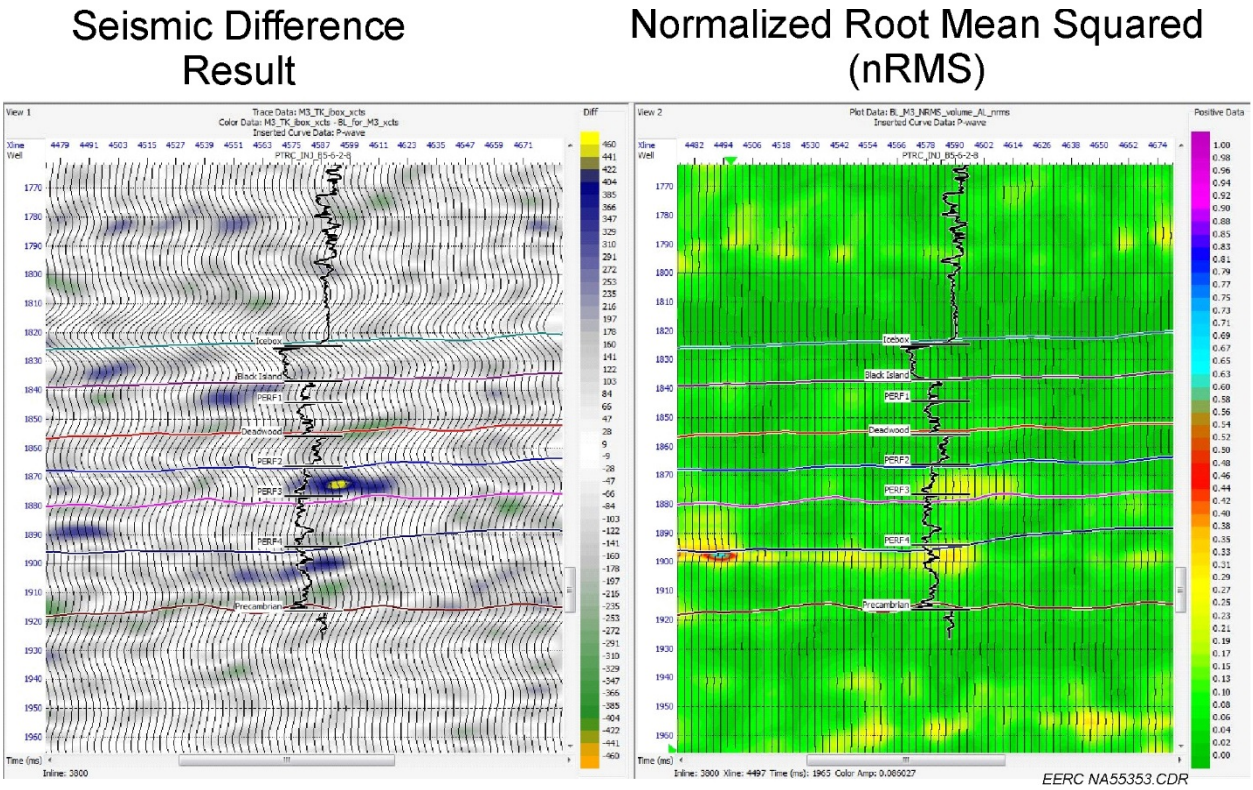


Figure A-11. Cross section intersecting the injection well showing (left) the difference calculated by subtracting the preinjection 3-D seismic volume from the postinjection 3-D seismic volume and (right) the cross-section nRMS values calculated over a 10-microsecond sliding window for the pre- and postinjection seismic data sets.

### 3.3 Mapping the Interpreted $CO_2$ Plume

The nRMS values were mapped across the areal extent of the model. The mapped nRMS amplitudes provide an aerial extent of the interpreted $CO_2$ plume and indicate that this change extends from the injection well to the observation well (Figure A-12). PNL measurements acquired from the observation well on February 24, 2016, around the time the postinjection seismic data

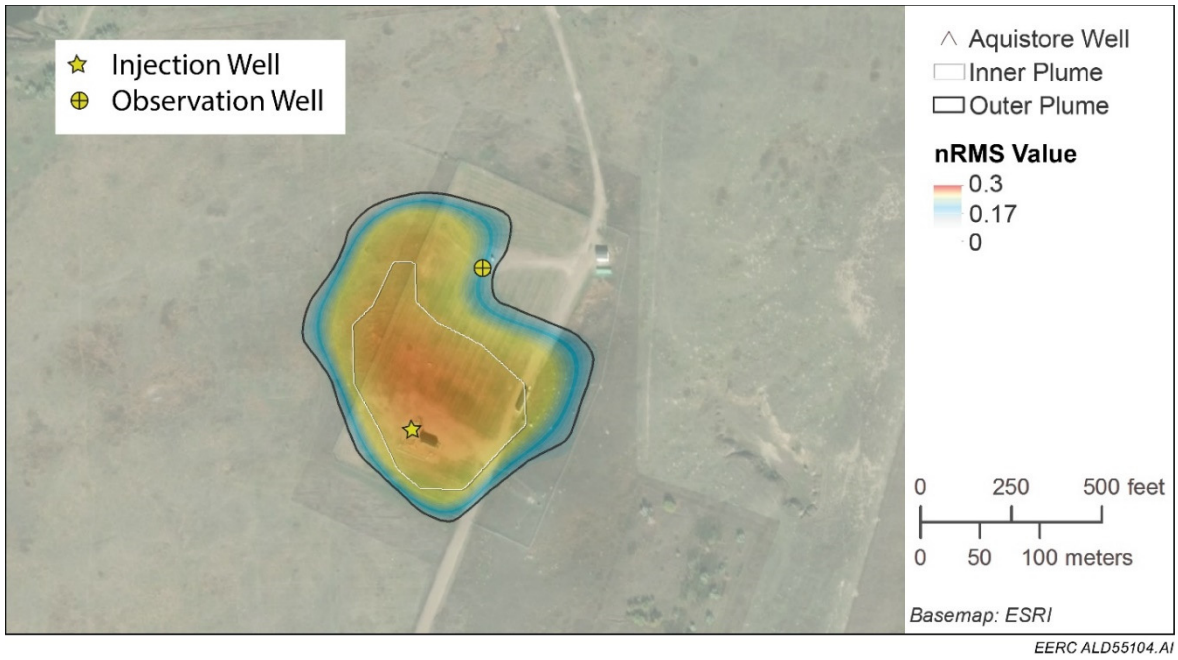


Figure A-12. Map of the nRMS difference values for the March 2012 and February 2016 3-D seismic data acquired at the Site. Values were calculated over a 10-microsecond window centered at 1874 microseconds. Smoothing was applied in ArcMap prior to interpretation. An outer plume extent was interpreted as shown by the black outline, and inner plume extent was interpreted as shown by the white outline.

were acquired, confirmed that $CO_2$ had reached the observation well in the Deadwood sand interval from 3233 to 3239 m that corresponds to the Perforation 2 interval in the injection well (Dalkhaa and others, 2017). Therefore, the differences evident in the Perforation 2 interval from 4-D seismic analysis of the two seismic data sets are likely attributable to the change in $CO_2$ saturation, and the extent of this change is representative of the extent of the injected $CO_2$ plume. The nRMS amplitude map generated for Perforation 2 was used to interpret the $CO_2$ plume extent. The results from this seismic time-lapse analysis were used as the observed $CO_2$ plume boundary input to the history-matching workflow for the inverse modeling. The inverse modeling will then provide greater model confidence for future forecasting scenarios.

## 4.0 AUTOMATED HISTORY-MATCHING WORKFLOW

### 4.1 Overview

The AHM workflow developed for Module 5 (CMR Analysis) uses inverse modeling made up of Python scripts that compare the dimensions of the observed $CO_2$ plume to the simulated $CO_2$ plume and quantify this comparison using an error criterion referred to as the "LOF." If the LOF is within a specified error tolerance (e.g., 10%), then the AHM workflow is complete. However, if the LOF is not met, then additional adjustments are made to update the porosity and/or permeability of the Baseline Geologic Model, and this updated geologic model is fed back into the

forward-modeling workflow. This updated geologic model is then used to simulate a new $CO_2$ plume for comparison against the observed $CO_2$ plume. This iterative process continues until the LOF is either achieved (i.e., LOF ≤10%) or until the process reaches the maximum number of iterations (e.g., ten iterations).

### 4.2 Forward- and Inverse-Modeling Theory

The term "history matching" in the AHM workflow context refers to a special kind of inverse problem where field measurements are used to estimate a set of reservoir simulation model parameters. Since these parameter estimates are conditioned on field measurements, they provide a model that can generate more accurate predictions. In the petroleum industry, history matching has become the standard validation step for a reservoir model prior to generating future scenario estimates (forecasts of oil production or subsurface saturation changes). The AHM workflow builds upon several decades of research on the upstream sector of the petroleum industry. Additional details on these concepts can be found in Oliver and others (2008) and Oliver and Chen (2011).

Prior to understanding the inverse problem, it is helpful review the forward-modeling approach. The prediction problem for a forward model is defined as follows:

$$G(m, v) = d_{pred} \quad \text{[Eq. 4]}$$

where $G$ denotes a mathematical function (i.e., the model) that describes the fundamental physics of the system being modeled. In the case of simulating $CO_2$ behavior in the reservoir in response to $CO_2$ injection, $G$ contains a set of partial differential equations describing the multiphase-flow ($CO_2$ and formation fluids) in porous media, which are solved in the form of a numerical reservoir simulator. The model parameters are represented by $m$, $v$ is the symbol for the input variables, and $d_{pred}$ refers to the predicted outcome. Equation 4 states that the model output can be calculated given the model parameters, the input variables, and the function [Oliver and others, 2008].

As the name implies, the inverse problem refers to the reverse calculation, i.e., treating the model parameters as unknowns and observing the data, $d_{obs}$. Observation data could be of several types, such as a time-series (e.g., fluid rates or wellbore pressures) or discrete data points (e.g., fluid breakthrough, production logs, or core samples). An important characteristic of real-world applications of the inverse problem is that the observation data generally contain some form of noise (uncertainty) component ($\eta$), which includes both natural variability in the true value of the measurement and measurement error. Therefore, the inverse problem can be expressed as follows:

$$d_{obs} = G(m, v) + \eta \quad \text{[Eq. 5]}$$

Equation 5 states that the set of model parameters ($m$) could be estimated from the information contained within the observed data, $d_{obs}$. However, the presence of measurement uncertainty creates challenges for accurately estimating the model parameters and is an important consideration for designing a robust AHM workflow. A primary objective of data preprocessing steps is to minimize the measurement uncertainty prior to converting the observed data into model inputs.

History matching is often an ill-posed problem, in the sense that there are many possible solutions that can honor the observations [Oliver and Chen, 2011]. While many techniques have been developed in the previous four decades, there will always be a component of uncertainty in the estimation of reservoir simulation parameters. Therefore, the ultimate goal of the AHM workflow used in the IMS should not be regarded as an attempt to generate the perfect model. Instead, the goal of the AHM workflow is to reduce model uncertainty through data integration and a careful process of model calibration. By reducing model uncertainty, the model outcomes will be more reliable, and the site operator will have more reliable data with which to make informed decisions for managing the $CO_2$ injection operations.

The process adopted in the current AHM workflow is to utilize the observed $CO_2$ plume as the observed data ($d_{obs}$) and to modify the porosity and permeability of the geologic model as the parameters of the model ($m$). Other aspects of the geologic model are considered constant in this application, as is the observed $CO_2$ plume. To preserve the information gathered from the seismic data integration, the AHM workflow begins with the porosity field from the Baseline Geologic Model. Subsequent iterations of the AHM workflow update the geologic realizations by varying porosity and/or permeability in the area surrounding the observed $CO_2$ plume boundary.

### 4.3 Incorporating Python Scripts

Integration of different data types into the AHM workflow required data structures and tools to favor coding efficiency, minimal maintenance, and flexibility. When possible, the project team utilized open-source packages maintained by an active scientific community in Python. For example, the data structures that store spatial and temporal data from the 3-D reservoir model (pressure, $CO_2$ saturation, porosity, permeability, etc.) utilize the multidimensional arrays provided by the Python extension module, *NumPy* (NumPy, 2018). This is crucial for being able to perform efficient computations with large arrays. *NumPy* also allows usage of advanced options for filtering and indexing, flexible array manipulation methods, and efficient memory allocation and storage. This allows the performance of efficient operations such as matrix calculations, plane slicing, and threshold definition. Most of the scientific computation functions (e.g., regression, interpolation, contour location, and statistical analysis) use the Python module, *SciPy* (SciPy, 2018). Lastly, the plotting library, *Matplotlib*, was used to visualize 2-D and 3-D data sets (Matplotlib, 2018), and the open-source package, *Pandas*, was used for working with time-series data sets (Pandas, 2018).

Python scripts execute and handle two CMG software applications for performing the AHM calculations: “Results Report” and GEM (Computer Modelling Group Ltd., 2016a; 2016b). The Results Report is a CMG postprocessing application, which can be executed in batch mode from an MS-DOS prompt. The “Results Report” allows extracting information from CMG’s simulation results files (SRF). Information in the original SRF files is stored in binary format. The Results Report allows exporting selected simulation results into ASCII files using a system of keyword commands. The keyword commands are placed in an input text file, which Results Report will read to produce the output files.

Although the AHM is implemented in the form of Python scripts, these functionalities are fully compatible with commercial tools such as CMOST. This flexibility permits the workflow to

be seamlessly adjusted to semiautomatic mode should the user encounter difficulties obtaining a satisfactory automated history match. Compatibility with commercial tools such as CMOST provides numerous advantages for future IMS development. For example, compatibility with commercial tools provides access to a number of state-of-the-art functionalities that are continuously being developed and improved by highly specialized research and development (R&D) teams. However, for the routine work of the monitoring activities, those functionalities should not be necessary to get a reasonable update of the geologic model and reservoir simulations.

### 4.4 Automation

There are three key components of the AHM workflow that perform the automated history match: i) preparing CMG input files (Builder), ii) running CMG simulations (Launcher), and iii) extracting results from CMG simulation files (Reader). The environment variables (project folder, file system, log files, etc.) and commands are labeled appropriately to identify and track each iteration. The scripts automatically handle data exchange and synchronize the file managements. Each iteration starts with the following three-step sequence:

i. Builder:
   - Prepare the environment variables (working path, CMG paths, historical data file, etc.).
   - Build the CMG inputs for the numerical experiments using the template (base case) and include files (model parameters).

ii. Launcher:
   - Prepare command lines and launch the external applications (Results Report, GEM, Python libraries, etc.).
   - Monitor the execution, and terminate programs if necessary.

iii. Reader:
   - If the simulation is successful, then extract the results, and return a vector with those simulation results needed to feed the objective functions.
   - If the simulation is not successful, then return a warning message.

The observed $CO_2$ plumes' actual shape and location, as determined through 4-D seismic time-lapse analysis, were transferred to the IMS Database in the form of an American Standard Code for Information Interchange (ASCII) table with coordinates and attributes per layer. The porosity and permeability of the Baseline Geologic Model are iteratively updated to match this 4-D seismic time-lapse analysis.

Porosity and permeability updates are stored in "include" files (text files containing an array with numerical values for each cell in the 3-D geologic model domain). These include files facilitate handling user-defined model parameters and, at the same time, managing large data arrays. The CMG simulation file is used as a master template, which contains keywords referring to each model parameter changed by the AHM workflow. Each numerical experiment is automatically built replacing parameter values into the master template.

The integration and automation scripts have a large degree of flexibility. Other geologic models and/or parameters can be adapted and automated with the existing AHM workflow.

### 4.5 Sector Model

Minimization of the AHM computational requirements is necessary for making the AHM workflow a real-time application. The size of the computational domain and the number of cells are important factors that affect the simulation time (simulation time tends to grow exponentially with the number of model grid cells). One common approach is finding the smaller model size that still fits the modeling needs regarding the areal distribution of the $CO_2$ plume, i.e., a model that is sufficiently large enough by areal extent to capture the pressure and saturation evolution. An effective method is to divide the reservoir into sector models that may be substantially smaller than the original domain while still capturing the main physics affecting the results (Dzyuba and others, 2012). Exploratory work conducted as part of the current study showed that during the first 2 years of $CO_2$ injection at the Site, large areas of the model domain remain unaffected because the injected volumes are relatively small in relation to the total reservoir volume. For that reason, one valid option to reduce the AHM time requirements is to run the numerical simulations using a sector model that incorporates an area sufficiently large to capture the $CO_2$ plume transport at the equivalent monitoring time. By using a sector model, the simulation time can be reduced between 10- to 60-fold as compared to the full simulation model. Preliminary tests showed that running sector models with an area of 2.5 km × 2.5 km significantly reduces the simulation time, from a few hours to less than 5 minutes. While the sector model is less accurate than the full model, this approach still provides sufficient information for helping to reduce the simulation uncertainty through improved geologic property distributions. Therefore, the current AHM workflow allows the user to select from two different options: running the full simulation model or running the sector model.

### 4.6 Evaluation of Goodness-of-Fit

The AHM workflow links CMG tools with Python scripts to compare the observed $CO_2$ plume from the 4-D seismic time-lapse analysis and the simulated $CO_2$ plume from dynamic simulations using a LOF. The goodness-of-fit between the observed and simulated $CO_2$ plumes is calculated using a formulation adapted after the work of Hiebert and others (2013). In Equation 6, the numerator measures the disagreement between the observed and simulated $CO_2$ plumes, while the numerator measures the agreement. This LOF has intuitive physical and mathematical meanings. When the observed and simulated parameters agree, then the term $\alpha_i$ in the numerator in Equation 6 will converge toward zero, so the LOF will tend toward zero. Conversely, when the observed and simulated parameters are in disagreement, then the term $(1-\alpha_i)$ in the denominator in Equation 6 will tend toward zero, and the LOF will tend toward a larger number. The LOF is always positive and bounded at zero.

The LOF is computed according the following equation:

$$LOF = \frac{\sum(S_{g,i*}V_i)\alpha_i}{\sum(S_{g,i*}V_i)(1-\alpha_i)} \text{ ; with } \alpha_i = (M_i - S_i)^2 \qquad \text{[Eq. 6]}$$

Where:

$V_i$ is the gas per unit area of each grid block; which is used as weighting factor

$S_{g,i}$ is the gas saturation in each grid block; which is used as feature

$M_i$ is a measurement-derived parameter, defined as a binary index to indicate if the block $i$ is inside the observed $CO_2$ plume ($M_i = 1$) or not ($M_i = 0$)
$S_i$ is a simulation-derived parameter, defined as a binary index to indicate if the block $i$ is inside the simulated $CO_2$ plume ($S_i = 1$) or not ($S_i = 0$)
$\alpha_i$, defined as the "agreement" factor, is a parameter that measures whether there is an intersection between the measured and simulated parameters

### 4.7 Porosity and Permeability Updates

The AHM workflow for updating porosity and permeability values in the geologic model follows a local updating approach. However, the current AHM architecture is flexible, such that if more advanced IMS prototypes are required, then the new functionality can be easily added as a new module.

The update of the geologic model properties uses the porosity volume derived from 4-D seismic difference data as a reference (Baseline Geologic Model). The AHM workflow then redefines the observed and simulated $CO_2$ plumes into binary outcomes. This process defines a measurement-derived binary index, $M_i$, from the 4-D seismic difference volume. $M_i$ is defined as a binary index to indicate if a grid block $i$ is inside the region enclosed by the observed $CO_2$ plume ($M_i = 1$) or not inside the region enclosed by the observed $CO_2$ plume ($M_i = 0$). Next, this process defines a simulation-derived binary index, $S_i$. $S_i$ is defined with the gas saturation results from the reservoir simulation. If the gas saturation is above or below 10%, then the block $j$ is considered inside the region enclosed by the simulated $CO_2$ plume ($S_i = 1$) or not inside the region enclosed by the simulated $CO_2$ plume ($S_i = 0$). The $M_i$ and $S_i$ values assigned to each of the nearly 1.5 million grid cells composing the 3-D model domain are then stored in 1-D numerical arrays, such that an elementwise numerical comparison can be performed efficiently, with the help of built-in functionalities in *NumPy*. After the $M_i$ and $S_i$ comparison, each block will fall into one of two possible categories: a region where there is agreement between $M_i$ and $S_i$, OR a region where $M_i$ and $S_i$ are in disagreement. Where there is a disagreement, the porosity and permeability values of the geologic model are updated. Where there is agreement, the porosity and permeability values of the geologic model from the prior iteration are retained (i.e., no changes are made).

The updates to the porosity and permeability values are done with multipliers and only change the model grid blocks that were identified as areas of disagreement between the predicted and observed $CO_2$ plumes. The porosity multiplier is ×1.02 (a 2% increase in porosity) or ×0.98 (a 2% decrease in porosity). Therefore, after five iterations of the AHM workflow, the porosity in regions of disagreement would change by approximately +/– 10% as compared to the Baseline Geologic Model. The permeability multiplier is ×2.0 (a 200% increase in permeability) or ×0.5 (a 50% reduction in permeability). The relationship between permeability and porosity is exponential, i.e., log permeability versus porosity. Consequently, the multipliers used for permeability are greater.

### 4.8 Stopping Criteria

The conventional procedure to stop the iterations during a history-matching workflow consists of finding the model parameters that produce the minimum value in a predefined objective

function. The residual sum of squares (RSS) is a commonly used metric for quantifying goodness-of-fit. Using 1-D arrays to store all the observation points, the objective function, *RSS(m)*, could be expressed in vectorial form as follows:

$$RSS(m)= ||d_{obs} - d_{sim}||^2 = (d_{obs} - d_{sim})^T * (d_{obs} - d_{sim}) \quad \text{[Eq. 7]}$$

where $d_{obs}$ and $d_{sim}$ are the observed values and simulated values, respectively. As different observations may have different degrees of relative importance, weighting factors are used to provide a quantitative way of expressing the users' confidence for each term. This can be expressed as:

$$RSS(m) = (d_{obs} - d_{sim})^T * \lambda * (d_{obs} - d_{sim}) \quad \text{[Eq. 8]}$$

where λ is a diagonal matrix containing individual weighting factors (positive values greater than zero). Equation 8 is a common choice as global objective function (GOF). This approach was successfully used in CMOST, for the assisted history-matching exercise (using mostly data collected at the wells but not the 3-D seismic data). However, the RSS approach faces several challenges in regard to matching the observed $CO_2$ plume from seismic data (Obidegwu and others, 2015). One of the problems with implementing RSS with seismic data is that multiple solutions to the inverse problem can produce a minimum value of the objective function. However, the existence of a minimum does not guarantee that the model represents the geologic structure or property distribution of the reservoir (Tavassoli and others, 2004). Therefore, to match the seismic data, the AHM workflow relies on a simpler objective function (the LOF explained in Section 4.8).

The main assumption underlying the AHM approach is that the key geologic structural features have already been captured in the geologic model through the initial forward-modeling efforts. The quality of the seismic interpretation work done (and transferring this information while building the Baseline Geologic Model) is paramount to the validity of the AHM workflow employed in this IMS. Therefore, the automatic update should be a relatively smooth process, taking advantage of the previous knowledge already incorporated into the Baseline Geologic Model. The solution space should be constrained to a range where the model parameters are relatively in close agreement with respect to the initial geologic model. If the AHM fails to converge using a reduced number of iterations, then this could indicate that something changed in the system or that some significant structural feature is missing in the geologic model, and because of these factors, warning flags should be raised in the AHM workflow. Rapid convergence (few iterations) suggests that the $CO_2$ plume is behaving within predicted limits. Conversely, greater disagreement means that the $CO_2$ plume is NOT behaving within predicted limits and, therefore, the model is taking longer to converge or is not converging.

The AHM workflow contains three stopping criteria:

1) LOF is smaller than a predefined tolerance (e.g., 10%).
2) LOF is higher than the predefined tolerance for Case 1, but there is an inflection point when considering changes in the LOF over successive iterations.

3) The maximum number of iterations is reached, which indicates a higher degree of uncertainty between observed and simulated $CO_2$ plumes and failure of the AHM workflow to achieve the LOF.

Case 3 does not necessarily mean that there is an unacceptable level of risk for the site; however, this outcome indicates to the operator that the observed subsurface conditions are outside of the expected range, which is an indication that the geologic model may need to be reexamined or other inputs must be reevaluated; i.e., human intervention is required.

## 5.0 EXAMPLE AHM CASES

This section presents examples intended to illustrate key aspects that should be considered when setting up and executing any AHM case within the IMS.

### 5.1 Value of Using a Sector Model

Building a sector model that captures the principal physical mechanisms of the full model is critical to successfully executing the AHM workflow. Sector models require cutting a region of the entire full model domain while keeping the rest of the model parameters the same. However, sometimes sector models require a bit more work and consideration because some model options need to be modified. For example, in the IMS work, the boundary condition in the sector model was changed to a closed reservoir where pressure and $CO_2$ are kept within the model instead of an infinite reservoir allowing for fluid and pressure to leave the model. Preliminary sensitivity analysis simulations were executed to verify that the boundary conditions and domain changes did not significantly alter the results. Note that the volume of gas injected was approximately 36,000 tonnes when the post-$CO_2$-injection Monitor 2 seismic survey was launched, which only represents a small fraction of the total reservoir storage capacity, which, according to Peck and others (2014), ranges from 8.4 to 27.1 million tonnes of $CO_2$.

### 5.2 Case 1: Fault Feature Analysis

Case 1 provides an example where the permeability field was updated within the five layers associated with the Perforation 2 (Layers 30 to 34 of the geologic model). The permeability updates were performed by constructing a 3-D subdomain enclosed by the projection of the $CO_2$ plume boundary contour observed in the top layer of Perforation 2. This 3-D subdomain only expands through five layers in Perforation 2.

Figure A-13 shows results that illustrate the importance of adding the geologic structural features into the model. Case 1a (Figure A-13a) compares the observed $CO_2$ plume contour from the 4-D seismic difference to the initial simulated $CO_2$ plume from the simulation model *prior to*

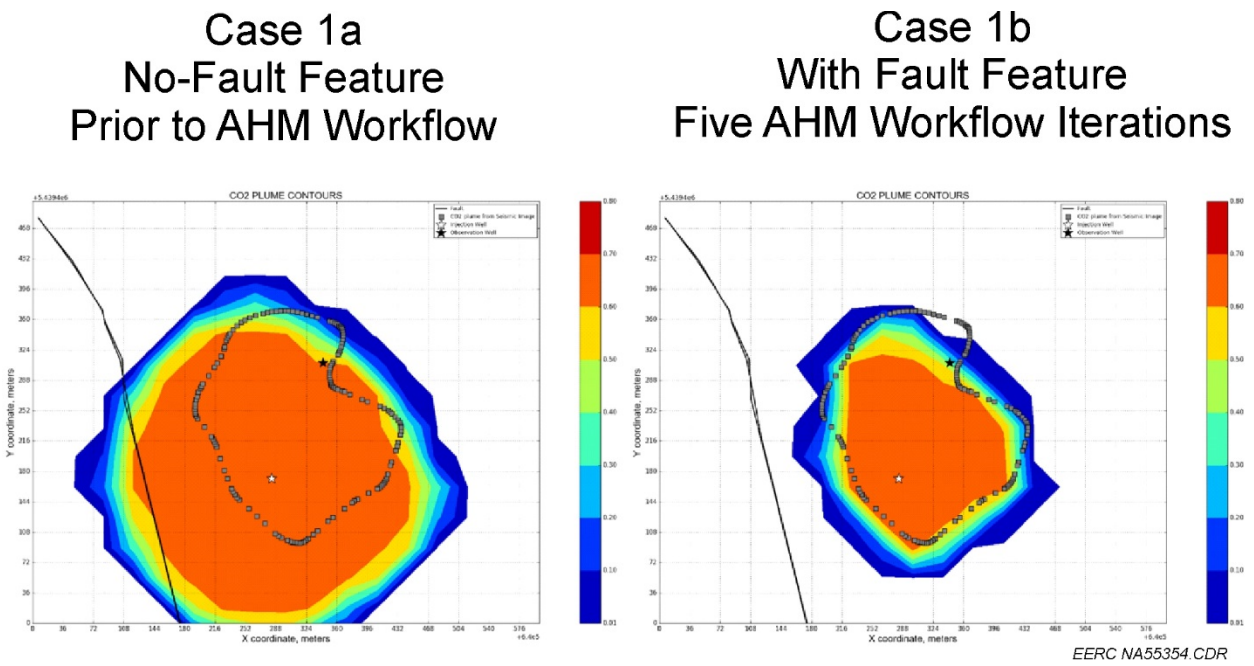


Figure A-13. Illustrative example showing contour maps of the simulated $CO_2$ plume as compared to the observed $CO_2$ plume outline (left) prior to going through the AHM workflow and without considering the fault feature (Case 1a) and (right) after five AHM workflow iterations and including the fault feature in the geologic model (Case 1b).

*running the AHM workflow* and *without incorporating the fault feature.* Case 1b (Figure A-13b) shows the simulated $CO_2$ plume *after five iterations within the AHM workflow*, with a model incorporating a fault feature that acts as a flow barrier (i.e., the model grid cells that intersect the fault feature have a low transmissivity value). This example highlights the importance of both the initial forward-modeling process for deriving the Baseline Geologic Model and the value of the AHM workflow for incrementally improving the accuracy of the simulated $CO_2$ plume.

Figure A-14 illustrates Cases 1a and 1b but shows the application of the criteria for identifying model grid cells located either within or outside of the observed $CO_2$ plume using the binary value, which is used in the AHM workflow to evaluate the LOF and for updating the porosity and permeability fields in subsequent iterations. Where there is agreement (Region 2), the porosity and permeability are maintained at their initial values. Where there is disagreement (Regions 1 and 3), the porosity and permeability are changed in subsequent iterations. The reduction and increase of the porosity and permeability values are handled using multipliers, which are limited to maintain the cell values within certain bounds, even though a successive number of iterations were needed. If the simulation results show $CO_2$ in a cell where $CO_2$ was not observed in the observed $CO_2$ plume, then the next iteration will reduce both porosity and permeability values. These changes will act to limit $CO_2$ migration toward this area of the model. If the simulation results do not show $CO_2$ in a cell where $CO_2$ was observed in the observed $CO_2$ plume, then the next iteration will increase both permeability and porosity values. These changes will act to increase $CO_2$ migration toward this area of the model.

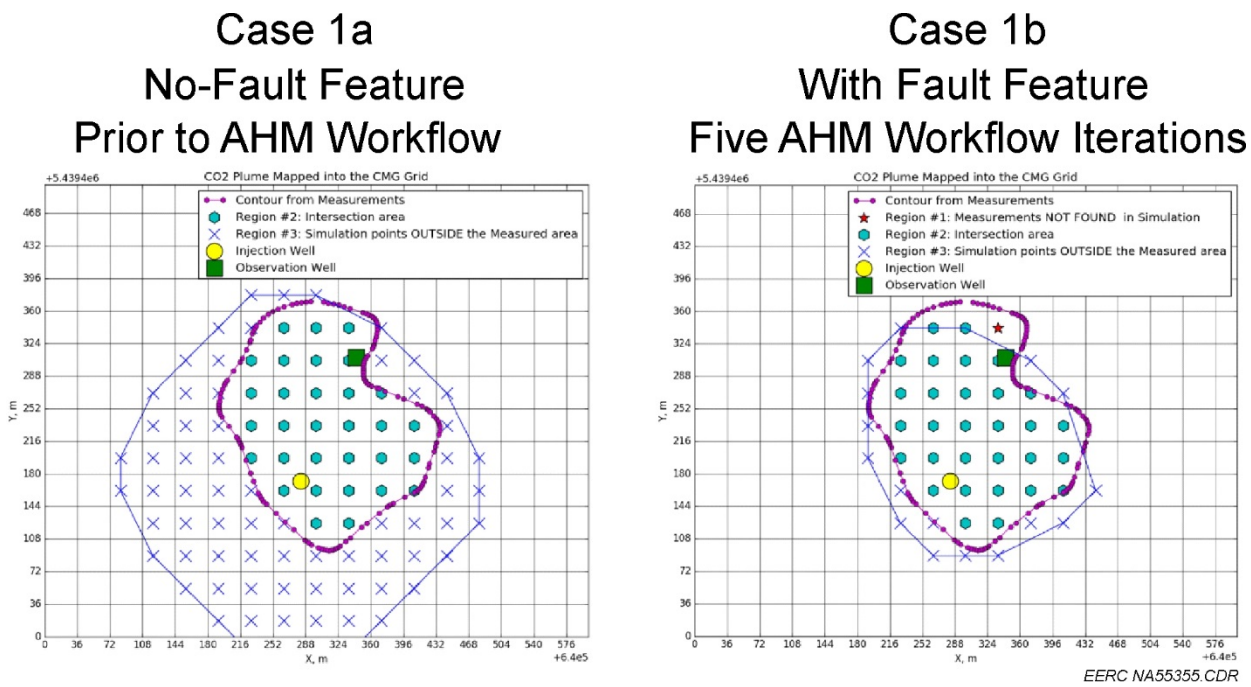


Figure A-14. Illustrative example showing model grid cells identified either within or outside of the observed $CO_2$ plume (left) prior to going through the AHM workflow and without considering the fault feature (Case 1a) and (right) after five AHM workflow iterations and including the fault feature in the geologic model (Case 1b).

Two factors cause the differences between Case 1a and Case 1b. First, in Case 1a (without the fault feature), a symmetrical simulated $CO_2$ plume shape is obtained where the center approximately corresponds to the injection well location (Figures A-13a and A-14a). In the reservoir, the dip of the geological strata is shallow (1 to 2 percent to the SSE after Stork and others [2018]) and does not significantly affect the shape of the simulated plume. After adding the fault feature (Case 1b, Figures A-13b and A-14b), the simulated plume shape exhibits an asymmetry, which is a consequence of the fluid transport being reduced (lower transmissivity) in the region of the fault feature. Results from Case 1b provide better agreement with previous work by Roach and White (2018). Their analyses showed that the $CO_2$ plume is "spreading predominantly along the NNW-SSE structural/permeability trends in the reservoir." In addition, White and others (2018) has identified a fault-related flexure after analyzing the seismic attributes in the Deadwood reservoir.

The second factor causing major differences between Case 1a and 1b is the horizontal permeability values. Horizontal permeability values obtained after five AHM workflow iterations (Case 1b) are in better agreement when compared with the operational data presented by Lee and others (2018). Their falloff test analysis showed an average permeability thickness of 70 mD*m. The initial model (Case 1a) had a higher average permeability; therefore, the $CO_2$ could travel laterally across longer distances.

Even with the inclusion of the fault feature and after five iterations through the AHM workflow (Case 1b), the simulated $CO_2$ plume is not an exact match of the outline of the observed $CO_2$ plume. This result is partially attributable to the fact that the simulation model has a grid resolution of 36 ft × 36 ft, which causes some discretization error in the sector model. While using a finer grid resolution could help to reduce the difference between the simulated $CO_2$ plume contours and the irregular outline of the observed $CO_2$ plume, the value of information obtained by having a perfect match does not outweigh the computational cost of running a sector model with a finer grid resolution.

### 5.3 Case 2: LOF Analysis

Figure A-15 shows plots with the outcome of the LOF as a function of the number of AHM workflow iterations for Case 1b (top) and Case 2 (bottom). Case 2 is a hypothetical stress test designed such that the AHM workflow does not converge over successive iterations. The "disagree" function refers to the numerator in Equation 6. Case 1b (Figure A-15, top) illustrates a case where the LOF trend eventually converges to a minimum value. While the minimum LOF value is not zero, the LOF trend shows a significant reduction from the first iteration to the last iteration; therefore, the iterations could be considered that converge to a reasonable minimum. The disagree function follows a similar trend for Case 1. In contrast, Case 2 (Figure A-15, bottom) illustrates a case where both the LOF value and disagree function stay relatively flat and there is little improvement as the number of iterations increase. While this example might converge to a local minimum, as both LOF and the disagree function are still far from zero, this outcome could be considered a failure to converge to a reasonable minimum. This LOF analysis illustrates how the LOF formulation provides a mathematical and intuitive basis for analyzing the evolution of the AHM convergence and for defining action levels (stopping criteria).

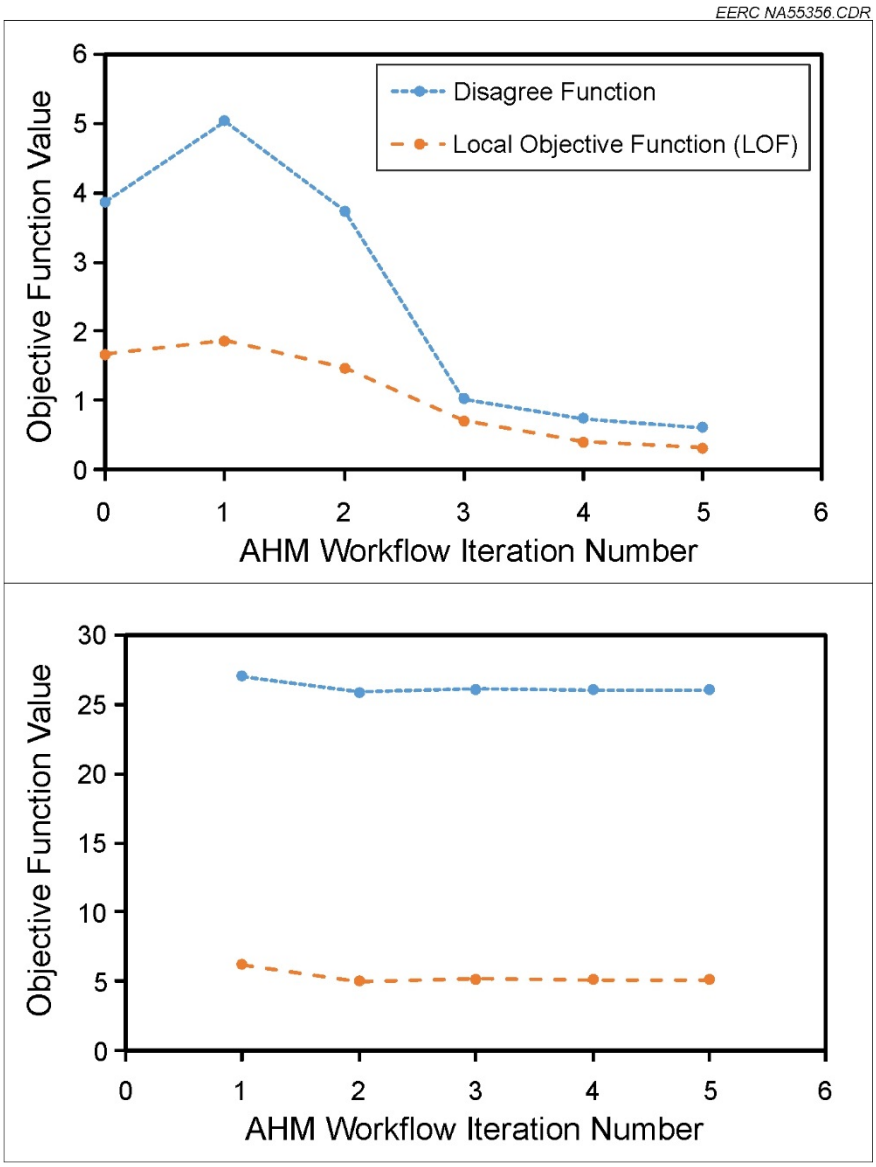


Figure A-15. Graph of the LOF versus number of AHM iterations showing (top) Case 1b (with the fault feature) and (bottom) Case 2. Case 2 is a hypothetical stress test designed such that the AHM workflow does not converge over successive iterations.

## 6.0 REFERENCES

Azzolina, N.A., Torres, J.A., Chimote, S., Burton-Kelly, M., Dotzenrod, N.W., Dalkhaa, C., Ayash, S., Pekot, L.J., Li, C., Gorecki, C.D., Nakles, D.V., and Vettleson, H., 2018, Development of intelligent monitoring system (IMS) modules for the Aquistore $CO_2$ storage project: Final Technical Report, Deliverable D5, November 14, 2018.

Computer Modelling Group Ltd. 2016a, CMOST user guide, Calgary, Alberta, Canada.

Computer Modelling Group Ltd. 2016b, GEM user guide, Calgary, Alberta, Canada.

Dalkhaa, C., Pekot, L.J., Jiang, T., Oster, B.S., Bosshart, N.W., Sorensen, J.A., and Gorecki, C.D., 2017, Aquistore $CO_2$ storage project—numerical modeling and simulation update: Plains $CO_2$ Reduction (PCOR) Partnership Phase III Task 9 Deliverable D93 (Update 3) for U.S. Department of Energy National Energy Technology Laboratory Cooperative Agreement No. DE-FC26-05NT42592, EERC Publication EERC-10-09, Grand Forks, North Dakota, Energy & Environmental Research Center, July.

Dzyuba, V.I., Litvinenko, Y.V., Bogachev, K.Y., Migrasimov, A.R., Semenko, A.E., Khachaturova, E.A., and Eydinov, D., 2012, Application of sector modeling technology for giant reservoir simulations (Russian): Society of Petroleum Engineers.

Hiebert, A.D., Morrish, I.C., Card, C., Ha, H., Porter, S., Kumar, A., Sun, F., and Close, J.C., 2013, Incorporating 4D seismic steam chamber location information into assisted history matching for a SAGD simulation: Society of Petroleum Engineers, doi:10.2118/165420-MS.

Lee, S.Y., Swagera, L., Pekot, L., Piercey, M., Will, R., and Zaluski, W., 2018, Study of operational dynamic data in Aquistore project: International Journal of Greenhouse Gas Control, v. 76, p. 62–77.

Matplotlib, 2018, Matplotlib, version 3.0.0: https://matplotlib.org/ (accessed October 2018).

Nakatsukasa, M., Kurosawa, I., Kato, A., Takanashi, M., White, D.J., and Worth, K., 2016, The performance of an ACROSS permanent seismic source for time lapse seismic at the Aquistore $CO_2$ storage site: Presented at the International Petroleum Technology Conference held in Bangkok, Thailand, November 14–16, 2016.

NumPy, 2018, http://www.numpy.org/ (accessed October 2018).

Obidegwu, D., Chassagne, R., and MacBeth, C., 2015, Seismic assisted history matching using binary image matching: Society of Petroleum Engineers, doi:10.2118/174310-MS.

Oliver, D.S., Reynolds, A.C., Liu, N., 2008, Inverse theory for petroleum reservoir characterization and history matching: p. 1–380.

Oliver, D.S., and Chen, Y., 2011, Recent progress on reservoir history matching—a review: Computational Geosciences, 115, no. 1, p. 185-221.

Pandas, 2018, Pandas: Python Data Analysis Library, https://pandas.pydata.org/ (accessed October 2018).

Peck, W.D., Bailey, T.P., Liu, G., Klenner, R.C., Gorecki, C.D., Ayash, S.C., Steadman, E.N., and Harju, J.A., 2014, Model development of the Aquistore $CO_2$ storage project: Energy Procedia, v. 63, p. 3723–3743.

Python Core Team, 2018, Python—a dynamic, open source programming language: Python Software Foundation, URL https://www.python.org/ (accessed 2018)/.

Roach, L.A.N., White, D.J., Roberts, B., and Angus, D., 2017, Initial 4D seismic results after $CO_2$ injection start-up at the Aquistore storage site: Geophysics, v. 82, no. 3, p. B95–B107, http://dx.doi.org/10.1190/geo2016-0488.1.

Schlumberger, 2017, Petrel: www.software.slb.com/products/petrel/petrel-2017/ (accessed October 10, 2017).

SciPy, 2018, SciPy: https://www.scipy.org/ (accessed October 2018).

Stork, A.L., Nixon, C.G., Hawkes, C.D., Birnie, C., White, D.J., Schmitt, D.R., and Roberts, B., 2018, Is $CO_2$ injection at Aquistore aseismic? A combined seismological and geomechanical study of early injection operations: International Journal of Greenhouse Gas Control, v. 75, p. 107–124, ISSN 1750-5836.

Tavassoli, Z., Carter, J.N., and King, P.R. 2004, Errors in history matching: Society of Petroleum Engineers, doi:10.2118/86883-PA.

White, D.J., Roach, L.A.N., and Roberts, B., 2015, Improved time-lapse seismic performance using a sparse permanent seismic array—experience from the Aquistore $CO_2$ storage site: Geophysics, v, 80, no. 2, p. WA35–WA48, doi:10.1190/geo2014-0239.1.

White, D.J., Hawkes, C.D., and Rostron, B.J., 2016. Geological characterization of the Aquistore $CO_2$ storage site from 3-D seismic data: International Journal of Greenhouse Gas Control, v. 54, p. 330–344.

Wyllie, M.R.J., Gregory, A.R., and Gardner, L.W., 1956, Elastic wave velocities in heterogeneous and porous media: Geophysics, v. 21, no. 1, p. 41–70.

# APPENDIX B

# PROGRAMMING AND SYSTEM REQUIREMENTS FOR THE INTELLIGENT MONITORING SYSTEM

## TABLE OF CONTENTS

# PROGRAMMING AND SYSTEM REQUIREMENTS FOR THE INTELLIGENT MONITORING SYSTEM

## 1.0 IMS OVERVIEW

The Energy & Environmental Research Center (EERC) has completed a 3-year project focused on developing new workflows, algorithms, and a user interface for the automation and integration of carbon dioxide ($CO_2$) storage site-monitoring and simulation data as part of an intelligent monitoring system (IMS). The design for the IMS was based on injection and monitoring data acquired by SaskPower and the Petroleum Technology Research Centre (PTRC) at the Aquistore $CO_2$ Storage Site of the Boundary Dam Power Station located near Estevan, Saskatchewan, Canada (hereafter "Storage Site").

The IMS comprises a database that stores the monitoring measurements (IMS Database) and a graphical user interface (IMS GUI) with which the user interacts to retrieve data from the IMS Database. Lastly, the IMS Workflow defines the linkage between the IMS GUI and the IMS Database.

The IMS GUI is divided into seven modules, which are separate pages within the user interface that address specific aspects of the monitoring system:

Module 1) Well Monitoring Measurements
Module 2) Distributed Temperature System (DTS) Measurements (DTS Profiles and DTS Time-Series)
Module 3) Bottomhole Temperature (BHT) and Bottomhole Pressure (BHP) Analysis
Module 4) DTS Analysis
Module 5) Continuous Modeling Refinement (CMR) Analysis
Module 6) $CO_2$ Plume Boundary
Module 7) System Evaluation

The IMS comprises a set of software packages and files that must be installed on the user's computer. This appendix describes the programming code used to develop the IMS and the system requirements needed to execute the IMS. Additional details about the Storage Site, IMS Database, Workflow, GUI, and modules are provided in the final technical report (Azzolina et al., 2018).

## 2.0 IMS PROGRAMMING AND SYSTEM REQUIREMENTS

### 2.1 Python

After various programming languages were considered, Python was selected as the programming language for the IMS (Python Core Team, 2018). Python is a high-level, general-purpose programming language that can be applied to many different classes of problems (Python Software Foundation, 2018b). Guido van Rossum developed the Python code in 1991, and the Python Software Foundation is a 501(c)(3) nonprofit corporation that holds the intellectual

property rights behind the Python programming language and manages the open-source licensing for Python version 2.1 and later (Python Software Foundation, 2018c). The IMS was developed using Python version 2.7.

Python was selected as the programming language for the IMS because it satisfied the following key requirements:

- **Ability to connect to a SQL database:** The IMS requires connecting to, and retrieving data from, the IMS Database, which is a T-SQL database. The Python application programming interface (API) module for open database connectivity (ODBC), *pyodbc*, provides an up-to-date, convenient interface with the IMS Database using native data types like date, time, and decimal (Python Software Foundation, 2018a).

- **Capability to quickly Retrieve and analyze a large data set:** The IMS Database contains more than 1 million records (i.e., rows of injection and monitoring data); therefore, the ability to quickly retrieve and analyze large amounts of data was an important requirement of the IMS. The Python library, *pandas*, is an open-source, Berkeley Software Distribution (BSD)-licensed library that provides high-performance, easy-to-use data structures and data analysis tools for the Python programming language (Pandas, 2018). In addition, the *pandas* library provides functions that are well-suited for the types of data included in the IMS Database.

- **Powerful GUI:** The IMS Data Workflow links the IMS Database to the IMS GUI, which is the primary means by which the user interfaces with the IMS. Thus a powerful GUI is essential to the IMS. *PyQt* brings together the Qt C++ cross-platform application framework and the cross-platform interpreted language Python, essentially combining the advantages of Qt with the simplicity of Python. *PyQt* provides an ideal combination for rapidly creating powerful and flexible GUI applications (Riverbank Computing Limited, 2018).

- **Flexible graphing tools:** Many of the IMS modules are visual tools that plot measurements onto graphs for decision-making about trends or correlations. Python provides two powerful graphing tools that are well-suited to these applications: *matplotlib* – a Python 2-D plotting library which produces publication-quality figures in a variety of hardcopy formats and interactive environments across platforms (matplotlib, 2018) and *seaborn* – a Python data visualization library based on *matplotlib* that provides a high-level interface for drawing attractive and informative statistical graphics (seaborn, 2018).

- **Ability to process and filter data:** Python offers some of the most powerful and versatile tools available for processing and filtering data by providing the ability to interact with the operating system console or external programs for additional data analysis.

- **Ability to interact with other software:** The ability of Python to leverage existing simulation packages, such as third-party reservoir simulation software, resulted in an expansion of the IMS capabilities.

- **Existence of a large number of scientific libraries:** The ability to utilize existing libraries minimized the time and resources required to develop the IMS code.

Using Python as a programming language (Invensis, 2018) has several additional advantages for example:

- **Open-source initiative (OSI)-approved:** The Python language is developed under an OSI-approved license, which makes Python free to use and distribute, including for commercial purposes. Python's open-source development is supported by a broad and diverse community, which collaborates for developing Python code through conferences, mailing lists, and other online resources.

- **Third-party modules:** The Python Package Index (*PyPI*) is a repository of software for the Python programming language and contains numerous third-party modules that make Python capable of interacting with most other software languages and platforms (Python Software Foundation, 2018a).

- **Extensive support libraries:** Python provides a large standard library, which includes areas like Internet protocols, string operations, Web services tools, and operating system interfaces. Many high-use programming tasks have already been scripted into the standard library, which can significantly reduce the length of code that needs to be written to perform an operation.

- **Learning ease and support available:** Python offers excellent readability and uncluttered simple-to-learn syntax, which helps beginners to utilize this programming language. The code style guidelines, Python Enhancement Proposal (PEP) 8, provide a set of rules to facilitate the formatting of code. Additionally, the wide base of users and active developers has resulted in a rich Internet resource bank to encourage development and the continued adoption of the language.

- **User-friendly data structures:** Python has built-in list and dictionary data structures, which can be used to construct fast run time data structures. Further, Python also provides the option of dynamic high-level data typing which reduces the length of support code that is needed.

- **Productivity and speed:** Python has clean object-oriented design, provides enhanced process control capabilities, and possesses strong integration and text processing capabilities and its own unit-testing framework, all of which contribute to the increase in its speed and productivity.

## 2.2 IMS System Requirements

### *2.2.1 Hardware and Software Requirements*

Installing the IMS software requires the following minimum system requirements:

- **Recommended operating system:** Windows 7 or Windows 10 (64 bit)
- **Random-access memory (RAM):** 8 GB (minimum), 16 GB (recommended)
- **Processor:** 64-bit Intel® or AMD® multicore processor
- **Python versions and dependent packages:**
  - *Python* 2.7 (64 bit) [https://www.python.org/download/releases/2.7/]
    - The minimum Python software requirements can also be satisfied by installing Python 2.7.12: Anaconda 4.2.0 (64-bit) [https://www.anaconda.com/download/]
  - *dateutil*: 2.5 [https://pypi.org/project/python-dateutil/2.5.3/]
  - *matplotlib*: 1.5 [https://matplotlib.org/users/installing.html]
  - *numexpr*: 2.6 [https://pypi.org/project/numexpr/]
  - *numpy*: 1.11 [https://www.scipy.org/scipylib/download.html]
  - *pandas*: 0.18 [https://pypi.org/project/pandas/0.18.1/#files]
  - *pip*: 18.1 [https://pypi.org/project/pip/]
  - *scipy*: 0.18 [https://www.scipy.org/]
  - *seaborn* 0.8 [https://pypi.org/project/seaborn/]
  - *setuptools*: 27.2 [https://pypi.org/project/setuptools/]
  - *sphinx*: 1.4 [https://pypi.org/project/Sphinx/]
  - *tables*: 3.2 [https://pypi.org/project/tables/]

### *2.2.2 Additional Software Requirements*

The preceding hardware and software requirements are necessary for executing the majority of the IMS modules. However, the IMS integrates seismic measurements and well logs using geologic models and numerical simulations. Therefore, the IMS must have the ability to access a licensed version of two software programs from the Computer Modelling Group (CMG): CMOST (Computer Modeling Group, 2016a) and GEM (Computer Modeling Group, 2016b). CMOST is CMG's application for performing sensitivity analysis, history matching, optimization, and uncertainty assessment with reservoir simulators. GEM is CMG's equation-of-state (EoS) reservoir simulator for compositional, chemical, and unconventional reservoir modeling. Lastly, the IMS also requires an executable called "Results Report" (Report.exe), which is GEM's postprocessing application that can be executed in batch mode from an MS-DOS prompt. Results Report allows the IMS to extract information from CMG's simulation results files (SRF).

## 3.0 REFERENCES


Azzolina, N.A., Torres, J.A., Chimote, S., Burton-Kelly, M., Dotzenrod, N.W., Dalkhaa, C., Ayash, S., Pekot, L.J., Li, C., Gorecki, C.D., Nakles, D.V., and Vettleson, H., 2018, Development of intelligent monitoring system (IMS) modules for the Aquistore $CO_2$ storage project: Final Technical Report, Deliverable D5, November 14, 2018.

Computer Modelling Group Ltd., 2016a, CMOST user guide: Calgary, Alberta, Canada.

Computer Modelling Group Ltd., 2016b, GEM user guide: Calgary, Alberta, Canada.

Invensis, 2018, Benefits of Python over other programming languages: www.invensis.net/blog/it/benefits-of-python-over-other-programming-languages/ (accessed October 2018).

matplotlib, 2018, matplotlib, version 3.0.0: https://matplotlib.org/ (accessed October 2018).

Pandas, 2018, pandas: Python Data Analysis Library, https://pandas.pydata.org/ (accessed October 2018).

Python Core Team, 2018, Python—a dynamic, open source programming language: Python Software Foundation, URL https://www.python.org/.

Python Software Foundation, 2018a, Find, install and publish Python packages with the Python package index: https://pypi.org/ (accessed October 2018).

Python Software Foundation, 2018b, General Python FAQ: https://docs.python.org/3/faq/general.html (accessed October 2018).

Python Software Foundation, 2018c, pyodbc 4.0.24: https://pypi.org/project/pyodbc/ (accessed October 2018).

Riverbank Computing Limited, 2018, What is PyQt?: https://www.riverbankcomputing.com/software/pyqt/intro (accessed October 2018).

seaborn, 2018, seaborn—statistical data visualization: https://seaborn.pydata.org/ (accessed October 2018).

# APPENDIX C

# STATISTICAL ACTION LEVELS FOR CONTINUOUS MEASUREMENTS USED IN THE INTELLIGENT MONITORING SYSTEM

## TABLE OF CONTENTS

## LIST OF FIGURES

# STATISTICAL ACTION LEVELS FOR CONTINUOUS MEASUREMENTS USED IN THE INTELLIGENT MONITORING SYSTEM

## 1.0 OVERVIEW

The Energy & Environmental Research Center (EERC) has completed a 3-year project focused on developing new workflows, algorithms, and a user interface for the automation and integration of carbon dioxide ($CO_2$) storage site-monitoring and simulation data as part of an intelligent monitoring system (IMS). The design for the IMS was based on injection and monitoring data acquired by SaskPower and the Petroleum Technology Research Centre (PTRC) at the Aquistore $CO_2$ Storage Site of the Boundary Dam Power Station located near Estevan, Saskatchewan, Canada (hereafter the "Site").

The IMS comprises a database that stores the monitoring measurements (IMS Database) and a graphical user interface (IMS GUI) with which the user interacts to retrieve data from the IMS Database. Lastly, the IMS Workflow defines the linkage between the IMS GUI and the IMS Database.

The IMS GUI is divided into seven modules, which are separate pages within the user interface that address specific aspects of the monitoring system:

Module 1) Well Monitoring Measurements
Module 2) Distributed Temperature System (DTS) Measurements (DTS Profiles and DTS Time-Series)
Module 3) Bottomhole Temperature (BHT) and Bottomhole Pressure (BHP) Analysis
Module 4) DTS Analysis
Module 5) Continuous Modeling Refinement (CMR) Analysis
Module 6) $CO_2$ Plume Boundary
Module 7) System Evaluation

This appendix is specific to the derivation of statistical action levels for three continuous measurements: 1) BHT and BHP measurements acquired at the casing-conveyed gauge located at 10,374 feet in the injection well and 2) DTS measurements acquired at 33 discrete sensors located along the 4.5-inch tubing within the injection wellbore. The action levels for BHT and BHP measurements are integrated within Module 3 of the IMS, and Module 4 includes action levels for the DTS measurements. Module 7 combines these action levels into a single graphical assessment page that helps the user quickly determine whether all three of these continuous measurements are or are not within normal operating limits. Additional details about the Site, IMS Database, Workflow, GUI, and modules are provided in the final technical report (Azzolina et al., 2018b).

## 2.0 DEFINITION OF NORMAL OPERATING LIMITS

As part of its effort at the Site, PTRC conducted an extensive review of the Site-monitoring data that have been collected, including additional measurements beyond those incorporated into the current IMS, and concluded that there have been no failures of the storage unit, e.g., $CO_2$ migration outside of the target injection horizon or leakage along the $CO_2$ injection wellbore. Thus the data set used to develop the current IMS is referred to in this document as representative of "normal operating limits" under a range of $CO_2$ injection conditions and contains the observed data which provide the basis for quantifying decision thresholds. Specifically, the current IMS uses monitoring data acquired from the injection well from April 15, 2015, through July 31, 2017, to establish a set of "action levels," or threshold values, that could be used to identify exceedances of normal operating limits. These action levels represent a retrospective analysis applied to the historical data set rather than an autonomous system that begins at the start of $CO_2$ injection, learns from the data, and derives action levels in real time. Nevertheless, these action levels provide a basis for decision-making about future monitoring measurements (i.e., acquired after July 31, 2017).

## 3.0 BOTTOMHOLE TEMPERATURE (BHT)

### 3.1 BHT Response to $CO_2$ Injection

When there is no $CO_2$ injection occurring at the Site, the measured BHT in the injection well is approximately 234°F, consistent with the formation-specific geothermal gradient. For example, Figure C-1 shows time-series plots of BHP, BHT, and Qg for the period from April 15, 2015, through July 31, 2017. The period from approximately June 21, 2015, through November 12, 2015, represents a period with little to no $CO_2$ injection, as Qg was at or near zero over this time. Consequently, the measured BHT during this period shows a horizontal line of nearly constant BHT of 234°F (Period A, middle panel of Figure C-1). However, in response to $CO_2$ injection, BHT decreases from this baseline value. In addition, the intermittent $CO_2$ injection, in which both Qg and the number of days of $CO_2$ injection vary, results in a sawtooth pattern in BHT corresponding to oscillating periods of $CO_2$ injection and shut-in (Period B, middle panel of Figure C-1). Finally, after $CO_2$ injection ceases on January 24, 2017, BHT increases toward the preinjection temperature of 234°F (Period C, middle panel of Figure C-1). The action levels developed for BHT utilize these observed correlations between Qg and BHT.

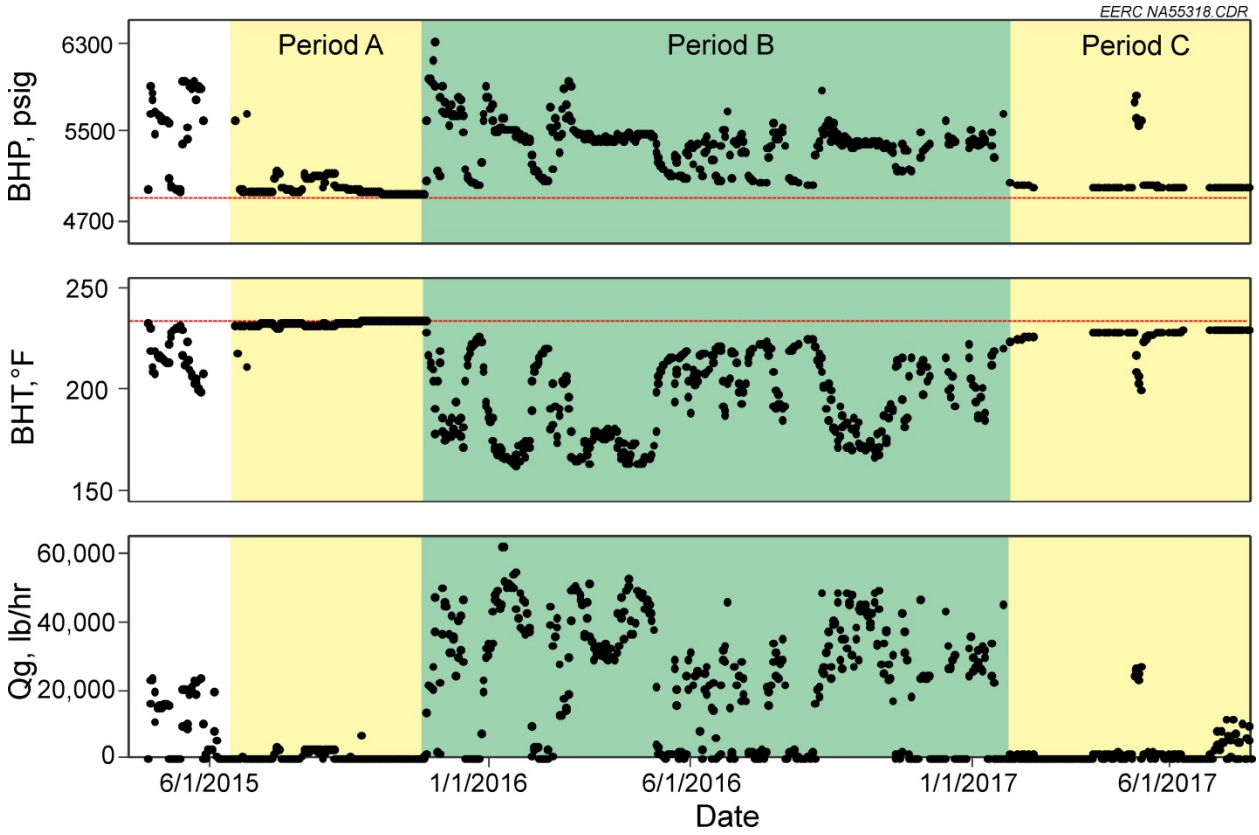


Figure C-1. Time-series plots of BHP (top), BHT (middle), and Qg (bottom) from the period beginning April 15, 2015, and ending July 31, 2017. Periods A and C (yellow highlights) show periods of no significant $CO_2$ injection, while Period B (green highlight) corresponds to oscillating periods of $CO_2$ injection and shut-in. The horizontal lines in the top and middle panels reflect the hydrostatic pressure gradient of 4940 psi and static geothermal gradient of 234°F, respectively.

### 3.2 BHT Action Levels

The BHT algorithms used in Module 3 of the IMS predict BHT given a set of operating conditions using injection and monitoring data acquired from the injection well during the period from April 15, 2015, through July 31, 2017. As described in Azzolina and others (2018a), the development of BHT action levels explored two different BHT prediction models, one based on heat transfer between the wellbore and surrounding rock and formation fluids (physical model) and one based on empirical correlations between Qg and BHT (empirical model). While the empirical model ignores time-dependency and heat-transfer, comparison of the two approaches showed that the empirical model was simpler to implement and more robust (less dependent upon input assumption) and provided comparable or better sensitivity to detecting change from normal operating conditions than the physical model. Thus the empirical model was selected for calculating action levels for BHT in Module 3.

The action levels for BHT were derived using regression on the natural log-transformed BHT measurement as the outcome and the measured $CO_2$ mass injection rate (Qg) as the predictor. The regression model form (Eq. 1) and fitted regression model (Eq. 2) were:

$$\ln(BHT) = \beta_0 + \beta_1 Qg \quad \text{[Eq. 1]}$$

$$\ln(BHT) = 5.433 - (6.517 \times 10^{-6})Qg \quad \text{[Eq. 2]}$$

Where:

ln(BHT) = the natural log transformed BHT
$\beta_0$ = the intercept (fitted value = 5.433)
$\beta_1$ = the slope (fitted value = 6.517E-06)

For example, the expected value for BHT given a Qg of 10,000 lb/hr would be:

$$BHT = \exp[5.433 - (6.517 \times 10^{-6})(10{,}000)] = 214°\text{F} \quad \text{[Eq. 3]}$$

Where "exp" returns the constant *e* (2.71828), the base of the natural logarithm, to the quantity inside the brackets.

While Eq. 3 allows the system to predict the *average* BHT outcome given Qg, there is variability (uncertainty) around this expected value that is attributable to several factors, including the duration of $CO_2$ injection and fluid properties of the wellbore and surrounding formation (McAdams, 1942; Ramey, 1962; Willhite, 1967; Wu and Pruess, 1990). Module 3 quantifies this uncertainty using *prediction intervals*, which incorporate the unexplained variability of the outcome variable (BHT in this example) in addition to uncertainties in the fitted parameter estimates of the regression ($\beta_0$ and $\beta_1$ in this example). These prediction intervals should contain approximately $1-\alpha\cdot(100)\%$ of the data within them, with $\alpha/2\cdot(100)\%$ of the data beyond each side of the intervals, assuming that the residuals are approximately normal (Helsel and Hirsch, 2002). Alpha ($\alpha$) refers to a fractional value between 0 and 1, commonly set to 0.01 (1%) or 0.05 (5%). For example, setting $\alpha = 0.05$, the prediction interval should contain 95% of the data within the lower and upper prediction intervals. The prediction interval should not be confused with a *confidence interval*, which estimates the confidence interval around the expected (mean) response.

Prediction intervals for the BHT outcome were calculated from the fitted regression equation (Eq. 3) and for the condition of Qg ranging from 0 to 100,000 lb/hr to define a framework for decision-making about BHT measurements within these constraints. The lower and upper prediction intervals were calculated according to Helsel and Hirsch (2002) using the following formula:

$$(\hat{y}) \pm ts\sqrt{1 + \frac{1}{n} + \frac{(x_0 - \bar{x})^2}{SS_x}} \quad \text{[Eq. 4]}$$

Where:

$\hat{y}$ = the estimate of *y* (BHT) given *x* (Qg)

$t$ = the quantile of the students' t-distribution having n−2 degrees of freedom with probability of exceedance of α/2
$s$ = the standard error of the fitted regression model ($s$ = 0.0377)
$n$ = the number of measurements used in the analysis ($n$ = 429)
$x_o$ = the value of Qg being evaluated (the range from 0 to 100,000 lb/hr)
$\bar{x}$ = the average $x$ (Qg) ($\bar{x}$ = 22,147)
$SS_x$ = the sum of squares $x$ ($SS_x$ = 1.25E11)

The product of $s$ and the quantity inside the square root of Eq. 4 is sometimes referred to as the "standard error of prediction," and the product of $t$ and the standard error of prediction is sometimes referred to as the "margin of error."

Continuing with the previous example of the expected value for BHT given a Qg of 10,000 lb/hr and setting α = 0.05:

$$\text{Std. Error of Prediction} = 0.03777\sqrt{1+\frac{1}{429}+\frac{(10{,}000-22{,}147)^2}{1.25E11}} = 0.0378 \qquad \text{[Eq. 5]}$$

$$\text{Margin of Error} = 1.966 \times 0.0378 = 0.0743 \qquad \text{[Eq. 6]}$$

$$\text{Lower Prediction Interval} = \exp[5.433 - (6.517 \times 10^{-6})(10{,}000) - 0.0743] = 199°\text{F} \qquad \text{[Eq. 7]}$$

$$\text{Upper Prediction Interval} = \exp[5.433 - (6.517 \times 10^{-6})(10{,}000) + 0.0743] = 231°\text{F} \qquad \text{[Eq. 8]}$$

Therefore, the expected result for the next BHT measurement acquired when Qg is 10,000 lb/hr would be 214°F, but this result would be expected to fall between 199° and 231°F with 95% confidence.

Two action levels were defined for BHT: Action Level 1 and Action Level 2. Action Level 1 represents a 2% false-positive rate, and Action Level 2 represents a 1% false-positive rate. Stated differently, fewer than 2% of the BHT measurements acquired from April 15, 2015, through July 31, 2017, plot outside Action Level 1, and fewer than 1% of the BHT measurements acquired over the same time span plot outside Action Level 2. These action levels were derived by using a numerical solver to modify α for the prediction interval until either 1% or 2% of the measurements were outside the prediction interval. Thus new BHT measurements (acquired after July 31, 2017) that plot outside of these action levels indicate BHT conditions that do not frequently occur, which may indicate BHT conditions that exceed normal operating limits observed during the first 2 years of operation at the Site.

Figure C-2 shows the output from Module 3 for the "BHT" page and the date range from April 15, 2015, through July 31, 2017. The default template will plot the BHT measurements (black circles), expected value from the regression (green line), Action Level 1 (blue dashed lines), and Action Level 2 (red dotted lines). As shown in the figure, few measurements plot beyond the action

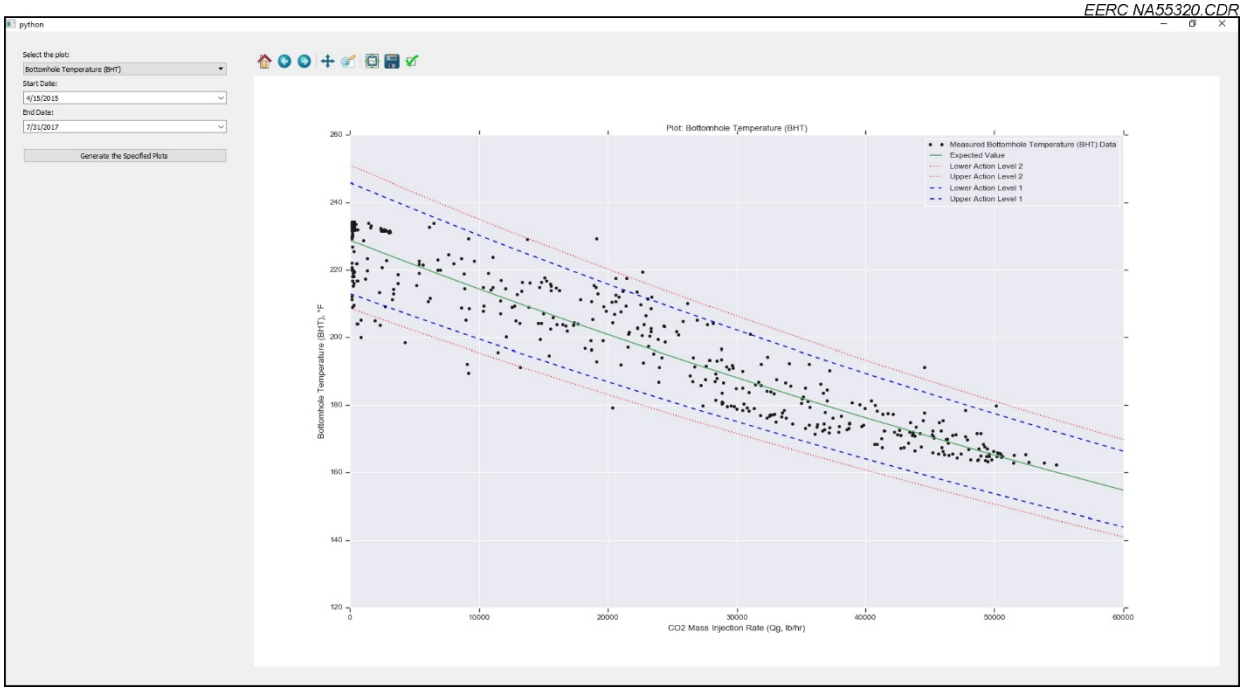


Figure C-2. Module 3 crossplot of Qg (x-axis, lb/hr) versus BHT (y-axis, °F) for the date range from April 15, 2015 through July 31, 2017, showing the BHT measurements (black circles), expected value (green line), Action Level 1 (blue dashed lines), and Action Level 2 (red dotted lines).

levels. As $CO_2$ injection continues at the Site, additional BHT measurements should plot within these action levels. New BHT measurements that plot outside of these action levels indicate BHT conditions that do not frequently occur, which may indicate BHT conditions that exceed normal operating limits and could trigger an operational response from the IMS user.

## 4.0 BOTTOMHOLE PRESSURE

### 4.1 BHP Response to $CO_2$ Injection

The current IMS utilizes BHP measurements acquired at the casing-conveyed pressure gauge located at 10,374 feet in the injection well. Similar to the measurements of BHT, when there is no $CO_2$ injection occurring at the Site, the measured BHP in the $CO_2$ injection well represents the local hydrostatic pressure, which is approximately 4940 psig. For example, as previously shown in Figure C-1, during the period from June 21, 2015, through November 12, 2015, which represents a period with little-to-no $CO_2$ injection, the measured BHP during this period shows a horizontal line at 4940 psig (Period A, top panel of Figure C-1). However, in response to $CO_2$ injection, BHP increases from this baseline value. In addition, the intermittent $CO_2$ injection, during which both Qg and the number of days of $CO_2$ injection vary, results in a sawtooth pattern in BHP corresponding to oscillating periods of $CO_2$ injection and shut-in (Period B, top panel of Figure C-1). These sawtooth patterns in BHP in response to $CO_2$ injection are roughly the inverse

of the patterns observed for BHT, which decreases in response to $CO_2$ injection. Finally, after $CO_2$ injection ceases on January 24, 2017, BHP begins to decrease and return toward the preinjection baseline of 4940 psig (Period C, top panel of Figure C-1). The action levels developed for BHP utilize these observed correlations between Qg and BHP; however, these BHP action levels also consider physics-based models. The remainder of this section builds upon and expands the process originally described in Azzolina and others (2018a).

## 4.2 BHP Action Levels

### *4.2.1 Overview*

One potential means for incorporating a physics-based model into the action levels for BHP would be to link the monitoring measurements to a numerical model of the injection well and surrounding formations. Numerical modeling of $CO_2$ injection into a deep saline formation is well established in the literature (e.g., Pruess and others, 2003) and commercial software packages such as CMG's GEM (Nghiem, 2002) are capable of modeling multiphase fluid flow like the $CO_2$-brine system at the Site (Jiang and others, 2017). However, the IMS modules for BHP require rapid calculations that do not rely on interfaces between the IMS Database and third-party software packages. Consequently, the IMS modules require a less computationally intensive solution.

An alternative to numerical models would be analytical or semianalytical solutions for modeling BHP in response to $CO_2$ injection. While analytical solutions exist (e.g., Noh and others, 2007; Azizi and Cinar, 2013), the $CO_2$ injection characteristics of the Site complicate using these simplified models to estimate BHP. One of the primary reasons that analytical or semianalytical models are challenging to implement for this specific site is that the intermittent $CO_2$ injection causes nonconstant flow rates, temperature variations in the wellbore and near-wellbore formation, and history-dependent performance effects surrounding the wellbore. Existing analytical solutions cannot account for these types of characteristics and are, therefore, not appropriate for estimating BHP at this Site.

However, in terms of providing information to the Site operator to more efficiently monitor and manage $CO_2$ injection and subsurface conditions, predicting BHP is perhaps less important than knowing how the measured BHP relates to the normally expected injectivity regime of the target injection zone at a given $CO_2$ injection rate. This is the approach used in the current IMS: integrating a physics-based model (rock geomechanics) with Qg and BHP. This approach estimates the Qg that corresponds to matrix- or fracture-flow regimes. These matrix- and fracture-flow regimes determine the expected BHP response during $CO_2$ injection, which are the action levels for BHP that are used in the IMS. Measured BHPs outside of this expected BHP response inform the operator of a potential change in subsurface conditions that may be outside of normal operating limits.

### *4.2.2 Injectivity Index*

This document defines the injectivity regime of the well across a range of operating conditions using the injectivity index (Bohloli and others, 2017):

$$\text{Injectivity Index} = \frac{Q_g}{(p_{wf} - p_i)} \quad \text{[Eq. 9]}$$

Where:

Qg = $CO_2$ mass injection rate, lb/hr
$p_{wf}$ = injection well BHP during injection, psig
$p_i$ = initial reservoir pressure, assumed a constant of 4940 psig

The injectivity index is a measure of the well performance and reflects the ability of the target injection zone to accept the $CO_2$ injection rate, which is primarily a function of the reservoir properties and the BHP. Geomechanical properties of the rock and the temperature differential between the injected $CO_2$ (bottomhole conditions) and the formation are known to affect the injectivity index. Examination of BHP versus Qg shows that BHP increases linearly with increasing Qg until reaching a threshold of approximately 30,000 lb/hr, above which the slope changes and BHP increases more gradually with increasing Qg (Figure C-3a). In contrast, the injectivity index increases nearly linearly with increasing Qg (Figure C-3b). This increasing injectivity index reflects a greater ability of the target injection zone to accept the $CO_2$ injection rate. The increasing injectivity is largely attributable to temperature changes in the injection well, as BHT decreases almost linearly with increasing Qg (i.e., the wellbore cools in response to $CO_2$ injection) (Figure C-3c) and injectivity is inversely proportion to the BHT (i.e., lower BHT yields higher injectivity and vice versa) (Figure C-3d).

If the injection pressure remains below the formation fracture opening pressure, then BHP will increase almost linearly with increasing Qg. This region represents matrix-flow injection, where the injected $CO_2$ flows into the rock proportional to the formation permeability. On the other hand, if injection pressure exceeds the formation fracture opening pressure, then flow regime changes and represents fracture-flow injection, where injectivity increases because the injected $CO_2$ flows into the rock via both the formation permeability and the fracture permeability (Bohloli and others, 2017). This fracture-flow regime changes the rate of increase in BHP in response to increasing Qg. The BHP module utilizes the relationships among Qg, BHT, and rock geomechanics to estimate the Qg that corresponds to matrix- or fracture-flow regimes.

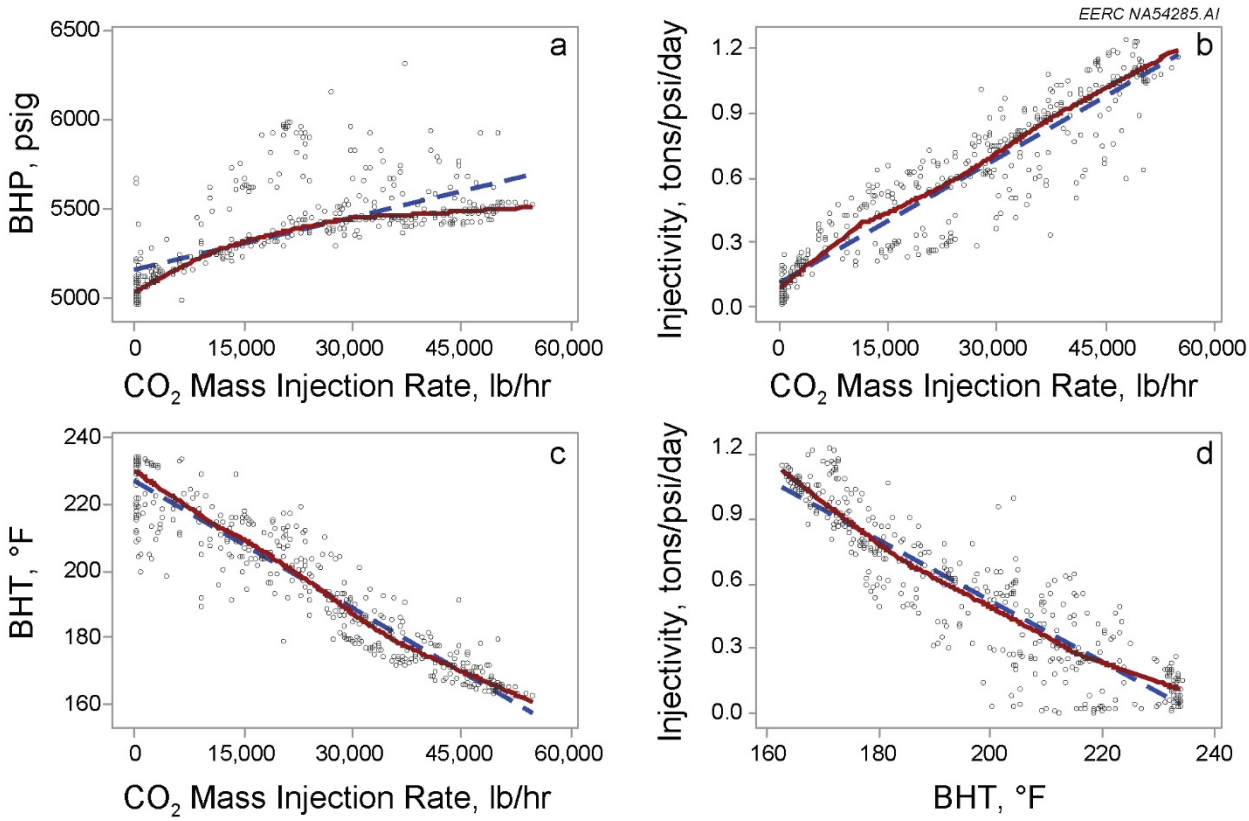


Figure C-3. Crossplots of a) Qg vs. BHP, b) Qg vs. injectivity index, c) Qg vs. BHT, and d) BHT vs. injectivity index. The blue dashed lines in each panel represent a linear regression line between panel-specific x- and y-axis variables. The red solid lines in each panel represent a LOWESS (LOcally WEighted Scatter-plot Smoother) line between the two variables. The LOWESS is a nonparametric smoother that captures a range of the data at each point and, therefore, better captures nonlinear trends.

### *4.2.3 Estimating Matrix- and Fracture-Flow Regimes*

The BHP module uses the injection well measurements acquired from April 15, 2015, through July 31, 2017, and rock geomechanics to estimate the fracture opening pressure of the target injection zone near the two predominant perforations that inject the majority of the injected $CO_2$ – Perforations 2 (Perf 2) and 4 (Perf 4). This geomechanical approach utilizes a series of equations, informed by downhole logging and testing data, to estimate the fracture pressure under static conditions and then adjusts these estimates to account for thermoelastic stress attributable to decreases in BHT that result from increasing Qg. Additional information gained through injection tests conducted at the Aquistore site prior to $CO_2$ injection also inform these estimates. The remainder of this section discusses these calculations and describes the derivation of action levels for measured BHP.

This document defines the formation fracture opening pressure as the fluid pressure required to open fractures in a rock formation, usually leading to a significant increase in permeability due to the induced fractures (Bohloli and others, 2017). This pressure is a function of the rock stress state, which is determined by the three principal stresses: vertical stress ($\sigma_v$) and the two horizontal principal stresses ($\sigma_H$, $\sigma_h$). Two of the most commonly used methods for determination of fracture pressure are 1) the minimum stress method and 2) the tensile failure method, which provide the lower and upper bounds, respectively, of the fracture opening pressure. The lower bound of this pressure ($P_{FPmin}$) and the upper bound of this pressure ($P_{FPmax}$) are defined as (Fjar and others, 2008):

$$P_{FP\min} = \sigma_{\min} \quad \text{[Eq. 10]}$$

$$P_{FP\max} = 3\sigma_{\min} - \sigma_H - P_P - \sigma_T + T_0 \quad \text{[Eq. 11]}$$

Where:

$\sigma_{\min}$ = minimum in situ stress, psi
$\sigma_H$ = maximum horizontal stress, psi
$P_P$ = pore pressure, psi
$\sigma_T$ = thermoelastic stress, psi
$T_0$ = tensile stress of the rock, psi

The individual terms in Eq. 10 and Eq. 11 are each functions of different geomechanical rock properties, as summarized in Eq. 12–Eq. 17 below (Fjar and others, 2008).

$$\sigma_{min} = \frac{v}{1-v}(S_v - \alpha P_P) + \alpha P_P + \frac{E\varepsilon_y}{1-v^2} + \frac{vE\varepsilon_x}{1-v^2} \quad \text{[Eq. 12]}$$

$$\sigma_H = \frac{v}{1-v}(S_v - \alpha P_P) + \alpha P_P + \frac{E\varepsilon_x}{1-v^2} + \frac{vE\varepsilon_y}{1-v^2} \quad \text{[Eq. 13]}$$

$$v = 0.5\left(\frac{\Delta t_s^2 - 2\Delta t_p^2}{\Delta t_s^2 - \Delta t_p^2}\right) \quad \text{[Eq. 14]}$$

$$E_s = 0.414E_d - 1.05 \quad \text{[Eq. 15]}$$

$$E_d = \left(\frac{\rho}{\Delta t_s^2}\right)\left(\frac{3\Delta t_s^2 - 4\Delta t_p^2}{\Delta t_s^2 - \Delta t_p^2}\right) \quad \text{[Eq. 16]}$$

$$S_V = Gz \quad \text{[Eq. 17]}$$

Where:

$v$ = Poisson's ratio derived from sonic log measurements, where $t_p$ and $t_s$ are the compression and shear sonic measurements, respectively, μs/ft
$S_v$ = vertical stress, calculated using a gradient ($G$) of 1.092 psi/ft calculated using bulk density logs from ground surface to depth of interest ($z$), as reported by White and others (2016)
$\alpha$ = Boit's coefficient = 1

$P_P$ = pore pressure, calculated using a gradient of 0.473 psi/ft, which was interpreted from well tests conducted in the Deadwood Formation, as reported by White and others (2016)

$E_s$ = static Young's modulus

$E_d$ = dynamic Young's modulus, which integrates the bulk density measurement from density logging ($\rho$) with the compression ($t_p$) and shear ($t_s$) sonic measurements

$T_0$ = rock tensile strength, assumed 290 psi (2 MPa) (Fjar and others, 2008)

$\varepsilon_x$, $\varepsilon_y$ = anisotropic coefficients, which were used to calibrate the value of $\sigma_{\min}$ to the results of the leak-off and Minifrac tests that were conducted at the injection well

Well logs, well tests, and laboratory data are required to correlate stress with rock mechanical properties. In the absence of laboratory results, the BHP module utilized a correlation between static and dynamic Young's modulus from the literature (Fjar and others, 2008). The density and sonic logs were acquired from the injection well in 2012 and 2015, respectively, while the Minifrac test was conducted in 2012. These measurements were used to populate the variables in Eqs. 12–17 and to estimate $P_{FPmin}$ (Eq. 10) and $P_{FPmax}$ (Eq. 11) from depths of approximately 9400 to 11,100 feet along the injection well assuming no thermoelastic stress (i.e., $\sigma_T = 0$). Then, these estimates were adjusted to account for thermoelastic stress under a range of $CO_2$ injection conditions (i.e., $\sigma_T > 0$), incorporating the temperature difference between the wellbore and the formation and several geomechanical properties.

Figure C-4 shows the estimated $P_{FPmin}$ and $P_{FPmax}$ as a function of depth along the injection well. These estimates are based on Eqs. 10 and 11, respectively, and density, sonic, and Minifrac measurements acquired from the injection well and used to inform Eqs. 12–17. These results suggest that the range in estimated $P_{FPmin}$ and $P_{FPmax}$ across the depth intervals corresponding to Perf 2 and Perf 4 is approximately 7000 to 10,000 psi, with an average value of approximately 8500 psi. Adjusting for the depth difference between Perf 2/Perf 4 and the tubing-conveyed pressure gauge (located approximately 600 feet higher) and assuming a $CO_2$-equivalent pressure gradient of 0.368 psi/ft, results in a lower-bound estimate for fracture opening pressure measured at the location of the BHP gauge of approximately 6780 psi. This adjustment assumes a $CO_2$ density of approximately 53 lb/ft$^3$, which is approximately 85% of fresh water (62.4 lb/ft$^3$) and results in a $CO_2$-equivalent pressure gradient of 0.85 × 0.433 psi/ft = 0.368 psi/ft. These estimates are for the static condition with no thermoelastic stress (i.e., $\sigma_T = 0$). These theoretical results, which were derived from injection well measurements, density and sonic log measurements, and geomechanical theory, are comparable to previous injection test interpretations conducted at the Site. Initial completion testing in 2012 determined through a pressure transient test analysis that the formation breakdown pressure was reached at a BHP range of 6560 to 6700 psi [SaskPower, personal communication], which is very close to the theoretical fracture pressure of 6780 psi.

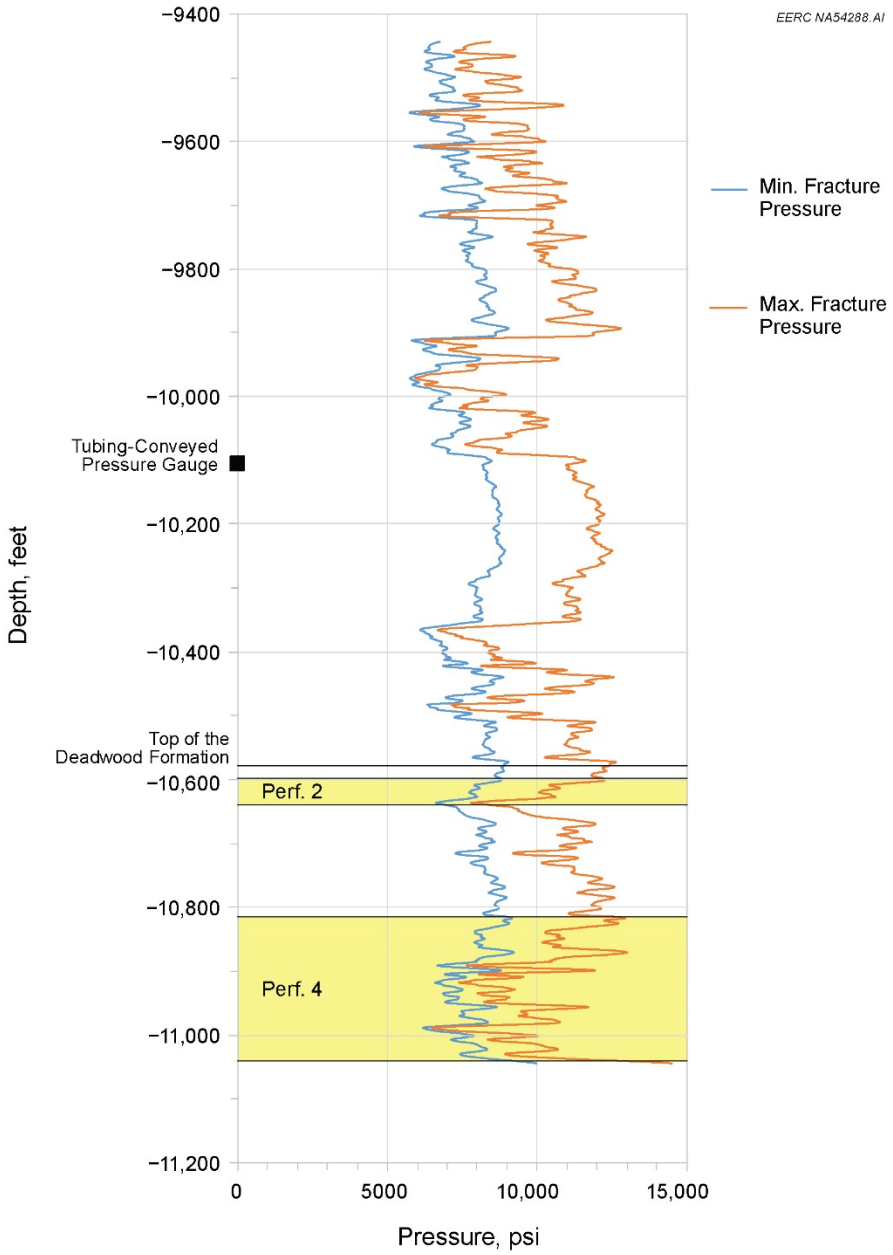


Figure C-4. Plot of estimated minimum fracture pressure ($P_{FPmin}$, blue line) and maximum fracture pressure ($P_{FPmax}$, red line) vs. depth along the injection well. Yellow highlights represent the approximate depth intervals of Perf 2 and Perf 4.

### *4.2.4 Incorporating Thermoelastic Stress*

The estimates shown in Figure C-4 assume no thermoelastic stress effects (i.e., $\sigma\ T = 0$). However, as described in Section 2.2 (BHT Action Levels) and illustrated in Figure C-3c, injection of $CO_2$ lowers the BHT, and the magnitude of the decrease in BHT is proportional to the $CO_2$ injection rate and duration. The difference between the BHT and the rock formation temperature ($\Delta T$) will affect the thermoelastic stress and lower the fracture pressure accordingly. Eq. 18 relates the change in the thermoelastic stress term ($\sigma_T$) to $\Delta T$ and the relevant geomechanical properties of the target injection zone (Fjar and others, 2008):

$$\Delta\sigma_T = \frac{\alpha_T\ E\ \Delta T}{1 - v} \qquad \text{[Eq. 18]}$$

Where:

$\Delta T$ = difference between measured BHT and the temperature of the target injection horizon under static conditions (234°F [385 K]), Kelvin
$\alpha_T$ = coefficient of thermoelasticity, Kelvin$^{-1}$
$E$ = Young's modulus, GPa
$v$ = Poisson's ratio, dimensionless

The current version of the BHP module uses a literature value of 1.5E-05 for $\alpha_T$ (Luo and Bryant, 2011) and derived values of 2,900,750 psi (20 GPa) for $E$ and 0.2 for $v$. The values for $E$ and $v$ were derived from the well log data across the depth intervals associated with Perf 2 and Perf 4. These inputs result in a thermoelastic stress of approximately 30 psi per °F. Stated differently, for every 1°F difference between the injection well BHT and the target injection zone under static conditions, the estimated fracture pressure decreases by approximately 30 psi as compared to the theoretical fracture pressure of 6780 psi at static conditions with no thermoelastic stress.

Figure C-5 shows an overlay of the measured BHP and the estimated fracture pressure adjusted for thermoelastic stress as a function of Qg. The red box identifies a region of overlap (transition) between matrix- and fracture-flow regimes, which corresponds to a measured BHP of approximately 5500 psi and a measured Qg of between approximately 28,000 and 32,000 lb/hr.

### *4.2.5 Decision-Making Framework*

At Qg rates below approximately 25,000 lb/hr, the estimated fracture opening pressure accounting for thermoelastic stress is generally above the observed BHP. Consequently, the $CO_2$ injection is predominantly in the matrix-flow regime, where pressure increases approximately linearly with increasing Qg. There is a transition zone between Qg rates of approximately 25,000 and 35,000 lb/hr, where the flow regime transitions from matrix- to fracture-flow regime. Finally, above Qg rates of approximately 35,000 lb/hr, the injectivity reflects an open fracture-flow regime. This information is important to the operator, as excessively high BHP measurements at low Qg rates or increases in BHP above approximately 6000 psi when Qg rates exceed 35,000 lb/hr indicate reduced injectivity.

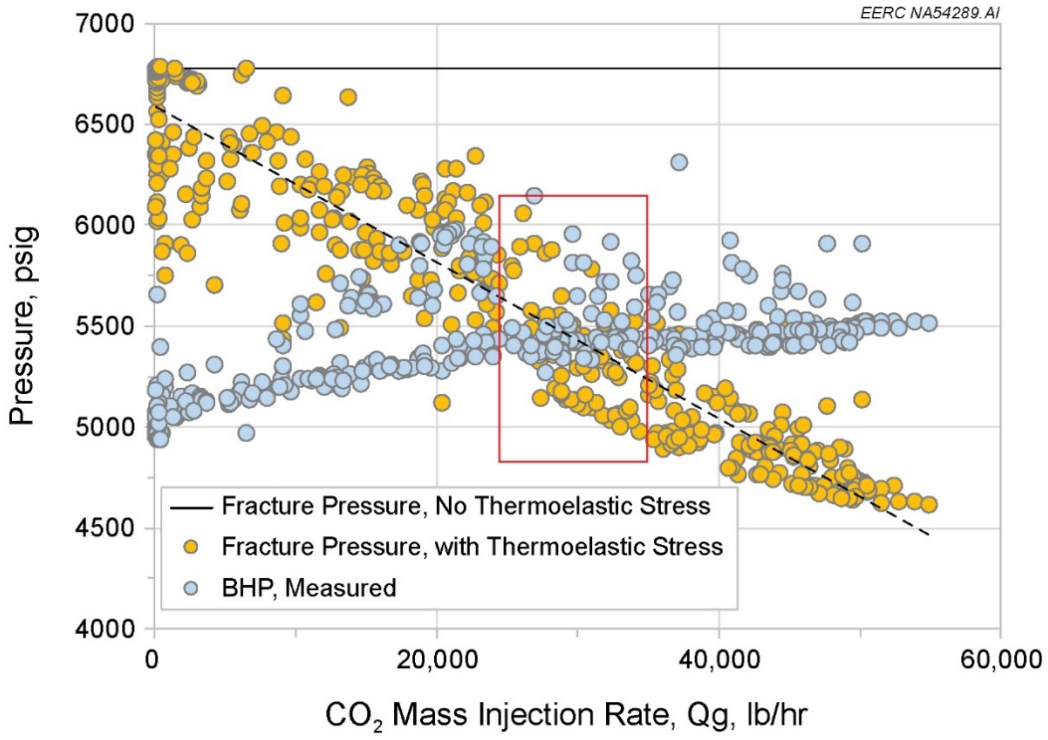


Figure C-5. Crossplot of Qg vs. measured BHP (blue circles) and the derived fracture pressure using Eqs. 10–17 and adjusting for thermoelastic stress via Eq. 18 (orange circles). The black horizontal line at 6780 psi is the lower-bound estimate for fracture pressure measured at the location of the BHP gauge with no thermoelastic stress. The black dashed line is a linear regression fit through the data points for derived fracture pressure adjusting for thermoelastic stress. The red box identifies a region of overlap (transition) between matrix- and fracture-flow regimes.

The BHP module uses the information from Figure C-5 to construct a decision-making framework within which new BHP measurements are classified into one of three Qg vs. BHP regions: Zone I, Zone II, and Zone III (Figure C-6). Zone 1 (blue region) represents the lower boundary of normal operating conditions for matrix or fracture flow. New BHP measurements plotting within Zone I could indicate either failure of the tubing-conveyed pressure gauge (if the measurement is less than the hydrostatic pressure value of 4940 psig) or that the $CO_2$ injection has fractured the formation, resulting in no commensurate increase in BHP with increasing Qg. Zone II (green region) represents the normal operating conditions. New BHP measurements falling within this region are within the expected injectivity regime of either matrix or fracture flow. Lastly, Zone III (red region) represents a region of above-normal BHP. For example, new BHP measurements plotting in Zone III when Qg exceeds 40,000 lb/hr indicate that the injectivity is not increasing as predicted, which could indicate potential problems with one or more perforation intervals.

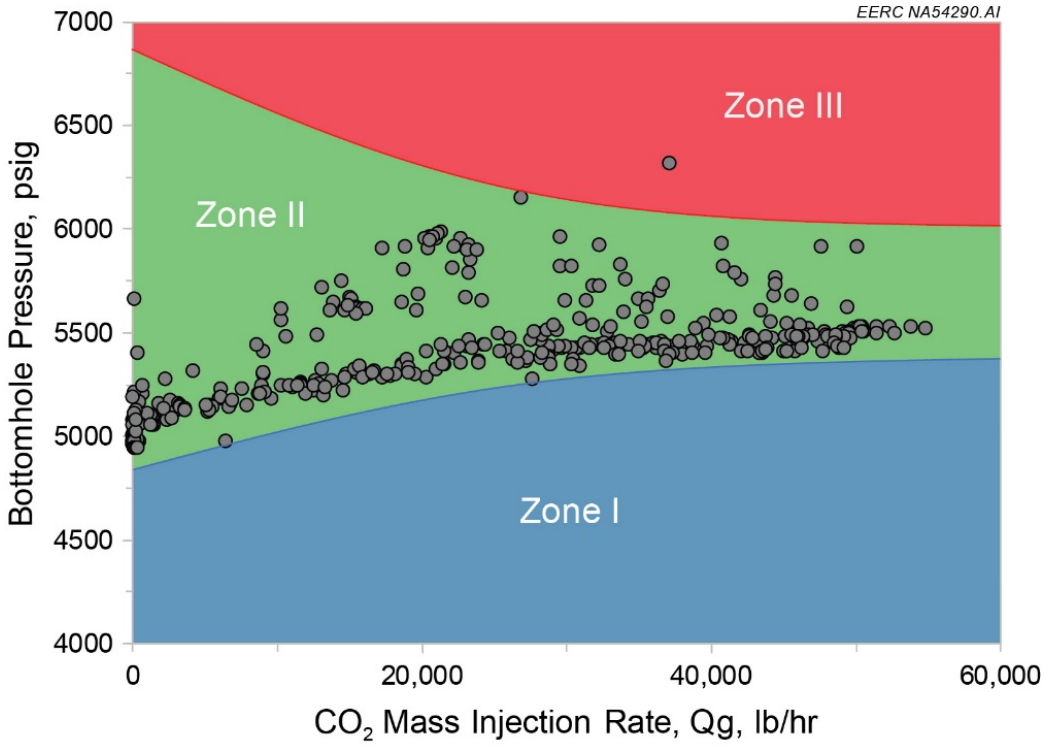


Figure C-6. Decision-making framework used to define injection-dependent action levels for BHP measurements.

The graphical construct illustrated in Figure C-6 was translated into mathematical expressions to define continuous BHP action levels as a function of Qg. A three-parameter, nonlinear equation was used to define the Zone I/II boundary and the Zone II/III boundary:

$$Y = a + b[1 - \exp(-cX)] \qquad \text{[Eq. 19]}$$

Where:

Y = the outcome variable, BHP (psig)
X = the predictor variable, Qg (lb/hr)
a, b, c = fitted parameters

The fitted equations used to define the Zone I/II boundary and the Zone II/III boundaries were:

$$Zone\,\frac{I}{II}\,boundary = 4940 + 450[1 - \exp(-0.00005X)] \qquad \text{[Eq. 20]}$$

$$Zone\,\frac{II}{III}\,boundary = 6800 - 800[1 - \exp(-0.00005X)] \qquad \text{[Eq. 21]}$$

These equations define the Zones I, II, and III in Module 3 of the IMS. Figure C-7 shows the output from Module 3 for the "BHP" page and the date range from April 15, 2015 through July 31, 2017. The default template will plot the BHP measurements (black circles), Zone I/II action level (blue dashed line [Eq. 20]), and Zone II/III action level (red dotted line [Eq. 21]). As shown in the figure, few measurements plot beyond the action levels. As $CO_2$ injection continues at the Site, additional BHP measurements should plot within these action levels. New BHP measurements that plot outside of these action levels indicate BHP conditions that do not frequently occur, which may indicate BHT conditions that exceed normal operating limits and could trigger an operational response from the IMS user.

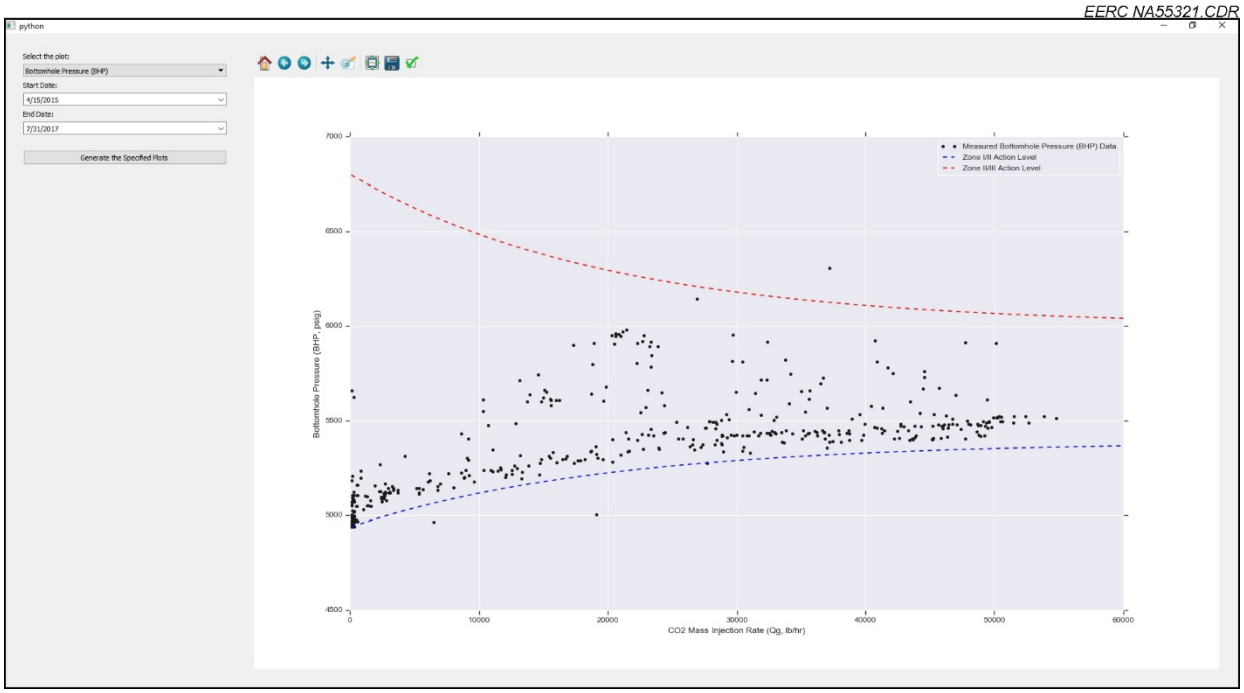


Figure C-7. Module 3 crossplot of Qg (x-axis, lb/hr) versus BHP (y-axis, psig) for the date range from April 15, 2015, through July 31, 2017, showing the BHP measurements (black circles), Zone I/II action level (blue dashed line), and Zone II/III action level (red dotted line).

## 5.0 DTS TEMPERATURE PROFILE

The DTS temperature profiles acquired at the injection well provide continuous measurements of temperature at discrete sensors located along the wellbore from the surface to the target injection horizon. Developing action levels for these DTS measurements required defining the baseline (no $CO_2$ injection) DTS temperature profile and the change in the DTS temperature profile in response to $CO_2$ injection. The output of these calculations provides the action levels for the DTS measurements, which are incorporated into Module 4 of the IMS.

### 5.1 DTS Baseline Temperature Profile

When there is no $CO_2$ injection occurring at the Site, the DTS temperature profile at the injection well reflects the local geothermal gradient, which was determined to follow a quadratic (second-order polynomial) of the form:

$$T_{\mathrm{DTS}} = 48.1 - 0.02699Z - 0.00000087Z^2 \qquad \text{[Eq. 22]}$$

Where:

$T_{\mathrm{DTS}}$ = temperature measurement within the DTS temperature profile (°F)

$Z$ =depth below ground surface (feet), where 0 is surface and −10,203 feet is the depth of the BHT gauge down into the injection well

Figure C-8 shows the average daily DTS temperature profile for the injection well during the period from June 8, 2015, through November 5, 2015, which represents a period with no significant $CO_2$ injection, as Qg was at or near zero over this time. The solid and dashed lines show a fit of the expected value and upper 95% prediction limit, respectively, of the Eq. 22 fit to these DTS measurements. The DTS measurements at the surface reflect the variability in ambient air temperatures, which ranged from 22° to 100°F over the period. However, DTS measurements acquired at greater depths reflect a relatively constant temperature gradient with little variance over the period. Subsequent figures showing DTS temperature profiles include the upper 95% prediction limit as a reference maximum temperature boundary for baseline conditions.

### 5.2 DTS Temperature Response to $CO_2$ Injection

In response to $CO_2$ injection, the DTS temperature profile will change, as several factors will influence the temperature along the wellbore. These factors primarily include 1) the temperature of the $CO_2$ at the time of injection; 2) the thermal properties of the wellbore casing, cement, and surrounding rock and formation fluids; 3) the thermal properties of the injected $CO_2$; 4) the Qg; and 5) the number of consecutive days of $CO_2$ injection.

Figure C-9 shows DTS temperature profiles acquired at the injection well during the period from April 15, 2015, through July 31, 2017, which represents periods with and without $CO_2$ injection. The DTS temperature profiles for the injection well illustrate the range of observed temperature profiles in response to $CO_2$ injection.

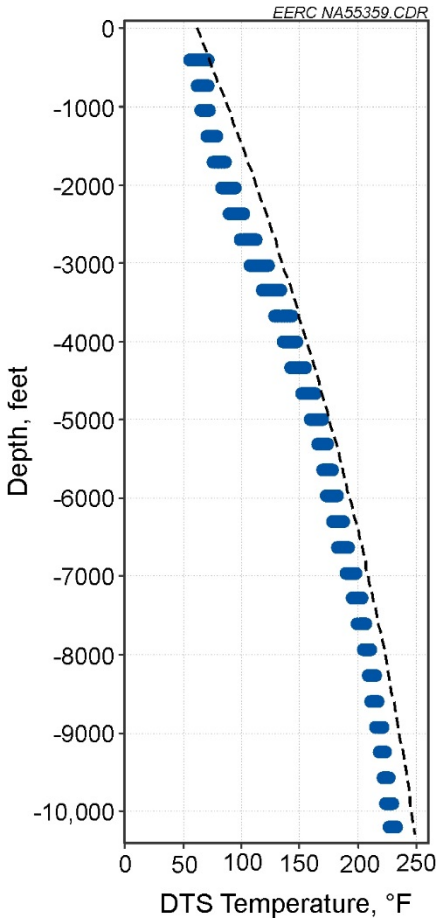


Figure C-8. Average daily DTS temperature profiles acquired at the injection well during the period from June 8, 2015, through November 5, 2015, which represents a period with no significant $CO_2$ injection. The dashed line shows a fit of the upper 95% prediction limit of Eq. 22 fit to these baseline (no $CO_2$ injection) DTS measurements.

### 5.3 Accounting for Intermittent $CO_2$ Injection

The Site receives intermittent $CO_2$ from SaskPower's Boundary Dam $CO_2$ capture facility, which results in periods with and without $CO_2$ injection. In addition, Qg varies as a function of the mass of $CO_2$ sent from the capture facility to the Site. For example, for the period from April 15, 2015, through July 31, 2017, 33% of the days had no $CO_2$ injection. When injecting $CO_2$, Qg was most frequently between 1000 and 50,000 lb/hr; however, there were days where Qg was less than or greater than this range (Figure C-10). This variability in Qg affects the wellbore temperature profile response to $CO_2$ injection, as the heat transfer between the wellbore and the surrounding formation is affected by the average wellbore temperature and the enthalpy and specific heat of the wellbore fluids (McAdams, 1942; Ramey, 1962; Willhite, 1967; Wu and Pruess, 1990). Thus decision-making with respect to whether the DTS temperature profile response is or is not within normal operating limits must account for the variability in Qg.

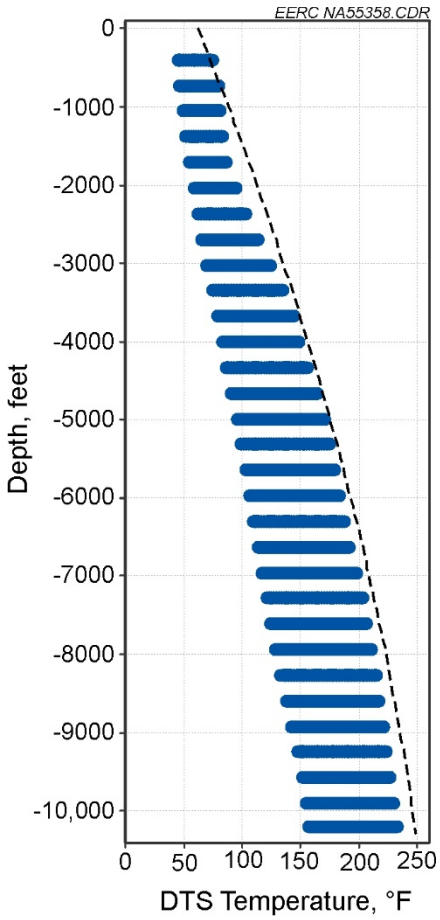


Figure C-9. Average daily DTS temperature profiles acquired at the injection well during the period from April 15, 2015, through July 31, 2017, which represents the full data set and periods with and without $CO_2$ injection. The dashed line shows a fit of the upper 95% prediction limit of Eq. 22 fit to the baseline (no $CO_2$ injection) DTS measurements.

In addition to the variability in Qg, the intermittent injection of $CO_2$ results in periods of different lengths of consecutive days of injection (injection duration) and periods with no $CO_2$ injection where the wellbore temperature profile rebounds toward the baseline geothermal gradient. For example, again for the period from April 15, 2015, through July 31, 2017:

- Only five periods had an injection duration of more than 20 consecutive days.
- Longest period of continuous $CO_2$ injection was 89 consecutive days.
- Five periods had more than 10 consecutive days with no $CO_2$ injection.
- Longest period with no $CO_2$ injection was 44 consecutive days.

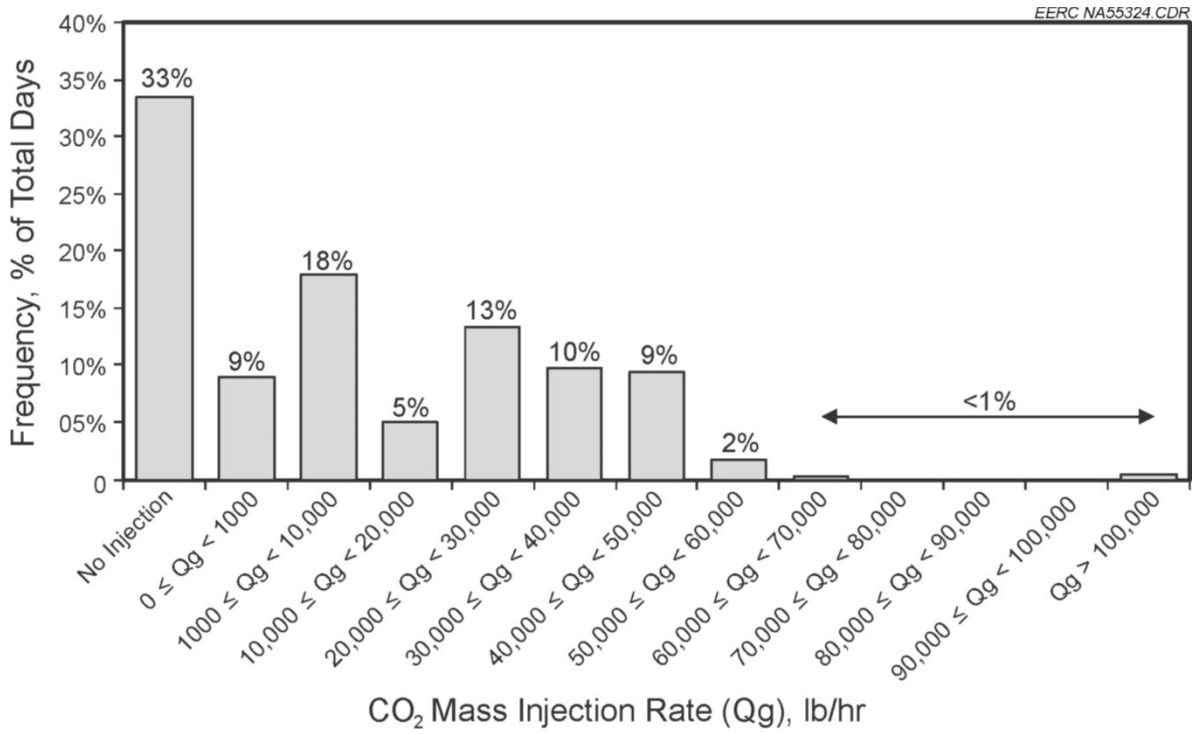


Figure C-10. Histogram showing the frequency percentage (percent of the total number of days) of the Qg for the period from April 15, 2015, through July 31, 2017.

These changes in the injection duration also affect the wellbore temperature profile response to $CO_2$ injection. Heat losses between the wellbore and the formations are large initially but decrease with time as thermal resistance to the flow of heat builds up in the formation (Ramey, 1962; Willhite, 1967). Consequently, decision-making with respect to whether the DTS temperature profile response is or is not within normal operating limits must also account for the variability in injection duration.

The action levels for the DTS temperature profiles address the combination of the effects of variability in Qg and injection duration on the DTS temperature profile by defining three groups of conditions and then providing action levels that are group-specific. Investigation into the sensitivity of the DTS temperature profile to the injection duration showed that the wellbore reached its minimum temperature profile relatively rapidly (in less than 5 days) and that Qg played a more significant role in determining the DTS temperature profile than the injection duration. An assessment of the combined effects of Qg and the injection duration resulted in the following three combinations used to derive action levels for the DTS temperature profile measurements in the injection well:

- **Group A:** Qg < 10,000 lb/hr and consecutive days < 5
- **Group B:** Qg < 10,000 lb/hr and consecutive days ≥ 5
- **Group C:** Qg ≥ 10,000 lb/hr

These three combinations of Qg and/or injection duration provided optimum sensitivity for detecting changes from normal operating conditions. Further parsing of the DTS measurement record into more groups resulted in fewer measurements in each group and commensurately wider action intervals (i.e., more uncertainty and, therefore, less sensitivity for detecting change).

### 5.4 DTS Action Levels

Nonparametric empirical percentiles were drawn for each group using methods described by Helsel and Hirsch (2002). The DTS temperature sensor measurements acquired between April 15, 2015, and July 31, 2017, were first classified into groups based on the above injection rate and duration criteria. Next, the measured temperatures for each DTS sensor were ranked from lowest to highest. Finally, Action Levels 1 and 2 were again defined as the 2% and 1% false-positive rates, respectively. For example, if there were 100 DTS temperature measurements in Group A, then Action Level 1 would be the second-lowest measurement (2/100 frequency of occurrence), and Action Level 2 would be the lowest measurement (1/100 frequency of occurrence).

Figure C-11 shows the DTS temperature profiles for the injection well grouped according to the three combinations of Qg and consecutive days of $CO_2$ injection. These action levels define the decision-framework used in Module 4 of the IMS to identify DTS temperature measurements that are outside of normal operating limits.

## 6.0 SYSTEM EVALUATION MODULE

The system evaluation module (Module 7) is the last module in the IMS and integrates the action levels for DTS, BHT, and BHP, in addition to the outcome from the automated history-match (AHM) in Module 5, into a single graphical assessment of whether the system is or is not operating within normal limits. The purpose of Module 7 is to provide a tool for the operator to quickly assess the color-coded outputs and determine whether they need to evaluate other modules within the IMS or implement further actions to control the storage site.

Module 7 incorporates algorithms to quickly classify new measurements as “Normal” (blue), “Caution” (pink), or “Flag” (red). In addition, NULL (missing) values in the IMS Database or BHP gauge readings less than 4940 psi (hydrostatic pressure) are reported as “possible error” (gray). Module 7 makes several simplifying assumptions to accommodate multiple measurements and action levels. Module 7 is designed with a global false-positive rate of 1% for “Flag” and 2% for “Caution” conditions; therefore, a system evaluation color-shading of blue denotes conditions that were observed 98% of the time during the period from April 15, 2015, through July 31, 2017, used to establish normal operating limits. However, the operator could modify these action levels depending on their specific risk tolerances.

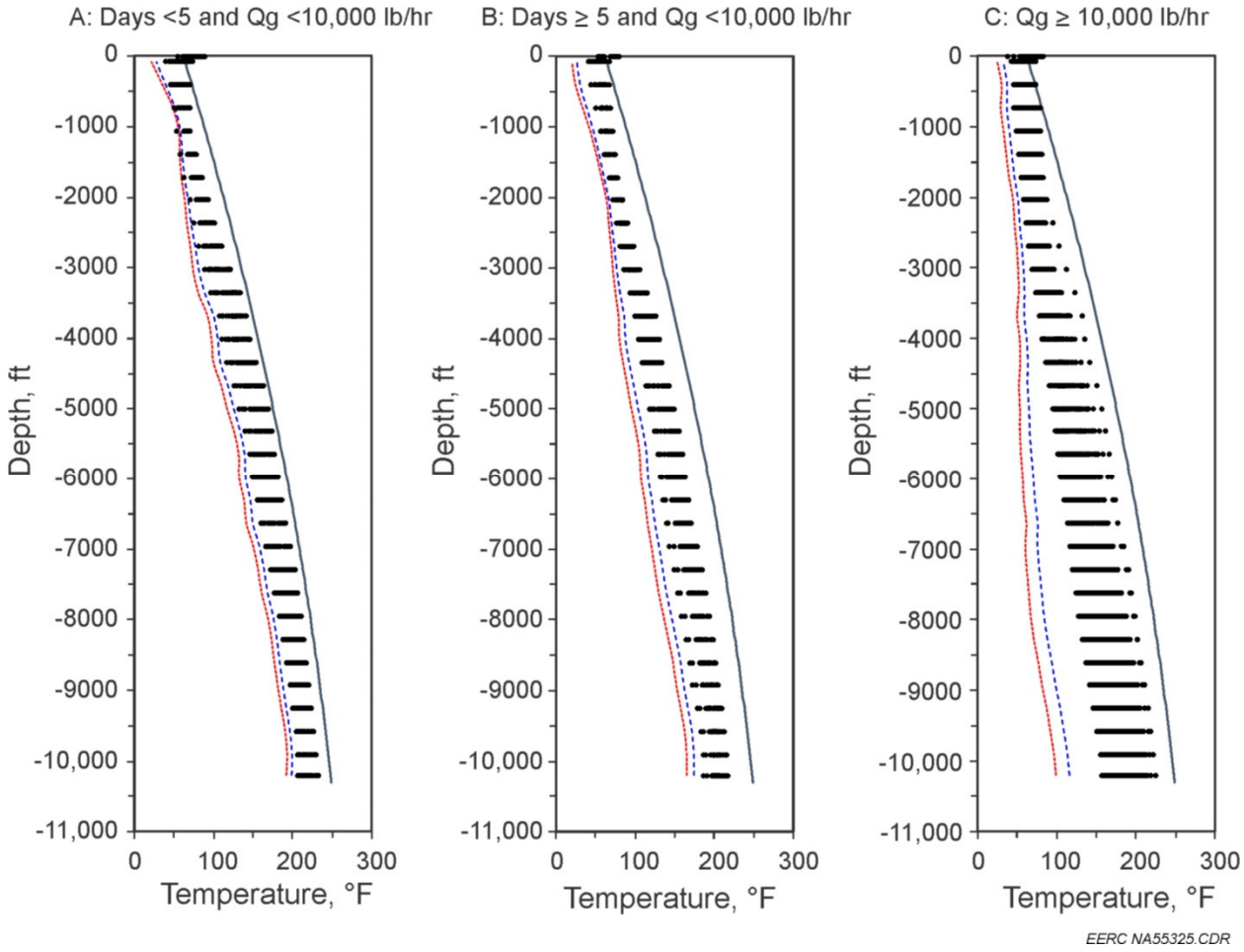


Figure C-11. Average daily DTS temperature profiles acquired at the injection well during the period from April 15, 2015, through July 31, 2017, grouped by three combinations: A) $CO_2$ Qg < 10,000 lb/hr and number of cumulative days of $CO_2$ injection (days) < 5, B) Qg < 10,000 lb/hr and days ≥ 5, and C) Qg ≥ 10,000 lb/hr. The solid black line to the right in each panel shows a fit of the upper 95% prediction limit of the Eq. 22 fit to the baseline (no $CO_2$ injection) DTS measurements. The blue and red dashed lines to the left in each panel represent the group-specific 2% (Action Level 1) and 1% (Action Level 2) action levels, respectively.

Figure C-12 shows an example output from Module 7 where the user has selected a Monitoring Date of December 10, 2015 and +45 days. After "Generate the Specified Plots" is selected, Module 7 will retrieve the DTS, BHT, and BHP measurements from the IMS Database, compare these measurements against respective action levels, and display the results. In addition, Module 7 takes the stopping criteria output from Module 5 and displays this result with the other measurements. As shown in the example in Figure C-12, the Module 7 output is organized as follows:

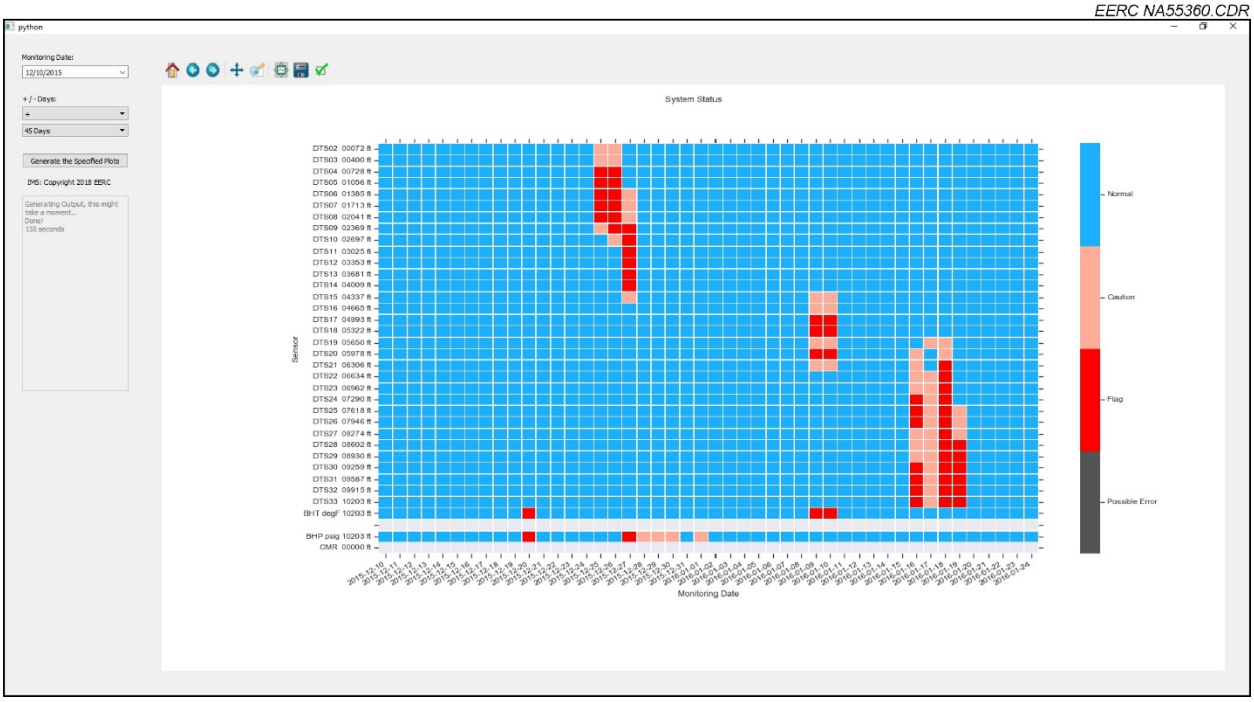


Figure C-12. Module 7 example showing +45 days from a Monitoring Date of December 10, 2015.

- Time (measurement acquisition date) is displayed across the x-axis as columns, with a minimum of 15 columns (+/– 15 days) and a maximum of 45 columns (+/– 45 days).

- DTS sensor results from DTS02 to DTS33 are displayed from top-to-bottom, which corresponds to the injection well temperature profile, identical to the configuration used in Module 2B (DTS Time-Series). The DTS sensor at the surface, DTS01, is excluded from this analysis, as the temperature measured at this gauge is significantly affected by surface conditions.

- The BHT results are shown at the bottom of the column of DTS sensors, which corresponds with the spatial relationship between the BHT sensor (bottomhole in the injection well) and the bottommost DTS sensor.

- A blank row is inserted between BHT and the last two measurements to distinguish between temperature-related measurements and the other measurements.

- The BHP results are displayed next and use a single row to flag either Zone I (pressure is less than expected) or Zone III outcomes (pressure is greater than expected).

- Lastly, the stopping criteria from the AHM workflow executed in Module 5 are shown in the final column, “CMR.” The stopping criteria are a function of the local objective

function (LOF), which compares the observed and predicted $CO_2$ plumes, and the number of iterations of the AHM workflow. The AHM workflow contains three stopping criteria:

A. Normal (blue) – The LOF is smaller than a predefined tolerance (currently set at 10%).

B. Caution (pink) – The LOF is higher than the predefined tolerance for Case A, but there is an inflection point when considering changes in the LOF over successive iterations.

C. Flag (red) – The maximum number of iterations is reached, which indicates a higher degree of uncertainty between observed and simulated $CO_2$ plumes and failure of the AHM to achieve the LOF. Case C does not necessarily mean that there is an unacceptable level of risk for the site; however, this outcome indicates to the operator that the observed subsurface conditions are outside of the expected range, which is an indication that the geologic model may need to be reexamined or other inputs must be reevaluated, i.e., human intervention is required.

The CMR portion of Module 7 can only be updated when the next 3-D seismic data set has been acquired, processed, and interpreted, which could be 1 year or more between updates. Consequently, the CMR criterion of the system evaluation has a much longer time-to-detection than the continuous measurements of DTS, BHT, or BHP

## 7.0 REFERENCES


Azizi, E., and Cinar, Y., 2013, Approximate analytical solutions for $CO_2$ injectivity into saline formations: SPE Reservoir Evaluation & Engineering, May 2013, p. 123–133, SPE-165575-PA.

Azzolina, N.A., Torres, J.A., Pekot, L.J., Li, C., and Gorecki, C.D., 2018a, Development of intelligent monitoring system (IMS) modules for the Aquistore $CO_2$ storage project—data integration algorithms for aiding decision-making about the subsurface risk profile: Revised Topical Report – Deliverable D4 – Data Integration for Risk Profiling, May 22, 2018.

Azzolina, N.A., Torres, J.A., Chimote, S., Burton-Kelly, M., Dotzenrod, N.W., Dalkhaa, C., Ayash, S., Pekot, L.J., Li, C., Gorecki, C.D., Nakles, D.V., and Vettleson, H., 2018b, Development of intelligent monitoring system (IMS) modules for the Aquistore $CO_2$ storage Project: Final Technical Report, Deliverable D5, November 14, 2018.

Bohloli, B., Ringrose, P., Grande, L., and Nazarian, B., 2017, Determination of the fracture pressure from $CO_2$ injection time-series datasets: International Journal of Greenhouse Gas Control, v. 61, p. 85–93.

Fjar, E., Holt, R.M., Raaen, A.M., Roamed, R., and Horsrud, P., 2008, Petroleum related rock mechanics, 2d ed.: Elsevier, v. 53, p. 514.

Helsel, D.R., and R. M. Hirsch, 2002, Statistical methods in water resources techniques of water resources investigations: U.S. Geological Survey, book 4, chapter A3, 522 p.

Jiang, T., Pekot, L.J., Jina, L., Peck, W.D., Gorecki, C.D., and Worth, K., 2017, Numerical modeling of the Aquistore $CO_2$ storage project: Energy Procedia, v. 114, p. 4886–4895.

Luo, Z., and Bryant, S., 2011, Influence of thermoselastic stress on fracture initiation during $CO_2$ injection and storage: Energy Procedia, v. 4, p. 3714–3721.

McAdams, W.H., 1942, Heat transmission, 2d ed.: New York, McGraw-Hill Book Co. Inc.

Nghiem, L., 2002, Compositional simulator for carbon dioxide sequestration: Calgary, Computer Modelling Group.

Noh, M., Lake, W., Bryant, S.L., and Martinez-Araque, A., 2007, Implications of coupling fractional flow and geochemistry for $CO_2$ injection in aquifers: SPE Reservoir Evaluation & Engineering, August, p. 406–414.

Pruess, K., Xu, T., Apps, J., and Garcia, J., 2003, Numerical modeling of aquifer disposal of $CO_2$: Society of Petroleum Engineers Journal, v. 8 no. 1, p. 49–60. SPE-83695-PA. doi: 10.2118/83695-PA.

Ramey, H.J., Jr., 1962, Wellbore heat transmission: Journal of Petroleum Technology, April, p. 427–435.

White, D.J., Hawkes, C.D., and Rostron, B.J., 2016, Geological characterization of the Aquistore CO2 storage site from 3-D seismic data: International Journal of Greenhouse Gas Control, v. 54, p. 330–344.

Willhite, G.P., 1967, Over-all heat transfer coefficients in steam and hot water injection wells: Journal of Petroleum Technology, May, p. 607–615.

Wu, Y., and Pruess, K., 1990, An analytical solution for wellbore heat transmission in layered formations: SPE Reservoir Engineering, November, p. 531–538.

# APPENDIX D

# SCHLUMBERGER TECHNICAL MEMORANDUM

Schlumberger

# Technical Memorandum

**To:** Nick Azzolina, EERC
**From:** Si-Yong Lee, Schlumberger
**Cc:**
**Ref. No.** CS1809-1-SL
**Date:** September 25, 2018
**Subject:** Review of IMS Modules

---

The purpose of this memo is to provide a technical review of the Intelligent Monitoring System (IMS) control system architecture and the compatibility of the IMS interface developed by the Energy & Environmental Research Center (EERC) as part of the DOE-funded project entitled, "Development of Intelligent Monitoring Modules for the Aquistore $CO_2$ Storage Project." To accomplish this technical review, an on-site review was held at the EERC located in Grand Forks, North Dakota, on August 21, 2018. Si-Yong Lee of Schlumberger and Nick Azzolina and Jose Torres of the EERC participated in the on-site review.

IMS is a real-time monitoring and analysis tool that connects PI/SCADA system colleting the downhole sensor data to a user/operator. The developed IMS system is designed to perform real-time monitoring of sensor data, to efficiently monitor and manage a geological $CO_2$ storage project, and to provide alarms for specified conditions/risks. The design and development of IMS is based on the operational dataset of the Aquistore project acquired from 4/15/2015 to 7/31/2017. See Azzolina et al. (2018) for the detailed description of IMS data integration algorithm.

At the time of the on-site IMS review meeting, the IMS consisted of seven modules:

1) Well monitoring measurements
2) DTS measurements
3) Area of review
4) Module A (DTS analysis)
5) Module B (BHT and BHP analysis)
6) Module C (CMR analysis)
7) IMS system evaluation.

Figure 1 shows the module selection window after launching the IMS, where the user can select one of the seven modules. At the time of the on-site review meeting, the IMS lacked general information such as the module version, copyright, disclaimer, license, and contact information. It is recommended to add this information in future updates. In addition, besides the full user manual, concise and easily accessible descriptions of each module would be helpful to the user. For example, the IMS should provide the user with pop-up balloons that provide a brief description of a module when the user moves a mouse pointer to the corner of a module selection button. In the following sections, this memo will go over each module and summarize its detailed review.

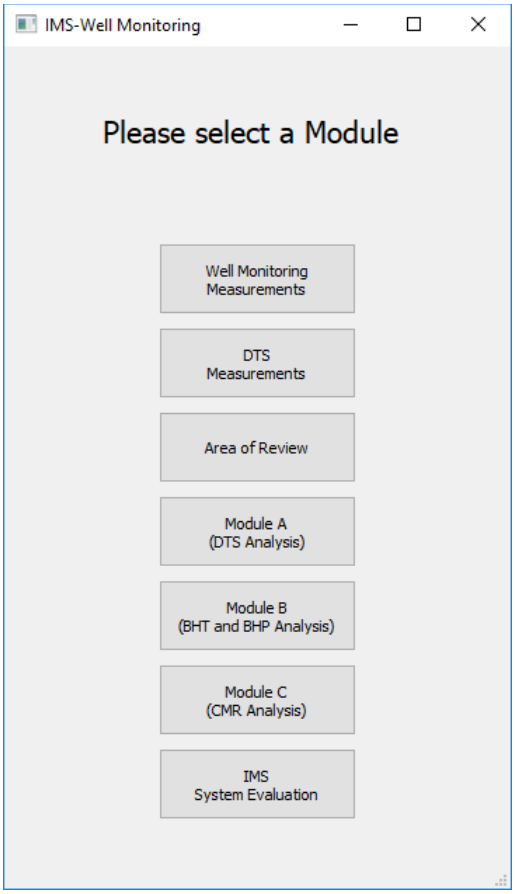


**Figure 1: IMS module selection window.**

**Well Monitoring Measurements Module**

The Well Monitoring Measurement Module is designed to allow the user to monitor, plot, and export the measurement data such as $CO_2$ injection rate (Q), wellhead temperature (WHT), wellhead pressure (WHP), bottomhole temperature (BHT), and bottomhole pressure (BHP) from a well. Figure 2 shows an example screenshot of the module with the plots of $CO_2$ injection rate on the top panel and bottom hole pressure at the bottom panel.

This module plots only one attribute in each separate panel, up to a maximum of two panels. It is often useful to plot multiple attributes in a single panel (for example, BHP and WHP along with the Q data) to examine the relationship among different attributes. It is therefore recommended to add plotting capability to this module in order to display multiple attributes in a single panel, which would require corresponding multiple y axes.

It was also noted that due to the nature of the offline dataset given from Aquistore, handling of real-time data was not demonstrable with the current IMS version. To fully apply to the field operation, it is recommended to equip the IMS with real-time monitoring capability. Instead of accessing the entire dataset at once, it might be possible to simulate real-time condition by sequentially reading the Aquistore dataset and updating the IMS.

Lastly, it is recommended to add the annular pressure measurement to the Well Monitoring Measurements Module. The annular pressure measurement is a measurement of the pressure in the space between the tubing and the production casing. This space is filled with water and sealed with the wellhead at the surface and sealed at the bottom by the production packer. Pressure is monitored at the surface in the wellhead where the annulus connects to the pressure management system.

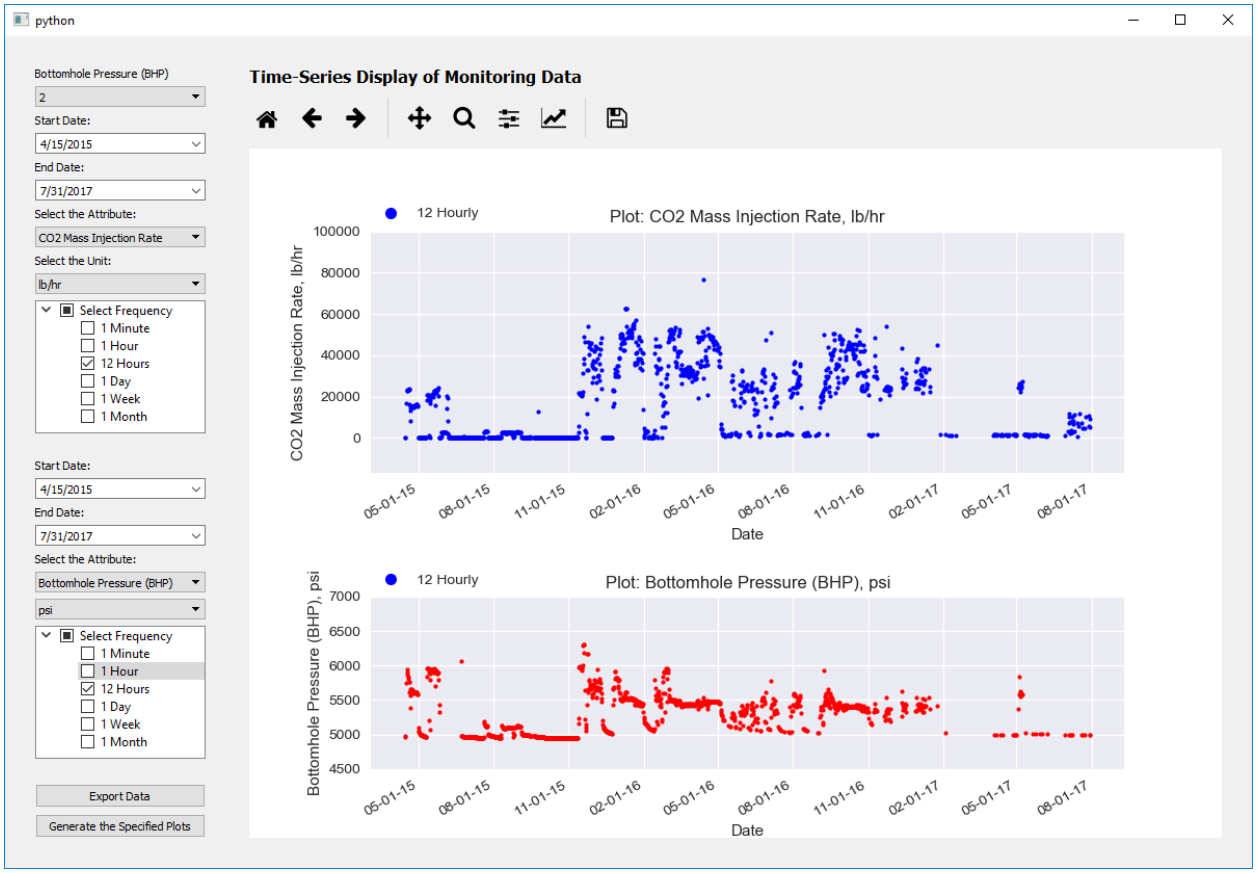


**Figure 2. Screenshot of well monitoring measurement module.**

## DTS Measurements Module

The distributed temperature sensor (DTS) installed on the outside of tubing is a fiber optic line that is used to measure temperature along the tubing. The DTS is useful when monitoring for potential leaks within the injection well system. Especially when assessing pressure changes in the annulus, the DTS can help in understanding whether the annular pressure change is caused by leaks or thermal expansion. Figure 3 shows the DTS Measurement Module which plots temperature measurement at approximately 100 m intervals in the Aquistore injection well.

After reviewing this module, it is recommended to consider the following:

- To add units (days) of sampling frequency
- To include display option for plotting DTS values (of each sensor) in temperature (y axis) against time (x axis)
- To plot DTS values (contour map) in depth (y axis) against time (x axis)
- To calculate and visualize DTS thermal gradient (contour map) along depth (y axis) against time (x axis)

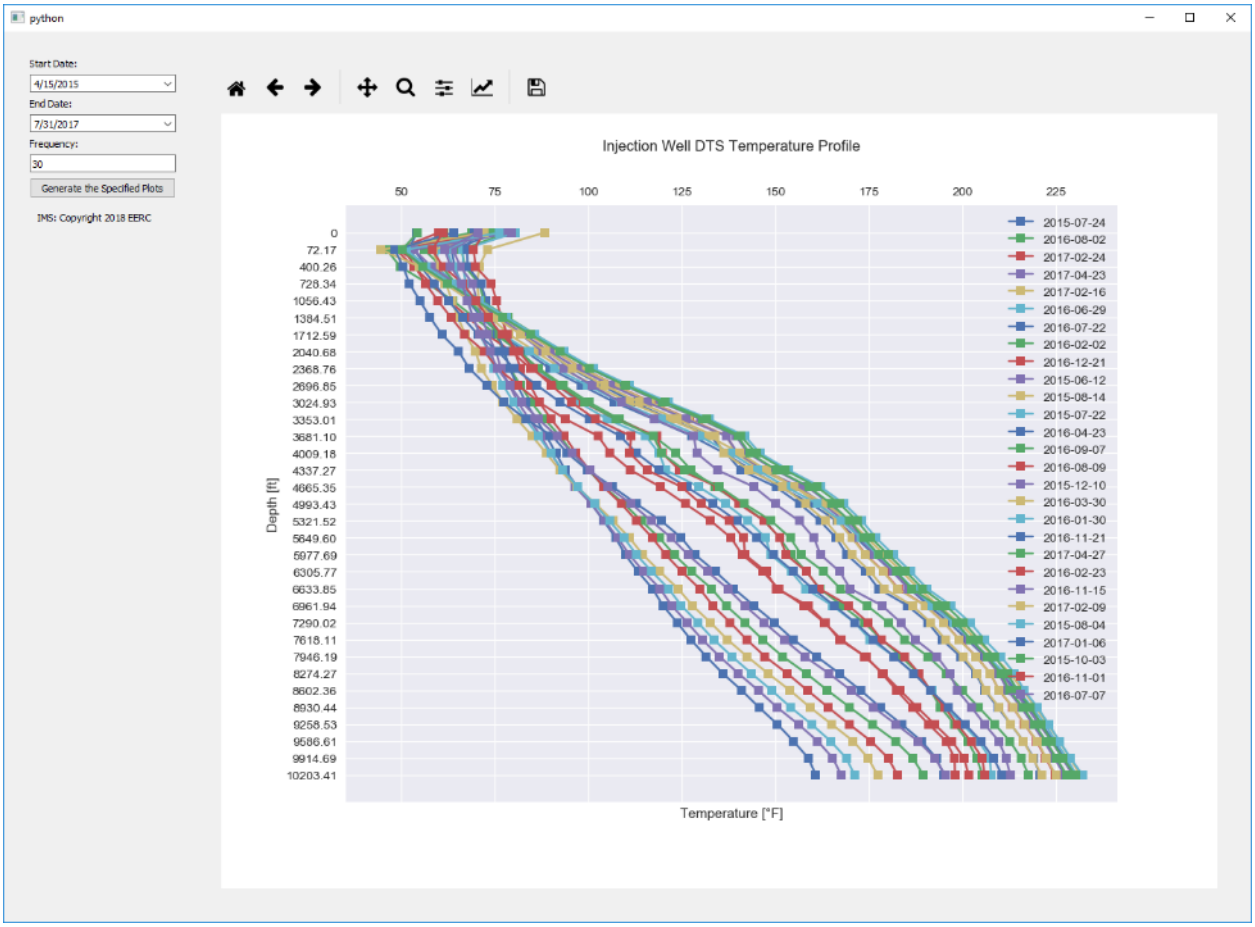


**Figure 3. Screenshot of DTS measurements module.**

**AOR**

The Area of Review (AOR) Module allows the user to display the files of $CO_2$ plume extents in 2D. Figure 4 shows the graphical display of $CO_2$ plumes from both seismic interpretation and dynamic modeling results, which provides a visual assessment of simulation results in comparison with the time lapse seismic analysis.

The AOR is defined by the US EPA as the area where the underground sources of drinking water may be endangered by $CO_2$ injection. Thus, evaluation of AOR typically involves both $CO_2$ plume and pressure migration. However, the current AOR module considers only the $CO_2$ plume extent as AOR. Thus, it is recommended to include additional AOR with pressure buildup ($\Delta P$) in future updates.

For the graphical display of $CO_2$ plume AOR, it is recommended to consider the following things:

- Time information of $CO_2$ plumes is missing and needs to be included.
- The interval of contour lines used in Figure 4 is very dense. It would be helpful to have an option to edit the contour lines such as minimum value, intervals, and display values.
- The color map used in Figure 4 is too simplistic to see the variations in gas saturation. It is recommended to use hot color (red) for high $CO_2$ saturation and cool color (blue) for low $CO_2$ saturation.

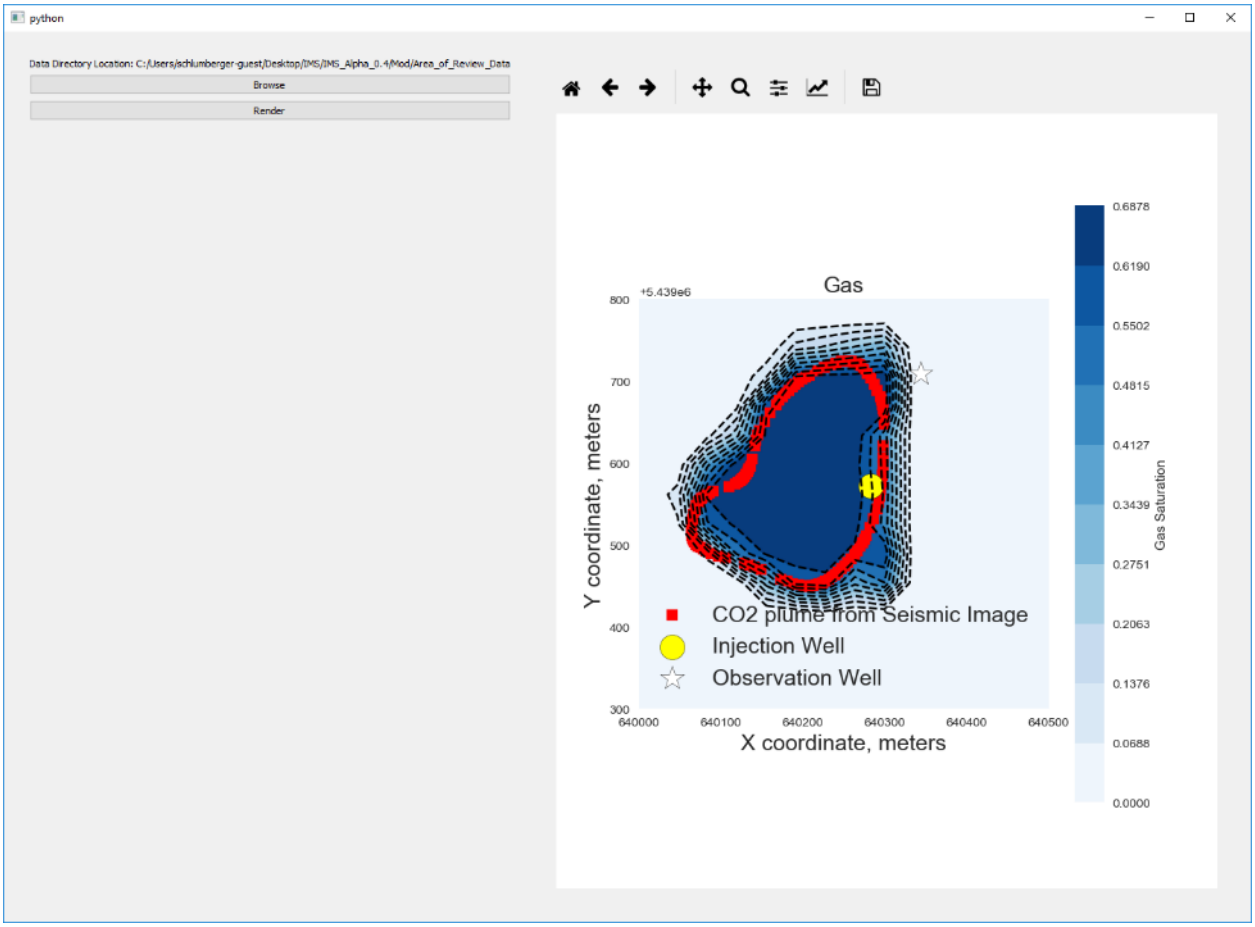


**Figure 4: Screenshot of AOR module.**

**Module A (DTS Analysis)**

Module A (DTS Analysis) evaluates the DTS data and provides a warning to a user when the action level is reached. Based on the injection rate and consecutive injection days, three possible groups and action levels for Module A were identified from the Aquistore dataset. Figure 5 shows the screenshot of Module A including the geothermal gradient, action levels 1 and 2 when the Q is greater than or equal to 10,000 lb/hr and consecutive injection days are greater than or equal to 5 days. Action levels 1 and 2 represents 1% and 2% false-positive rate action levels, respectively.

The identified three possible groups and action levels were pre-determined from the Aquistore dataset. In reality, however, real-time data are transmitted to the IMS continuously and the possible groups need to be identified concurrently (i.e., in real-time). In addition, the action levels should be updated accordingly over time. Therefore, the application of this module under the real-time condition would require the readiness of the algorithm for real-time data.

As mentioned in the DTS Measurement Module, since the DTS records the temperature along the outside of tubing, the DTS profile needs to be better understood when there is a leak in the injection well. In addition to the DTS raw data, it may also be useful to consider the use of the DTS thermal gradient and/or annular pressure for detecting abnormal behavior. The annular pressure measurement is a measurement of the pressure in the space between the tubing and the production casing. This space is filled with water and sealed with the wellhead at the surface and sealed at the bottom by the production packer. Pressure is monitored at the surface in the wellhead where the annulus connects to the pressure management system. If a leak were to develop in

the injection system, then it would be present in the annulus pressure as the higher injection pressure from tubing bleeds off into the annulus space.

While testing Module A, the following observations were also noted:

- Pop-up balloon or help button for the brief description of geothermal gradient, action level 1, and 2 would be helpful to the user.
- Unlike the DTS Measurements Module, the sampling interval (or frequency) input is not included in the Module A. It is recommended to describe how the single frequency value is chosen for Module A in the user's manual. Note that the appropriate sampling frequency for a different project may be different from the one found in the Aquistore dataset.

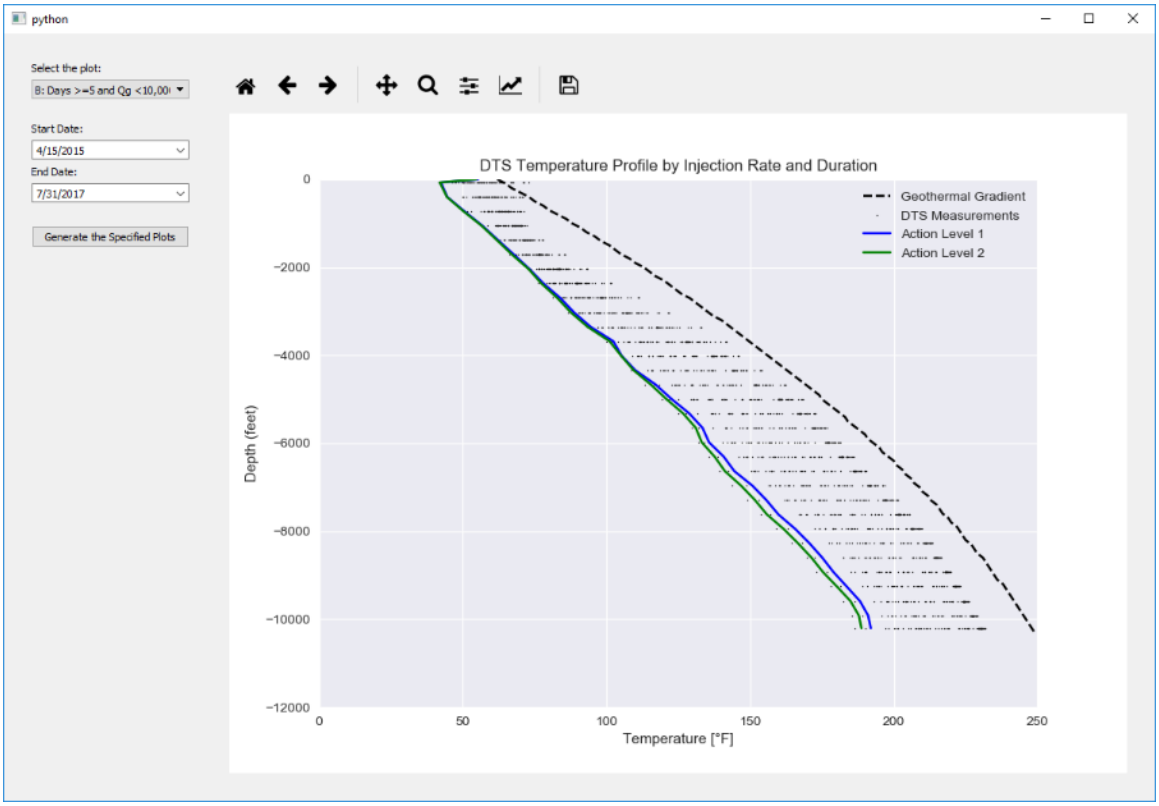


**Figure 5. Screenshot of Module A DTS (DTS analysis) when Q ≤ 10,000 lb/hr and consecutive injection days ≥ 5 days.**

**Module B (BHT & BHP analysis)**

Similar to Module A, Module B is designed to plot and evaluate BHT and BHP data with the pre-defined action levels from the Aquistore dataset. Three zones (I, II, and III) for BHP were identified with the Aquistore dataset in terms of risk identification with BHP. Figure 6 shows the BHT (upper panel) and BHP (lower panel) against time with action level 1 and 2 for BHT and zone I and II for BHP.

As pointed out in the Module A, the determination of action levels with BHT or three zones with BHP under the real-time condition may not be straightforward for the application of IMS to a newly beginning project. In addition, Lee et al. (2018) recently identified the temporal evolution of injectivities (three injection regimes) in the Aquistore injection well. It is likely that the lower and upper action level would be narrower if these three

injection regimes are introduced. Thus, it would be useful if the IMS can identify these injection regimes and apply them accordingly when evaluating BHT and BHP. Lee et al. (2018) also suggested that the thermal effect due to the introduction of cold $CO_2$ injection may not be negligible. The monitoring of the thermal effect with the IMS may be an important update if possible in the future. Lastly, it appears that the sampling frequency is fixed and excluded purposely in the module. As mentioned in Module A, the appropriate frequency for Module B may vary in a different injection well.

Due to the malfunctioning of downhole BHP gauge since late August of 2017 in the Aquistore project, BHP recordings from September of 2017 is not the downhole gauge data but the values from the multi-order regression equation. Assuming that the effect of frictional loss and $CO_2$ column pressure within the injection well is minimal, the relationship between BHP and WHP would be linear. However, detailed dynamic flow modelling within the injection well is needed to use the WHP for history match and operational guidance instead of BHP. Although the dataset used in the review of IMS did not include the period of BHP gauge failure, application of IMS needs to consider the worst case with one or multiple gauge failures.

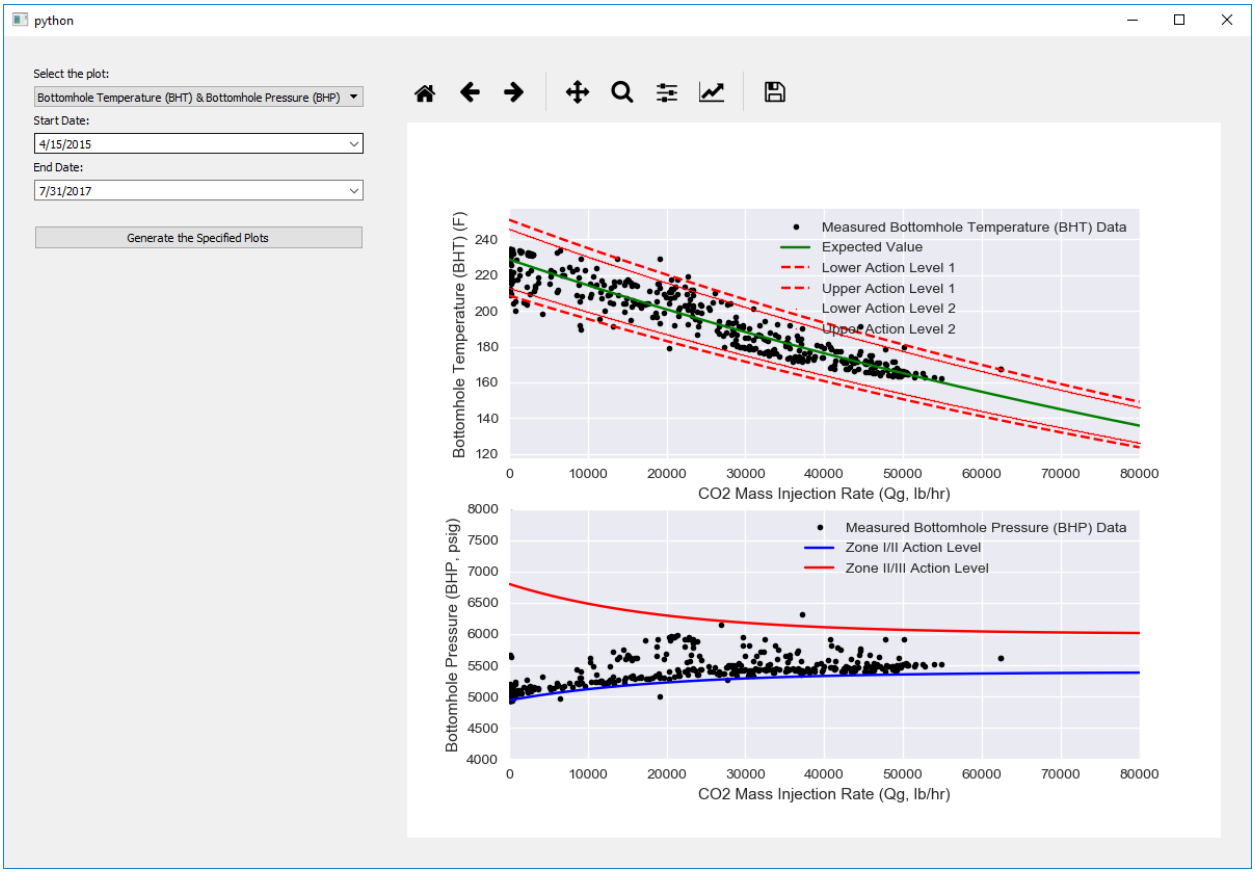


**Figure 6. Screenshot of Module B (BHT & BHP analysis).**

### Module C (CMR analysis)

Module C is intended to run Continuous Modeling Refinement (CMR) routines and evaluate history matching performance. This module includes the automatic history-matching workflow in which an objective function calculates volume-weighted error between the observed and simulated results. Because the detection of $CO_2$ plume with a seismic survey would require minimum thickness or saturation, rather than solely relying on

the volume weighted function, it is recommended to consider using the mass-weighted function as the objective function in future updates.

Figure 7 is the screenshot of Module C showing an example run. Typically, a full dynamic model requires significantly long computational time to finish. It is recommended to include the display of the simulation time/date on the screen so that a user can find the status of simulation run. In addition, it would be useful for the user to include a link to the manual as well as a technical document of this module.

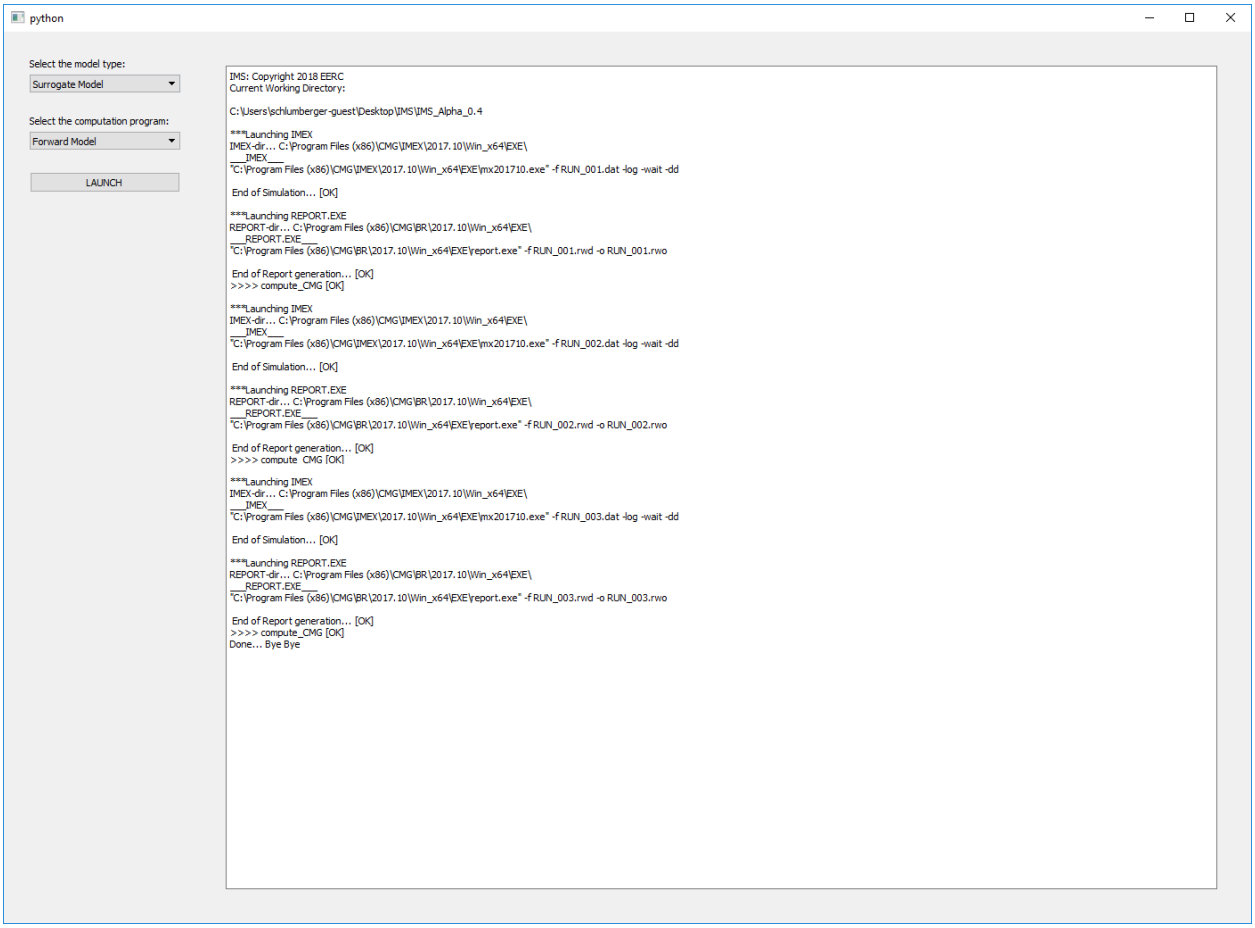


**Figure 7: Screenshot of Module C.**

## System Evaluation

The System Evaluation Module is intended to integrate and graphically display the action levels associated with DTS, BHT, BHP, CMR analysis. Figure 8 illustrates the screenshot of module with 1% (red color, flag) and 2% (salmon color, caution) action levels, while otherwise normal (blue). As discussed in Module A, DTS thermal gradient and/or annular pressure can be considered for the assessment of the $CO_2$ leakage into the annular in addition to DTS raw data. The following things were also noted during the review meeting:

- The monitoring date could not be modified manually. It is recommended to add an option to type in the date manually.

- Since this module is intended to provide an alarm to a user based on the action levels, in addition to the manual operation, it is recommended to provide an automated alarm to notify the specified users via a phone call, email, and/or text message when the action level is reached.

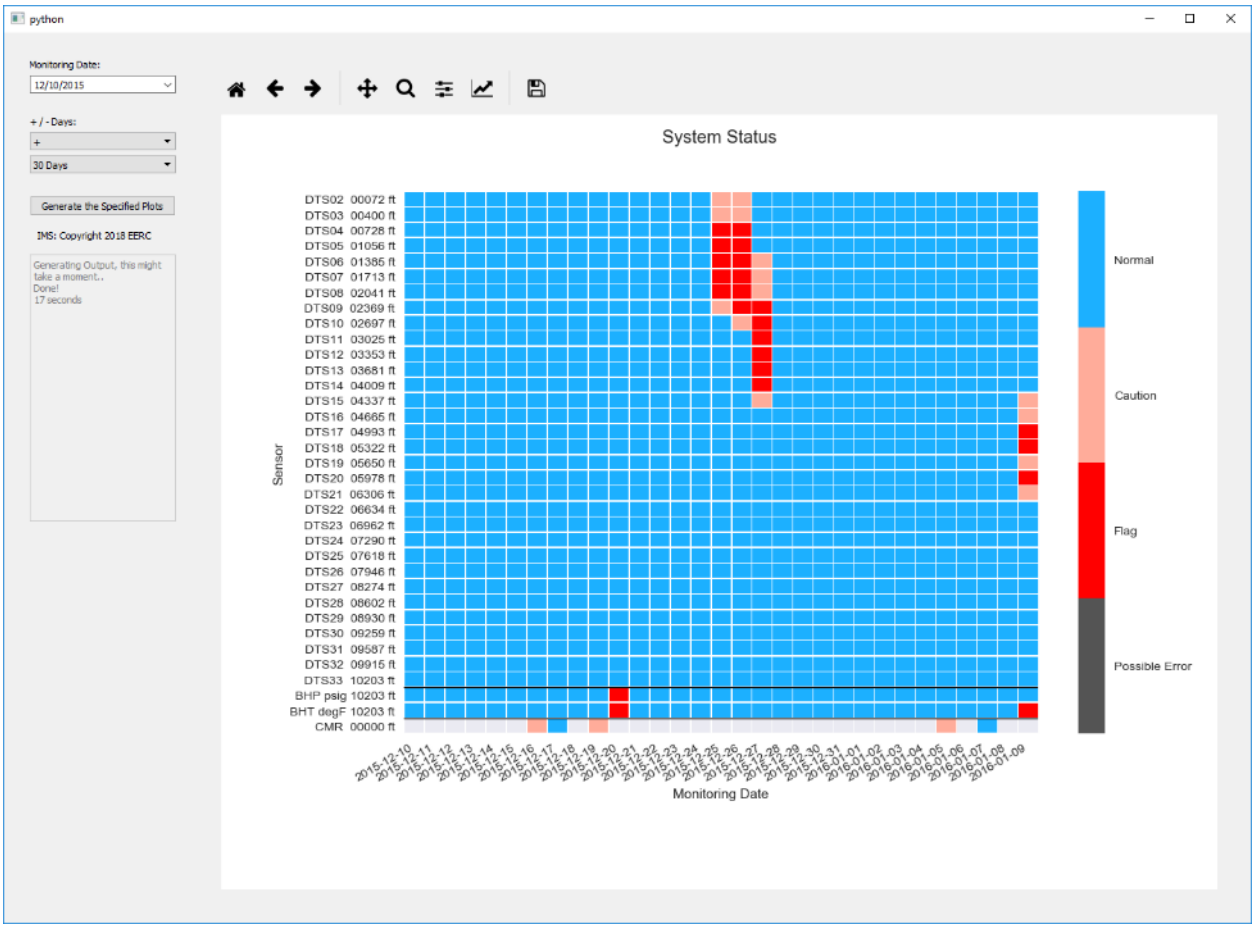


**Figure 8: Screenshot of system evaluation module.**

## Summary of Recommendations

The following is a summary of recommendations in each IMS module for the future updates:

- Module Selection Window
  - ➢ Include general information of module version, copyright, disclaimer, license, and contact information
  - ➢ Add brief descriptions of each module
- Well Monitoring Measurements Module
  - ➢ Plot multiple attributes in a single panel
  - ➢ Demonstrate real-time monitoring capability
- DTS Measurements Module
  - ➢ Add units (days) of sampling frequency

- Include display options for DTS values (of each sensor) in temperature (y axis) against time (x axis)
- Plot DTS values (contour map) in depth (y axis) against time (x axis)
- Calculate and visualize DTS thermal gradient (contour map) along depth (y axis) against time (x axis)

- AOR
  - Add additional AOR with pressure buildup ($\Delta P$)
  - Include time information of $CO_2$ plumes
  - Consider an option for the contour lines such as minimum value, intervals, and display values
  - Use hot colors (red) for high $CO_2$ saturation and cool colors (blue) for low saturation in the color map
- Module A (DTS Analysis)
  - Prepare for real-time data
  - Consider the use of DTS thermal gradient and/or annular pressure
  - Add a pop-up balloon or help button for a brief description of geothermal gradient, action level 1, and 2
  - Describe which and why single frequency value is used in the user's manual
- Module B (BHT & BHP analysis)
  - Prepare for real-time data
  - Describe which and why single frequency value is used in the user's manual
  - Add a pop-up balloon or help button for a brief description of action level 1 and 2
  - Consider the worst case scenario when the downhole gauges fail
- Module C (CMR analysis)
  - Consider the use of mass-weighted function as objective function
  - Include the display of the simulation time/date on the screen
  - Add a link to the manual and a technical document of this module
- System Evaluation
  - Consider the use of DTS thermal gradient and/or annular pressure in the system evaluation in addition to DTS raw data
  - Provide an automated alarm to notify the specified users via a phone call, email, and/or text message when the action level is reached.

**References**

Azzolina N, Torres J, Vettleson H, Pekot L, Li C (2018) Development of Intelligent Monitoring System (IMS) modules for the Aquistore $CO_2$ storage project: Data integration algorithms for aiding decision-making about the subsurface risk profile. Energy & Environmental Research Center,

Lee S-Y, Swager L, Pekot L, Piercey M, Will R (2018) Study of operational dynamic data in Aquistore project. International Journal of Greenhouse Gas Control:76:62-77